

Characterization of polyethylenes : from thermal fractionation techniques to spectrometry

Olivier Boyron

▶ **To cite this version:**

Olivier Boyron. Characterization of polyethylenes : from thermal fractionation techniques to spectrometry. Polymers. Université de Lyon, 2021. English. ⟨NNT : 2021LYSE1090⟩. ⟨tel-03647604⟩

HAL Id: tel-03647604

https://theses.hal.science/tel-03647604v1

Submitted on 20 Apr 2022

HAL is a multi-disciplinary open access archive for the deposit and dissemination of scientific research documents, whether they are published or not. The documents may come from teaching and research institutions in France or abroad, or from public or private research centers.

L'archive ouverte pluridisciplinaire **HAL**, est destinée au dépôt et à la diffusion de documents scientifiques de niveau recherche, publiés ou non, émanant des établissements d'enseignement et de recherche français ou étrangers, des laboratoires publics ou privés.



HAL Authorization

N°d'ordre NNT : 2021LYSE1090

THESE de DOCTORAT DE L'UNIVERSITE DE LYON

opérée au sein de
l'Université Claude Bernard Lyon 1

Ecole Doctorale N° 206
Ecole doctorale de Chimie de Lyon

Spécialité de doctorat : Chimie
Discipline : Chimie des polymères

Soutenue le 01/06/2021, par :

Olivier Boyron

CHARACTERIZATION OF POLYETHYLENES:
FROM THERMAL FRACTIONATION TECHNIQUES TO SPECTROMETRY

Devant le jury composé de :

Stéphane Daniele Professeur des universités, *Université de Lyon*	Président
Laurence Charles Professeure des Universités, *Université Aix-Marseille*	Rapporteure
Stéphanie Reynaud Directrice de recherche, *CNRS*	Rapporteure
Catherine Ladavière Directrice de recherche, *CNRS*	Examinatrice
Anne-Françoise Mingotaud Chargée de recherche, *CNRS*	Examinatrice
Nadia Delon-Anik Ingénieur de recherche, *Solvay*	Examinatrice
Christophe Boisson Directeur de recherche, *CNRS*	Directeur de thèse
Timothy F.L. McKenna Directeur de recherche, *CNRS*	Co-directeur de thèse

UNIVERSITE CLAUDE BERNARD – LYON 1

Administrateur provisoire de l'Université	M. Frédéric FLEURY
Président du Conseil Académique	M. Hamda BEN HADID
Vice-Président du Conseil d'Administration	M. Didier REVEL
Vice-Président du Conseil des Etudes et de la Vie Universitaire	M. Philippe CHEVALLIER
Vice-Président de la Commission de Recherche	M. Jean-François MORNEX
Directeur Général des Services	M. Pierre ROLLAND

COMPOSANTES SANTE

Département de Formation et Centre de Recherche en Biologie Humaine	Directrice : Mme Anne-Marie SCHOTT
Faculté d'Odontologie	Doyenne : Mme Dominique SEUX
Faculté de Médecine et Maïeutique Lyon Sud - Charles Mérieux	Doyenne : Mme Carole BURILLON
Faculté de Médecine Lyon-Est	Doyen : M. Gilles RODE
Institut des Sciences et Techniques de la Réadaptation (ISTR)	Directeur : M. Xavier PERROT
Institut des Sciences Pharmaceutiques et Biologiques (ISBP)	Directrice : Mme Christine VINCIGUERRA

COMPOSANTES & DEPARTEMENTS DE SCIENCES & TECHNOLOGIE

Département Génie Electrique et des Procédés (GEP)	Directrice : Mme Rosaria FERRIGNO
Département Informatique	Directeur : M. Behzad SHARIAT
Département Mécanique	Directeur M. Marc BUFFAT
Ecole Supérieure de Chimie, Physique, Electronique (CPE Lyon)	Directeur : Gérard PIGNAULT
Institut de Science Financière et d'Assurances (ISFA)	Directeur : M. Nicolas LEBOISNE
Institut National du Professorat et de l'Education	Administrateur Provisoire : M. Pierre CHAREYRON
Institut Universitaire de Technologie de Lyon 1	Directeur : M. Christophe VITON
Observatoire de Lyon	Directrice : Mme Isabelle DANIEL
Polytechnique Lyon	Directeur : Emmanuel PERRIN
UFR Biosciences	Administratrice provisoire : Mme Kathrin GIESELER
UFR des Sciences et Techniques des Activités Physiques et Sportives (STAPS)	Directeur : M. Yannick VANPOULLE
UFR Faculté des Sciences	Directeur : M. Bruno ANDRIOLETTI

À ma grand-mère,

REMERCIEMENTS

À la suite d'une expérience en analyse dans le domaine de l'environnement dans le groupe CARSO, j'ai intégré le CNRS en 2001. Mes activités ont débuté au sein du Service Central d'Analyse. Riche de ces diverses expériences, j'ai choisi en 2006 de me rapprocher du monde de la recherche et d'intégrer le laboratoire C2P2 alors dirigé par Roger Spitz. Cette thèse est donc une suite logique de mon immersion dans la recherche.

Dans un premier temps, je souhaite remercier l'ensemble des membres du jury. J'ai beaucoup d'admiration pour vos carrières et vos travaux et je suis très fier que vous ayez accepté d'évaluer mes travaux de thèse.

Je ne pensais pas la tâche si compliquée pour exprimer avec justesse l'ampleur de mes remerciements.

J'ai naturellement une pensée de remerciement pour les anciens directeurs de l'unité, Roger Spitz et Bernadette Charleux qui m'ont fait confiance et m'ont soutenu dans mes envies de développement analytique.

Un grand merci à mes encadrants, Tim McKenna et Christophe Boisson, qui m'ont guidé dans le monde exigeant et rigoureux de la recherche. C'est un honneur d'être sur la liste des docteurs que vous avez initiés. Merci Tim pour m'avoir « bousculé » tout le long cette thèse et d'avoir su me transmettre régulièrement le message : « il est plus que temps d'achever cette thèse ». Cela a porté ces fruits. Merci Christophe pour les débats scientifiques tellement riches, tes corrections toujours pertinentes et les discussions personnelles si amicales. Merci pour ton immense bienveillance, c'est sans nul doute la combinaison de tes qualités scientifiques et de ton altruisme qui ont rendu cette expérience aussi passionnante.

« Les personnes silencieuses ont les esprits les plus bruyants. »
Stephen Hawking

Plus particulièrement, je souhaite exprimer toute mon affection à mes amies du laboratoire. Manel, tu as été le catalyseur pour démarrer cette thèse, mon bras droit qui m'a permis de dégager du temps pour m'investir dans ce projet et aussi mon bras gauche pour y avoir participé si activement et si généreusement. Nathalie et Muriel, merci pour votre bonne humeur, votre sourire et les précieuses pauses-café (elles sont loin).

Je veux tout spécialement remercier mon copain de bureau, Franck, tes conseils en général et en particulier pour la rédaction m'ont été précieux. Sébastien et Franck(s) le running avec vous et nos confabulations pendant ces sorties sont toujours agréables. Damien, Fabrice, merci pour vos idées précieuses qui ont enrichi ce manuscrit et alimenté mes réflexions. Elodie, Pierre-Yves, Vincent, Jean je suis très fier de vous avoir comme collègue. Merci très particulier à Mathieu et à Edgar pour votre disponibilité et vos inestimables contributions.

Je tiens à témoigner toute ma reconnaissance aux personnes extérieures au laboratoire qui m'ont aidé, discrètement, et sont au fil du temps devenu des amis : Fernande Da Cruz-Boisson pour le support en RMN, Stéphane Lebras pour le support en infrarouge, Ronan Cozic pour l'aide en spectrométrie de masse, Laurent Constant pour ton efficacité à réparer la chromatographie.

I would also like to express my friendship and gratitude to Benjamin Monrabal and Alberto Ortin from PolymerChar, Joao Soares from University of Alberta and Tibor Macko from Fraunhofer institute for many friendly and valuable discussions about thermal fractionation techniques.

Nombreux sont ceux que je veux, aussi, remercier pour leur implication dans ce travail lors de stages de Master (Alissa, Anne, Arnaud, Bérangère, Claire Marie, Emilie, Gisèle, Islem, Laetitia, Sofia), de projets CPE (Nicolas, Constance, Florence, Rémi, Thibault, Alexane, François) et de stages d'IUT (Guillaume, Nicolas, Pierre). Ce travail a abouti grâce à votre investissement toujours passionné et vos idées continuellement passionnantes.

Merci aux étudiants et doctorants du laboratoire c'est un bonheur et une grande richesse de vous côtoyer.

Et surtout, merci à ma famille, trouver les mots justes est compliqué. Ma femme tout d'abord, merci pour ton soutien, ta patience et pour m'avoir épousé pendant cette thèse. Merci à ma belle-famille qui m'a appris les plaisirs de se dépasser pour atteindre des sommets. Merci à ma belle-famille avec qui j'aime partager, dans la fumée d'un « Romeo y Julieta », des mystères de la science. Merci à mes enfants pour vos illustrations, je vous chéris. Merci à mes parents pour vos encouragements. Vous m'avez donné tellement d'armes pour réaliser ce type de défis. Cette thèse est probablement pour vous, avant tout. Je sais la fierté que vous éprouvez et je n'ai pas toujours les mots pour vous exprimer la mienne.

"Ce qui compte ne peut pas toujours être compté,
et ce qui peut être compté ne compte pas forcément."
Albert Einstein

ABSTRACT

Eighty-eight copolymers of ethylene with α-olefins (propene, hexene, octene, octadecene and norbornene) have been prepared using the $Et(Ind)_2ZrCl_2$ and $(nBuCp)_2ZrCl_2$ complexes activated with methylaluminoxane. These complexes led to a large range of high-density polyethylene (HDPE) linear low-density polyethylene (LLDPE) with various chemical compositions. They were referred as PE models. Their average comonomer contents were determined by ^{1}H- and ^{13}C-NMR.

The PE models (HDPE and LLDPE) were characterized by high temperature size exclusion chromatography (HT-SEC) and showed a narrow molar mass distribution as expected for polymers obtained with single site catalysts. A method was developed to access to the degree of long chain branching (LCB) in polyethylene (PE). The viscometer detector of the SEC was used to determine the LCB by measuring the ratio of the intrinsic viscosity of a PE sample and a standard linear polyethylene. An original approach has been proposed to investigate the effect on the intrinsic viscosity of short chain branching (SCB) in LLDPE and correct this effect for the LCB measurement. The results agreed well with that of NMR studies.

The LLDPE models which are homogeneous in chemical composition, were used as standards to calibrate thermal fractionation techniques: TREF, CRYSTAF, CEF, TGIC and SGIC. The main purpose of this work was to provide calibration curves for all existing thermal fractionation techniques, for various types of comonomers and for a wide range of α-olefin contents. The obtained calibration curves have been gathered for the first time in a unique work. They have been used and will be used to access the chemical composition distribution (CCD) of polyethylenes with heterogeneous chemical compositions.

The well-defined and well-characterized LLDPE models were exploited for the development of rapid methods to determine the comonomer content for polyethylene samples. Chemometric methods, applied to mid and near IR spectra, were constructed and provided accurate results. Consecutive to this work a similar approach was established to quantify the chemical composition of ethylene-butadiene copolymers that exhibit more complex structures. Finally, a method using thermogravimetric analysis (TGA) coupled to mass spectrometry (MS) revealed a new way to access the type of comonomer used in the synthesis of LLDPE.

In summary, this thesis work shows on the one hand the interest of separative techniques to access to CCD and on the other hand the power of spectrometry to rapidly obtain the average chemical composition of unknown polyolefin samples.

KEYWORDS

Polyethylene – LLDPE – SEC – TREF – CRYSTAF – CEF – TGIC – SGIC – thermal fractionation techniques – DSC – polyolefins characterization – FTIR spectroscopy – chemometrics



TITRE

Caractérisation des polyéthylènes : des techniques de fractionnement thermique à la spectrométrie.

RESUME

Quatre-vingt-huit copolymères d'éthylène avec des α-oléfines (propène, hexène, octène, octadécène et norbornène) ont été synthétisés en utilisant les complexes $Et(Ind)_2ZrCl_2$ et $(nBuCp)_2ZrCl_2$ activés par le méthylaluminoxane. Ces complexes ont permis d'obtenir une large gamme de polyéthylène haute densité (PEHD) et de polyéthylène basse densité linéaire (PEBDL) de compositions chimiques variées. Leurs teneurs moyennes en comonomères ont été déterminées par la RMN ^{1}H et du ^{13}C.

Les PE modèles (HDPE et LLDPE) ont été analysés par chromatographie d'exclusion stérique haute température et ont montré une distribution de masse molaire étroite comme prévu avec des catalyseurs mono-site. Ces polymères modèles ont été utilisés pour créer une méthode de mesure du degré de ramification à longue chaîne (LCB) dans le PE. Le détecteur de viscosimétrie de la SEC a été utilisé pour déterminer le LCB en mesurant le rapport de la viscosité intrinsèque du polymère ramifié et d'un polymère linéaire. Une approche originale a été proposée pour étudier la ramification à chaîne courte (SCB) dans le LLDPE et corriger leurs effets dans la mesure du LCB. Les mesures concordaient bien avec les études RMN.

Comme ces copolymères ont une composition chimique homogène, ils ont été utilisés comme étalons pour calibrer les techniques de fractionnement thermique : TREF, CRYSTAF, CEF, TGIC et SGIC. Ces travaux ont fourni des courbes d'étalonnage pour toutes les techniques de fractionnement existantes, pour différents types de comonomères et pour une large gamme de teneurs en α-oléfines. Ces courbes d'étalonnage sont rassemblées pour la première fois dans un travail unique. Elles ont été utilisées et seront utilisées pour accéder à la distribution de composition chimique (CCD) de copolymères hétérogènes.

Les PE modèles, bien définis et bien caractérisés, ont ensuite pu être utilisés pour le développement d'autres méthodes plus rapides de mesure de composition chimique. Ils ont servi à construire des méthodes chimiométriques, appliquées aux spectres moyen et proche IR, pour la prédiction de la teneur en comonomère dans des échantillons inconnus.

Suite à ces travaux, une approche similaire a été mise en place afin de quantifier la composition chimique de copolymères éthylène-butadiène qui présentent des structures plus complexes. Comme elles sont rapides, simples et sans préparation d'échantillons, ces méthodes chimiométriques ont montré leur potentiel pour caractériser les polymères.

Enfin, une méthode utilisant l'analyse thermogravimétrique (ATG) couplée à la spectrométrie de masse a montré une nouvelle façon d'accéder au type de comonomère utilisé lors de la synthèse du LLDPE.

Ce travail de thèse a montré d'une part l'apport unique des techniques de séparation pour accéder à la CCD et d'autre part la puissance de la spectrométrie pour obtenir rapidement la composition chimique moyenne d'un copolymère.

MOTS-CLES

Polyéthylène – LLDPE – caractérisation des polymères – chromatographie d'exclusion stérique – fractionnement thermique – TREF – CRYSTAF – CEF – TGIC – SGIC

RESUME SUBSTANTIEL

Il y a un siècle, en 1920, Staudinger a démontré l'existence de « longues molécules » qu'il décrivait comme de longues chaînes constituées d'unités moléculaires répétitives liées par des liaisons covalentes.[1] Ses travaux pionniers, récompensés par le prix Nobel de chimie en 1954,[2] ont conduit à de nombreuses avancées.

Aujourd'hui, les polymères forment l'un des groupes de matériaux les plus attractifs grâce à leurs propriétés polyvalentes et uniques qui les rendent omniprésents dans notre vie quotidienne. Ils ont des atouts indéniables qui permettent à la société de répondre à de multiples défis. Par exemple, les plastiques d'emballage réduisent le gaspillage alimentaire ; les matériaux isolants synthétiques utilisés dans les bâtiments nous aident à réduire notre consommation d'énergie ; les matériaux légers dans les transports permettent d'économiser l'énergie et réduisent les émissions de CO_2 ; les polymères biocompatibles sont impliqués dans des avancées médicales et sauvent des vies. En répondant aux exigences de plus en plus strictes de nombreuses applications, ils sont encore au cœur de nombreuses innovations dans les domaines de l'emballage, du transport, du BTP, de la médecine et même de l'écologie.

En particulier, l'industrie des polyoléfines a évolué de façon spectaculaire. Aujourd'hui, avec une production annuelle d'environ 170 millions de tonnes, elle représente à elle seule plus de 60% de la production de plastique et progresse encore tous les ans d'environ 4%.[3] Les polyoléfines sont constituées simplement d'atomes de carbone et d'hydrogène qui selon leurs organisations aboutissent à divers matériaux aux propriétés spécifiques. Plusieurs centaines de grades de polyoléfines, qui possèdent autant de propriétés variées, sont actuellement commercialisés.

Avec le polypropylène (PP), le polyéthylène (PE) est une classe majeure de polyoléfines. II existe principalement trois types de polyéthylènes regroupés selon leur densité (Table 1) : (1) Le polyéthylène haute densité (HDPE) présente une structure assez linéaire, (2) le polyéthylène basse densité (LDPE) présente une structure très ramifiée comprenant des ramifications longues et courtes (LCB et SCB) (3) et le polyéthylène basse densité linéaire (LLDPE) est caractérisé par des ramifications courtes (SCB). Les LLDPE industriels sont issus de la copolymérisation d'éthylène avec une α-oléfine par catalyse Ziegler-Natta. La longueur des ramifications dépend directement du comonomère utilisé lors de la synthèse.

Table 1 : Classification des polyéthylènes selon leurs structures.

Type de PE	**HDPE**	**LLDPE**	**LDPE**
Structure			

Bien que le LDPE soit produit par procédés radicalaires, la majorité des polyoléfines sont synthétisées par catalyse de coordination. Ils sont mis en œuvre dans des unités de production en continu utilisant des procédés en phase gazeuse et en suspension.

Les récents développements en chimie de polymérisation utilisant des catalyseurs mono-sites ont donné naissance à des systèmes catalytiques toujours plus performants. Ils permettent de contrôler finement la structure des chaînes de polymères. Associés aux avancées en procédés de polymérisation avec l'utilisation de réacteurs multiples en cascade, ils ont conduit à la production directe de polyoléfines de performances.

Tous ces progrès ont permis, entre autres, d'orienter la composition chimique (organisation des carbones et hydrogènes) des matériaux pour atteindre des propriétés spécifiques. Ces remarquables avancées représentent de grands défis pour la caractérisation de ces matériaux. Il est donc essentiel de développer des outils analytiques nouveaux pour explorer et comprendre ces structures de plus en plus complexes. La mesure de la composition chimique moyenne, obtenue habituellement par densité ou « melt flow index » en milieu industriel ou par RMN en laboratoire de recherche, ne suffit plus. Il faut accéder à la distribution de composition chimique seulement accessible par des techniques de fractionnement thermique. Ces techniques dédiées à la caractérisation des polyoléfines sont assimilées à des méthodes séparatives de chromatographie liquide.

Ce travail de thèse est focalisé sur l'implantation et le développement de méthodes basées sur ces techniques séparatives.

Pour mettre en place ces nouvelles méthodes, il a été nécessaire, dans un premier temps, de préparer nos propres étalons. Ainsi, 88 copolymères d'éthylène avec des α-oléfines (propène, hexène, octène, octadécène et norbornène) ont été synthétisés en utilisant les complexes $Et(Ind)_2ZrCl_2$ (Figure 1) et $(nBuCp)_2ZrCl_2$ activés par le méthylaluminoxane.

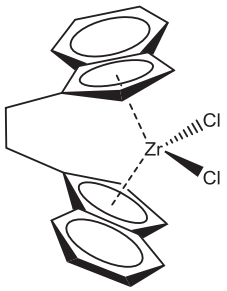


Figure 1 : Complexe $Et(Ind)_2ZrCl_2$ utilisé pour la synthèse des copolymères

Ces catalyseurs ont permis la synthèse d'une large gamme de HDPE et de LLDPE (Figure 2) avec des compositions chimiques variées. Ces valeurs de compositions chimiques, équivalentes à la teneur moyennes α-oléfines, ont été déterminées par la RMN ^{1}H et du ^{13}C.

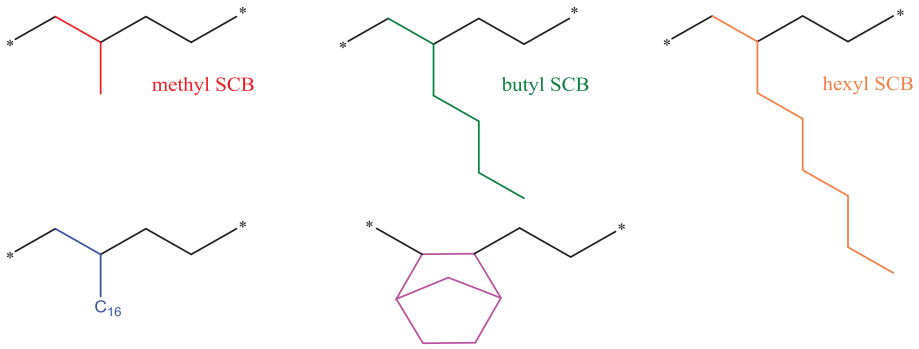


Figure 2 : Familles de copolymères synthétisés dans cette étude

Les PE modèles ont été analysés par chromatographie d'exclusion stérique (SEC) haute température et ont montré une distribution de masse molaire étroite comme prévu avec des catalyseurs mono-site. La SEC a été aussi utilisée pour mesurer le nombre de ramifications longues (LCB, long chain branching) dans nos polymères modèles. Comme les ramifications courtes elles impactent les propriétés des PE. Le détecteur viscosimétrique a été exploité pour déterminer le taux de LCB en mesurant le rapport de la viscosité intrinsèque du polymère étudié et d'un polyéthylène linéaire modèle. Une approche originale a été proposée pour mesurer l'effet des ramifications courtes (SCB, short chain branching) sur la viscosité intrinsèque dans les LLDPE et corriger cet effet pour une mesure quantitative du taux de LCB. Nous avons montré que les mesures concordaient bien avec les valeurs obtenues en parallèle par RMN.

Comme les copolymères préparés ont une composition chimique homogène, ils ont pu être utilisés comme référence pour étalonner les techniques de fractionnement thermique : TREF, CRYSTAF, CEF, TGIC et SGIC.

Ces travaux ont fourni des courbes d'étalonnage pour toutes les techniques de fractionnement existantes, pour différents types de comonomères et pour une large gamme de teneurs en α-oléfines. Outre les étalonnages pour les α-oléfines classiques (propylène, hexène et octène) des étalonnages ont été établis pour des copolymères avec des ramifications plus longues (C_{16}) et des cycles (norbornène). Ils ont permis d'étudier l'effets de ces unités sur la cristallisation du polymère (DSC) et sur les températures d'élution (TREF, CEF). Ces courbes d'étalonnage sont rassemblées pour la première fois dans un travail unique. Elles ont été utilisées et seront utilisées pour accéder à la distribution de composition chimique (CCD) de copolymères hétérogènes comme présenté en Figure 3.

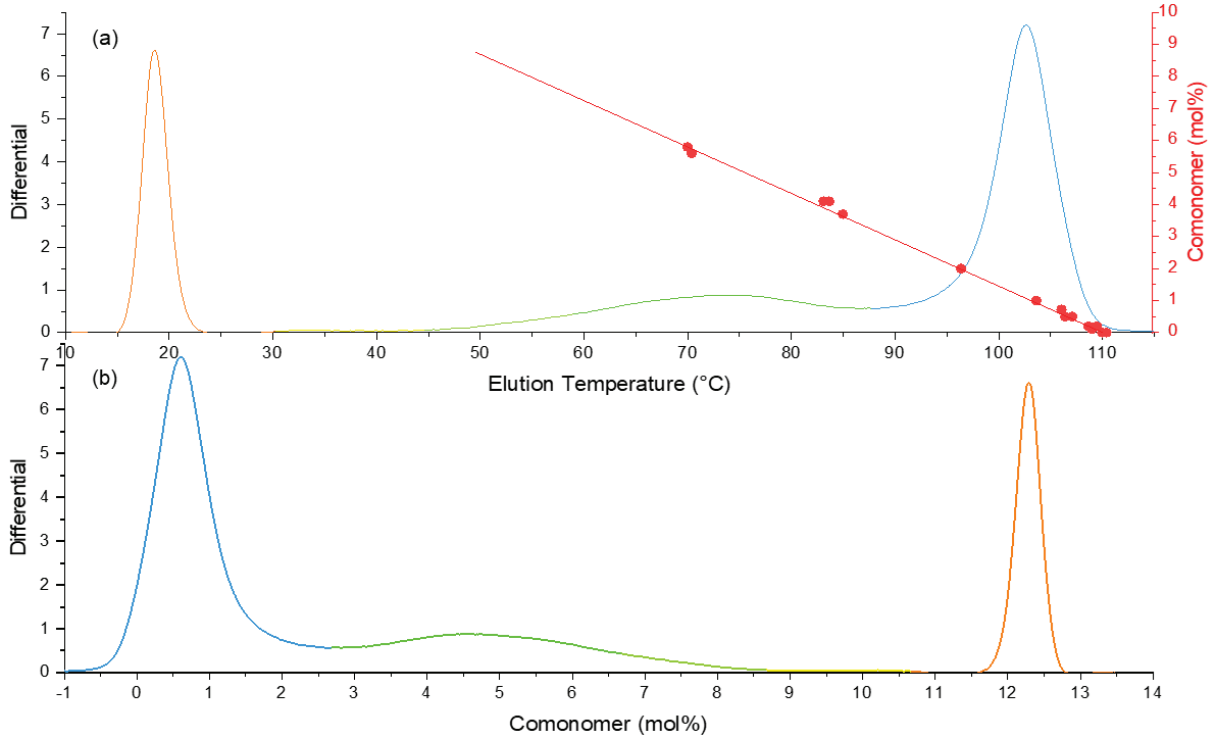


Figure 3 : Chromatogramme CEF pour un échantillon de composition chimique hétérogène (a) et distribution de composition chimique obtenue grâce aux étalonnages mis en place (b).

Suite à la présentation de cette première étape d'étalonnage des différentes techniques de fractionnement, trois publications soumises et acceptées dans des journaux à comités de lecture illustrent la fin du chapitre. Elles (1) décrivent l'étalonnage de la TREF et son application à l'analyse de copolymères hétérogènes en composition chimique obtenus par catalyse Ziegler-Natta, (2) comparent les techniques CRYSTAF et SGIC et (3) discutent des interactions enthalpiques et entropiques qui entrent en jeu entre les chaines de LLDPE et la colonne en graphène utilisée en TGIC. Je suis auteur principal de la première publication et co-auteur des deux suivantes.

Nous avons montré dans le chapitre 3 que les techniques de fractionnement sont des moyens uniques pour accéder à la distribution en composition chimique de polyéthylènes. Ces techniques séparatives, tout comme l'analyse RMN, requièrent une mise en solution des échantillons ; ce qui pour les polyoléfines nécessitent l'utilisation de solvants agressifs et toxiques (DCB, TCB, xylène) ainsi que des températures élevées (130°C à 150°C). Dans ce contexte de préparation des échantillons, il faut à la fois être vigilant sur la bonne mise en solution du polymère et éviter sa dégradation. Cette préparation délicate demande des temps d'analyse souvent longs. Il est d'un réel intérêt pour les laboratoires de recherche et d'analyse de développer en parallèle des techniques plus rapides et plus simples pour accéder à la composition chimique moyenne.

Les LLDPE modèles, bien définis et bien caractérisés, ont ainsi pu être utilisés pour le développement de méthodes alternatives de mesure de la composition chimique. Ce sont les techniques de spectrométrie, largement utilisés par les laboratoires de recherche, qui ont été envisagées comme outils alternatifs. Dans ce 4ème chapitre nous nous sommes intéressés en particulier à la spectroscopie infrarouge à transformée de Fourier (FTIR) et au couplage de l'analyse thermique et de la spectrométrie de masse.

La spectroscopie infrarouge est utilisée depuis de nombreuses années pour la caractérisation des polyoléfines. Le développement de la chimiométrie, outils mathématiques et statistiques pour obtenir des informations à partir d'un grand nombre de données, permet une nouvelle approche dans l'exploitation des spectres obtenus. La chimiométrie permet d'atteindre des informations sur les polymères en observant l'ensemble des longueurs d'ondes significatives des informations recherchées. Nous avons montré qu'elle peut s'appliquer efficacement à la fois au moyen infrarouge et au proche infrarouge sur les LLDPE (première partie du chapitre) mais aussi sur d'autres types de copolymère comme des copolymères éthylène-butadiène qui présentent des structures complexes (seconde partie du chapitre). Nos polymères modèles ont ainsi servi à construire des méthodes chimiométriques, appliquées aux spectres IR, pour la prédiction de la teneur en comonomère dans des échantillons inconnus. Comme elles sont rapides, simples et sans préparation d'échantillons, ces méthodes chimiométriques ont montré leur potentiel pour caractériser les polyéthylènes (Figure 4).

La dernière partie du chapitre concerne la spectrométrie de masse particulièrement difficile à employer pour l'analyse des polymères. Le couplage de l'analyse thermo gravimétrique (ATG) avec la spectromètrie de masse a révélé tout son potentiel pour comprendre la structure de LLDPE inconnus. Le couplage a permis, par dégradation thermique, d'obtenir des fragments significatifs des LLDPE analysés qui ont été

ensuite identifiés par la spectrométrie de masse. Cette méthode permet d'identifier le type d'α-oléfines utilisé lors de la synthèse.

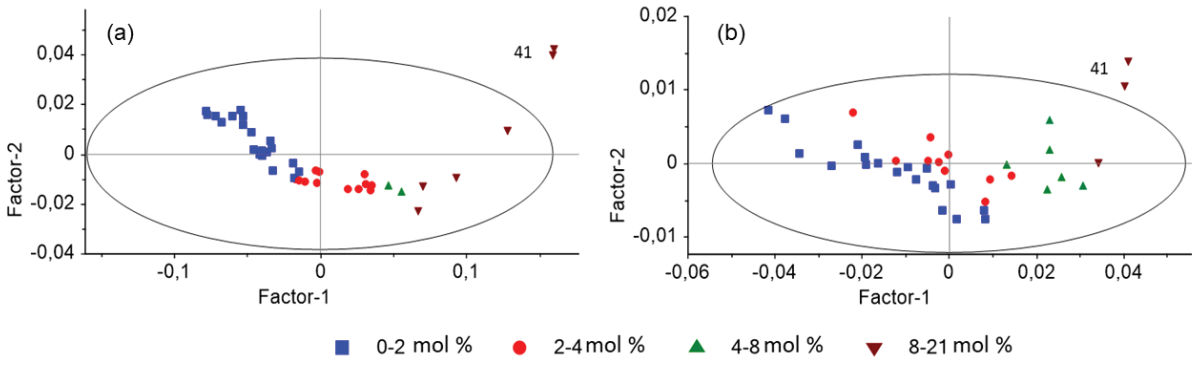


Figure 4 : Analyse en composantes principales (PCA, principal component analysis) pour un intervalle de confiance de 95% moyen infrarouge (a) et en proche infrarouge (b) pour des copolymères éthylène-hexène. Les échantillons ont été séparés de manière distincte en quatre groupes (bleu, rouge, vert et marron) en fonction de leur teneur en 1-hexène (en mol%).

Ce travail de thèse a montré d'une part l'apport unique des techniques séparatives de fractionnement thermique pour accéder à la CCD et d'autre part la puissance de la spectrométrie pour obtenir rapidement la composition chimique moyenne de copolymères.

REFERENCES

[1] H. Staudinger, *Berichte der deutschen chemischen Gesellschaft (A and B Series)* **1920**, *53*, 1073.

[2] *Chemical & Engineering News Archive* **1954**, *32*, 162.

[3] T. J. Hutley, M. Ouederni, "Polyolefins—The History and Economic Impact", in *Polyolefin Compounds and Materials: Fundamentals and Industrial Applications*, M. Al-Ali AlMa'adeed and I. Krupa, Eds., Springer International Publishing, Cham, 2016, p. 13.

TABLE OF CONTENT

Nomenclature....19

Introduction....22

1 Literature review 1-28

1.1 Introduction to polymers 1-30

1.2 Polyethylenes 1-32

1.2.1 Classification based on density 1-32

1.2.2 Classification based on branching structure 1-33

1.3 Polypropylenes 1-35

1.3.1 Types of Polypropylenes 1-35

1.4 Polymerization of olefins 1-37

1.4.1 Phillips catalysts 1-40

1.4.2 Ziegler-Natta catalysts 1-41

1.4.3 Metallocene catalysts 1-42

1.5 Properties of polyolefins 1-45

1.5.1 Structure of polyethylene 1-46

1.5.2 Crystallinity 1-49

1.5.3 Molar masses 1-52

1.5.4 Chemical composition 1-57

1.6 Conclusion 1-65

2 Synthesis of LLDPE models and their characterization 2-73

2.1 Reaction medium 2-75

2.1.1 Pre-catalysts 2-75

2.1.2 Co-catalyst 2-75

2.1.3 Solvent 2-76

2.1.4 Monomer 2-76
2.1.5 Comonomers 2-76
2.2 Copolymerization 2-78
2.2.1 Copolymerization conditions 2-78
2.2.2 Behavior of metallocene complexes 2-81
2.3 Determination of comonomer content by NMR 2-84
2.3.1 Quantification by ^{1}H NMR 2-85
2.3.2 Quantification by ^{13}C NMR 2-87
2.4 Determination of molar mass and branching by HT-SEC 2-90
2.4.1 Calibration methods 2-90
2.4.2 Long chain branching 2-97
2.5 Conclusion 2-109
3 Use of LLDPE to calibrate thermal fractionation techniques 3-113
3.1 Role of comonomers in thermal behavior of LLDPE by DSC 3-115
3.1.1 Equipment and analytical conditions 3-115
3.1.2 Temperature and heat flow calibration 3-116
3.1.3 Effect of molar mass on DSC profiles 3-117
3.1.4 Effect of comonomer content on DSC profiles 3-120
3.2 Melting and crystallization enthalpy 3-124
3.2.1 Ethylene-norbornene copolymers 3-124
3.2.2 Ethylene-hexene copolymers - Effect of low comonomer content 3-124
3.2.3 Ethylene-hexene copolymers - Onset melting temperature 3-125
3.3 Calibration of thermal fractionation techniques 3-128
3.3.1 Analytical conditions 3-128
3.3.2 Fractionation techniques based on crystallization 3-132

3.3.3 Fractionation techniques based on interaction 3-143

3.3.4 Comparison of techniques (CEF and TGIC) 3-148

3.3.5 Ultra-high molecular weight polyethylene (UHMWPE) 3-150

3.4 Conclusion 3-157

4 Chemical composition of ethylene copolymers using spectrometry 4-198

4.1 Chemical composition of hexene based LLDPE by IR spectroscopy and chemometrics 4-201

4.1.1 Introduction 4-201

4.1.2 Experimental Section 4-203

4.1.3 Results and discussion 4-206

4.1.4 Conclusion 4-220

4.2 Rapid determination of the chemical composition of ethylene-butadiene copolymers using FTIR spectroscopy and chemometrics 4-225

4.2.1 Introduction 4-225

4.2.2 Experimental Section 4-226

4.2.3 Results and discussion 4-228

4.2.4 Conclusion 4-240

4.3 An advanced technique for linear low-density polyethylene composition determination: TGA–IST16–GC–MS coupling 4-243

4.3.1 Introduction 4-244

4.3.2 Experimental Part 4-245

4.3.3 Results and discussion 4-249

4.3.4 Conclusions 4-258

General conclusion 265

Appendix: List of LLDPE models 274

NOMENCLATURE

Acronyms

*a*PP	Atactic polypropylene
aTREF	Analytical temperature rising elution fractionation
CCD	Chemical composition distribution
CEF	Crystallization elution fractionation
^{13}C NMR	Carbon-13 nuclear magnetic resonance
CR	Cooling rate
CRYSTAF	Crystallization analysis fractionation
DC	Dynamic crystallization
DSC	Differential scanning calorimetry
ELSD	Evaporative light scattering detector
E/P	Ethylene-propylene copolymer
EPDM	Ethylene propylene diene monomer
EVA	Ethylene vinyl acetate
FTIR	Fourier transform infrared spectroscopy
GPC	Gel-permeation chromatography
^{1}H NMR	Proton nuclear magnetic resonance
HDPE	High density polyethylene
HPLC	High performance liquid chromatography
HR	Heating rate
HT-SEC	High temperature size exclusion chromatography
SGIC	Solvent gradient interactive chromatography
TGIC	Thermal gradient interactive chromatography
*i*PP	Isotactic polypropylene
IR	Infrared spectroscopy
IV	Intrinsic viscosity
LAC	Liquid adsorption chromatography
LC	Liquid chromatography
LCCC	Liquid chromatography at critical conditions
LCB	Long chain branching
LDPE	Low density polyethylene

LLDPE	Linear low-density polyethylene
LS	Light scattering detector
MAO	Methylaluminoxane
MHS	Mark-Houwink-Sakurada
m-LLDPE	Metallocene linear low-density polyethylene
MW	Molecular weight
MWD	Molecular weight distribution
NMR	Nuclear magnetic resonance
ODCB	1,2-dichlorobenzene
PE	Polyethylene
PGC	Porous graphitic carbon
PP	Polypropylene
PS	Polystyrene
RI	Refractive index
SAXS	Small-angle X-ray scattering
SCB	Short chain branching
SCB/1000 C	Number of short chain branching per 1000 carbons
SEC	Size exclusion chromatography
*s*PP	Syndiotactic polypropylene
TMA	Trimethylaluminum
TCB	1,2,4-trichlorobenzene
TREF	Temperature rising elution fractionation
UHMWPE	Ultra-high molecular weight polyethylene

LLDPE models	This term will be frequently used throughout the document and includes all ethylene-α-olefin copolymers synthesized to calibrate analytical techniques

Symbols

$\bar{B}_w$	Weight-average number of branch per molecule
C_P	Cyclopentadienyl
Đ	Dispersity
D	Diffusivity

D_T	Density of the solvent at temperature T
dn/dc	Refractive index increment
ℓ	Lamella thickness
E_α	Activation energy
g	Branching factor based on radius of gyration
g'	Branching factor based on intrinsic viscosity
L_P	Long period of the crystalline structure
M	Molar mass
$\bar{M}_n$	Number-average molar mass
$\bar{M}_w$	Weight-average molar mass
mol.%	Mole percent
R	Alkyl group
R_h	Hydrodynamic radius
R_g	Radius of gyration
$\langle R_g^2 \rangle$	Mean-square radius of gyration
T_c	Crystallization temperature
T_g	Glass transition temperature
T_m	Melting temperature
T_p	Peak elution temperature
V_h	Hydrodynamic volume
wt.%	Weight percent
[η]	Intrinsic viscosity

INTRODUCTION

Polymers form one of the most attractive groups of materials thanks to their versatile and unique properties which make them ubiquitous in our daily lives. They have assets that allow society to respond to multiple challenges. For example, packaging plastics reduce food waste; high performance synthetic insulation materials help us to reduce our energy consumption; lightweight materials in transport save fuel and reduce CO_2 emissions; biocompatible polymers enable medical advances that save human lives. And they still have great potential for development.

Thanks to the progress made in synthesis, polymers remain at the heart of many innovations in medicine, electronics, transport, ecology, and construction. Indeed, the development of polymerization techniques makes it possible to envisage the preparation of a large variety of macromolecules with well-defined structures and compositions. Thus, recent polymerization tools have made it possible to modulate the composition of macromolecule chains and therefore their properties to better meet the increasingly strict requirements of numerous applications. In particular, the development of catalyst systems has greatly contributed to facilitating the production of polyolefins with new properties which constitute a fascinating range of materials.

With an annual production of around 170 million tons per year and an annual increase of around 4%, polyolefins alone represent more than 60% of plastic production.[1] Depending on the arrangement of the carbon and hydrogen atoms, various polyolefin materials with different properties can be obtained. This combination of carbon atom and hydrogen leads to the composition of several hundred grades of polyolefins.

Polypropylene (PP) is an important class of polyolefins. Atactic polypropylene (aPP), in which methyl groups are randomly distributed along the chain, is also manufactured, and exhibits characteristics similar to waxes. Syndiotactic polypropylene (*s*PP) results in a regular alternation in the orientation of these methyl groups. Isotactic polypropylene (*i*PP) includes all the methyl groups placed on the same side of the polymer backbone, leading to the formation of a helix. The stack of these helices forms polypropylene crystals which give the polymer high flexural rigidity, which is the basis of most of its properties. *i*PP is by far the most commonly produced polypropylene.

With polypropylene, polyethylene (PE) is a major class of polyolefins. Basically, there are three classes of polyethylene. High-density polyethylene (HDPE) displays a fairly linear structure, low-density polyethylene (LDPE) features highly branched structures comprising long and short branching (LCB and SCB), and linear low-density polyethylene (LLDPE) is characterized by short chain branches (SCB). LLDPE are produced with

Ziegler-Natta catalysts by copolymerization of ethylene with an α-olefin, the branch length depends directly on the comonomer used during the synthesis.

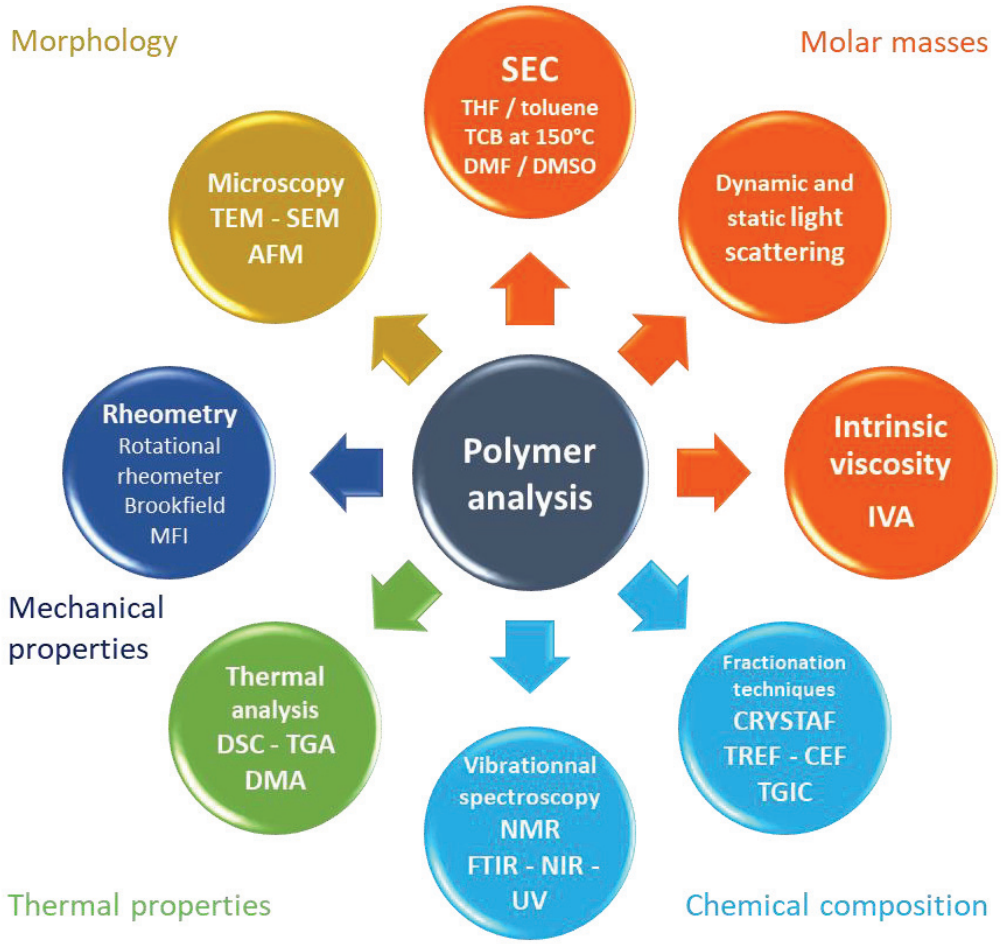
Although LDPE is produced by a radical process, the vast majority of polyolefins are synthesized by coordination catalysis. Catalysts have undergone many developments which have given rise to ever more efficient catalytic systems. They are generally obtained in continuous production units using gas phase and slurry processes. Advances in catalyst systems and in polymerization processes make it possible to manipulate polymer chain structures and combine polymers in the form of blends. The modification of polymerization conditions in a single reactor and the use of cascade reactors have led to the direct production of blends constituting high performance materials.

All this progress has made it conceivable to orient the distribution of molar mass and the distribution of chemical composition during polymerization to achieve specific properties. It is therefore essential to develop analytical tools to explore and understand these increasingly complex structures.

This thesis work is centered on the characterization of polyolefins and in particular semi-crystalline polyethylene (HDPE et LLDPE), a topic which presents particular constraints and challenges. Indeed, polymer materials are mixtures of various chains called distributions. There can be several types of distributions in the same material: chain length distributions or molar mass distributions, chemical composition distribution and structure distribution. Furthermore, as semi-crystalline polymers, polyolefins are insoluble in any solvent at room temperature which makes their analysis trickier than for most other polymers. The analysis of such complex entities cannot be limited to the use of a single characterization technique but must involve an array of several techniques. The C2P2 laboratory has gradually acquired and expanded its analytical capacity with coherent and complementary techniques which are summarized in the Figure below.

The main objective of this thesis work was to extend the analytical capabilities of the laboratory with modern tools and new characterization methods.

Part of this work lies on the implementation of original fractionation techniques for polyolefin characterization, to develop state of the art methods and to use these techniques to their maximum capacities. These techniques, based on the ability to separate polymer chains in solution according to their composition, belong to a specific part of the liquid chromatography family.



Liquid chromatography is a technique widely used for the characterization of polymers. Indeed, the modularity of this analytical technique regarding polymer elution possibilities allows obtaining a great deal of information such as the distribution of molar masses and of the chemical composition of polymer chains. Several liquid chromatography techniques were used in this work for the characterization of LLDPE by various separation modes.

- **the steric exclusion mode**, which is governed by only the loss of entropy. The macromolecule enters the pores of the stationary phase without interaction with it. The higher the molar mass of the macromolecules, the faster they will be excluded from the pores. When this elution mechanism is used, the analytical method is called size exclusion chromatography (SEC).
- **the interactive mode**, which is governed by the variation of the enthalpy energy generated during interactions between the polymer and the stationary phase. This technique is then called interactive chromatography (IC). Liquid chromatography under critical conditions (LCCC) allows the elution of polymers regardless of their molar mass. This method is widely used to separate amphiphilic block

copolymers. In this work two methods based on this mode and functioning for LLDPE were developed: solvent gradient interactive chromatography (SGIC) and thermal gradient interactive chromatography (TGIC).

- **the crystallization mode**, which is governed by the capacity of a polymer to crystallize, as in crystallization analysis fractionation (CRYSTAF), or be re-eluted after a crystallization step as in temperature rising elution fractionation (TREF) and crystallization elution fractionation (CEF). These methods can be applied only for semi-crystalline polymers and are actually used only to separate polyolefins.

In this work, these different existing separation modes were used, developed, and installed in our laboratory to achieve fine characterizations of the complex structures of LLDPE samples. To fully exploit these recent techniques, our strategy was based on successive stages: the synthesis of well-defined LLDPE models, the complete characterization of these LLDPE by conventional techniques (NMR, SEC, DSC), and the calibration of thermal fractionation methods. Finally, taking advantage of the synthesis of LLDPE models that are well controlled regarding composition and well characterized, new analytical tools based on spectroscopy have been developed. This second line of research focused on the development of original tools with coupling methods (TGA and mass spectrometry) and the exploitation of complex spectroscopic data by chemometric tools.

This manuscript is divided into four chapters that describe these different steps:

Chapter 1 reviews the main industrialized polyolefin materials. In the second part, the various methods used for ethylene polymerization and copolymerization with α-olefins are described. Particular attention is paid to the coordination polymerization carried out with Phillips, Ziegler-Natta and metallocene catalysts. Finally, the different analytical tools used to understand the structure (molar mass, long chain branching, regioregularity) and the composition (chemical composition with short chain branching) of polyolefins are presented and described in-depth. Both well-known techniques such as size exclusion chromatography, spectroscopy (NMR, infrared) and thermal analysis (differential scanning calorimetry), and original fractionation techniques are presented (CRYSTAF, TREF, CEF, TGIC).

We synthetized LLDPE models before calibrating our original fractionation techniques which are described beforehand. In **Chapter 2,** the copolymerization conditions of ethylene with various types of α-olefins (propylene, hexene, octene, octadecene, and norbornene) are described. The complex rac-ethylene bis(indenyl)zirconium (IV) dichloride (rac-Et(Ind)$_2$ZrCl$_2$) was used due to its efficient incorporation of

comonomers and its ability to produce homogeneous LLDPE samples with respect to their molar masses and their composition. Afterwards, the chemical composition of all the samples was measured precisely with ^{1}H and ^{13}C NMR. In parallel, high temperature size exclusion chromatography was used to measure the molar masses of the samples and also to study the ability of the viscometer to measure their long and short chain branching in PE.

Chapter 3 is the heart of this thesis work. Prepared LLDPE models were used to calibrate the various thermal fractionation techniques recently installed in our unit. The advantages and specificities of each technique are discussed and illustrated. Finally, a complete calibration panel is provided for all these techniques and applicable for most industrial LLDPE samples. Some examples of applications are given to illustrate their uses. Three published articles based on these works are presented at the end of the chapter.

Finally, **Chapter 4** is dedicated to the development of the spectroscopic method. The NMR and fractionation techniques described previously are time consuming and sometimes a faster analysis is preferred. The spectroscopic method coupled with chemometric tools and thermal analysis coupled with mass spectrometry provided a rapid and precise solution to measure the chemical composition of polyolefins. This chapter consists of three publications published in peer-reviewed journal.

The main objective of all these developments is to support researches in the field of polyolefin synthesis and polymerization processes.

REFERENCES

[1] T. J. Hutley, M. Ouederni, "Polyolefins—The History and Economic Impact", in *Polyolefin Compounds and Materials: Fundamentals and Industrial Applications*, M. Al-Ali AlMa'adeed and I. Krupa, Eds., Springer International Publishing, Cham, 2016, p. 13.

CHAPTER I

LITERATURE REVIEW



Plastics are widely used in automobile parts.

Polyolefins are made from simple and commonly accessible monomers which only contain carbon and hydrogen. Despite their simplicity, they are used in a wide range of applications: packaging, car bumpers, construction, agriculture, toys, gas pipelines, etc. Since many years, they have been the largest class of synthetic polymers. The success of polyolefins is mainly due to their low production cost, large-volume production processes, reduced environmental impact, and adjustable mechanical properties.

For all these reasons, the polymerization of olefins into polymers with various microstructures continues to be widely studied by industrial and academic laboratories. The PCM (polymérisation, catalyse, matériaux) team in the CP2M (catalyse, polymérisation, proceeds et matériaux) laboratory focuses its research activity on polymer synthesis and polymerization processes. It is of great importance for researchers to understand the chemistry that is involved during the different steps of polymer synthesis. This PhD project is mainly focused on the integration in the laboratory of new characterization techniques and original analytical methods to improve understanding of the impact of polymerization chemistry and processes on polymer properties.

This bibliographic study is organized on the basis of polymer properties. First, an overview of ethylene polymerization is provided with the presentation of the different industrial processes used to produce polyolefins. The second section focuses on advanced analytical techniques for the characterization of polyolefins.

1.1 INTRODUCTION TO POLYMERS

Since they were developed in the 1950s, polymers have achieved spectacular success because of their indisputable qualities: ease of manufacturing, low cost, mechanical strength, transparency, lightness, etc. For instance, polymers contribute to reduce transport emissions with lighter materials. They have been revealed as ideal materials for many applications like packaging, building construction, automobiles, agriculture (Figure 1-1a), and are gradually taking the place of other materials, such as metals and glass. Today, between 100 and 140 kg of polymers per year and per citizen are consumed in Europe and the United States. This consumption will be further accelerated (Figure 1-1b), so it seems essential to maintain research and development efforts in this field.

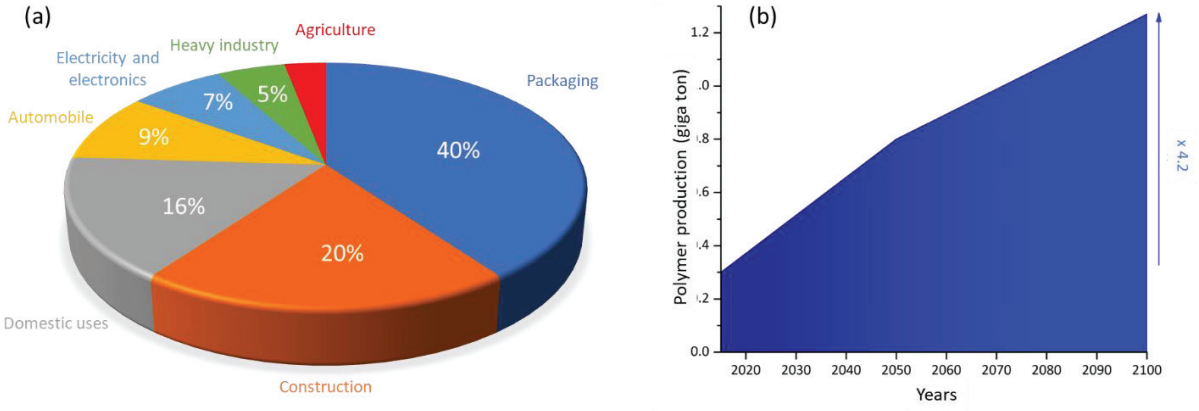


Figure 1-1: Distribution of demand for plastics in Europe in 2018 (a) and prediction of the evolution of polymer production in giga ton per year.(b) Source: PlasticsEurope Market Research Group (PEMRG)

A polymer is a set of macromolecules formed by the covalent linking of a large number of repeating units called monomers. There are different families of synthetic polymers that can be characterized by their properties. These properties are defined by both the monomer chemistry and the molecular organization in the polymer chain. First, polymers can be classified into two vast families distinguished by their heat behavior: thermosets and thermoplastics.

Thermoset polymers contain chains that cross-link together during the synthesis process to form an irreversible chemical bond. They are ideal for high temperature applications and cost-effective, but they cannot be remolded, reformed, or recycled.

Thermoplastic resins feature a broad range of performances. They generally offer high impact resistance, remolding capacity and mostly high recyclability. Among the thermoplastics, polymers may exist in amorphous and crystalline form. In the amorphous state, macromolecules become entangled in complex ways. In the crystalline state the macromolecular chains are organized and must therefore have a very regular structure. However, polymers are never totally crystalline and are considered as a mixture of amorphous and crystalline phases.

Polyolefins belong to the thermoplastic family. They are produced from a simple family of monomers, the α-olefins, with the general formula C_nH_{2n}. They can be divided into polyethylene (PE), isotactic polypropylene (*i*PP) and olefin-based elastomers such as ethylene-propylene-diene monomer rubber (EPDM), polyisobutylene (PIB), and ethylene propylene rubber (EPR). PE, the polyolefin used most, will be an important subject of this work.

1.2 POLYETHYLENES

Polyethylene, a basic repetition of -CH_2- groups, is produced by polymerizing the ethylene molecule. With an annual global production of approximately 100 million tons, polyethylenes (PEs) are the main commercial polymeric material[1, 2] and the most widely used polymers in the world (Figure 1-2). Their use has grown rapidly because they are composed of simple monomers (they contain only carbon and hydrogen) and they offer a very varied range of products whose mechanical, rheological, and optical properties provide many applications.

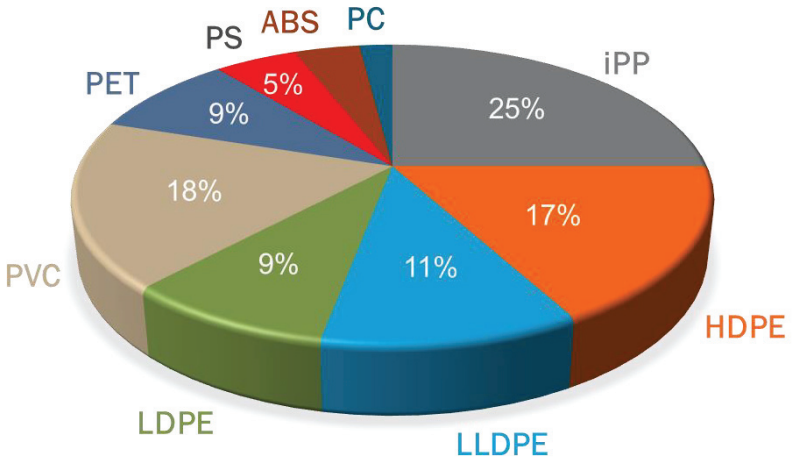


Figure 1-2: Distribution of European plastics demand by type in 2017. Source: PlasticsEurope Market Research Group (PEMRG)

1.2.1 CLASSIFICATION BASED ON DENSITY

Polyethylenes are commonly classified according to density into the following 3 classes per ASTM D883:

- high-density polyethylene (HDPE); 0.940 to 0.970 g cm^{-3}
- low-density polyethylene (LDPE); 0.910 to 0.940 g cm^{-3}
- linear low-density polyethylene (LLDPE); 0.916 to 0.940 g cm^{-3}

Additionally, ASTM D1248 further defines two additional density classes at either density extreme:

- very low-density polyethylene; ≤0.910 g cm^{-3}
- very high-density polyethylene; >0.960 g cm^{-3}

Some examples of PE applications according to their density are shown in Figure 1-3.



Figure 1-3: Polyethylene uses and applications according to their density.

1.2.2 CLASSIFICATION BASED ON BRANCHING STRUCTURE

PEs can be classified according to their branching structure (Table 1-1). The mechanism of polymerization controls the organization of the monomers linked in the polymer chain and the branching structure. HDPE has no or only a small amount of branching and is a very crystalline polymer (around 70% of crystallinity). They are manufactured with Ziegler-Natta or Phillips catalysts. LDPE contains a combination of long and short chain branching from 20 to 30 CH_3 groups per 1000 carbons. They are produced via radical polymerization and have typical properties: flexibility, processability, transparency.

The branching in LLDPE is predominantly short chain branching. This class of PE is synthetized by copolymerization of ethylene with an α-olefin which allows the insertion of a short-chain branching into the main chain and thus impacts the crystallinity of the material.[3] The α-olefins frequently used are 1-butene, 1-hexene and 1-octene. [1, 4] The crystallinity and then the physical properties of LLDPE can be adjusted by varying the comonomer content.[3, 5] Consequently, it is highly relevant to quantify the amount of comonomer units incorporated into LLDPE during the polymerization process.

Table 1-1: Classification of polyethylenes according to their branching structure. The three architectures result in various physical properties.

PE type	**HDPE**	**LLDPE**	**LDPE**
Molecular structure			
Branching			
Type	Short or long[a]	Short	Short and long
Content	Low or none	Various	High
Polymerization process	Slurry, gas phase, solution phase	Slurry, gas phase, solution phase	Supercritical ethylene
Pressure (Mpa)	2.0 – 5.0	2.0 – 5.0	70 - 300

[a] from Phillips catalysts

1.3 POLYPROPYLENES

Polypropylenes belong to the polyolefin family and has applications both as a plastic and a fiber. It is distributed in 3 families according to its geometry: isotactic (*i*PP), syndiotactic (*s*PP) and atactic (*a*PP) (Figure 1-4). The properties of *i*PP are similar to that of polyethylene but it is slightly harder and more heat and chemical resistant.[1]

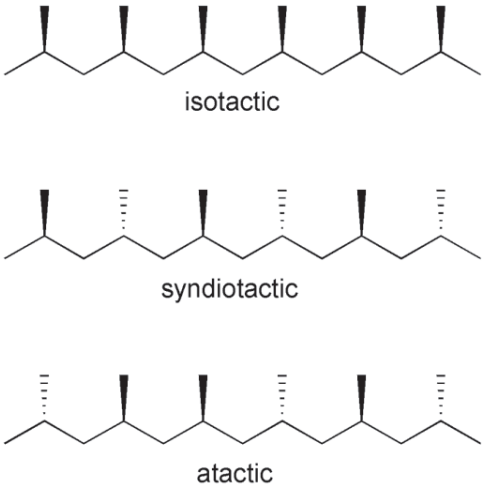


Figure 1-4: Polypropylene tacticity - Isotactic (*i*PP), methyl groups (CH_3) arranged on one side of the carbon chain - syndiotactic (*s*PP), alternating methyl group (CH_3) arrangement - atactic (*a*PP), irregular methyl group (CH_3) arrangement

*a*PP is amorphous and has almost no commercial value. Both *i*PP and *s*PP exhibit high melting temperatures due to the organization of their chains. They are both semi-crystalline. *s*PP can only be produced with specialized metallocene catalysts, resulting in expensive production. In 1988, Ewen et al. described the first efficient polymerization system for *s*PP synthesis based on *ansa*-fluorenyl-cyclopentadienyl catalysts.[6] *i*PP production is based on heterogenous Ziegler-Natta catalysts[7] and supported metallocene catalysts.[8] Compared to *s*PP, it offers an attractive properties/cost ratio and leads the market.

1.3.1 TYPES OF POLYPROPYLENES

1.3.1.1 Homopolymers

*i*PP homopolymer is the grade most developed; the main applications include packaging, textiles, pipes, automotive and electrical applications. PP copolymer grade is separated into random copolymers and block copolymers produced by co-polymerization with ethylene. Polypropylene random copolymer is

produced by polymerizing together propene and up to 6 mass % of ethylene. These polymers are flexible and optically clear, making them suitable for applications requiring transparency and for products requiring excellent appearance.

1.3.1.2 Block copolymers

In polypropylene block copolymers, the amount of ethylene is higher, up to 15%. It has comonomer units arranged in blocks.[9, 10] The regular arrangement makes polymer more rigid and less brittle than the random copolymer.[11] These materials are appropriate for applications demanding high impact strength.[12]

1.3.1.3 High impact polypropylene

*i*PP is very fragile at low temperatures due to its elevated glass transition temperature (around 20°C)[13]. Its application in cold environments is therefore not possible. The incorporation of an ethylene-propylene elastomer (EPR) in this material improves its toughness and its impact resistance in subzero temperatures.[14, 15] The addition of a certain amount of EPR into an *i*PP semi-crystalline matrix serves to adapt the final properties of the resulting material called high impact polypropylene (hiPP). The inclusions of the amorphous EPR phase prevents the propagation of cracks in the crystal matrix and absorbs the energy of impacts, while the *i*PP provides rigidity to the material. This balance between toughness and stiffness will depend on the final percentage of rubber in the material.[16-18]

hiPP is useful in applications which require impact resistance. hiPPs are mainly used in packaging, houseware, film, pipe applications, automotive bumpers and electrical segments.[15, 16]

The development of these essential polymers largely used in everyday life, requires the control and understanding of chemistry and reaction engineering via the development of advanced and specific characterization techniques. This thesis work resides fully in this framework. It aims to develop novel analytical methods to better understand the structure of polymers and thus better interpret the chemical processes involved during the polymerization steps.

To effectively achieve this objective, it is first necessary to understand the chemistry and processes of olefin polymerization.

1.4 POLYMERIZATION OF OLEFINS

Depending on the polymerization process, several grades of polyethylene can be produced. They are obtained by chain reactions via various synthesis methods:

- **Free-radical polymerization** under high pressures (120-300 MPa) and high temperatures (140-325°C) produces LDPE containing long and short chain branching. The process was developed in 1933.
- **Chromium catalysis or Phillips process**, the first catalytic polymerization of ethylene by the Phillips Petroleum Company (CrO_3-silica catalyst, Figure 1-5). The process was developed in the 1950s.

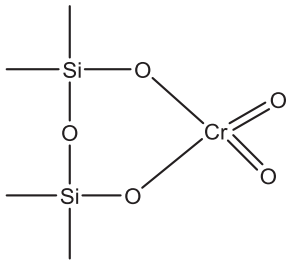


Figure 1-5: Chromium catalyst

• The **Ziegler-Natta catalysis process** was developed by Karl Ziegler and Giulio Natta in the 1950s. Originally, Ziegler and co-workers at the Max Planck Institute in Germany proved the ability of the Al-C bond of trialkylaluminium to insert ethylene via the "Aufbau" reaction.[19] Afterwards, a major breakthrough was achieved when they polymerized ethylene with the $TiCl_4/AlEt_3$ system under mild conditions.[20] Subsequently, Natta and co-workers at Milan Polytechnic were the first to produce *i*PP with a $TiCl_3/AlEt_2Cl$ combination.[21, 22] For these major discoveries Karl Ziegler and Giulio Natta were awarded the Nobel Prize for chemistry in 1963.

Several generations of Ziegler-Natta catalyst have been successively developed to improve activities and stereoregularity in the case of propylene polymerization.[23] In particular, the evolution towards the supported catalyst $TiCl_4$ on $MgCl_2$ developed by Mitsui Chemical Inc. improves not only the activity but also the control of the polymer structure and particle morphology. The use of the heterogeneous system (with a support in contrast with a homogeneous or soluble system) has enabled the production of new grades of polymers such as HDPEs and LLDPEs. Despite developments, Ziegler-Natta catalysts are multisite.

• **Metallocene complexes** used for single site catalysis have led to new evolutions in polymer structure. The metallocene complexes consist of two aromatic groups such as cyclopentadienyl ligands (Cp) linked to the metal center. The first titanocene dichloride (Cp_2TiCl_2), activated by aluminium alkyls $AlEt_2Cl$ and

$AlEt_3$, was reported by Breslow, Newburg and Natta.[24-26] Although the cocatalysts proved ineffective for the activation of complexes and led to poor activity, these catalysts contributed to understand the mechanism of polymerization. Later, Ewen and Kaminsky discovered the highly active Cp_2ZrCl_2/MAO.[27-29] Methylaluminoxane (MAO, Figure 1-9) was revealed to be a major activator for group 4 metallocene complexes (Figure 1-6).

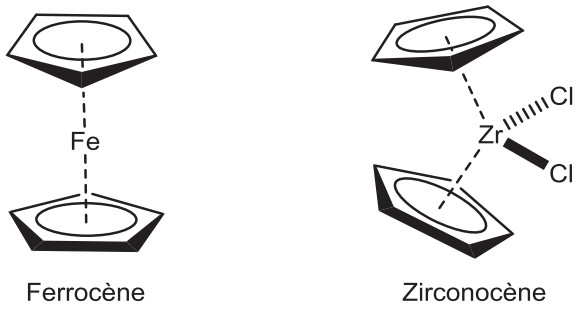


Figure 1-6: Example of metallocene complexes with sandwich structure: ferrocene[30] which is not active for olefin polymerization and zirconocene.

• The development **of post-metallocene catalysts** has given rise to intense interest in understanding ligand/metal effects on the catalyst behavior.[31] For instance, Brookhart and co-workers have reported catalysts with a late transition metal (nickel(II) and palladium(II)) combined with a bulky diimine ligand, which produce high molar mass polyolefins and a well-controlled microstructure (Figure 1-7).

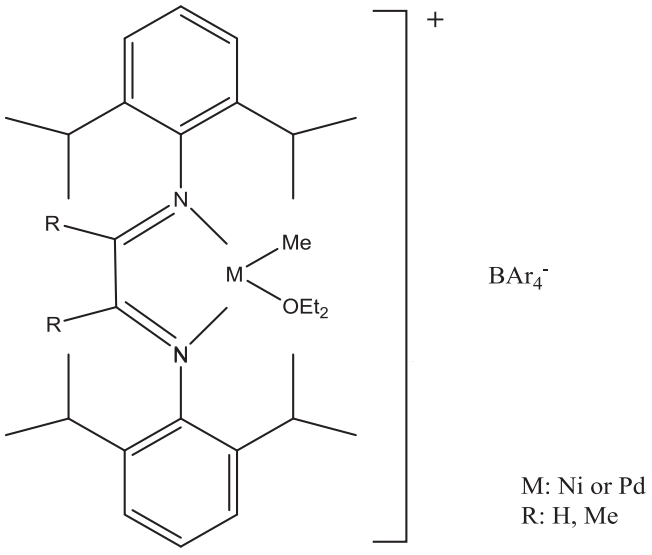


Figure 1-7: Brookhart α-diimido metal catalysts.

This catalyst system offers a complete range of materials from highly branched polyolefins, without the need for an α-olefin, to linear ones.[32]

Post-metallocene catalysts that have received commercial attention were initially developed by DOW and Exxon with the constrained geometry catalysts (CGC).[33] The CGCs feature more accessible active site than metallocene catalysts (Figure 1-8). Thus, the open nature of the active site allows the efficient copolymerization of ethylene with α-olefins such as hexene and octene[34, 35]. Stevens et al. also have reported that high molar mass polymers could be produced.[36]

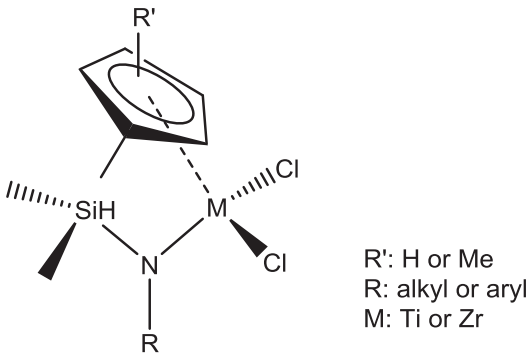


Figure 1-8: General structure of constrained geometry complexes (CGC).

A wide range of molecular catalysts have been developed, expanding the tool box for making polyolefin materials with improved performances.[37] However, investigating the development of olefin polymerization catalysts falls outside the scope of this chapter.

Table 1-2: Commercial catalysts and their characteristics.

Catalyst	**Transition metal**	**Process**	**Characteristics**
Phillips	Cr	Heterogeneous[a]	No cocatalyst / Broad molar mass distribution
Ziegler-Natta	Ti	Heterogeneous and Homogeneous[b]	Alkyl aluminum cocatalysts / Broad molar mass distribution
Metallocene	Zr, Ti, Hf	Heterogeneous and Homogeneous	Methylaluminum or borate cocatalyst / narrow molar mass and chemical distribution

[a] supported catalysts, [b] soluble catalysts

Table 1-2 summarizes the main types of industrial catalyst used to produce HDPE and LLDPE. Ziegler-Natta and Phillips catalysts are considered as multiple-site catalysts leading to heterogeneous polymers with broad molar mass distribution (MWD) and broad chemical composition distribution (CCD). Conversely, metallocene catalysts, as single site catalysts, produce homogenous polyolefins with narrow MWD and CCD. Note that the association of molecular catalysts (metallocene and post-metallocene) has led to advanced multi-site catalysts providing high performance resins via the control of short branching in low and high molar masses fractions.[38]

Some of the analytical methods developed in this work have required the use of ethylene copolymers with narrow MWD and CCD. Metallocene catalysts were therefore logically used to produce well-defined polymers that were used as standards.

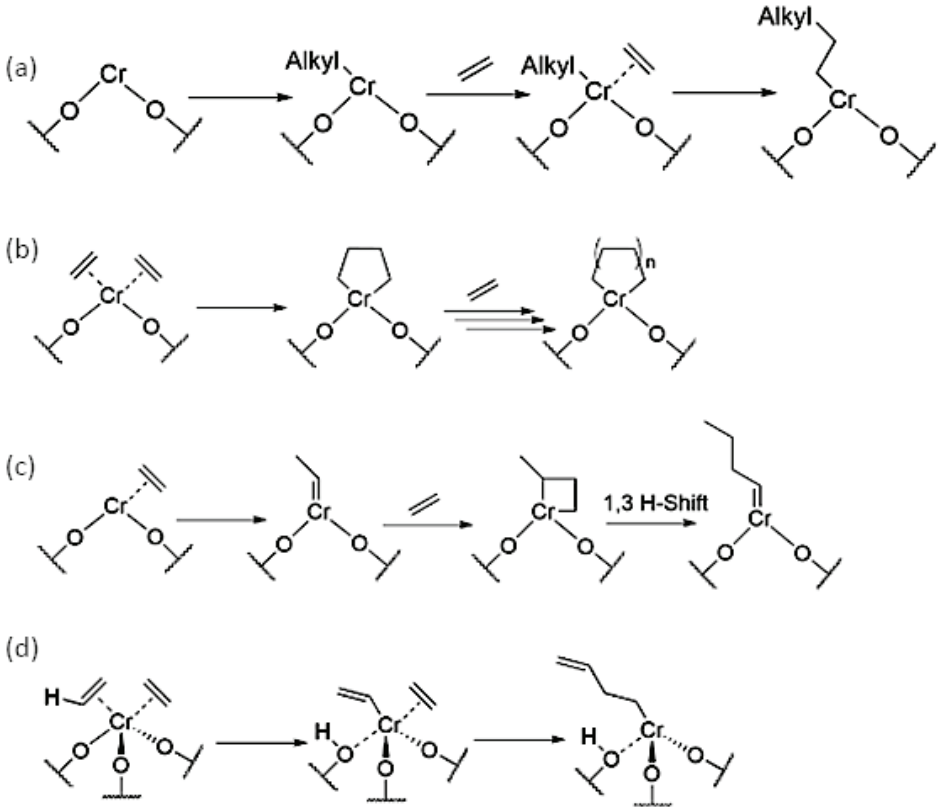
1.4.1 PHILLIPS CATALYSTS

Phillips catalysts were the first catalysts to be industrialized, in the 1950s, to produce HDPE. At present, Phillips Petroleum utilizes a highly active catalyst, chromium oxide on a high-surface area silica, to produce high-density polyethylene. It gives a highly linear and very crystalline polymer, but the presence of LCB characterizes this class of HDPE.[39]

Phillips catalysts lie on a hexavalent chromium supported on a silica surface. To make the catalysts, the silica gel carrier is impregnated with a chromic (III) acetate compound followed by calcination to “activate” the catalyst. During this activation, chromium (III) oxidizes to Cr(VI) on the silica surface. Chromate species including monochromate, dichromate and polychromate are formed. Only a fraction of about 1 wt% chromium is catalytically active.[4, 40] The chromate species of the Phillips catalysts in contact with the ethylene monomer may be reduced to lower valence states of Cr (II), leading to elevated ethylene polymerization activity without using any co-catalysts. [40]

Although Phillips catalysts are used to produce some 40-50% of the world’s HDPE, the polymerization mechanism is still under investigation, the main question being the structure of the active species.

Various initiation mechanisms have been proposed in the literature including the Cossee mechanism,[41-43] the metallacycle mechanism,[44-46] the carbene mechanism[46-48] and the proton transfer mechanism.[42]



Scheme 1-1: Overview of Cossee (a) metallacycle (b) carbene (c) and proton transfer (d) mechanism for Phillips catalysts.

1.4.2 ZIEGLER-NATTA CATALYSTS

Heterogeneous Ziegler-Natta catalysis is based on a transition metal salt as precursor, such as $TiCl_4$ or VCl_4, supported on silica or magnesium chloride and associated with a co-catalyst. Among the common trialkylaluminums (AlR_3) used as co-catalysts, $AlMe_3$ (TMA), $AlEt_3$ (TEA), $Al(i\text{-}Bu)_3$ (TIBA) are the most popular. The activation process with AlR_3 features several steps including chlorine abstractions, metal alkylation and reduction to Ti (III).

The variation of the atomic arrangements around the titanium impacts the properties of the catalyst and consequently its activity and its selectivity. First generation Ziegler-Natta catalysts for propylene polymerization consist of particulate titanium trichloride crystals. The main advances of this system are the use of a support ($MgCl_2$) and internal donors which improve the activity, the control of molar mass distribution and the particle morphology. [20, 26, 49, 50] Internal donors help to control catalyst selectivity by blocking certain sites. Ziegler-Natta catalytic polymerization follows a coordination-insertion mechanism.

The full polymerization mechanism, which comprises several steps with initiation, propagation and chain termination, was described by Cossee and Arlman.[43, 51-53]

1.4.3 METALLOCENE CATALYSTS

The structure of metallocene catalysts adopts a sandwich-type form, where the transition metal is located between two cyclopentadienyl (Cp) rings (Figure 1-6). A well-studied example of a metallocene catalyst is based on Cp_2ZrCl_2. Since metallocene catalysts are soluble, they can be used as homogeneous and heterogeneous catalysts, where they are carried on inert supports such as silica, alumina and magnesium dichloride.

Commonly used to activate the Ziegler-Natta catalysts, trimethylaluminum was logically first chosen as an activator for metallocene catalysts but led to low activity. Kaminsky and Sinn discovered that methylaluminoxane (MAO) efficiently activated metallocene pre-catalysts.[27, 54] The complex structure of MAO is produced by the hydrolysis of trimethyl-aluminum.[55-57] Many structural models have been proposed (Figure 1-9).

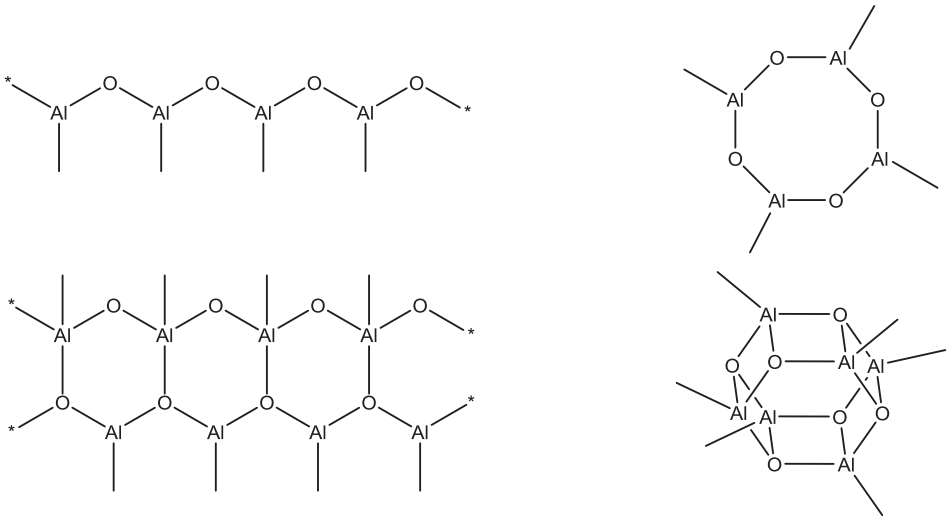


Figure 1-9: Schematic structures of methyaluminoxane

With the modification of the ligands attached to the metal, it is possible to modulate the polymerization behavior of catalysts. After activation with MAO, an active cationic species is formed. The general representation of a cationic metallocene catalyst is shown in Figure 1-10. It is composed of a group 4 metal supported by two cyclopentadienyl rings (Cp) via $\sigma\pi$ bonds. The metal is also linked to an alkyl ligand, methyl, when MAO is used as an activator.

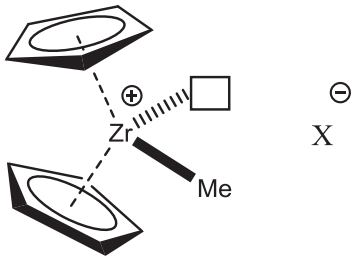
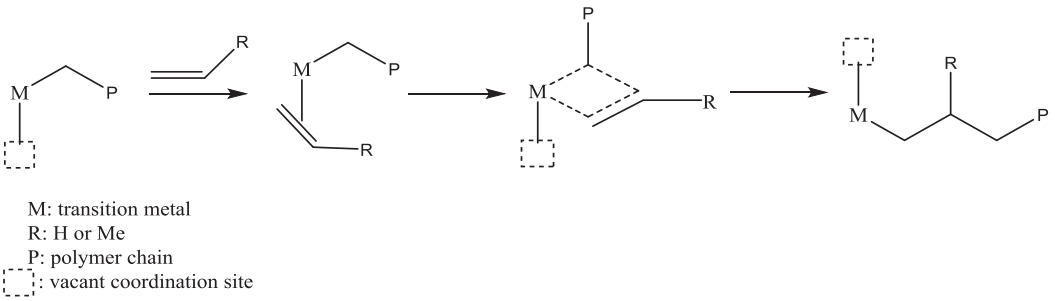


Figure 1-10: Generalized structure of a metallocene catalyst with M = Ti^{IV}, Zr^{IV}, Hf^{IV} and X = MAO-Me or $B(C_6F_5)_4$.

Many factors can be changed to adapt the catalytic behavior of metallocene catalysts such as the nature of transition metal, the co-catalyst/catalyst ratio, the substituent on the cyclopentadienyl rings and the polymerization conditions. These factors regulate the catalyst's activity, the comonomer response, the regioselectivity and the stereospecificity of olefin insertion.[58] The symmetry forced by the ligands around the active site determines the coordination and insertion of the monomers and, consequently, the orientation of the growing polymer chain.

The polymerization mechanism with metallocene catalysts is similar to the Ziegler-Natta mechanism.[59, 60] The first step of the polymerization mechanism is the formation of an active site. It is created by the reaction of a pre-catalyst and the co-catalyst. The co-catalyst alkylates the pre-catalysts and extracts one ligand (halogen or methyl) to form a cationic active site and a non-coordinating anion. As a Lewis acid, the cocatalyst also serves to protect active species by trapping impurities (water traces, oxygen, CO_2, mercaptans, etc.) which poison the reaction.

Polymerization occurs via a coordination-insertion mechanism. The active species has both a metal-carbon bond and a coordination site for the monomer in cis position. Polymerization takes place in two steps. The first corresponds to the coordination of the olefin, and the second step consists of the insertion of the olefin into the metal-carbon bond, releasing a coordination site capable of accepting a new olefin. Transfer reactions are key elements of the catalytic mechanism because they make it possible to form a large number of chains per metal center. Among these transfer reactions, the β-H elimination reaction is the main transfer reaction, leading to vinyl terminated polymer chains.



Scheme 1-2: Simplified mechanism of the catalytic polymerization of olefins.

Advances in olefin polymerization have been achieved due to the unique active sites available on metallocene catalysts, unlike traditional Ziegler Natta catalysts. Indeed, these single site catalysts can have better control over key polyolefin parameters such as molar mass distribution, comonomer distribution, amount of long chain branching, and stereospecificity. The reason for the great versatility of polyolefins is that these microstructure parameters have a significant impact on their properties. The structure-property relationship is one of the most important issues in polymer science. Consequently, detailed and accurate measurement of the microstructure of polyolefins is of crucial importance. The following section presents the techniques for measuring the main characteristics of polyolefins: the crystallinity by DSC, the molar mass distribution by size exclusion chromatography, and the chemical composition distribution by fractionation techniques.

1.5 PROPERTIES OF POLYOLEFINS

The properties of polyolefins are defined by several important factors. New tools in chemistry with the control of catalyst behavior, and in chemical reaction engineering, can tailor the properties of polyolefins such as:

- Molar mass distribution,
- Chemical composition distribution with short chain branching or comonomer content,
- Long chain branching,
- Stereo and regioregularity.

To efficiently control the microstructure, and then the properties of polyolefins, a wide variety of dedicated techniques can be used:

- Molar mass distribution and average molar masses:
  - High temperature size exclusion chromatography (HT-SEC),
  - High temperature asymmetrical flow field-flow fractionation (AF4).
- Average chemical composition (comonomer content):
  - ^{13}C and ^{1}H nuclear magnetic resonance (NMR),
  - Fourier transform infrared spectroscopy (FTIR),
  - Differential scanning calorimetry (DSC).
- Chemical composition distribution:
  - Temperature rising elution fractionation (TREF),
  - Crystallization analysis fractionation (CRYSTAF),
  - Crystallization elution fractionation (CEF),
  - High temperature thermal gradient interaction chromatography (TGIC),
  - High temperature solvent gradient interaction chromatography (SGIC).
- Long chain branching[1]:
  - HT-SEC with viscometer or light scattering detector,
  - NMR (for branching with more than 6 carbon atoms),
  - Rheology.

[1] *The branching is classified as LCB when the length of the branches is longer than a few hundred carbon atoms, corresponding to 2 or 3 times the entanglement molar mass.*[61-64]

In this work, all these techniques (except AF4) were employed and contributed to the development of new characterization methods. They were established in our laboratory to be used as routine techniques and to help research subjects in chemistry and processes of polymerization.

1.5.1 STRUCTURE OF POLYETHYLENE

The structure of polyethylene can be described on different levels, starting from the macromolecule chain to the macroscopic material. Five levels can be observed:

- (I) the macromolecular structure resulting directly from the polymer synthesis reactions,
- (II) the conformational structure, i.e. the spatial arrangement of the macromolecular chain,
- (III) the level of the amorphous and crystalline phases,
- (IV) the organization between them in the form of spherulites constitutes the microscopic level,
- (V) and finally, the last level represents the macroscopic material.

1.5.1.1 Macromolecular structure (level I)

The macromolecular structure is defined by the polymerization method (single site catalysts, multi-site catalysts, radical polymerization) and can be characterized by different analytical techniques (NMR, HT-SEC, TREF, CRYSTAF, CEF).

1.5.1.2 Conformational structure (level II)

The macromolecular chain is characterized by a local conformation which corresponds to the relative orientation of the lateral groups of the chains. The local conformation depends on the local covalent structure and the interactions between atoms. It results from the possibilities of rotation around the covalent bonds as a function of the steric hindrance of the various groups attached to the chain. A second characteristic of macromolecular chains is the overall chain conformation. PE macromolecular chains can adopt two global conformations: linear or random coil (Figure 1-11).

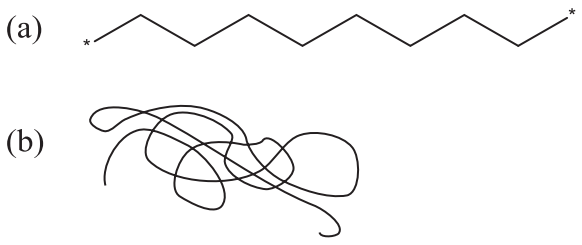


Figure 1-11: Global chain conformation of polyethylene; linear conformation (a), random coil conformation (b)

The random coil arrangement of the macromolecular chain concerns the amorphous phase of the polymer. The tangled structure of polyethylene plays an important role in the mechanical behavior of the polymer by giving it viscoelastic properties. The linear organization of chains is related to the crystalline phase of the polyethylene.

1.5.1.3 Crystalline structure (level III)

The crystalline structure of polyethylene is formed by the periodic assembly of chains having a regular conformation, linked together by Van Der Walls bonds (Figure 1-12).

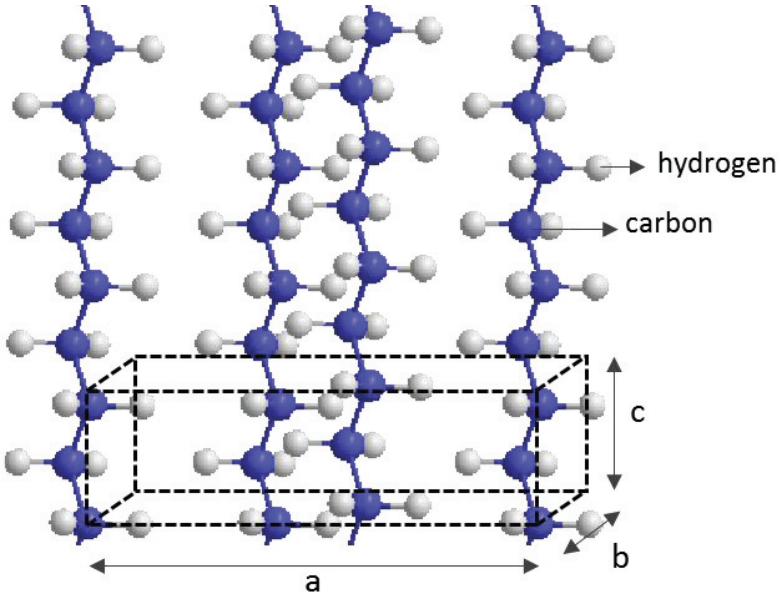


Figure 1-12: Schematic representation of the crystal structure of polyethylene.

The most stable configuration is the orthorhombic phase whose parameters, determined by Bunn[65], are: a = 0.740 nm, b = 0.493 nm, c = 0.253 nm, c axis corresponds to the orientation of the macromolecular chains. Later, the crystalline structures were also determined by X-ray scattering[66, 67] and neutron scattering for deuterated PE.[68, 69]

The stability of the PE is ensured by the inter-macromolecular Van der Waals force between the chains, which is weaker in energy than the intra-molecular covalent bonds between the atoms constituting the chain (Table 1-3).

Table 1-3: Energy and distance of covalent bonds and Van der Waals interactions in PE.

	Covalent bonds		**Van der Walls interactions**		
	C-C	C-H	C…C	C…H	H…H
Energy (KJ mol^{-1})	19.8	23.7	0.1-0.5	0.7-1.2	0.1-0.5
Distance (nm)	0.154	0.109	0.34-0.85	0.29-0.70	0.23-0.60

1.5.1.4 Spherulite (level IV)

In the molten state the polyethylene chains are randomly aligned and entangled. If they are cooled quickly, the chains remain frozen and the resulting polymer structure is disordered. Nevertheless, if the crystallization is slow enough, the polymer chains tend to take an orderly configuration in crystalline lamella. The growth of the polyethylene crystal occurs radially in all directions, resulting in a spherical arrangement called spherulites (Figure 1-13). They are organized in a succession of structured crystalline lamellae interrupted by amorphous regions. These semi-crystalline arrangements have sizes that vary from a few micrometers to several millimeters [70-72] depending on the number of nucleation sites. Larger spherulites are obtained in the case of a few nucleation sites.

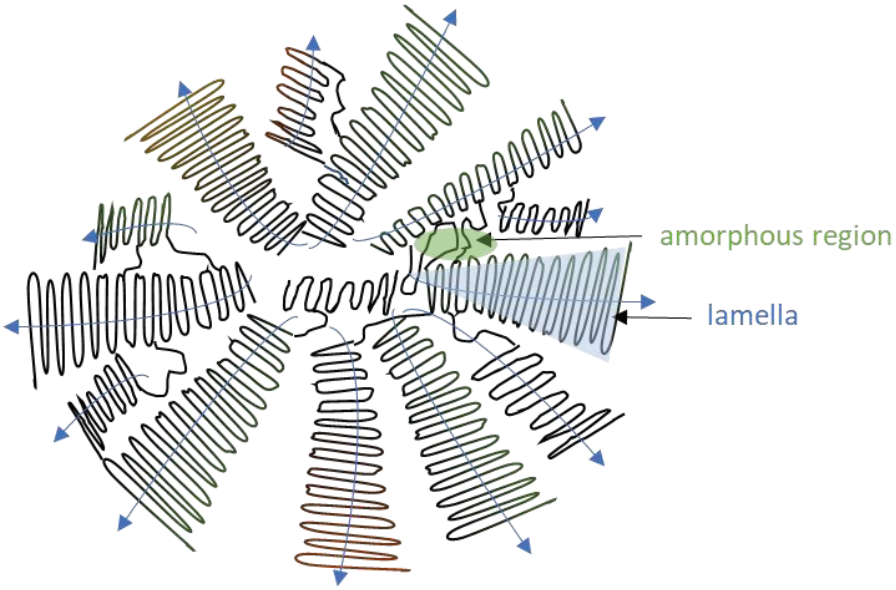


Figure 1-13: Spherulite structure showing the molecular level of the chain arrangements and the alignment of polymer chains.

1.5.2 CRYSTALLINITY

Depending on their entanglement, the polyolefin chains exist in two states: amorphous or semi-crystalline. If they are not organized, the polymer is amorphous. To be organized and form crystals, the chains should have a regular structure which allows their stacking, as shown in Figure 1-14.

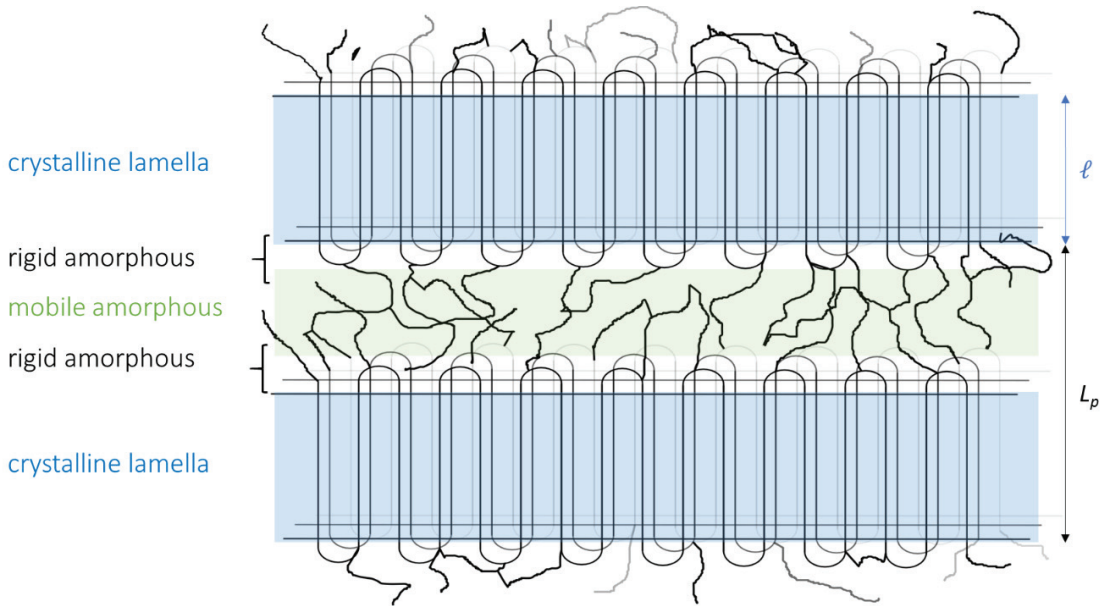


Figure 1-14: The semi-crystalline microstructure of PE containing crystalline and amorphous regions. Inside the crystalline lamellae, the polymer chains are parallel to each other and perpendicular to the amorphous regions. Amorphous and crystalline regions are intimately linked. ℓ is the lamella thickness (5-10 nm); L_P is the long period of the crystalline structure.

The crystalline phase is characterized by the melting temperature (Tm), the crystallization temperature (Tc) and the enthalpies associated with these phenomena. These parameters, linked to the ability of the polymer to crystallize, are usually determined by the following techniques:

- Differential scanning calorimetry (DSC)

Differential scanning calorimetry (DSC) is a thermal analysis technique that measures the differences in heat exchange between an analyzed sample and a reference. It is used to determine phase transitions: the glass transition temperature (T_g) of amorphous phases, the melting and crystallization temperatures and, the enthalpies of reaction, melting and crystallization.

Heat exchanges between the polymer and the equipment can be endothermic or exothermic depending on the transition event. Thus, for example, a melting absorbs heat in order to be able to increase its

temperature at the same rate as the reference. The melting is, therefore, an endothermic phase transition because it absorbs heat. Conversely, the sample can undergo exothermic events, such as crystallization, when it releases heat to the system.

The heat energy required during the melting of a semi-crystalline PE is the melting enthalpy. It can be quantified (Figure 1-15) and compared to that required by 100% crystalline PE with a known melting enthalpy value. An enthalpy of 293 J g^{-1} for a 100% crystalline material is commonly used.[73, 74] This analytical technique was widely used in this work.

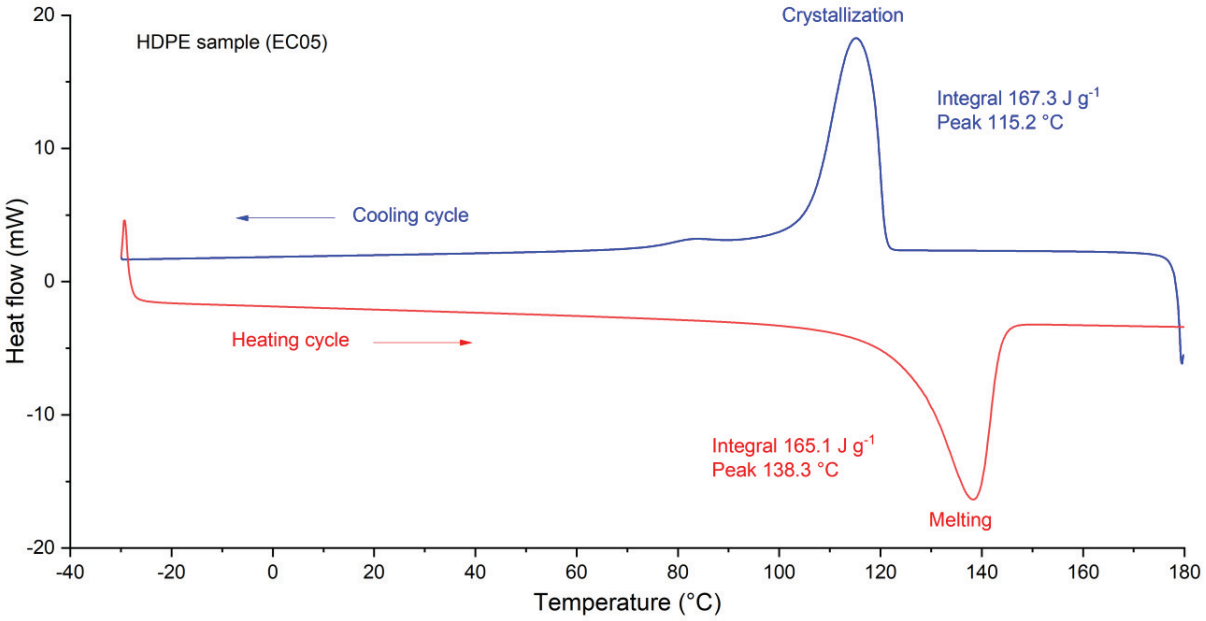


Figure 1-15: DSC thermogram of an HDPE with the second heating cycle (red) and the cooling cycle (blue).

The dependence of the melting temperature on crystallite thickness (ℓ) can be expressed by the Gibbs-Thomson equation:

$$T_m = T_m^0 \left(1 - \frac{2\sigma_e}{\Delta H_u \times \ell}\right) \qquad (1\text{-}1)$$

where T_m is the melting temperature, T_m^0 is the equilibrium melting temperature of the infinitely thick crystal, σ_e is the interfacial free energy, ΔH_u is the melting enthalpy per repeating unit, and ℓ is the crystallite thickness (Figure 1-14).

This relation can be applied directly to DSC measurement to calculate the lamellae thickness. However, this value can be also obtained by direct experimental measurement.

- X-ray scattering

Small angle X-ray scattering (SAXS) revealed the stacking of crystallites. This regular arrangement of chains produces narrow diffraction peaks while the amorphous regions produce broad halos. The lamellae thickness and the degree of crystallinity can be measured by integrating the relative intensities of the peaks and halos. [75-79]

- Infrared (IR) and Raman spectroscopy

The infrared absorption spectra of crystalline polymers exhibit characteristic peaks which are missing in amorphous polymers. The degree of crystallinity can be estimated from the analysis of these bands. [80] As an alternative, Raman spectroscopy using vibrational bands in the wavenumber region 900-1500 cm^{-1} can provide a reliable calculation of crystallinity.[81, 82]

- Nuclear magnetic resonance (NMR)

The mobility of protons differs in the crystalline and amorphous regions of polyethylene. Solid state ^{1}H NMR spectroscopy is affected by the different mobilities of atoms. The spectrum of a semi crystalline PE shows the overlap of a narrow peak and a broad peak. The mobile protons of the amorphous phase contribute to the narrow peaks, whereas the protons blocked in the crystalline phase contribute to the broadening of the peaks. The degree of crystallinity, related to the number of protons in each region, is obtained by the deconvolution of the spectrum.[83, 84]

Solid-state ^{13}C NMR signals can also be studied to estimate the degree of crystallinity. The nuclei of the same atoms in the amorphous and crystalline parts do not encounter exactly the same magnetic field, resulting in different signals in the ^{13}C NMR spectrum. The degree of crystallinity of PP samples, estimated by the deconvolution of CH_3 signals, has been reported in previous works.[85-88]

The degree of crystallinity depends slightly on the molar mass (mostly for low molar masses) and especially on the chemical composition of the polymer. These are, therefore, two essential parameters for the characterization of materials which are determined respectively by size exclusion chromatography and thermal fractionation techniques. These techniques will be described in the next sections.

1.5.3 MOLAR MASSES

Chain length is expressed in terms of molar masses, corresponding to the molar mass of the monomers and the number of monomer units inside the chain. The molar masses of polymers dictate numerous properties such as thermal behavior, chemical resistance, viscosity, tensile strength, toughness, impact resistance, etc. Higher molar masses are associated with higher physical properties, while lower molar masses are associated with lower properties.[89] Excessively low molar masses are not appropiate for industrial applications that require that products preserve their shape.

A polymer is a statistical set of macromolecular chains of different lengths and therefore of different molar masses. We often need to describe the shape of a distribution using only a few numbers. For this reason, polymer molar masses are described as averages calculated from the molar masses of all the chains.

The commonly used average molar masses,[90] classically determined by size exclusion chromatography, are described below.

1.5.3.1 Number average molar mass: $\bar{M}_n$

The number average molar mass is the statistical molar mass average of all the polymer chains in the sample. It is based on the number of polymer chains in a sample. This is the first moment of the distribution and is defined by:

$$\bar{M}_n = \frac{\sum N_i . M_i}{\sum N_i} \quad \text{or} \quad \bar{M}_n = \sum x_i . M_i \qquad (1\text{-}2)$$

where M_i is the molar mass of a chain (g mol^{-1}), N_i is the number of chains having a molar mass of M_i, and x_i is the mole fraction of chains having a molar mass of M_i.

$\bar{M}_n$ can be measured by methods that determine the number of molecules in a sample of a given weight; for example, colligative methods such as the end-group assay.

1.5.3.2 Weight average molar mass: $\bar{M}_w$

The weight average molar mass is calculated from the weight fraction distribution of different sized molecules (Equation 1-3). This is the second moment of the distribution.

$$\bar{M}_w = \frac{\sum N_i . M_i^2}{\sum N_i . M_i} \quad \text{or} \quad \bar{M}_w = \sum w_i . M_i \qquad (1\text{-}3)$$

where M_i is the molar mass of a chain (g mol^{-1}), N_i is the number of chains having a molar mass of M_i and w_i is the weight fraction of chains having a molar mass of M_i.

$\bar{M}_w$ considers the molar mass of a chain in determining contributions to the molar mass average. The larger the chain, the more the chain contributes to $\bar{M}_w$. $\bar{M}_w$ is changed to higher values and is always greater than $\bar{M}_n$. $\bar{M}_w$ can be determined by techniques that are sensitive to the molar size, such as light scattering techniques. There is an equivalent weight proportion of macromolecules on each side of $\bar{M}_w$ in the molar mass distribution.

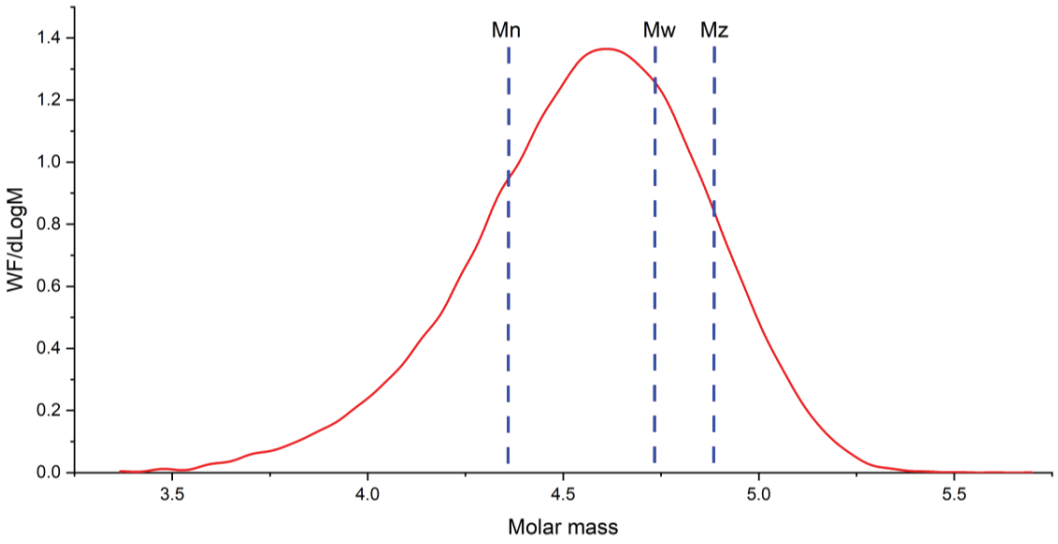


Figure 1-16: Molar mass distribution and position of the average molar masses.

1.5.3.3 Higher average molar masses: $\bar{M}_z$, $\bar{M}_{z+1}$

As a general formula, different average molar masses can be calculated using the nth moment of the distribution defined as follows.

$$\bar{M} = \frac{\sum N_i . M_i^{n+1}}{\sum N_i . M_i^n} \qquad (1\text{-}4)$$

where:

- n = 1 gives $\bar{M}_w$
- n = 2 gives $\bar{M}_z$
- n = 3 gives $\bar{M}_{z+1}$

The higher averages are increasingly sensitive to high molar masses and therefore are more difficult to measure with precision. They are associated with methods that measure the motion of polymer chains, such as diffusion.

As shown in Figure 1-16, for all polymers, the average molar mass always ranks in the following order: $\bar{M}_n < \bar{M}_w < \bar{M}_z < \bar{M}_{z+1}$.

1.5.3.4 Viscosity average molar mass

Molar mass can also be calculated from the viscosity of a polymer in a solution. Viscosity is the measure of resistance to flow. Long polymer chains have difficulty in flowing due to friction and entanglement between the chains presenting higher viscosity. In the viscosity average molar mass measurement method, the flow of the polymer solution through a capillary is measured. This method is also known as intrinsic viscosity analyzer (IVA).

First, Staudinger and then Flory assumed the [η] to be proportional to the polymer molar mass. [91, 92] Later, Mark,[93] Houwink[94] and Sakurada[95] correlated the intrinsic viscosity with molar mass using the Mark-Houwink-Sakurada Equation 1-5:

$$[\eta] = K.M^{\alpha} \qquad (1\text{-}5)$$

where K and α (0.5 – 1) are constants varying with the polymer, solvent, and temperature.

The value of α gives information about the conformation of the polymer in the solvent. It is equal to 0 for spherical conformation, 0.5 for statistical coil conformation, 0.8 for chains in good solvent and up to 1 for rigid rod conformation. These constants must be determined experimentally by plotting the logarithm of the intrinsic viscosity as a function of the logarithmic molar mass (Figure 1-17) and fitting the best straight line to the following Equation 1-6:

$$\log [\eta] = \log K + \alpha.\log M \qquad (1\text{-}6)$$

The intersection with the y-axis of a linear fit of data gives the constant log K, the slope of the curve gives the constant α. These parameters, relating viscosity to molar mass, can be found in the literature for polyethylene in commonly used solvents.[96, 97] For PE in 1,2,4 TCB at 135°C, the value of α is around 0.7.

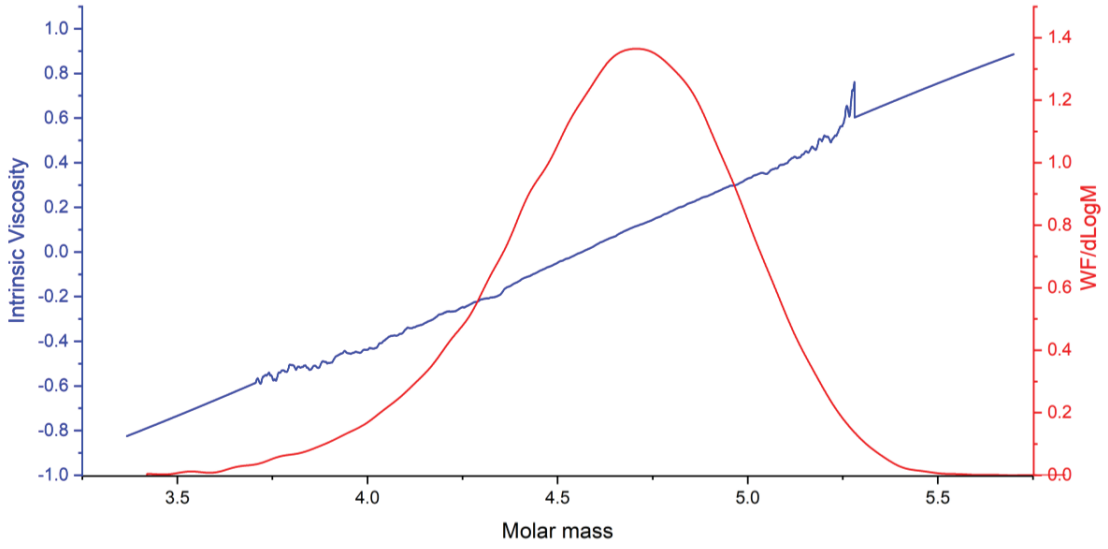


Figure 1-17: Molar mass distribution (red) and Mark Houwink plot (blue) of a broad polyethylene sample. The slope of the linear fitting of the Mark Houwink curve gives α (0.669) and the intercept gives log K (-3.362).

The viscosity average molar mass $\bar{M}_v$, which is not measured by SEC but by a viscometer analyzer (IVA) is calculated as:

$$\bar{M}\mathrm{v} = \left[\frac{\sum N_i . M_i^{1+\alpha}}{\sum N_i . M_i}\right]^{1/\alpha} \qquad (1\text{-}7)$$

Where M_i is the molar mass of a chain, N_i is the number of chains having a molar mass of M_i, α is the Mark Houwink value.

1.5.3.5 Dispersity

The dispersity is a representation of the broadness of a molar mass distribution of a polymer and is defined by Equation 1-8:

$$Đ = \bar{M}_w / \bar{M}_n \qquad (1\text{-}8)$$

The larger the dispersity, the broader the molar mass distribution. A narrow polymer where all the chain lengths are equal (such as a protein) has a Đ = 1. The best controlled synthetic polymers have a Đ of 1.02 to 1.10. Ziegler-Natta and Phillips catalysts typically yield polymer with a high Đ, whereas metallocene catalysts yield Đ values of 2.0, in theory (Table 1-4).

High temperature size exclusion chromatography (HT-SEC) is used to measure the average molar masses of polyolefins requiring high analysis temperatures. It is because of their high crystallinity that polyolefins

display limited solubility at room temperature and must therefore be dissolved at high temperature in particular solvents, such as toluene, xylene, *ortho*-dichlorobenzene and 1,2,4-trichlorobenzene.[98]

Table 1-4: Dispersity obtained with different polymerization reactions.

Polymerization	**Dispersity**
Anionic polymerization	1.02 – 1.5
Cationic polymerization	Broad
Chain polymerization	1.5 – 3.0
Step polymerization	2.0 – 4.0
Ziegler-Natta	2 - 40
Metallocene	2.0 – 3.0
Natural proteins	*1.0*

Average molar masses and molar mass distribution are, therefore, relevant parameters to be measured to characterize polymers. The most widely recognized technique to determine the MWD of polyolefins is high temperature size exclusion chromatography (HT-SEC). [99, 100] *However, many LLDPEs are produced with the incorporation of comonomers to extend and tune PE performances. Therefore, it is also necessary to measure the so-called chemical composition, which depends on comonomers content, to characterize these materials.*

1.5.4 CHEMICAL COMPOSITION

For LLDPE, the average chemical composition and its distribution (CCD)[101] are important parameters because they strongly impact the properties of LLDPE. The chemical composition corresponds to the comonomer or to the short chain branching (SCB) content in LLDPE chains. The increase in comonomer content will therefore decrease the crystallinity by breaking the regularity of the chains.

The heterogeneity of this distribution is due to the behavior of the multi-site catalysts, where each site gives a chain with different microstructures, and possibly to variations in the monomer concentration and the temperature during polymerization. To completely define the structure of a copolymer, it is therefore necessary to have access to the distribution in chemical composition in addition to the average.

Various techniques, which will be discussed in the following part, are available for measuring the CCD of polyolefins. These are separative techniques that allow, in the same way as SEC, to determine a distribution.

1.5.4.1 Crystallization based techniques

Most polyolefins are semi-crystalline, and their melting temperatures can reach up to 165 °C for *i*PP. The crystallization temperature mainly depends on the structure of the polymer with the comonomer content, and the degree of branching for PE (chemical composition) and tacticity for the PP. The polymer chains, with low crystallinities will crystallize out of the solution at a temperature lower than those with a higher crystallinity. Flory developed the crystallization theory of polymers[102] that was used to propose the principles of polymer fractionation in solution. Monrabal[103] summarized it in Equation 1-9.

$$T_m = T_m^0 - \frac{R(T_m^0)^2}{\Delta H_u} N_2 \qquad (1\text{-}9)$$

where T_m^0 is the melting temperature of the pure polymer, T_m is the melting temperature of the copolymer in the solvent, R is the gas constant (8.314 J mol^{-1} K^{-1}), ΔH_u is the melting heat per polymer repeating unit, and N_2 is the amount of comonomer incorporated.

This equation, which assumes that ΔH_u is constant over the whole range of crystallization temperatures, links the chemical composition of a polymer to its elution temperature. It can be applied for ethylene copolymers. This equation has been the basis for developing thermal fractionation techniques such as temperature rising elution fractionation (TREF), crystallization analysis fractionation (CRYSTAF) and the more recent crystallization elution fractionation (CEF) techniques.

The working principles and advantages of each approach will be discussed in the next sections.

1.5.4.2 Temperature rising elution fractionation TREF

The experimental TREF technique was the first well-established method to fractionate chains according to their crystallizability. The method was initially described by Desreux and Spiegels in 1950[104] and has been applied since the 1990s by Wild[105, 106] for polyolefins. The fractionation by TREF involves three main steps (Figure 1-18).

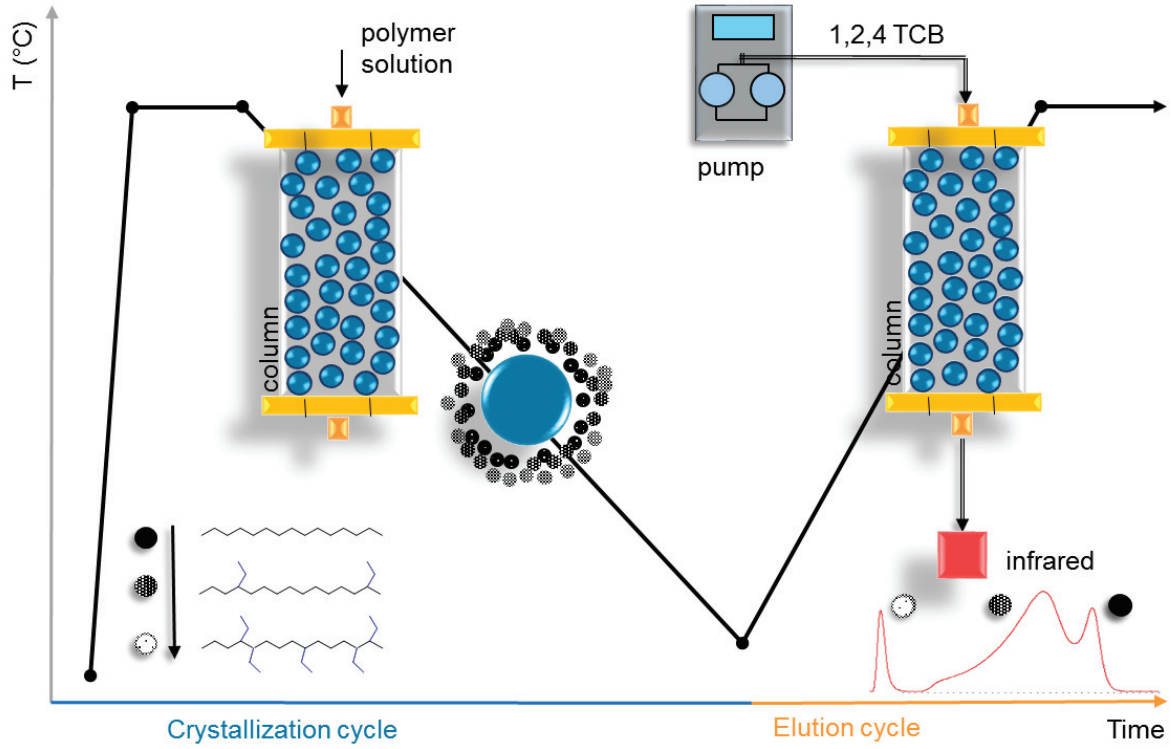


Figure 1-18: Schematic representation of a TREF experiment with two separation cycles. The column connected to a pump and to the IR detector is filled with an inert support like glass beads or stainless-steel shot.

First, the sample is dissolved in a suitable solvent (generally TCB or DCB) at high temperature and then introduced into a column. A slow decrease in temperature causes the polymer to crystallize. During this step, the polymer is deposited in a less and less crystalline layer on a solid support constituting the stationary phase of the column. Although the polymer is separated into layers of different crystalline structures at the end of this step, TREF requires a second temperature cycle. During this step, the polymer fractions with different crystallizabilities are dissolved by increasing the temperature. As the temperature increases, the solvent elutes the different fractions in increasing order of crystallinity. Soares and Hamielec

reported that the crystallization step has a strong influence on the separation, and that the decrease in the cooling rate results in better resolution.[107]

Elution is monitored by an infrared detector which generates the distribution curve of the chemical compositions. This detector has little dependence on temperature fluctuations and good sensitivity to the C-H bonds widely present in polyolefins. Absorbance is measured at 3.5 µm which correspond to the symmetrical elongation frequency of the C-H bonds. An additional viscometer detector which is molar mass sensitive can be added in the system.

TREF was used to analyze the composition of various polyolefins such as copolymers of ethylene[108, 109] and propylene,[110-112] polyolefin blends[113, 114] and separate isotactic polypropylenes according to their tacticity.[111, 115] More details on the analytical conditions are described in the various reviews published on TREF by Wild,[116] Fonseca, Harrison, Soares and Hamielec[117] and Monrabal.[118]

1.5.4.3 Crystallization analysis fractionation (CRYSTAF)

As TREF is time-consuming, a more recent technical approach was developed by Monrabal in 1991.[119, 120] Crystallization analysis fractionation (CRYSTAF) analyzes the distribution of short chain branching only during the crystallization step, which is performed in a similar way to TREF.

The CRYSTAF analysis is based on the continuous crystallization of polymer chains in dilute solution. When the temperature decreases, the chains progressively crystallize. First, the most crystalline chains precipitate at high temperatures and are followed by the chains of lower crystallinity. At a given temperature interval, an aliquot of the polymer solution is collected and filtered, and its concentration is determined by an IR detector. In CRYSTAF, the analysis is carried out in stirred crystallization vessels without support. When the temperature decreases, the most crystalline fractions (linear chains) precipitate first, resulting in a decrease in the concentration of the polymer solution. This step is followed by the precipitation of increasingly branching fractions (or less crystalline chains) as the temperature decreases (Figure 1-19). At the lowest temperature, there remains in solution the amorphous fraction corresponding to highly branched chains that have not crystallized.

The IR detector measures the concentration of the solution at each step of sampling. A curve (orange curve in Figure 1-19a) is obtained, representing the concentration of the polymer remaining in solution as a function of the temperature. The first derivative (blue curve in Figure 1-19a) of this curve represents the variation of the polymer concentration in the solution as a function of the temperature.

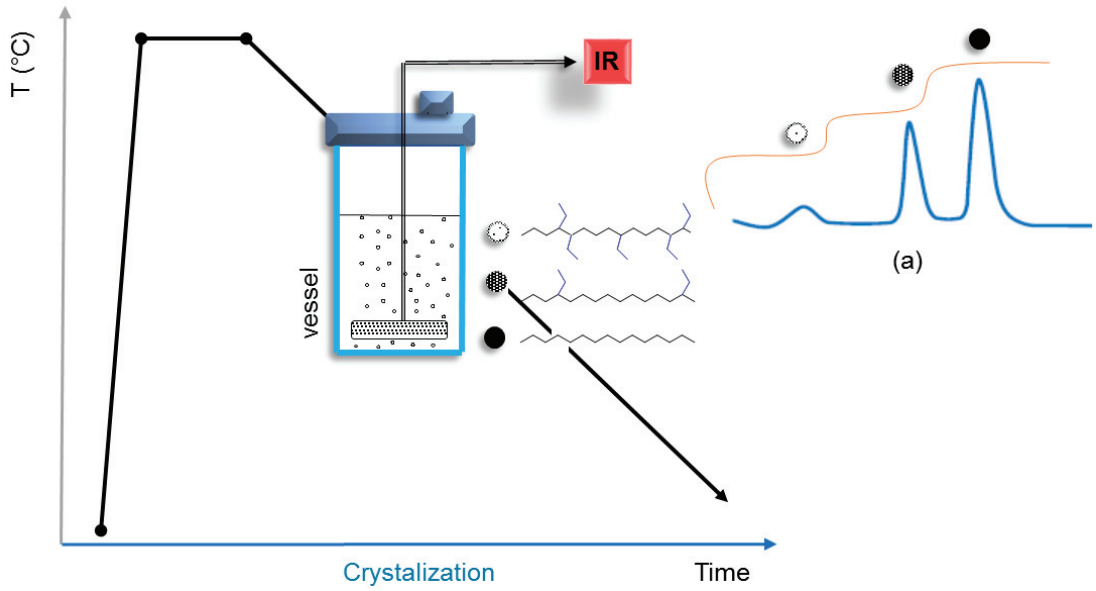


Figure 1-19: Schematic representation of a CRYSTAF experiment. The device is similar to that of TREF without the need for a column. Cumulative curve (orange) and CCD curve (blue) (a).

Characterizations of ethylene[121-123] and propylene[124, 125] copolymers were described by various teams. Furthermore, Sarzotti et al reported the molar mass effect on CRYSTAF separation above 10,000 g mol^{-1}.[126] CRYSTAF is an indisputably fast technique for separating samples, however it presents a poor resolution compared to TREF.

1.5.4.4 Crystallization elution fractionation (CEF)

In 2007, Monrabal et al developed a new experimental technique based on a similar separation principle and offering considerable time savings: crystallization elution fractionation (CEF).[127, 128]

CEF (Figure 1-20) was developed by combining the separation power obtained in the crystallization cycle (equivalent to CRYSTAF), with that obtained in the elution melting cycle (equivalent to TREF). The dynamic mode used during the crystallization stage requires a longer column than TREF but allows rapid separation and better resolution than TREF and CRYSTAF. Despite this improvement, various problems are still present:

- Co-crystallization has further complexified the separation of various families with poor precision and accuracy.

- Polyolefins with a comonomer content greater than about 8 mol % are unable to crystallize. This limit can be increased using cryogenic options, but the high freezing temperature of the solvent is a constraint.

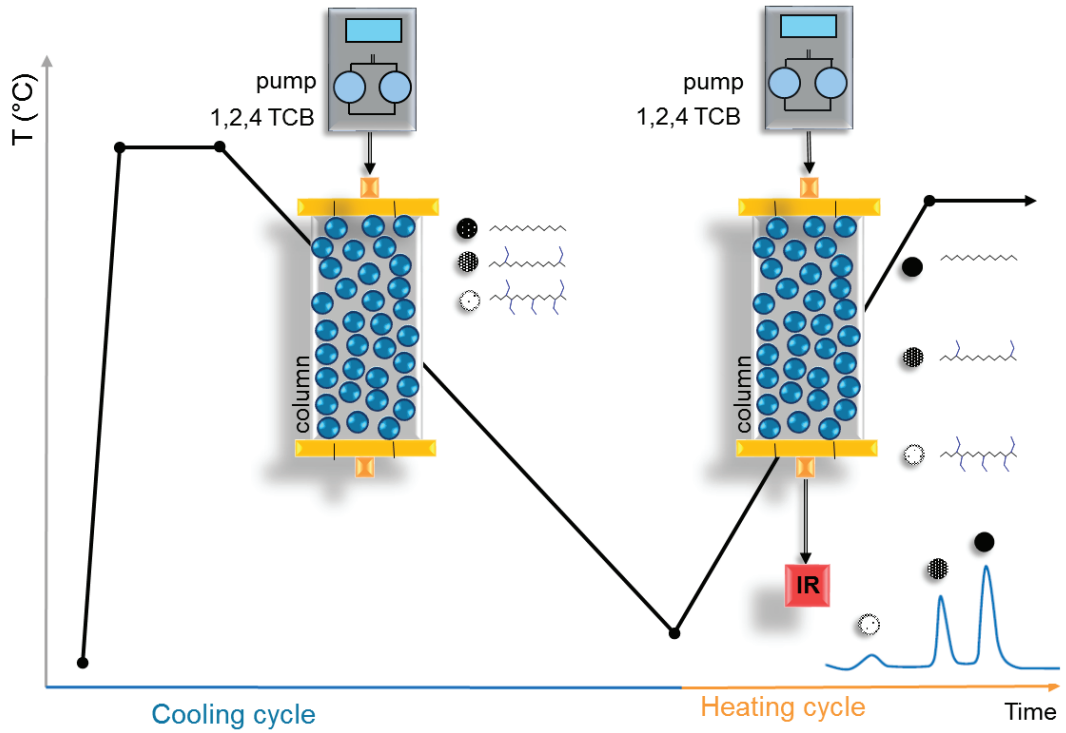


Figure 1-20: Schematic representation of a CEF experiment; the device is similar to that of TREF.

Two new techniques, well described by Monrabal,[129] have been developed to improve chemical composition measurement: Solvent Gradient Interaction Chromatography and Thermal Gradient Interaction Chromatography (SGIC and TGIC). With these techniques, the negative effect of co-crystallization is reduced, and amorphous polymers can finally be analyzed. These techniques combine both separation by crystallization as in previously described techniques and separation by adsorption on the stationary phase of the column.

1.5.4.5 Solvent gradient interactive chromatography, SGIC

High performance liquid chromatography is a well-known technique used to separate polymer chains according to their composition. For a long time it was limited to ambient temperature with liquid adsorption chromatography (LAC). The interaction mechanisms involved in LAC have been widely studied.[130, 131] In 2003, Macko et al reported for the first time the use of high temperature HPLC to separate polyolefins with a silica-based column.[132-135] Later, Macko and Pasch showed that polyolefins can be adsorbed and separated in a Hypercarb porous graphitic carbon column using a solvent gradient from decanol to TCB.[136-140] The use of the Hypercarb column was a major discovery in polyolefin characterization. Following this, a large variety of ethylene-α-olefin copolymers were separated using this approach known as solvent gradient interaction chromatography (SGIC).[141-146]

SGIC (Figure 1-21) can be used to separate for the first-time amorphous polyolefins with high α-olefin content. Due to the variation of the solvent composition during analysis, most common detectors cannot be employed. Classically, the evaporative light scattering detector (ELSD) , insensitive to the solvent gradient, is used even if the detector's output is nonlinear with concentration. A technical approach using a temperature gradient instead of a solvent gradient has recently enabled the use of conventional detectors for polyolefin characterization.

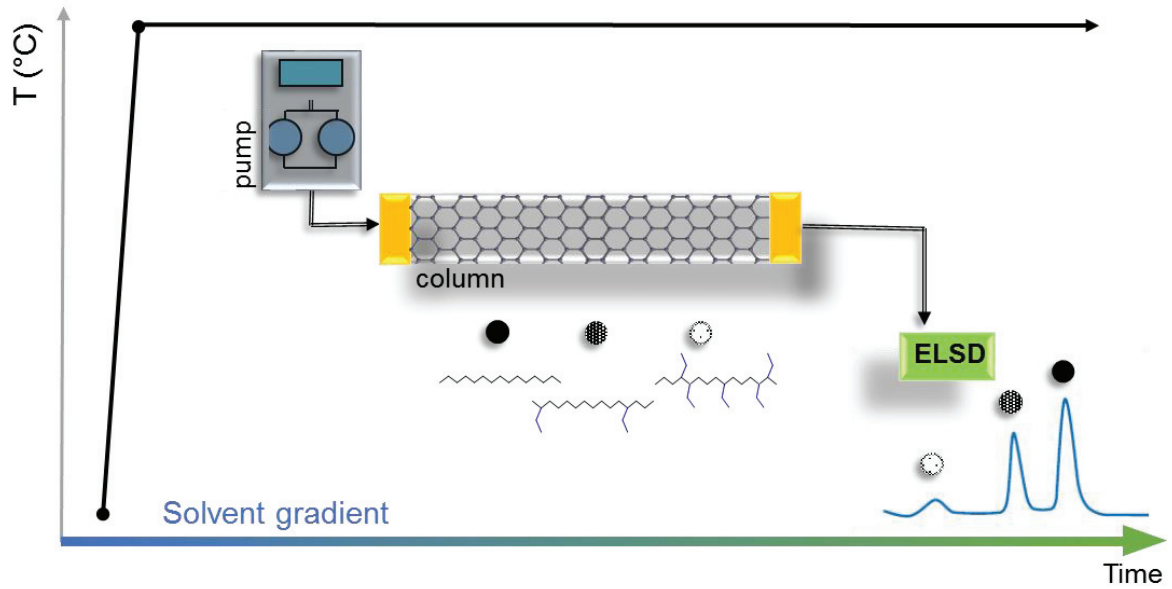


Figure 1-21: Schematic representation of an SGIC experiment.

1.5.4.6 Temperature gradient interaction chromatography (TGIC)

A temperature gradient interaction chromatography (TGIC) instrument, based on an adsorption-desorption mechanism under a temperature gradient, has recently been developed by Cong et al. [147]

The TGIC instrument (Figure 1-22) consists of an isocratic pump, an autosampler, an adjustable temperature oven and detectors (IR and viscometer). The experiments are similar to those of CEF, with two analytical cycles. Initially, the polymer solution is injected into the top of the graphite carbon column at high temperature. Then, separation can start with the cooling cycle in which the polymer chains with low α-olefin content are adsorbed first at the higher temperatures. As the column temperature decreases, the chains with higher amounts of α-olefin are adsorbed. Conversely, when the temperature increases, during the second cycle, the chains can be desorbed and eluted from the column according to their chemical composition. An on-line IR detector measures the concentration of polymer eluted from the column. Finally, since the fractionation mechanism is not based on polymer crystallization, three main advantages can be highlighted compared to crystallization techniques: (1) the copolymers are separated over a wider range of composition, (2) the analysis time is reduced by adsorption and desorption processes which are quicker than crystallization, (3) there are no co-crystallization effects.

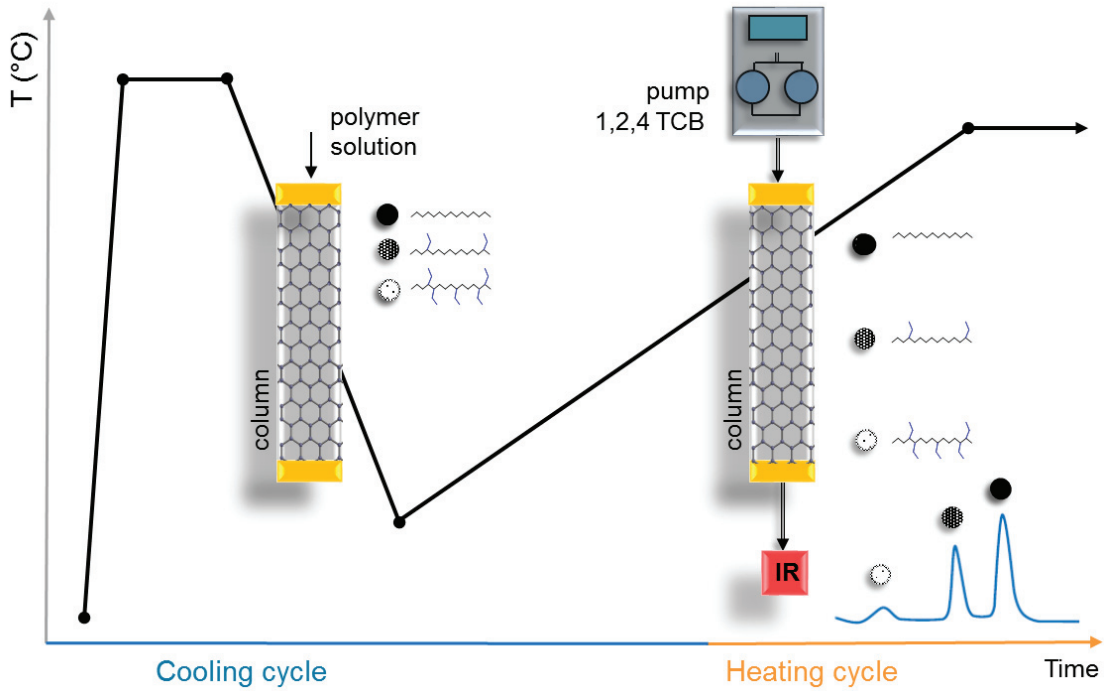


Figure 1-22: Schematic representation of a TGIC experiment. The device is similar to that of CEF with a graphite carbon column instead of an inert support column.

However, TGIC chromatography has lower peak resolution than crystallization-based techniques. This is reflected in calibration curves (elution temperature versus comonomer content) with lower slopes for TGIC. Enhancing its resolution is an active topic of research[148-151] that could further increase the number of its applications. A few publications have discussed the separation mechanism and the effect of analysis conditions. Monrabal et al. proposed that it is the ethylene segments in ethylene-α-olefin copolymers which adsorb strongly on the support, and that the tertiary branched carbons weaken this interaction. Therefore, copolymers with a low α-olefin content have longer ethylene sequences and desorb from the surface at higher temperatures than copolymers with higher α-olefin contents.[152, 153]

Graphitic carbon is the most common support for polyolefin separation. Nevertheless, Monrabal et al. proposed that all supports having atomically flat surfaces can be useful for TGIC fractionation, strengthening the case that copolymers interact with the column via flat ethylene sequences.[152, 153] They showed that adsorption is based on a weak interaction of van der Waals forces between the polyolefin chains and the flat surface. The increase in α-olefin content inhibits this interaction, thus lowering the desorption temperature.

Soares et al. studied the effect of the solvent, the characteristics of the column (particles size, column length) and various analytical conditions on the TGIC chromatograms of individual samples and their blends.[148-150] Neither average particle size (3 and 5 µm) nor column length (10 and 25 cm) played a major role in the fractionation. They showed that o-dichlorobenzene increased elution temperatures and had slightly better resolution than 1,2,4-TCB. Furthermore, they found that smaller injection volumes reduced column loading effects and minimized the co-adsorption/co-desorption effects. Finally, they demonstrated that the heating rate and the elution flow rate strongly impacted separation, while the cooling rate had no significant effect on the TGIC profiles.

Inwong et al. developed a mathematical model for TGIC fractionation based on population balances, assuming a non-equilibrium, multi-stage adsorption-desorption mechanism. Their model fitted the experimental results of individual ethylene-octene samples and their binary blends were measured under several operating conditions adequately.[148]

All these fractionation techniques are limited by the molar masses of the polymers that can be studied. Indeed, several researchers have agreed that molar mass has no impact on separation if it is high enough (> 25,000 g mol^{-1}).[149, 154]

1.6 CONCLUSION

Many innovations concerning polyolefins characterization have been developed over the last twenty years. New original techniques developed by Monrabal, Macko, Brull, Pash, Soares, Cong and their co-workers offer promising developments that lead to better understanding of polyolefin structures. These techniques make it possible for the first time to measure the complete chemical composition of polyolefins and not only their average composition. They are still undergoing development. Co-crystallization effects were studied, as were the effects of heating and cooling rate on separation. These techniques must be calibrated in order to adapt them to our polymer samples. The capacity of our group to provide very well-defined samples using metallocene catalyst and a complete range of characterizations (from size exclusion to NMR) was a unique opportunity to add my modest contribution to polyolefin characterization. Since the installation of the first instrument (CRYSTAF-TREF) in our laboratory, I have been convinced of the potential of these separative techniques to support and enhance our group's research in the fields of polymerization chemistry and process.

The next chapters focus first on LLDPE synthesis to provide a complete set of various comonomer contents and types. The aim of the following part is to demonstrate and propose new tools and methods with various items of equipment to characterize polyolefins structures.

The distributions of molar masses and chemical compositions are a direct consequence of the polymerization conditions: catalyst type, process, and so forth. Therefore, the accurate characterization of molar mass and structure, including short and long chain branching, is of great importance when establishing final composition-property relationships and conducting research on polymerization.

REFERENCES - CHAPTER I

[1] R. Mulhaupt, *Macromol. Chem. Phys.* **2003**, *204*, 289.

[2] W. D. Sauter, M. Taoufik, C. Boisson, *Polymers* **2017**, *9*.

[3] V. Kumar, C. R. Locker, P. J. in 't Veld, G. C. Rutledge, *Macromolecules* **2017**, *50*, 1206.

[4] M. P. McDaniel, *Adv. Catal.* **2010**, *53*, 123.

[5] S. Bensason, J. Minick, A. Moet, S. Chum, A. Hiltner, E. Baer, *Journal of Polymer Science Part B: Polymer Physics* **1996**, *34*, 1301.

[6] J. A. Ewen, R. L. Jones, A. Razavi, J. D. Ferrara, *Journal of the American Chemical Society* **1988**, *110*, 6255.

[7] P. Cossee, *Tetrahedron Letters* **1960**, *1*, 17.

[8] A. Tullo, *Chemical & Engineering News* **2010**, *88*, 10.

[9] G. Cecchin, G. Morini, A. Pelliconi, *Macromolecular Symposia* **2001**, *173*, 195.

[10] F. Ramsteiner, G. Kanig, W. Heckmann, W. Gruber, *Polymer* **1983**, *24*, 365.

[11] J. Karger - Kocsis, A. Kalló, A. Szafner, G. Bodor, Z. Sényei, *Polymer* **1979**, *20*, 37.

[12] A. J. Lovinger, M. L. Williams, *Journal of Applied Polymer Science* **1980**, *25*, 1703.

[13] D. L. Beck, A. A. Hiltz, J. R. Knox, *Polymer Engineering & Science* **1963**, *3*, 279.

[14] J. Z. Liang, R. K. Y. Li, *Journal of Applied Polymer Science* **2000**, *77*, 409.

[15] P. Galli, S. Danesi, T. Simonazzi, *Polymer Engineering & Science* **1984**, *24*, 544.

[16] M. Gahleitner, C. Tranninger, P. Doshev, *Journal of Applied Polymer Science* **2013**, *130*, 3028.

[17] P. Doshev, R. Lach, G. Lohse, A. Heuvelsland, W. Grellmann, H. J. Radusch, *Polymer* **2005**, *46*, 9411.

[18] P. Doshev, G. Lohse, S. Henning, M. Krumova, A. Heuvelsland, G. Michler, H.-J. Radusch, *Journal of Applied Polymer Science* **2006**, *101*, 2825.

[19] K. Ziegler, *Angewandte Chemie International Edition* **1952**, *64*, 323.

[20] K. Ziegler, E. Holzkamp, H. Martin, H. Breil, *Angew. Chem.* **1955**, *67*, 541.

[21] G. Natta, *Journal of Polymer Science* **1955**, *16*, 143.

[22] G. Natta, P. Pino, P. Corradini, F. Danusso, E. Mantica, G. Mazzanti, G. Moraglio, *Journal of the American Chemical Society* **1955**, *77*, 1708.

[23] W. Kaminsky, "*Polyolefins: 50 years after Ziegler and Natta I: Polyethylene and Polypropylene*", Springer Berlin Heidelberg, 2013.

[24] D. S. Breslow, N. R. Newburg, *Journal of the American Chemical Society* **1957**, *79*, 5072.

[25] D. S. Breslow, N. R. Newburg, *Journal of the American Chemical Society* **1959**, *81*, 81.

[26] G. Natta, P. Pino, G. Mazzanti, U. Giannini, *Journal of the American Chemical Society* **1957**, *79*, 2975.

[27] H. Sinn, W. Kaminsky, H.-J. Vollmer, R. Woldt, *Angewandte Chemie International Edition in English* **1980**, *19*, 390.

[28] H. Sinn, W. Kaminsky, "Ziegler-Natta Catalysis", in *Advances in Organometallic Chemistry*, F.G.A. Stone and R. West, Eds., Academic Press, 1980, p. 99.

[29] W. Kaminsky, M. Miri, H. Sinn, R. Woldt, *Makromol. Chem., Rapid Commun.* **1983**, *4*, 417.

[30] G. Wilkinson, M. Rosenblum, M. C. Whiting, R. B. Woodward, *Journal of the American Chemical Society* **1952**, *74*, 2125.

[31] A. L. McKnight, R. M. Waymouth, *Chem. Rev.* **1998**, *98*, 2587.

[32] L. Johnson, C. M. Killian, M. Brookhart, *Am Chem Soc* **1995**, *117*, 6414.

[33] P. J. Shapiro, E. Bunel, W. P. Schaefer, J. E. Bercaw, *Organometallics* **1990**, *9*, 867.

[34] J. Stevens, F. Timmers, *Y.(Dow): Eur. Pat. Appl. 0* **1991**, *416*, A2.

[35] T. R. Boussie, G. M. Diamond, C. Goh, K. A. Hall, A. M. LaPointe, M. Leclerc, C. Lund, V. Murphy, J. A. W. Shoemaker, U. Tracht, H. Turner, J. Zhang, T. Uno, R. K. Rosen, J. C. Stevens, *Journal of the American Chemical Society* **2003**, *125*, 4306.

[36] J. C. Stevens, "Constrained geometry and other single site metallocene polyolefin catalysts: A revolution in olefin polymerization", in *Stud. Surf. Sci. Catal.*, J.W. Hightower, W. Nicholas Delgass, E. Iglesia, and A.T. Bell, Eds., Elsevier, 1996, p. 11.

[37] M. C. Baier, M. A. Zuideveld, S. Mecking, *Angewandte Chemie International Edition* **2014**, *53*, 9722.

[38] M. Stürzel, S. Mihan, R. Mülhaupt, *Chem. Rev.* **2016**, *116*, 1398.

[39] M. P. McDaniel, D. C. Rohlfing, E. A. Benham, *Polymer Reaction Engineering* **2003**, *11*, 101.

[40] M. P. McDaniel, "Supported Chromium Catalysts for Ethylene Polymerization", in *Adv. Catal.*, D.D. Eley, H. Pines, and P.B. Weisz, Eds., Academic Press, 1985, p. 47.

[41] J. P. Hogan, *J. Polym. Sci.* **1970**, *8*, 2637.

[42] M. P. Conley, M. F. Delley, G. Siddiqi, G. Lapadula, S. Norsic, V. Monteil, O. V. Safonova, C. Copéret, *Angewandte Chemie International Edition* **2014**, *53*, 1872.

[43] P. Cossee, *J. Catal.* **1964**, *3*, 80.

[44] G. Ghiotti, E. Garrone, A. Zecchina, *J. Mol. Catal.* **1991**, *65*, 73.

[45] E. Groppo, C. Lamberti, S. Bordiga, G. Spoto, A. Zecchina, *Chemical Reviews* **2005**, *105*, 115.

[46] G. Ghiotti, E. Garrone, A. Zecchina, *J. Mol. Catal.* **1988**, *46*, 61.

[47] G. Ghiotti, E. Garrone, S. Coluccia, C. Morterra, A. Zecchina, *J. Chem. Soc. Chem. Commun.* **1979**, 1032.

[48] K. J. Ivin, J. J. Rooney, C. D. Stewart, M. L. H. Green, J. R. Mahtab, *J. Chem. Soc. Chem. Commun.* **1978**, 604.

[49] G. Natta, *J. Polym. Sci.* **1955**, *16*, 143.

[50] G. Natta, *Angew. Chem. Int. Ed.* **1956**, *68*, 393.

[51] G. Allegra, *Die Makromolekulare Chemie* **1971**, *145*, 235.

[52] P. Cossee, *Journal of Catalysis* **1964**, *3*, 80.

[53] E. J. Arlman, *Journal of Catalysis* **1964**, *3*, 89.

[54] W. Kaminsky, *Macromolecular Chemistry and Physics* **1996**, *197*, 3907.

[55] C. J. Harlan, S. G. Bott, A. R. Barron, *Journal of the American Chemical Society* **1995**, *117*, 6465.

[56] M. R. Mason, J. M. Smith, S. G. Bott, A. R. Barron, *Journal of the American Chemical Society* **1993**, *115*, 4971.

[57] W. Kaminsky, *Macromolecules* **2012**, *45*, 3289.

[58] W. Kaminsky, *Journal of Polymer Science Part A: Polymer Chemistry* **2004**, *42*, 3911.

[59] T. F. L. M. J. B. P. Soares, "Polymerization Catalysis and Mechanism", in *Polyolefin Reaction Engineering*, Wiley, Ed., 2012, p. 53.

[60] Y. Sarazin, M. Schormann, M. Bochmann, *Organometallics* **2004**, *23*, 3296.

[61] C. B. Gell, W. W. Graessley, V. Efstratiadis, M. Pitsikalis, N. Hadjichristidis, *Journal of Polymer Science Part B: Polymer Physics* **1997**, *35*, 1943.

[62] N. J. Inkson, T. C. B. McLeish, O. G. Harlen, D. J. Groves, *Journal of Rheology* **1999**, *43*, 873.

[63] T. C. B. McLeish, R. G. Larson, *Journal of Rheology* **1998**, *42*, 81.

[64] S. Shanbhag, *ISRN Materials Science* **2012**, *2012*.

[65] C. W. Bunn, *Transactions of the Faraday Society* **1939**, *35*, 482.

[66] M. Matsuo, C. Sawatari, *Macromolecules* **1986**, *19*, 2036.

[67] J. Clements, R. Jakeways, I. M. Ward, *Polymer* **1978**, *19*, 639.

[68] G. Avitabile, R. Napolitano, B. Pirozzi, K. D. Rouse, M. W. Thomas, B. T. M. Willis, *Journal of Polymer Science: Polymer Letters Edition* **1975**, *13*, 351.

[69] Y. Takahashi, *Macromolecules* **1998**, *31*, 3868.

[70] G. C. Claver Jr., R. Buchdahl, R. L. Miller, *Journal of Polymer Science* **1956**, *20*, 202.

[71] A. Keller, *Nature* **1952**, *169*, 913.

[72] J. J. Janimak, L. Markey, G. C. Stevens, *Polymer* **2001**, *42*, 4675.

[73] B. Wunderlich, "Thermal Analysis ", in *Thermal Analysis*, B. Wunderlich, Ed., Academic Press, 1990, p. 417.

[74] C. Schick, *Anal. Bioanal. Chem.* **2009**, *395*, 1589.

[75] F. H. Chung, R. W. Scott, *Journal of Applied Crystallography* **1973**, *6*, 225.

[76] B. Post, *Journal of Polymer Science Part B: Polymer Letters* **1971**, *9*, 635.

[77] A. Barlow, M. Young, *Journal of Applied Polymer Science* **1970**, *14*, 1731.

[78] D. E. Bosley, *Journal of Applied Polymer Science* **1964**, *8*, 1521.

[79] P. H. Hermans, A. Weidinger, *Die Makromolekulare Chemie* **1961**, *44*, 24.

[80] F. Happey, *Nature* **1969**, *222*, 603.

[81] G. R. Strobl, W. Hagedorn, *Journal of Polymer Science: Polymer Physics Edition* **1978**, *16*, 1181.

[82] R. Mutter, W. Stille, G. Strobl, *Journal of Polymer Science Part B: Polymer Physics* **1993**, *31*, 99.

[83] R. R. Eckman, P. M. Henrichs, A. J. Peacock, *Macromolecules* **1997**, *30*, 2474.

[84] J. S. Kauffman, C. Dybowski, *Journal of Polymer Science Part B: Polymer Physics* **1989**, *27*, 2203.

[85] O. Fricova, M. Uhrinova, V. Hronsky, M. Kovalakova, D. Olcak, I. Chodak, J. Spevacek, *Express Polym. Lett.* **2012**, *6*, 204.

[86] A. Bunn, M. E. A. Cudby, R. K. Harris, K. J. Packer, B. J. Say, *Polymer* **1982**, *23*, 694.

[87] S. Saito, Y. Moteki, M. Nakagawa, F. Horii, R. Kitamura, *Macromolecules* **1990**, *23*, 3256.

[88] R. Kitamaru, F. Horii, K. Murayama, *Macromolecules* **1986**, *19*, 636.

[89] H. E. Bair, R. Salovey, *Journal of Macromolecular Science, Part B* **1969**, *3*, 3.

[90] H. T. Pasch, B., *HPLC of polymers* **1998**.

[91] C. Tanford, "*Physical chemistry of macromolecules"*, Wiley, 1961.

[92] P. J. Flory, "*Principles of polymer chemistry"*, Cornell University Press, 1953.

[93] H. Mark, **1938**.

[94] R. Houwink, *Journal für praktische Chemie* **1940**, *157*, 15.

[95] I. Sakurada, "Nihon Kagakusenikenkyusho Koensyo", in *Proc. Symp. Jpn. Textile Res. Lab*, 1940, p. 5/33.

[96] H. L. Wagner, C. A. J. Hoeve, *Journal of Polymer Science: Polymer Physics Edition* **1973**, *11*, 1189.

[97] H. L. Wagner, *Journal of Physical and Chemical Reference Data* **1985**, *14*, 611.

[98] L. Carbognani, *Journal of High Resolution Chromatography* **1996**, *19*, 549.

[99] A. Striegel, W. W. Yau, J. J. Kirkland, D. D. Bly, "*Modern size-exclusion liquid chromatography: practice of gel permeation and gel filtration chromatography"*, John Wiley & Sons, 2009.

[100] T. G. Scholte, N. L. J. Meijerink, H. M. Schoffeleers, A. M. G. Brands, *Journal of Applied Polymer Science* **1984**, *29*, 3763.

[101] B. Monrabal, "Polyolefin Characterization: Recent Advances in Separation Techniques", 2013, p. 203.

[102] P. J. Flory, A. D. McIntyre, *Journal of Polymer Science* **1955**, *18*, 592.

[103] B. Monrabal, "Temperature Rising Elution Fractionation and Crystallization Analysis Fractionation", in *Encyclopedia of Analytical Chemistry*, Meyers, 2006.

[104] V. Desreux, M. C. Spiegels, *Bulletin des Sociétés Chimiques Belges* **1950**, *59*, 476.

[105] L. Wild, G. Glöckner, "Temperature rising elution fractionation", in *Separation Techniques Thermodynamics Liquid Crystal Polymers*, Springer Berlin Heidelberg, Berlin, Heidelberg, 19911.

[106] L. Wild, C. Blatz, *New Adv. Polyolefins, Ed. T. Chung, Plenum Press, New York* **1993**, 147.

[107] J. B. P. Soares, A. E. Hamielec, *Polymer* **1995**, *36*, 1639.

[108] S. Zhang, N. Zhao, Y. Wu, Q. Dong, Q. Wang, Y. Tang, Y. Yu, J. Da, X. He, R. Cheng, B. Liu, *Macromolecular Symposia* **2012**, *312*, 63.

[109] W. Liu, W. J. Wang, H. Fan, L. Yu, B. G. Li, S. Zhu, *European Polymer Journal* **2014**, *54*, 160.

[110] M. Kakugo, T. Miyatake, K. Mizunuma, Y. Kawai, *Macromolecules* **1988**, *21*, 2309.

[111] J. Xu, L. Feng, S. Yang, Y. Yang, X. Kong, *Polymer Journal* **1997**, *29*, 713.

[112] L. Wild, T. R. Ryle, D. C. Knobeloch, I. R. Peat, *Journal of Polymer Science, Polymer Physics Edition* **1982**, *20*, 441.

[113] J. Xu, Z. Fu, Z. Fan, L. Feng, *European Polymer Journal* **2002**, *38*, 1739.

[114] E. C. Kelusky, R. E. Murray, *Polym. Eng. Sci.* **1987**, *27*, 1562.

[115] M. Kakugo, T. Miyatake, Y. Naito, K. Mizunuma, *Macromolecules* **1988**, *21*, 314.

[116] L. Wild, *Adv. Polym. Sci.* **1991**, *98*, 1.

[117] C. A. S. J. Fonseca, *Modern techniques for Polymer Characterisation* **1999**, 1.

[118] B. Monrabal, "Temperature Rising Elution Fractionation and Crystallization Analysis Fractionation", in *Encyclopedia of Analytical Chemistry*, R.A. Meyers, Ed. Wiley: New York, Ed., Meyers, 2000, p. 8074.

[119] WO9306479A1 (1993), Dow Chemical Co., USA . inv. B. Monrabal;

[120] B. Monrabal, *J. Appl. Polym. Sci.* **1994**, *52*, 491.

[121] J. B. P. Soares, B. Monrabal, J. Nieto, J. Blanco, *Macromol. Chem. Phys.* **1998**, *199*, 1917.

[122] B. Monrabal, J. Blanco, J. Nieto, J. B. P. Soares, *Journal of Polymer Science, Part A: Polymer Chemistry* **1999**, *37*, 89.

[123] A. Albrecht, R. Bruell, T. Macko, P. Sinha, H. Pasch, *Macromol. Chem. Phys.* **2008**, *209*, 1909.

[124] H. Pasch, R. Brull, U. Wahner, B. Monrabal, *Macromol. Mater. Eng.* **2000**, *279*, 46.

[125] R. Brüll, H. Pasch, H. G. Raubenheimer, R. Sanderson, A. J. van Reenen, U. M. Wahner, *Macromolecular Chemistry and Physics* **2001**, *202*, 1281.

[126] D. M. Sarzotti, J. B. P. Soares, A. Penlidis, *Journal of Polymer Science Part B: Polymer Physics* **2002**, *40*, 2595.

[127] B. Monrabal, J. Sancho-Tello, N. Mayo, L. Romero, *Macromolecular Symposia* **2007**, *257*, 71.

[128] B. Monrabal, "Crystallization based separations for semicrystalline polymers", American Chemical Society, 2008ANYL.

[129] B. Monrabal, N. Mayo, R. Cong, *Macromolecular Symposia* **2012**, *312*, 115.

[130] A. M. Skvortsov, A. A. Gorvunov, *Journal of Chromatography A* **1986**, *358*, 77.

[131] B. Trathnigg, O. Jamelnik, A. Skvortsov, *Journal of Chromatography A* **2006**, *1128*, 39.

[132] T. Macko, J. F. Denayer, H. Pasch, G. V. Baron, *J. Sep. Sci.* **2003**, *26*, 1569.

[133] T. Macko, D. Hunkeler, *Adv. Polym. Sci.* **2003**, *163*, 61.

[134] T. Macko, H. Pasch, J. F. Denayer, *J. Chromatogr. A* **2003**, *1002*, 55.

[135] T. Macko, M. Adler, H. Pasch, J. F. Denayer, A. Raphael, *J. Liq. Chromatogr. Relat. Technol.* **2004**, *27*, 1743.

[136] T. Macko, R. Brüll, R. G. Alamo, Y. Thomann, V. Grumel, *Polymer* **2009**, *50*, 5443.

[137] T. Macko, H. Pasch, *Macromolecules* **2009**, *42*, 6063.

[138] T. Macko, R. Bruell, C. Brinkmann, H. Pasch, *J. Autom. Methods Manage. Chem.* **2009**, No pp. given.

[139] T. Macko, R. Bruell, Y. Wang, *Polym. Prepr. (Am. Chem. Soc., Div. Polym. Chem.)* **2009**, *50*, 228.

[140] H. Pasch, A. Albrecht, R. Bruell, T. Macko, W. Hiller, *Macromol. Symp.* **2009**, *282*, 71.

[141] R. Chitta, A. Ginzburg, G. van Doremaele, T. Macko, R. Bruell, *Polymer* **2011**, *52*, 5953.

[142] T. Macko, R. Bruell, Y. Wang, B. Coto, I. Suarez, *J. Appl. Polym. Sci.* **2011**, *122*, 3211.

[143] V. Dolle, A. Albrecht, R. Bruell, T. Macko, *Macromol. Chem. Phys.* **2011**, *212*, 959.

[144] R. Chitta, T. Macko, R. Bruell, G. Van Doremaele, L.-C. Heinz, *J. Polym. Sci., Part A: Polym. Chem.* **2011**, *49*, 1840.

[145] T. Macko, R. Bruell, R. G. Alamo, F. J. Stadler, S. Losio, *Anal. Bioanal. Chem.* **2011**, *399*, 1547.

[146] R. Chitta, A. Ginzburg, T. Macko, R. Bruell, G. van Doremaele, *LC-GC Eur.* **2012**, *25*, 352.

[147] R. Cong, W. DeGroot, "High temperature liquid chromatography of Polyolefin", American Chemical Society, 2015POLY.

[148] N. Inwong, S. Anantawaraskul, J. B. P. Soares, A. Z. Al- Khazaal, *Macromolecular Symposia* **2015**, *356*, 54.

[149] A. Z. Al-Khazaal, J. B. P. Soares, *Macromolecular Chemistry and Physics* **2014**, *215*, 465.

[150] A. Alghyamah, J. B. P. Soares, *Industrial & Engineering Chemistry Research* **2014**, *53*, 9228.

[151] D. Mekap, F. Malz, R. Bruell, Z. Zhou, R. Cong, A. W. deGroot, A. R. Parrott, *Macromolecules (Washington, DC, U. S.)* **2014**, *47*, 7939.

[152] B. Monrabal, *Macromol. Symp.* **2015**, *356*, 147.

[153] B. Monrabal, E. Lopez, L. Romero, *Macromol. Symp.* **2013**, *330*, 9.

[154] R. Cong, W. de Groot, A. Parrott, W. Yau, L. Hazlitt, R. Brown, M. Miller, Z. Zhou, *Macromolecules (Washington, DC, U. S.)* **2011**, *44*, 3062.

EXPERIMENTAL PART



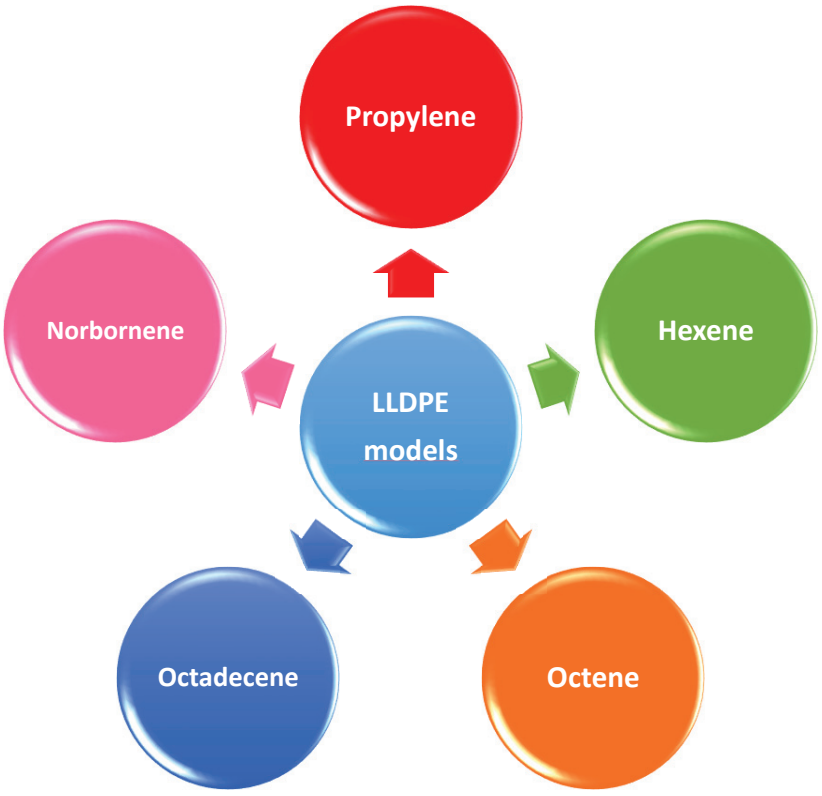
« La connaissance s'acquiert par l'expérience,
tout le reste n'est que de l'information »
Albert Einstein

CHAPTER II

SYNTHESIS OF LLDPE MODELS AND THEIR CHARACTERIZATION

There are no commercial LLDPE with known and certified chemical compositions. A specific know-how is available in our laboratory for the controlled synthesis of well-defined polymers. I decided to take advantage of the CP2M researchers' skills, and in particular those of Christophe Boisson, in metallocene catalysis to conceive polymers that will serve as standards for the development of new analytical methods. With the support of Christophe Boisson, I supervised three internship students who produced a wide range of well-defined copolymers. We have tested and chosen catalyst systems already known and studied by our laboratory in previous works.

The objective of the following part was to synthetize LLDPE models with various types and amount of comonomer as illustrated in the figure below.



2.1 REACTION MEDIUM

2.1.1 PRE-CATALYSTS

In order to obtain model polymers with homogeneous chains both in molar mass and in chemical composition, metallocene-type catalysts were used. The choice of catalysts was guided by previous work carried out in the laboratory[1] where homogeneous LLDPEs with low dispersity were obtained.

The complex used first, *rac-ethylene bis(indenyl)zirconium* (IV) *dichloride* (rac-Et(Ind)$_2$ZrCl$_2$), allows efficient incorporation of comonomers, and it is known in particular for its use in the synthesis of isotactic polypropylene, because of the C2-symmetry of the complex and the presence of two homotopic sites for active cationic species (Figure 2-1).

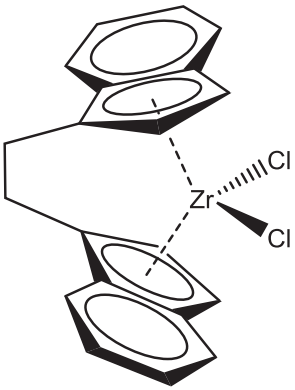


Figure 2-1: Complex Et(Ind)$_2$ZrCl$_2$.

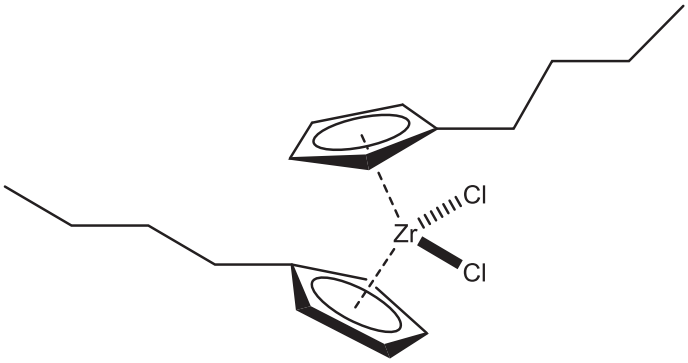


Figure 2-2: Complex (nBuCp)$_2$ZrCl$_2$.

The second complex used, *Bis (n-butylcyclopentadienyl) zirconium dichloride* ((nBuCp)$_2$ZrCl$_2$), leads to less efficient copolymerization (Figure 2-2). A lower response to the comonomer is obtained due to the steric hindrance of its ligands. However, polymers with narrow molar mass distribution were prepared.

2.1.2 CO-CATALYST

Methylaluminoxane (MAO) is the co-catalyst of choice for metallocene complexes. For the experiments, a commercial solution of MAO at 10% by mass in toluene was purchased from Aldrich. It was stored under inert atmosphere at -20°C.

2.1.3 SOLVENT

The toluene used as solvent was purchased from Biosolve and dried in a Mbraun solvent purification system equipped with activated alumina and copper catalyst columns.

2.1.4 MONOMER

Ethylene (99.95%) was purchased from Air Liquid and purified by passing it through 3 different columns in order to remove the impurities (H_2O, O_2, CO_2 and H_2):

• a copper oxide support CuO (from BASF) for the elimination of O_2 and CO,

• an activated molecular sieve which eliminates water,

• an alumina column which eliminates the sulfur compounds.

2.1.5 COMONOMERS

The tested comonomers are the α-olefins most often used industrially for the synthesis of polyolefins.

• Propylene, a gaseous compound, was used directly without purification.

• 97% commercial hexene is placed on CaH_2 overnight and then distilled by cryo-distillation for purification.

• 98% commercial octene is bubbled through a molecular sieve and used without further purification.
• Octadecene (90%) is purified by simple degassing under vacuum.

• Norbornene is in solid form at room temperature (melting temperature = 42 °C). Norbornene in a melting state is placed on sodium for one day and then distilled for purification. A solution of norbornene in toluene is then prepared in order to simplify the sampling.

The various comonomers used in this work and the corresponding copolymers that were obtained are summarized in Figure 2-3.

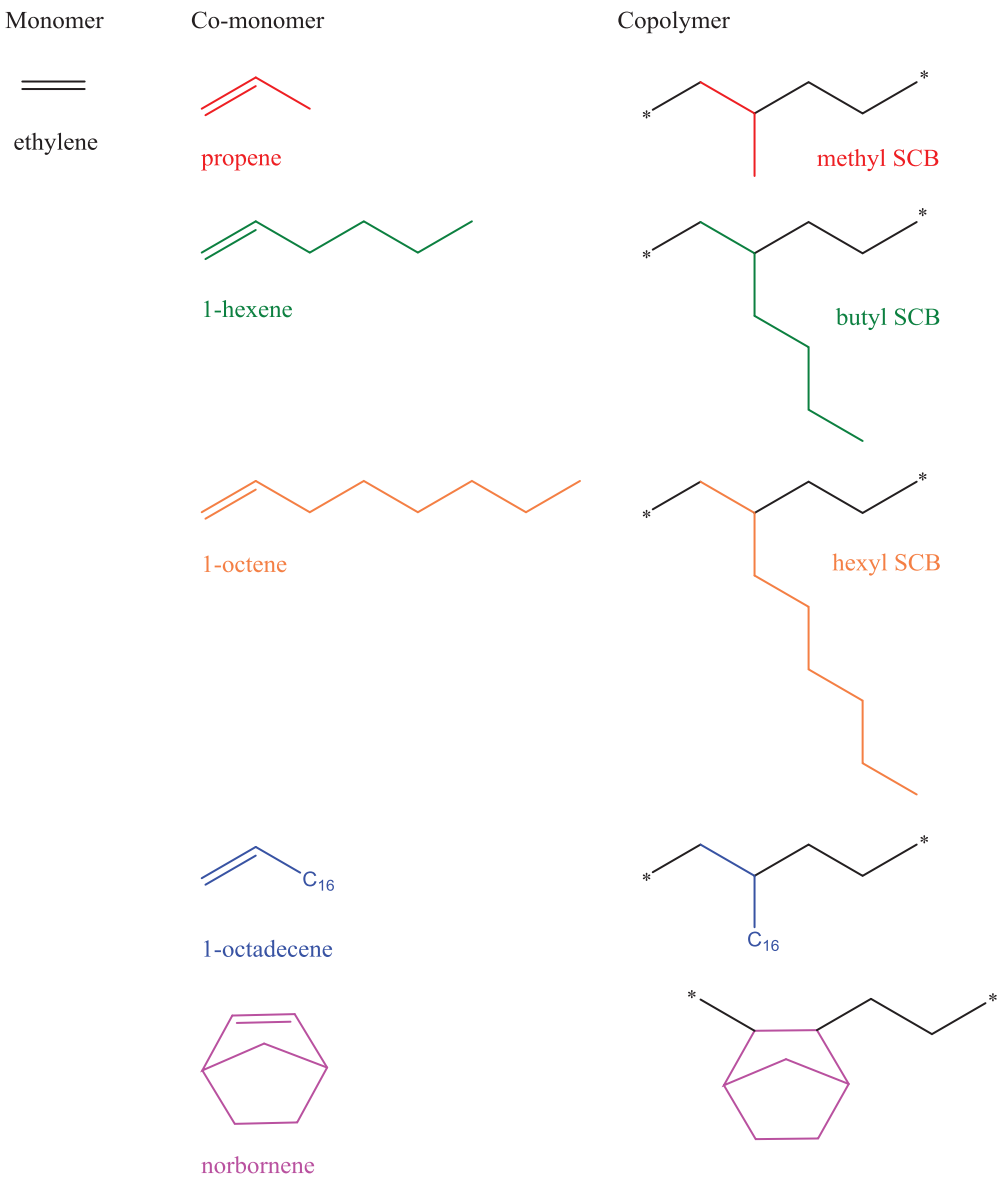


Figure 2-3: Copolymers synthesized by coordination polymerization.

2.2 COPOLYMERIZATION

A general procedure of the copolymerization is described below:

The complex was weighed in a glove box, and 25 mL of toluene was added. The solutions were stirred until dissolved. 300 mL of toluene, 0.3 mL of MAO, and between 0 and 20 mL of the comonomer were introduced into a 500 mL reactor. 100 µL of the pre-catalyst solution (1.5 mM), prepared previously, was either introduced in the reactor before ethylene pressurization. Polymerization was performed at 80°C under a constant pressure of 4 bar. The reaction exotherm was controlled to keep the reaction conditions as stable as possible. At the end of the reactions, the ethylene feed was stopped, and 5 ml of methanol was introduced in the reactor. The polymer was cleaned with acidified methanol and dried under vacuum at 90°C for 3 hours.

For the series with propylene as comonomer, gas mixtures with different ethylene-propylene ratios were prepared. They were introduced at 3 bar into the reactor that already contained toluene, MAO and the pre-catalyst.

2.2.1 COPOLYMERIZATION CONDITIONS

To obtain a homogeneous polymer with the most stable polymerization conditions, an injection chamber was implemented to inject the catalyst under ethylene pressure. Firstly, the comonomer, the solvent and the MAO were added in the reactor. In the next step, the reactor was fed with 3.8 bar of ethylene pressure and heated to 80 °C. Once the temperature was stable, 100 µL of the pre-catalyst solution, previously diluted in 10 ml of toluene and introduced into the injection chamber, was pushed inside the reactor using an ethylene pressure of 4 bar (Figure 2-4). This protocol allows the rapid injection of the pre-catalyst solution in stable conditions.

The distribution of the chemical composition of the LLDPE obtained when injecting the catalyst under ethylene pressure was compared to a sample synthetized without the injection chamber. In these conditions the pre-catalyst was introduced directly in the reactor at ambient temperature. Indeed, the catalysts and the α-olefin capable of polymerizing were present inside the reactor. In addition, when they were introduced into the reactor fed with ethylene, they did not immediately attain the polymerization temperature (80 °C). A temperature drift occurred with the risk of forming different microstructures of chains at the beginning of the reaction, affecting the homogeneity of the material.

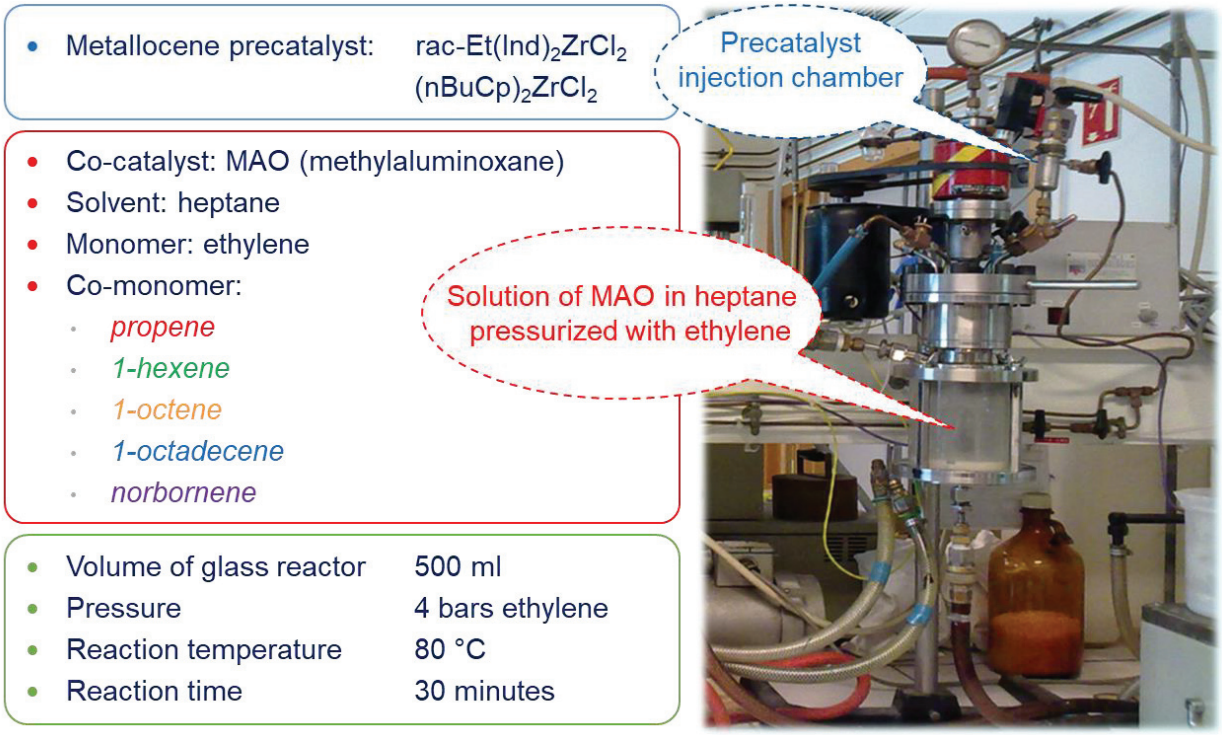


Figure 2-4: Reactor and synthesis conditions used to obtain our copolymer models.

DSC using the stepwise isothermal segregation technique (SIST) was chosen to evaluate the homogeneity of the chemical composition of the two samples obtained with and without the injection chamber. The analysis by SIST consisted of crystallizing the material in several steps. The melting profile obtained after these consecutive crystallization steps was characteristic of small changes in the polymer microstructure. Variations in comonomer insertion and subsequently in the polymerization process could thus be detected.

First, LLDPE samples were melted at 220 °C for 10 minutes and then cooled to the first crystallization temperature (Tc = 130 °C) at 50 °C min^{-1}. The samples could crystallize isothermally for 1 hour at this temperature. Subsequently, they were rapidly cooled again at 50 °C min^{-1} to the next crystallization temperature, 5 °C less, and again allowed to crystallize for 1 hour.

As represented in Figure 2-5 (a), this procedure was repeated for a series of 20 isothermal steps of 5 °C intervals, down to 40 °C. Finally, the samples were cooled to -20 °C before acquiring the melting DSC profile from -20 °C to 180 °C at 5 °C min^{-1}.

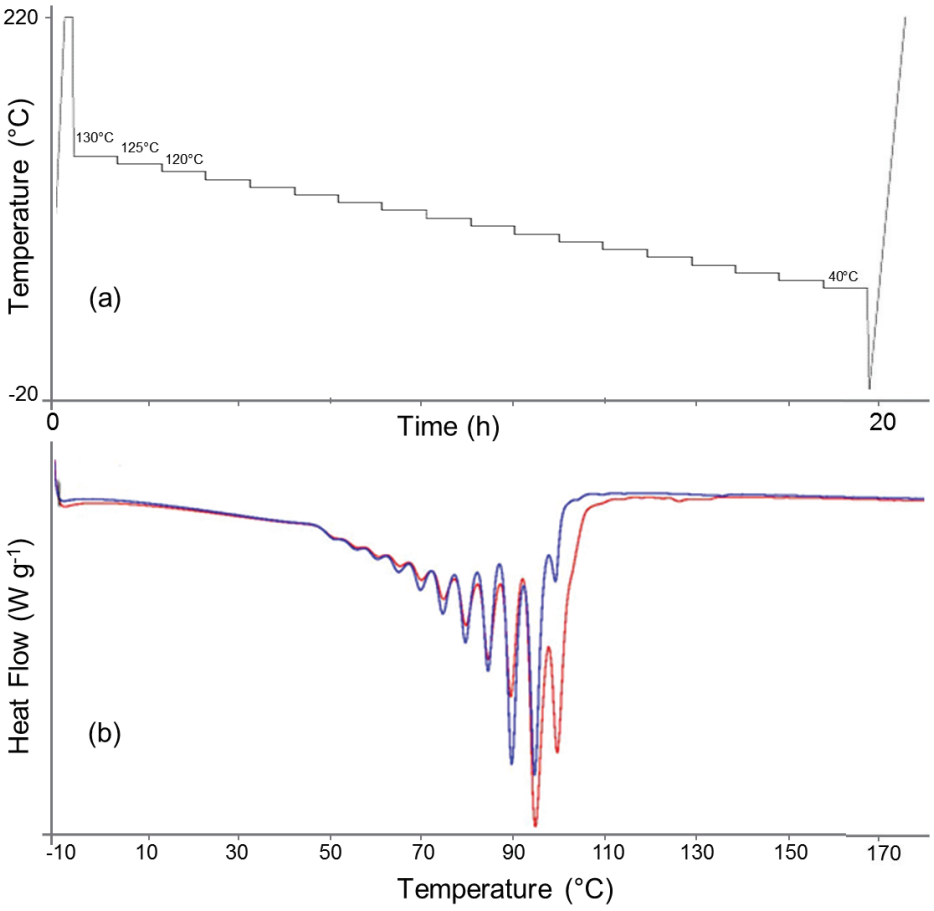


Figure 2-5: Temperature program used for the DSC SIST (a) and DSC thermogram during heating after SIST treatment for the sample obtained with the standard protocol (red curve) and the sample obtained using the injection chamber (blue curve) (b).

Chains with a high comonomer content have shorter ethylene sequences that are more difficult to crystallize. These chains form thinner lamellae and consequently melt at lower temperatures. On the contrary, chains with fewer comonomer and longer ethylene sequences melt at higher temperatures. Thus, the different peaks obtained after the SIST treatments reveal the different crystals due directly to the comonomer distribution. The DSC curve from LLDPE synthetized with the injection chamber (blue curve in Figure 2-5 (b)), clearly shows a narrower distribution compared to the LLDPE obtained with the classical protocol (red curve in Figure 2-5 (b). Indeed, the population of strong crystallinity (peak of higher temperature) is greatly reduced, leading to a narrower distribution. This population appeared at the beginning of polymerization when the thermal conditions were not yet stable. The injection chamber protocol appeared to be effective in achieving better homogeneity for our sample and was used systematically thereafter.

2.2.2 BEHAVIOR OF METALLOCENE COMPLEXES

Six series of copolymer models were prepared with these synthesis conditions. For each series, various comonomer contents were added in the reactor in order to obtain different comonomer contents inserted in the chain. The synthesis conditions are reported in Table 2-1.

Table 2-1: Polymerization conditions of the six series of LLDPE models

Série	**1**	**2**	**3**	**4**	**5**	**6**
Comonomer	Propylene	1-Hexene	1-Hexene	1-Octene	Octadecene	Norbornene
Feed[a]	2-39 mol%	1-88 mol%	11-64 mol%	9-59 mol%	21-69 mol%	5-68 mol%
Catalysts	$Et(Ind)_2ZrCl_2$	$Et(Ind)_2ZrCl_2$	$(nBuCp)_2ZrCl_2$	$Et(Ind)_2ZrCl_2$	$Et(Ind)_2ZrCl_2$	$Et(Ind)_2ZrCl_2$
Catalyst	$1.5x10^{-7}$ mol	$1.5x10^{-7}$ mol	$1.6x10^{-7}$ mol	$1.5x10^{-7}$ mol	$1.8x10^{-6}$ mol	$1.5x10^{-6}$ mol
Co-catalysts[b]	MAO	MAO	MAO	MAO	MAO	MAO
Ratio Al/Zr	3000	3000	3000	3000	3000	3000
Temperature	80°C	80°C	80°C	80°C	80°C	80°C
Reaction time	15 min	30 min	30 min	30 min	30 min	30 min

Volume of toluene = 330 mL, [a] % of comonomer in the reactor, [b] $[Al]_{MAO}$ = 2.4–3.0 mM. For each reaction the activity changed according to the following values:

(1) variation in activity from 3.9×10^6 up to 1.5×10^8 g mol^{-1} h^{-1}

(2) variation in activity from 1.8×10^7 up to 7.6×10^8 g mol^{-1} h^{-1}

(3) variation in activity from 3.4×10^7 up to 1.5×10^8 g mol^{-1} h^{-1}

(4) variation in activity from 9.4×10^6 up to 1.4×10^8 g mol^{-1} h^{-1}

(5) variation in activity from 3.8×10^6 up to 2.6×10^8 g mol^{-1} h^{-1}

(6) variation in activity from 2.5×10^5 up to 2.7×10^7 g mol^{-1} h^{-1}

The evolution of comonomer in the polymer versus comonomer in the feed is plotted in Figure 2-6. The ability of both catalyst systems to incorporate comonomer was evaluated according to the content of comonomer available in the reaction medium. As reported by Lehmus and co-workers, we observed that the content of incorporated comonomer is proportional to the α-olefin in the reaction medium.[2] A linear

response of insertion was observed for low comonomer content. When the comonomer content in the reactor was greater than 50 mol%, the insertion was no longer linear but was greatly increased.

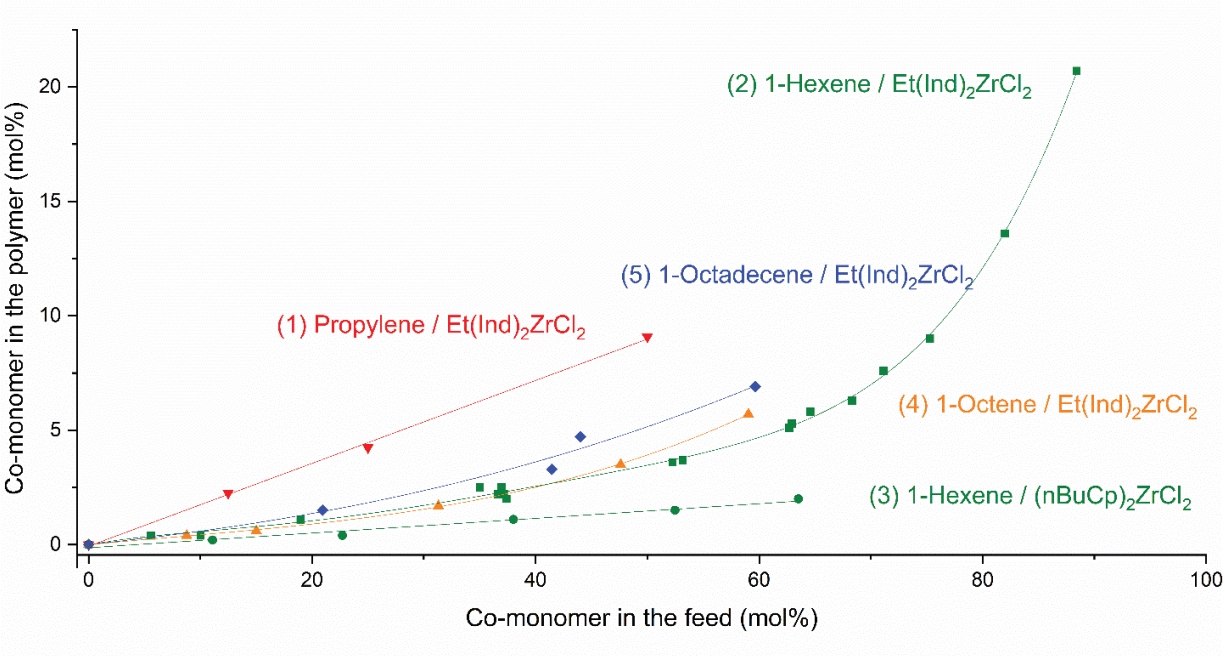
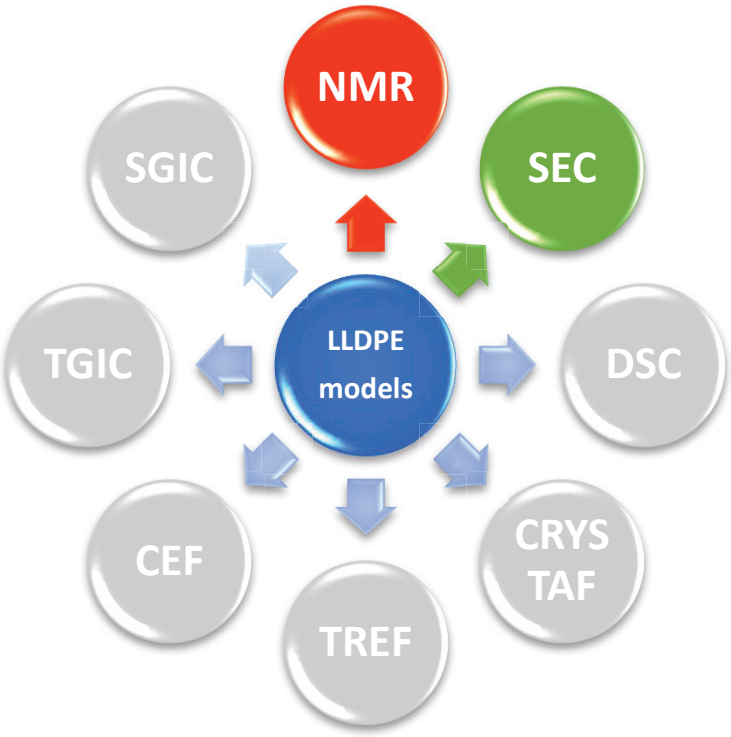


Figure 2-6: Influence of comonomer concentration in the reactor on their incorporation in ethylene-propyle, ethylene-hexene, ethylene-octene and ethylene-octadecene copolymers.

A major difference in the incorporation of 1-hexene was observed between both catalysts. The comonomer was incorporated more easily when using the $Et(Ind)_2ZrCl_2$. This behavior depending on the steric hindrance provided by the ligand, in $Et(Ind)_2ZrCl_2$ complex, was reported previously.[3, 4] The authors also calculated the reactivity ratio for ethylene by ^{13}C NMR for both complexes. They were evaluated at 51 and 160 for $Et(Ind)_2ZrCl_2$ and $(n\text{-}BuCp)_2ZrCl_2$ complexes, respectively. These values confirm the better comonomer insertion that we observed for the $Et(Ind)_2ZrCl_2$ complexes.

Following the synthesis of our model samples, the next step was the characterization by NMR to measure the average comonomer content, and by high temperature size exclusion chromatography (HT-SEC) to measure the average molar masses and the molar mass distribution. The SEC's viscometric detector was also used to measure the long chain branching and to propose a method for measuring the short chain branching.


NMR
SEC
DSC
CRYS TAF
TREF
CEF
TGIC
SGIC
LLDPE models

2.3 DETERMINATION OF COMONOMER CONTENT BY NMR

NMR uses an external magnetic field which interacts with the magnetic properties of nuclei to obtain information about the molecular structure of a sample. Different nuclei can be chosen for NMR experiments depending on the need: ^{1}H, ^{13}C, ^{15}N, ^{19}F, ^{31}P… ^{1}H and ^{13}C are generally applied for polyolefin NMR spectroscopy. The structural information was obtained thanks to the chemical shift (ppm) in the spectrum which represents the ΔE (Equation 2-1) relative to the reference proton. Tetramethylsilane (TMS), whose chemical shift is assigned at 0 ppm, is generally chosen as the reference.

$$\Delta E = \frac{h\gamma}{2\pi} B \qquad (2\text{-}1)$$

Where h is Planck's constant, γ the gyromagnetic ratio and B the external magnetic field.

For the LLDPE samples, NMR spectroscopy requires a high temperature and specific solvents which do not evaporate at high temperature. To perform a quantitative analysis, certain universal spectrometer parameters should be selected, as described by Malz and coworkers.[5] In particular, probe tuning and the relaxation delay should be specifically adjusted for LLDPE.

For ^{1}H NMR, the area of each signal is directly proportional to the number of protons associated with the signal. ^{1}H NMR is widely used to determine composition of polyolefins such as end-groups,[6] unsaturation,[7, 8] functional groups[9] and alkyl branches. Since the signal area can be quantitative, NMR has the great advantage of giving a direct value of the comonomer content in our copolymers without calibration.

^{13}C NMR is widely applied to explore the microstructure of polyolefins. It has been successfully applied to assess tacticity[10-12] and comonomer sequences.[13-16]

Because, in our case, the copolymers have a homogenous composition, the average value obtained by NMR is a fair representation of the structure of our samples. This part describes the instrumentation, parameter setting, and methods used to quantify the comonomer units inserted in the copolymer chains by ^{1}H NMR and ^{13}C NMR spectroscopy.

NMR experiments were performed in the NMR Polymer Service of the Institut de Chimie de Lyon (FR5223) with the friendly and expert support of Fernande Da Cruz-Boisson.

2.3.1 QUANTIFICATION BY ^{1}H NMR

The mole fraction of the comonomer in the copolymers was measured by proton NMR on a Bruker Avance III 400 spectrometer operating at 400MHz.

Analytical conditions:

- Analysis temperature = 100 ° C,
- 3: 1 volume mixture of 1,2,4-trichlorobenzene and toluene-d8,
- Concentration: 10 mg ml^{-1},
- 5 mm QNP (Quadrupole Nuclear Probe) probe,
- Calibration: chemical shifts of CHD_2 at 2.185 ppm.

The samples were dissolved in the NMR tube by heating the tube in a heating block at 150°C for 2 hours.

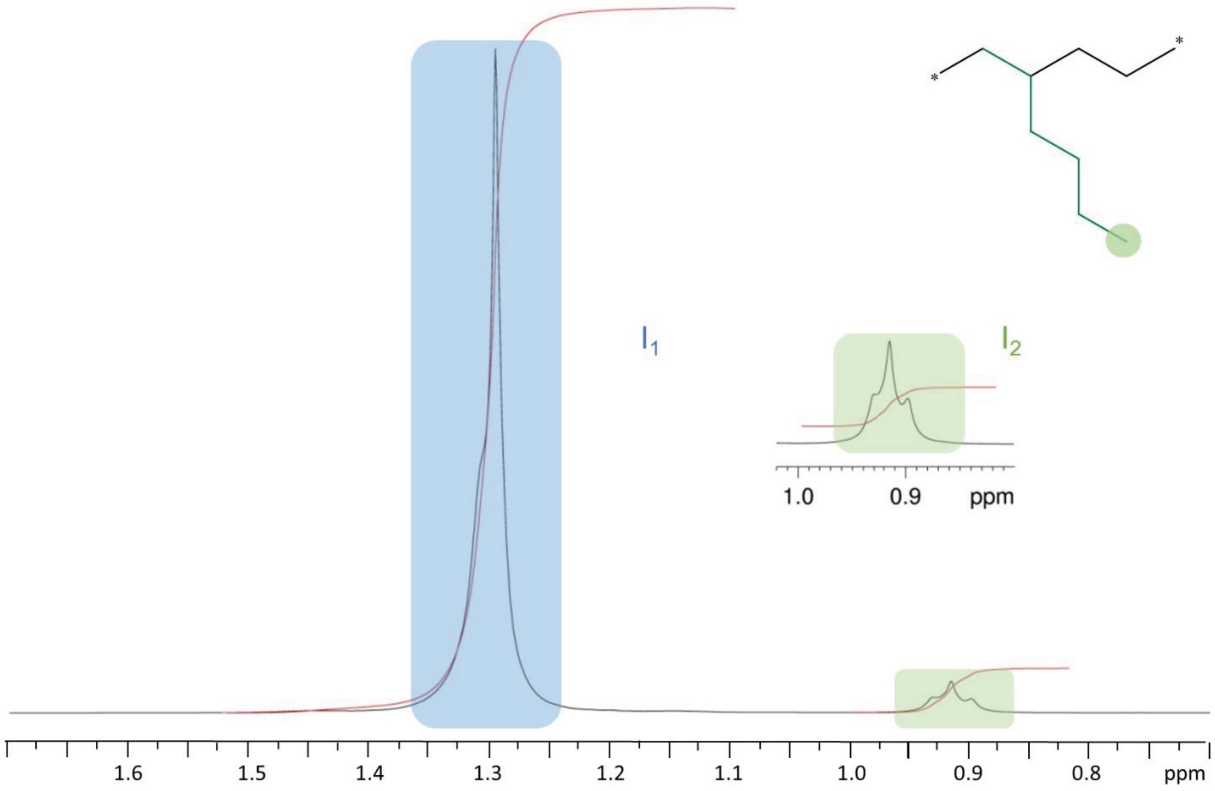


Figure 2-7: ^{1}H NMR spectrum of an ethylene-hexene copolymer in TCB/toluene-d8 at 373 K.

The ^{1}H NMR spectrum is composed of only two main signals. The methyl branches at 0.9 ppm can be easily distinguished from the proton signals of the ethylene backbone at 1.3 ppm (Figure 2-7). Regarding propylene, octene and octadecene comonomers the signal assignments are similar.

Methyl chain-ends were neglected in the calculations because the molar masses of the copolymers are high (> 20 kg mol^{-1}). Nevertheless, at low comonomer content, lower than 2 mol%, the sensitivity of ^{1}HNMR was not sufficient. In this case ^{13}C NMR was used as an alternative for the determination of the α-olefin content.

Ethylene-norbornene copolymer:

For ethylene-norbornene, the NMR spectra shown in Figure 2-8 are quite different. The peaks were assigned according to Bergström's publication.[17] I_2 is the integral of bridgehead hydrogen signals from norbornene, and I_1 is the integral of the remaining hydrogen signals (from norbornene and ethylene).

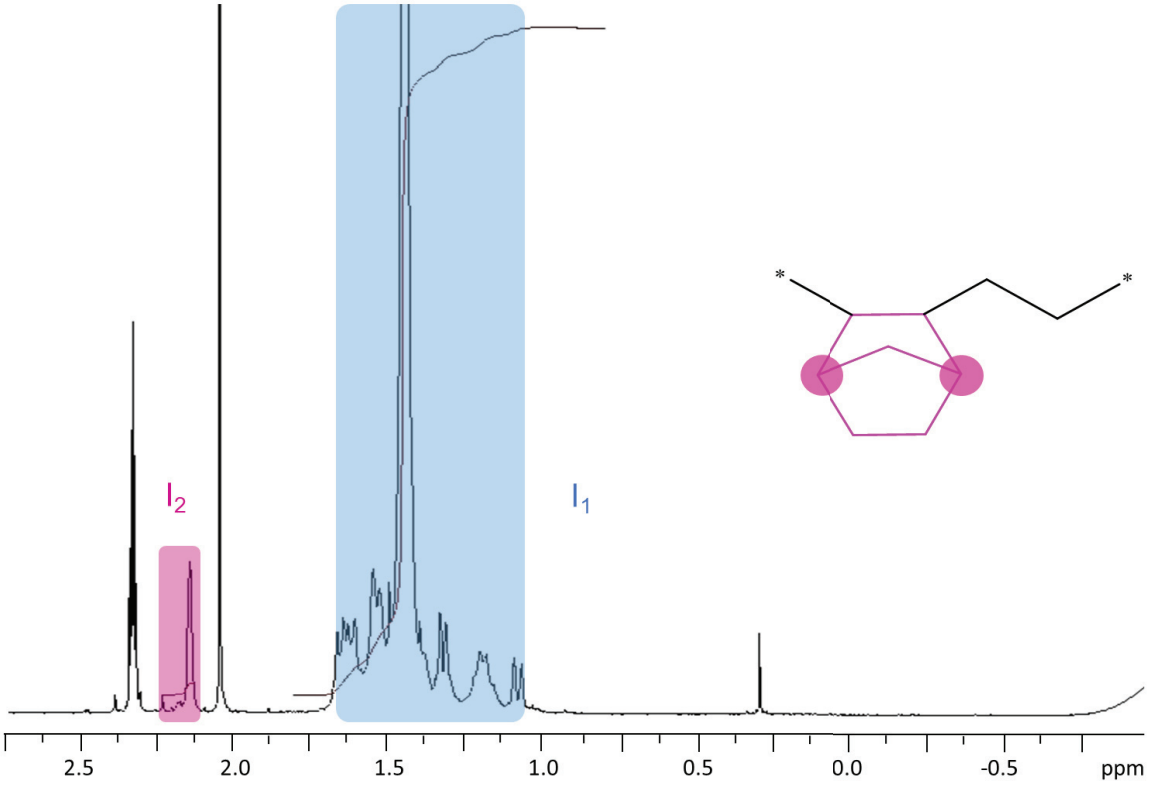
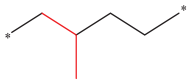
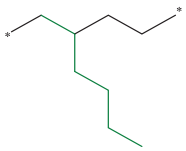
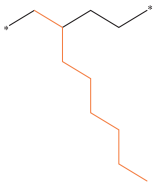
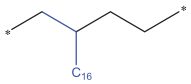
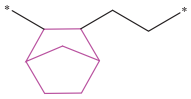


Figure 2-8: ^{1}H NMR spectrum of an ethylene-norbornene copolymer in TCB/toluene-d8 at 373 K.

After integrating the spectral regions with Topspin software (Bruker), the mole fractions of the comonomer were calculated by applying the following equations in Table 2-2.

Table 2-2: Comonomer content calculation by proton NMR.

Comonomer	Intensity	Mol fraction
Propene 	$I_1 = 4E + 3P$ $I_2 = 3P$	$\%=\frac{P}{E+P}=\frac{4\times I_2}{3\times I_1+I_2}$
Hexene 	$I_1 = 4E + 9H$ $I_2 = 3H$	$\%=\frac{H}{E+H}=\frac{4\times I_2}{3\times I_1- 5\times I_2}$
Octene 	$I_1 = 4E + 13O$ $I_2 = 3O$	$\%=\frac{O}{E+O}=\frac{4\times I_2}{3\times I_1- 9\times I_2}$
Octadecene 	$I_1 = 4E + 33OD$ $I_2 = 3OD$	$\%=\frac{OD}{E+OD}=\frac{4\times I_2}{3\times I_1-29\times I_2}$
Norbornene 	$I_1 = 4E + 8N$ $I_2 = 2N$	$\%=\frac{N}{E+N}=\frac{2\times I_2}{I_1-2\times I_2}$

with I_1 being the signal intensity of the CH2 and CH protons of the polyethylene chain at 1.3 ppm, I_2 is the signal intensity of the methyl at 0.9 ppm and CH at 2.15 ppm for norbornene. E, P, H, O, OD and N are the relative intensities of ethylene, propylene, hexene, octene, octadecene and norbornene units, respectively.

2.3.2 QUANTIFICATION BY ^{13}C NMR

For low amounts of α-olefin comonomers the triplet intensity at 0.9 ppm was low, the signal to noise ratio was not acceptable to ensure reliable results. ^{13}C NMR (Figure 2-9) was then carried out under the following conditions:

- Analysis temperature = 100 °C,
- 3: 1 volume mixture of 1,2,4-trichlorobenzene and toluene-d8,
- Concentration: 100 mg ml^{-1},
- 10 mm PA-SEX (Selective X) probe,
- Calibration: chemical shifts of PE at 30.06 ppm.

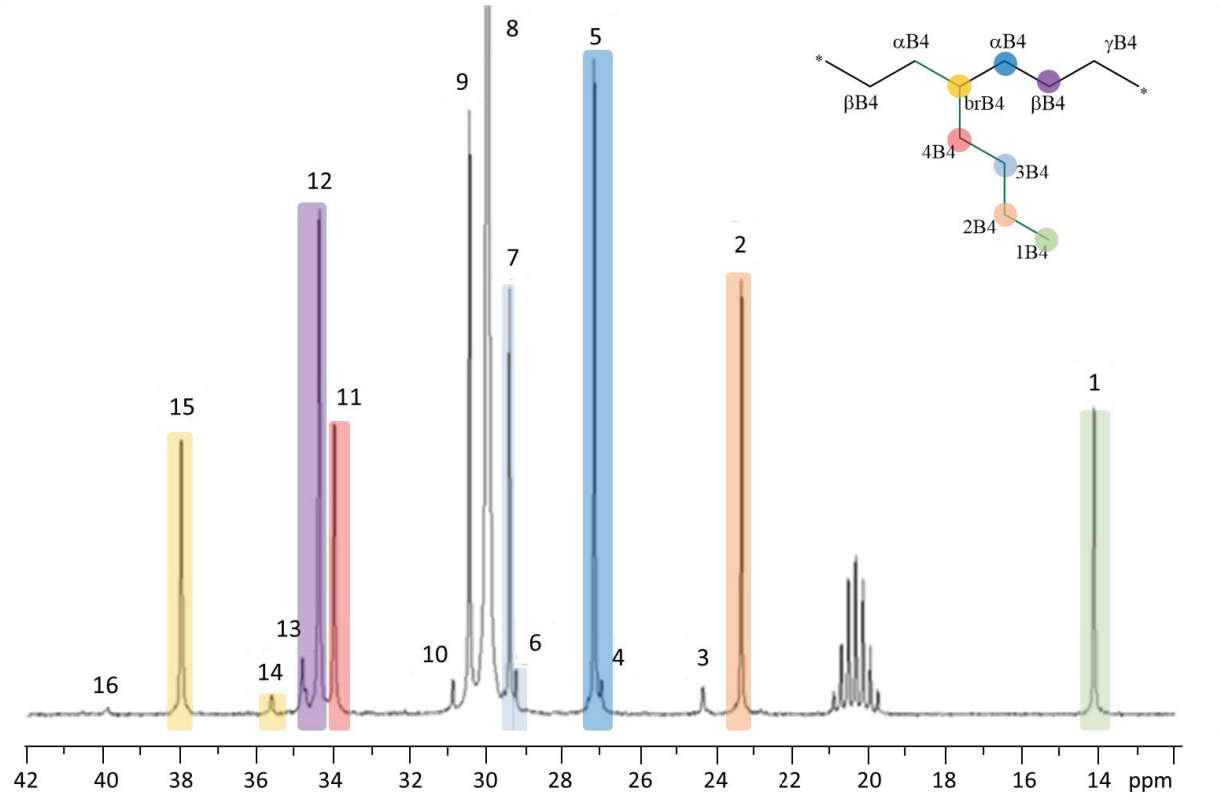
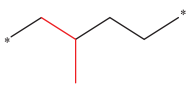
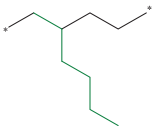
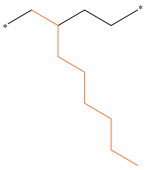
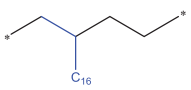


Figure 2-9: ^{13}C NMR spectrum of an ethylene-hexene copolymer (9 mol% of hexene) and peak assignments in TCB/toluene-d8 at 373 K (b). 1: 1B4; 2: 2B4; 3: ββ HEH; 4: βδ EEHH; 5: βδ EEHE; 6: 3B4 EHH; 7: 3B4 EHE; 8: δδ EEE; 9: δγ EEEH; 10: γγ HEEH; 11: 4B4; 12: αδ EEHE; 13: 4B4 EHH + αγ EEHH + αγ HEH; 14: CH EHH; 15: CH EHE; 16: αα EHH.

The ^{13}C NMR spectra is somewhat more complex; the peaks were assigned according to the publications by Randall[13] and Galland[18]. After integrating the spectral regions, the mole fractions of the comonomer were calculated by applying the following equations in Table 2-3.

Table 2-3: Comonomer content calculation by 13C NMR

Comonomer	**m = (I_α+I_β)/2**		**I (CH_2)**		**Mol fraction**
	δ (ppm)	Expres	δ (ppm)	Expression	
Propene 	I_α: 37.5 I_β: 27.4	m = 2xP	29 - 31	$I(CH_2)=2xE-3P$	$\%=\frac{m}{I(CH_2)+3/2\ m}$

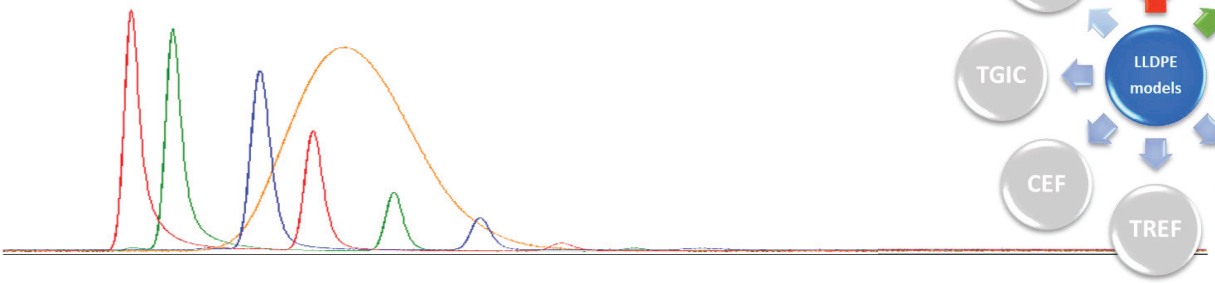
Hexene 	I_α: 34.4 I_β: 27.2	m = 2xH	29 - 31	$I(CH_2)=2x(E–H)$	$\%=\frac{m}{I(CH_2)+2m}$
Octene 	$I_{\alpha\,(\alpha B6+6B6)}$: 34.4 $I_{\beta\,(\beta B6+5B6)}$: 27.2	m = 3xO	29 - 31	$I(CH_2)=2x(E-O)$	$\%=\frac{2m}{3I(CH_2)+4m}$
Octadecene 	$I_{\alpha\,(\alpha B16+6B16)}$: 34.4 $I_{\beta\,(\beta B16+5B16)}$: 27.2	m = 3xOD	29 - 31	$I(CH_2)=2xE+8OD$	$\%=\frac{2m}{3\,(I(CH_2)-2m)}$

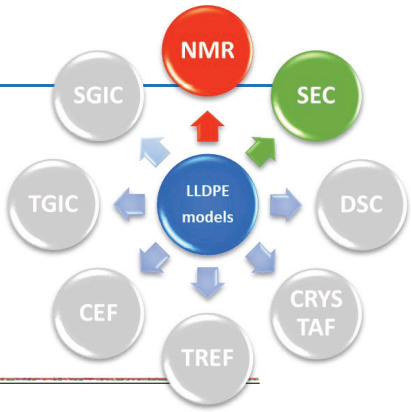
with I_α and I_β being the carbon atoms located in α and β positions, respectively, of the branch in the backbone chain (Figure 2-9). To improve the accuracy on the measurement, we use the average value (m) defined as $m = (I_\alpha + I_\beta)/2$, $I(CH_2)$ is the integral value of the signals between 29 and 31 ppm. E, P, H, O and OD are the relative intensities of ethylene, propene, hexene, octene and octadecene units, respectively.

A large number of each type of copolymer has been synthesized and characterized by NMR. The mole fractions calculated by NMR are reported in Appendix 1. These copolymers could then be used as standards to construct calibration curves for the different fractionation techniques: TREF, CRYSTAF, CEF and TGIC. For SGIC technique, a collaboration with Tibor Macko of the Fraunhofer Institute for Structural Durability and System Reliability, Darmstadt (LBF) has been undertaken. The copolymers were employed to correlate the elution times obtained by fractionation techniques to the amount of comonomers.

After measuring the comonomer content, we determined their average molar mass and their molar mass distribution by HT-SEC. To obtain a complete view of the microstructure of our model copolymers, we furthermore studied the presence of long chain branching (LCB).

2.4 DETERMINATION OF MOLAR MASS AND BRANCHING BY HT-SEC





I am in charge of the high temperature size exclusion chromatography (HT-SEC) in our laboratory. After setting up the instrument, I developed the sample preparation and analysis and performance evaluation protocols for the highly specific measurement of polyolefins.[19] The beginning of this section outlines the results of these evaluations in order to fully understand the accuracy of the measurements obtained on our LLDPE models.

First, the SEC has been used for the measurement of the molar masses according to several implanted methods which are described below. Afterwards, it has also applied to better understand the structure of our polymers through the advanced exploitation of light scattering and viscosimetric detectors.

The HT-SEC analyses were performed using a Viscotek system (Malvern Panalytical, Worcestershire, UK) equipped with three columns (PLgel Olexis 300 mm x 7 mm I.D. from Agilent Technologies). 200 µL of sample solution with a concentration of 5 mg mL^{-1} was eluted in 1,2,4-trichlorobenzene at a flow rate of 1 mL min^{-1} at 150°C. The mobile phase was stabilized with 2,6-di(tert-butyl)-4-methylphenol (200 mg L^{-1}). Online detection was performed with a differential refractive index detector, a dual light scattering detector (LALS and RALS) and a viscometer for absolute molar mass measurement. OmniSEC 5.12 software from Malvern Panalytical (Worcestershire, UK) was used for the calculations.

2.4.1 CALIBRATION METHODS

Three main methods using different types of detector were established to measure the molar mass of the sample.

2.4.1.1 Conventional Calibration

Conventional calibration needs only a single concentration detector, a refractive index (RI), to obtain the relative molar masses. They are determined from the elution volume measured by means of a calibration

curve, set up with the standards of known molar masses. The PS and PE standards were used to construct the calibration curves for our HT-SEC.

2.4.1.2 Universal Calibration

To improve conventional calibration, we use an additional detector, the four capillary differential viscometer detector. The viscometer coupled with the refractive index detector makes it possible to construct the universal calibration introduced by Benoit and co-workers in 1967.[20] The universal calibration method has proved to be very convenient. The column is calibrated with a series of certified narrow standards, PS in our case. Using this calibration, absolute molar masses can be assessed for polymers whose chemical composition or structure differs from those of the calibration standards. Nevertheless, a universal calibration curve is available only for a set of columns in a particular solvent and at a particular temperature.

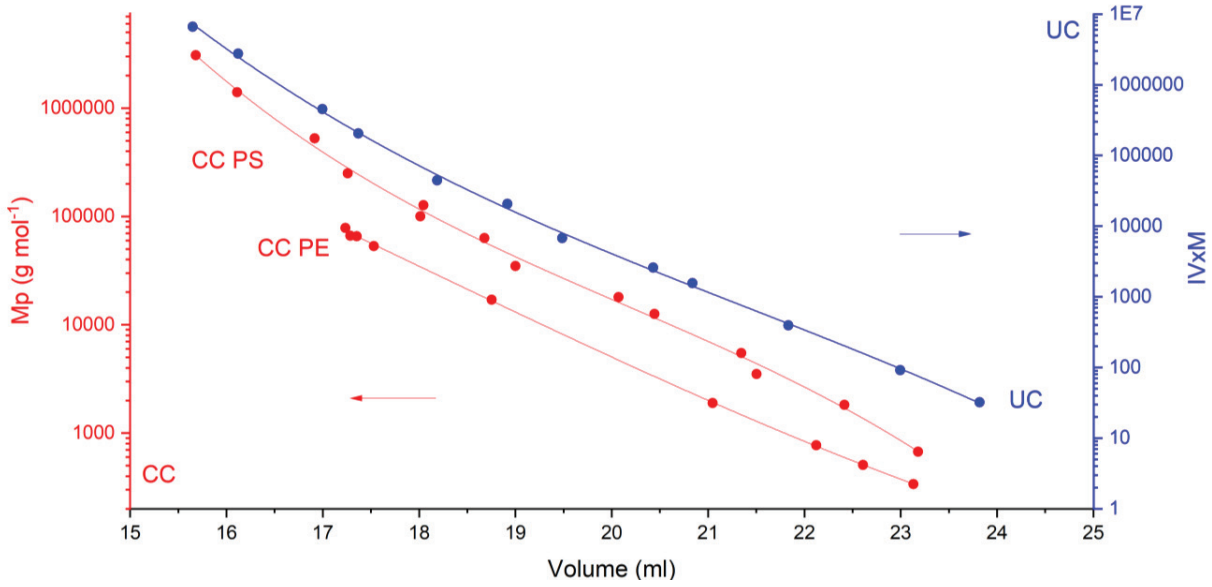


Figure 2-10: Calibration curves for HT-SEC with a curve fit of order 3. Conventional calibration with PS standards (CC PS, red curve), conventionnal calibration with PE standards (CC PE, red curve) and universal calibration with PS standards (UC, blue curve). PLgel Olexis columns (inner diameter: 7.5 mm, length: 300mm, particle size: 13µm) from Agilent were used.

The various calibration curves used in this work are plotted in Figure 2-10. A curve fit order of three was used to correlate the molar mass of standards and the elution time. We observed that the calibrations with PS and PE standards are distinct, showing that the steric hindrances of PS and PE, in 1,2,4-TCB are different.

The universal calibration with the viscometer allows the measurement of absolute molar masses as well as other parameters related to the structure of polymers such as intrinsic viscosity ([η]), hydrodynamic radius (R_h), Mark Houwink parameters (α and K), branching number (Bw), and frequency (λ).

2.4.1.3 Light scattering

With the introduction of online light scattering detection, which also provides the absolute molar mass of a sample, the use of universal calibration has begun to decline. The light scattering method does not depend on column calibration to correlate sample retention volume to molar mass. Light scattering measures the overall intensity of the light scattered from a molecule which is directly proportional to its molar mass using the Rayleigh equation[21] and Debye theory[22, 23]. The treatment method of Zimm[24-26] allowed condensing the results of the light scattering theory in a straightforward equation: [27]

$$\frac{K.c}{R_\theta} = \frac{1}{\bar{M}_w.P(\theta)} + 2.A_2.c \qquad (2\text{-}2)$$

with R_θ being the excess Raylelgh ratio of the scattered light (intensity of the scattered light by the sample in excess of the light scattered by the pure solvent), c is the mass concentration, $\bar{M}_w$ is the weight average molar mass, A_2 is the second virial coefficient.

P(θ), the angular dependence of the scattered light is defined by:

$$P(\theta) = \left(1 + \frac{q^2 R_g^2}{3}\right) \qquad (2\text{-}3)$$

with R_g being the root mean square radius or radius of gyration and q is the form factor calculated by:

$$q = \frac{4\pi.n_0}{\lambda}\sin\left({}^{\theta}/_{2}\right) \qquad (2\text{-}4)$$

where n_0 is the index of refraction of the solvent, λ is the vacuum wavelength of the laser.

Finally, K is a constant calculated by:

$$K = \frac{4\pi^2.(dn/dc)^2 n_0}{N_A.\lambda^4\,.} \qquad (2\text{-}5)$$

Where N_A is Avogadro's number and dn/dc is the refractive index increment of the polymer solution.

To obtain the value of molar mass $\bar{M}_w$ we must calculate the virtual intensity of light scattered at θ=0°. In this case, according to Equations (2-3) and (2-4) sin θ and, therefore, q are both equal to zero, which implies that P(θ) is equivalent to 1. To obtain the intensity of light scattered at θ=0°, two methods can be used. The first method uses an extrapolation of the light scattered at different angles to get that at zero degrees (multi-angle light scattering, MALS). The second solution is the direct measurement of the scattered light close to θ=0° and assume that the difference is negligible. The measurement at θ=0° is practically impossible because the non-scattered laser light overloads the photodiode detector. Therefore, the determination of molar mass is performed with a single angle at θ=7° (low angle light scattering, LALS).

The LALS instrument, with a complementary measurement angle at 90°, is proposed by Malvern Panalytical. Alternatively, MALS instruments are commercially available with two angles (Agilent Technologies), 3 angles, 18 angles (Wyatt Technology), 7 angles (Brookhaven Instruments) and 20 angles (Malvern Panalytical).

According to Equations (2-1) and (2-4) we also need to measure the polymer concentration (c) or to know the value of the refractive index increment (dn/dc).

Light scattering calibration requires no outside standards for column calibration as the sample is measured directly. Nevertheless, it remains necessary to calibrate the system with a standard sample to obtain the detector responses reported in Table 2-4.

Table 2-4: Offset (volume between detector) and calibration factors (constant for each detector) for the light scattering method.

	Offset (ml)	**Calibration factor**
RI	0	287794
RALS	-0.066	5.36×10^{-7}
LALS	-0.066	1.36×10^{-7}
IV	0.099	1.2

RI is the viscometer, RALS and LALS are the right-angle light scattering detector and the low angle light scattering detector, respectively, IV the viscometer detector. The offset is the volume of tubing between the detectors, and the calibration factor is the instrumental constant of each detectors.

2.4.1.4 Reproducibility of molar mass average

The reproducibility of the measurements by HT-SEC was evaluated. A same sample was analyzed under the same conditions over a period of several weeks (Figure 2-10). For each measurement, it was dissolved in TCB at a concentration of 5 mg mL^{-1} and lightly stirred for one hour at 150 °C before injection.

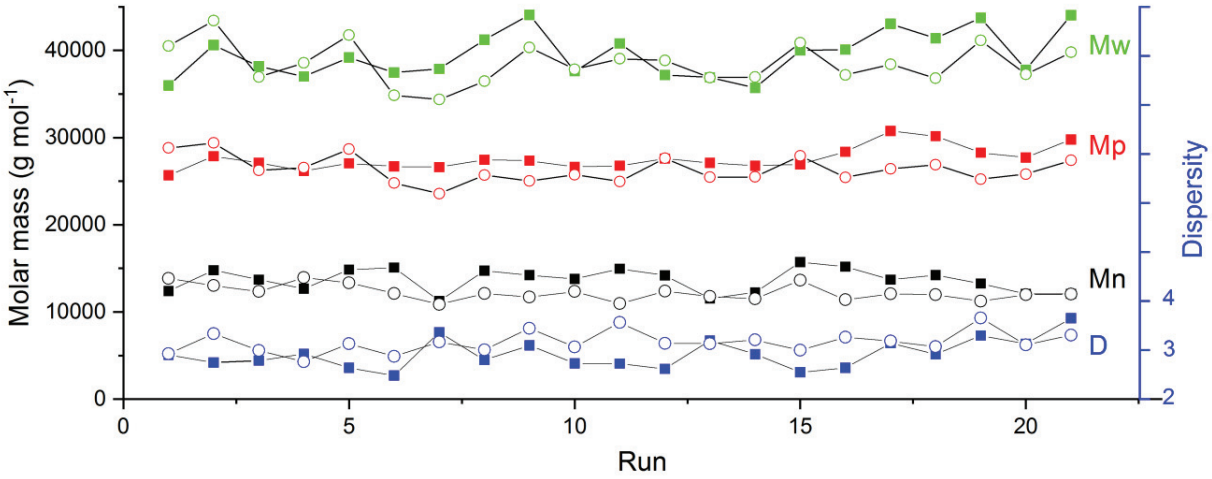


Figure 2-11: Repeatability of average molar masses and dispersity obtained by light scattering (square) and conventional calibration (circle) for a sample of LLDPE.

The data were acquired and processed by light scattering to obtain the absolute molar mass as well as by conventional calibration (created with narrow and certified polyethylene standards) where only the signal from the refractometer was used.

Table 2-5: Values of repeatability measurements obtained by HT-SEC with 21 runs for molar mass average, dispersity and intrinsec viscosity (viscometer detector).

	Light scattering				**Conventional calibration**				**Viscometer**
	$\bar{M}_n$ kg mol^{-1}	M_p kg mol^{-1}	$\bar{M}_w$ kg mol^{-1}	Đ	$\bar{M}_n$ kg mol^{-1}	M_p kg mol^{-1}	$\bar{M}_w$ kg mol^{-1}	Đ	$[\eta]^a$ dl g^{-1}
Average	13.6	27.5	39.5	2.9	12.2	26.3	38.4	3.2	1.30
Standard deviation	1.3	1.3	2.7	0.3	0.9	1.5	2.2	0.2	0.04
%	9.7	4.7	6.7	10.3	7.3	5.7	6.0	6.9	3.1

[a]intrinsic viscosity obtained with the viscometer detector.

The data in Table 2-5 show that the determination of $\bar{M}_n$ has more error than the other values. This is mainly due to the difficulty of integrating the distribution in a repeatable way in the low molar mass side

of the distribution due to the noise and this impacts the value of $\bar{M}_n$ more than that of $\bar{M}_w$. Concerning the measures of intrinsic viscosity ([η]), they show good reproducibility, demonstrating that the viscometer can be used efficiently for the branching calculation in the following part.

Using these experiments, we subsequently consider that the average molar mass will be given with an accuracy of 10% (Table 2-5). This value is higher for HT-SEC compared to ambient temperature SEC because of the noisier detector signal whose noise increases with temperature.

2.4.1.5 Degradation during sample preparation

The analysis conditions, 150 °C in the TCB, are aggressive. Polymers may be degraded during the dissolution step. To limit degradation, an antioxidant (BHT, Butylhydroxytoluene or 2,6-Di-tert-butyl-4-methylphenol) was added in the solvent. This degradation affects the values of the molar masses. Thus, to optimize the dissolution time of the samples, an LLDPE was subjected to high temperature (150 °C) for several hours. This sample was injected regularly, and we monitored the evolution of the molar masses as a function of the time spent at 150 °C (Figure 2-12).

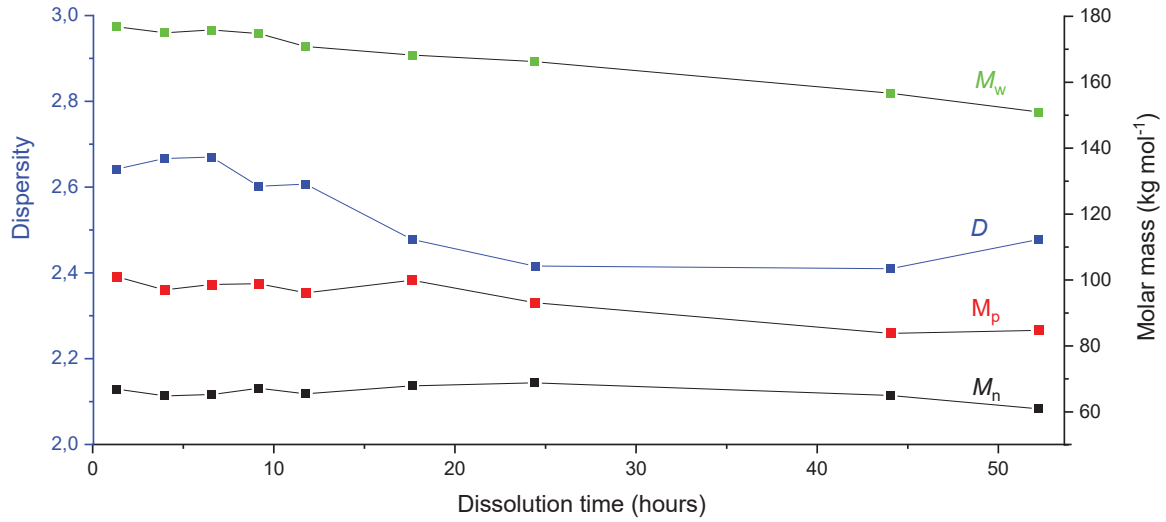


Figure 2-12: Effects of dissolution time at 150°C on the molar masses and dispersity for an LLDPE sample.

The molar masses are stable (inside the measurement error) for up to ten hours at 150 °C, afterwards the values measured decrease significantly. The $\bar{M}_w$ values are more impacted, meaning that the long chains are degraded first and become more breakable.

Therefore, in order to avoid any degradation during preparation, it was necessary to reduce the dissolution time to a maximum of 10 hours. Nitrogen can also be added in the vials during dissolution to remove oxygen and avoid the degradation of the polymer chains.

2.4.1.6 Determination of the molar mass of our LLDPE samples

Various parameters must be known to calibrate the system and analyze the unknown samples.

Table 2-6: Parameters for high temperature size exclusion measurement in 1,2,4 TCB at 150°C.

dn/dc_{PS} [a]	0.052
dn/dc_{PE} [b]	-0.105
dn/dc_{PP} [c]	-0.096
Refractive index of TCB [d]	1.5717
[η] (PS 99 Kg mol^{-1}) [e]	0.41
Factor of concentration variation [f]	0.86

[a]Used to perform universal calibration with PS standards; [b,c]required to measure the absolute molar masses with light scattering and universal calibration for PE and PP samples; [d]used to measure the absolute molar masses with light scattering; [e]Intrinsic viscosity of PS sample with a weight average molar mass of 99 Kg mol^{-1}; used to calibrate the viscometer. [f]Factor used to correct the sample concentration at high temperature, required to obtain the absolute molar masses with light scattering and universal calibration if the dn/dc is not known or to obtain sample recovery.

The factor of concentration variation must be explained since it is specific to HT-SEC and has an impact on the accuracy of the molar mass measurement. The samples are prepared at ambient temperature and analyzed at 150°C; because of the volume expansion due to the temperature, the concentration of the sample decreases. To obtain the volume variation factor, we need to measure the density of TCB at 150°C according to Equation 2-6.

$$D_T = D_{To} e^{-k(T-To)} \qquad (2\text{-}6)$$

Where D_T (g ml^{-1}) is the effective density of the solvent at temperature T, D_{To} (g ml^{-1}) is the density of the solvent at a reference temperature, at 25°C it is equal to 1.4547 g ml^{-1}, k is the temperature coefficient (0.0012), T is the experimental temperature and To is the reference temperature (°C).

At 150°C, the calculated value for D_T is 1.252 g ml^{-1}. The volume variation factor is therefore 1.4745/1.252 = 1.1619. Therefore, the factor used to correct the concentration is 1/1.1619 = 0.86. The concentration of the samples prepared at ambient temperature and analyzed at 150°C should be multiplied by this factor.

Our model samples were analyzed by the different calibration methods, but the results showed similar values. Therefore, only the molar masses obtained by light scattering were reported in the characterization results which are summarized in Appendix 1. We observed that the molar masses of the copolymers prepared with $Et(Ind)_2ZrCl_2$ and $(n\text{-}BuCp)_2ZrCl_2$ were dependent on the comonomer content. They decreased slightly as the comonomer content increased. This behavior was observed and reported previously.[28]

2.4.2 LONG CHAIN BRANCHING

Molar mass and its distribution, short chain branching (SCB) and long chain branching (LCB) are the key parameters that control the properties of LLDPE. The LCB can change the melt rheological behavior and enhance the processability of PE. During polymerization, few polymer chains are produced with unsaturated vinyl chain ends. Depending on the conditions, these macromonomers can be inserted into a growing polymer chain resulting in LCB. Although this has not been discussed extensively in the literature, we can assume that LCB may influence the elution time measured by thermal fractionation techniques. It is, therefore, of great importance to evaluate the LCB content in our samples. This part will discuss the method used to measure LCB by HT-SEC.

2.4.2.1 Calculation method

Depending on the polymerization method, PEs have different amounts of long chain branching (LCB). HDPEs obtained with Ziegler-Natta catalysts have a linear structure and contain only a few SCBs and no LCBs. For LDPE, obtained by free-radical polymerization at high temperatures and pressures, LCB is due to intermolecular chain transfer instead of short chain branching, resulting from intramolecular chain transfer.[29] Chromium catalysts produce polyethylene with small amounts of LCB. LCB has been the topic of intense investigation in the case of polymers obtained with metallocene catalysis. CGC catalyst was the first single site system reported to produce LCB.[30] The Cp_2ZrCl_2 and $Et(Ind)_2ZrCl_2$ catalysts with MAO have been reported to also produce few LCBs in polyethylene.[31]

This part of the work consists in investigating LCB content and frequency using size exclusion chromatography. Both the molar mass and the intrinsic viscosity of each fraction of the eluted polymer can be determined with light scattering detector (LALS and RALS) and viscometer detector. The LCB frequency can be obtained from either the viscometer detector or the light scattering detector, as explained in the following part.

The product of the intrinsic viscosity $[\eta]$ and molar mass M is proportional to the size of the molecule (hydrodynamic volume V_h), which is the basis of the separation performed in the chromatograph column (Equation 2-7).

$$V_h = k \,.\, M\,[\eta] \qquad (2\text{-}7)$$

The intrinsic viscosity of a dilute polymer is described by the empirical Mark-Houwink-Sakurada (MHS) Equation 2-8.

$$[\eta] = K.M^{\alpha} \qquad (2\text{-}8)$$

where K and α are the MHS constants.

Parameter α depends on the temperature and solvent and according to Flory[32] it varies from 0.5 for theta conditions to 0.8 in a good solvent.

For a given molar mass, branched polymer chains have a smaller hydrodynamic volume than linear ones.[33-35] The intrinsic viscosity ratio between a branched polymer and a linear one with the same molar mass leads to the viscosity branching factor, g' (Equation 2-9). Its value is comprised between 0 and 1.

$$g' = \frac{[\eta]_b}{[\eta]_l} \qquad (2\text{-}9)$$

where $[\eta]$ is the intrinsic viscosity for the branched (b) and linear polymer (l) considered at the same molar mass fraction.

The branching factor g (Equation 2-10), obtained by the ratio of the radius of gyration of the branched polymer to the radius of gyration of a linear one, is calculated by light scattering detection.

$$g = \frac{< R_g^2 >_b}{< R_g^2 >_l} \qquad (2\text{-}10)$$

where $\langle R_g^2 \rangle$ is the mean-square radius of gyration for the branched (b) and linear polymer (l) considered at the same molar mass fraction.

g is used for measuring the number of LCBs, according to equation 2-10, when the measurement is performed with a light scattering detector. To reach this value, the gyration radius (R_g) of the macromolecule should be accessed, and for this purpose the molar masses must be sufficiently high. This is not the case for our samples. As described below, conditions of angular dependence are necessary to be able to measure R_g.

Angular dependence: *At high molar mass (R_g > 15 nm), the intensity of scattered light varies with the measurement angle (anisotropic scatterers), but for low molar mass (R_g < 15 nm) there is no angular dependence on the intensity of the scattered light (isotropic scatterers). R_g (Equation 2-2) is calculated by measuring the slope of the angular dependence curve with the intensity of the scattered light. In isotropic condition, the slope of the curve is zero and does not allow the measurement of R_g. The data cannot be used to calculate R_g. We commonly estimate that R_g has a value of 15 nm for a PE around 100 Kg mol^{-1}, meaning that for our polymers with lower molar mass, light scattering cannot be used to measure R_g and therefore the number of LCBs. In this case, the viscometer data should be used.*

Assuming Flory-Fox[32] the relationship between the viscosity branching factor (g') and the branching factor (g) can be expressed by Equation 2-11.

$$g' = g^{\varepsilon} \qquad (2\text{-}11)$$

where ε is the drainage factor.

It depends on the measurement conditions (solvent, temperature) and also on the type of branching.[36] The reported values of ε for polymer samples are in the range of 0.5-1.5.[34, 37, 38] It is 0.5 for a star branched polymer and 1.5 for a comb branched polymer. For LLDPE under identical experimental conditions, a value of 0.75 for ε was determined previously.[39, 40] We have used this value for our calculations.

Zimm and Stockmayer proposed different formulae corresponding to each type of branching. They demonstrated that for randomly branched polymers whose branches are tri-functional and randomly distributed in length, the branching factor (g)[34] and the branching frequency (λ) can be deduced from Equation 2-12 and 2-13, respectively.

$$g = \frac{6}{\bar{B}_w}\frac{1}{2}\left[\left(\frac{2+\bar{B}_w^{\frac{1}{2}}}{\bar{B}_w}\right) ln\left(\frac{(2+\bar{B}_w)^{\frac{1}{2}}+\bar{B}_w^{\frac{1}{2}}}{(2+\bar{B}_w)^{\frac{1}{2}}-\bar{B}_w^{\frac{1}{2}}}\right)-1\right] \qquad (2\text{-}12)$$

where $\bar{B_w}$ is the weight-average number of branch points per molecule (branching number).

$$\lambda = \frac{1000\ \mathrm{M_0}\ \bar{\mathrm{B}}\mathrm{w}}{M_i} \qquad (2\text{-}13)$$

where M_0 is the molar mass of the repetitive unit (CH_2: 14 g mol^{-1}) and M_i the molar mass for the elution fraction i.

2.4.2.2 Long chain branching content in LDPE and HDPE

Multidetector HT-SEC allows the simultaneous and independent calculation of intrinsic viscosity and molar mass for each elution fraction.

The intrinsic viscosity versus molar mass, also called the Mark-Houwink-Sakurada plot (MHS)[41], can be plotted on the entire molar mass distribution. In this work we have used the MHS plot to quantify the LCB in our LLDPE, as described by various researchers.[42-45]

Before analyzing our LLDPE samples, we studied 3 commercial LDPE samples containing SCB and LCB. In contrast, a certified polyethylene sample (BRPE0) was used as non-branched sample. Unfortunately, its range of molar masses is rather low and was not appropriate for comparison with the other samples. Hence, it seemed interesting to add an HDPE sample synthetized with a Ziegler-Natta catalyst known to have no branching (dark blue curve in Figure 2-12). In addition, a certified branched LDPE (BRPE14) was also analyzed (green curve in Figure 2-12).

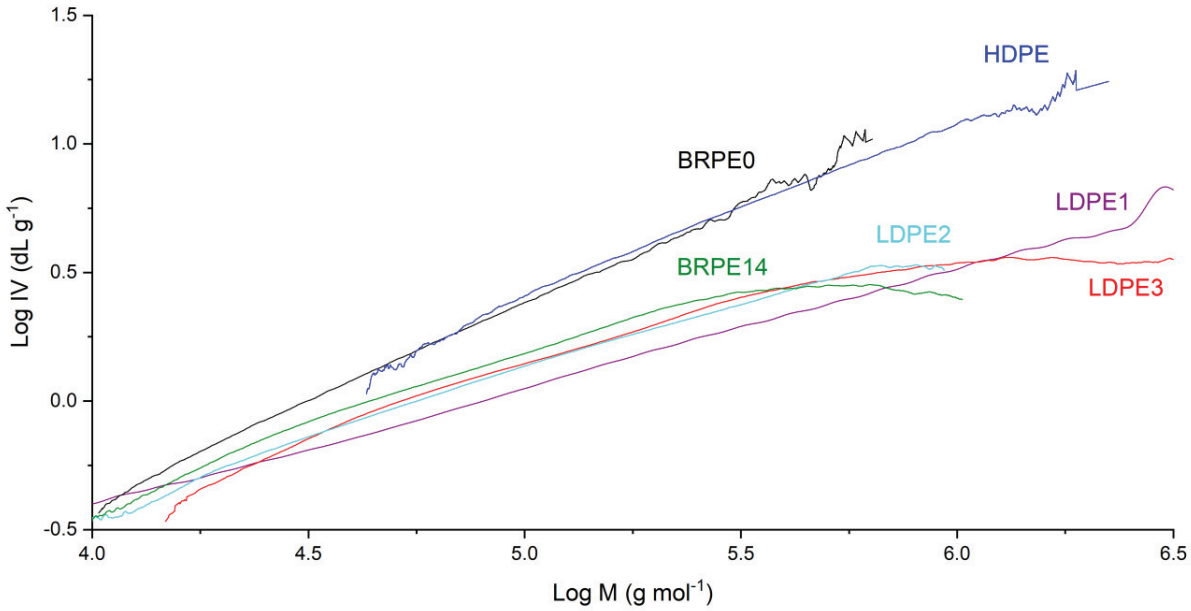


Figure 2-13: Mark-Houwink-Sakurada plot for 5 PE samples and a linear reference polymer (black line). The dark blue curve is an HDPE from the Ziegler-Natta catalyst, LDPE1 is LPDE 165 from Exxon Mobil, LDPE2 and LDPE3 are LDPE3020 and LDPE Lupolen 3020, respectively, from LyondellBasell. BRPE0 and BRPE14, linear and branched, respectively, are reference materials.

The MHSs plotted of the LDPE samples were constructed and compared to the linear certified reference and HDPE. The MHS plot of the HDPE fits well with the linear reference and shows that the sample has no

branch. It was used, as a linear reference in addition to the certified polyethylene, to increase the molar mass range that can be studied.

Concerning LDPE, the MHS plot shows that, at a given molar mass, the intrinsic viscosity is lower than that of the linear structure due to the smaller hydrodynamic size of the branched molecules. The amplified deviation of the LDPE viscosity from the linear reference with an increase in molar masses is characteristic of a randomly branched polymer.

It can be seen that the intrinsic viscosity curves of HDPE and LDPE do not intersect at low molar mass. Wood-Adams[41] reported that this behavior is correlated to the presence of SCB in the LDPE.

Table 2-7: Zimm-Stockmayer equations applied to HDPE, LDPE and certified PE samples.

Sample	$\bar{M}_w$ Kg mol^{-1}	$\bar{M}_n$ Kg mol^{-1}	[η] dL g^{-1}	R_h[a] nm	α[b]	Log K[b]	λ[c] for 1000 C
LDPE1	240.6	24.4	1.2	16.0	0.47	-2.30	5.5
LDPE2	100.3	27.1	1.1	11.7	0.54	-2.62	2.8
LDPE3	90.5	19.1	1.0	10.8	0.53	-2.53	2.8
BRPE 0[d]	48.5 (52.0)	17.1 (18.3)	1.0 (1.01)	8.4	0.71	-3.20	(0)
BRPE 14[d]	79.9 (88.2)	22.2 (23.0)	0.9 (0.90)	9.8	0.57	-2.67	1.6 (1.4)
HDPE	254.8	110.7	4.6	25.8	0.69	-3.01	0.01

[a]hydrodynamic radius calculated with intrinsic viscosity and molar mass, [b]MHS parameters obtained with the slope and the intercept of the curve, [c]long chain branching frequency per 1000 carbon atoms, [d]certified PE samples purchased from American Polymer Standards, the certified values given by the producer are in brackets, the other values were acquired by HT-SEC.

Some parameters can be obtained with the MHS plots to characterize the polymers, they are reported in Table 2-7. The hydrodynamic radius of the polymer is calculated according to the viscosity relation (Equation 2-14) where the volume of the macromolecule is replaced by the hydrodynamic radius, as proposed by Flory and Fox:[32]

$$R_h = \left(\frac{3\,[\eta]\,M}{10\,\pi\,N_A}\right)^{1/3} \qquad (2\text{-}14)$$

with N_A being the Avogadro's constant, and [η] the intrinsic viscosity.

The slope and intercept of the MHS curve provide the α and K Mark-Houwink parameters, respectively, according to Equation 2-15.

$$\log [\eta] = \log K + \alpha \log M \qquad (2\text{-}15)$$

The calculation of the MHS parameters clearly shows that the slope, affected by the branching, is lower for LDPE (α = 0.5) than for HDPE (α = 0.7). LDPE1 with the lower α value is the most branched polymer. These values are in accordance with values reported in previous work on polyethylene in TCB.[46-48]

The Zimm-Stockmayer equations can be used to quantify the branching content, step by step, following the procedure below. The value λ represents the LCB frequency for 1,000 carbon atoms. To obtain this value, initially, the intrinsic viscosity of the sample was divided by the intrinsic viscosity of the linear reference (HDPE) for each slice of the molar mass distribution. The ratio g' was calculated using Equation 2-9. It is plotted for each slice of the distribution with the blue curve in Figure 2-14. The next step was the calculation of the branching factor (g) obtained with Equation 2-11 and 0.75 as the value for ε. Afterwards, Equation 2-12 allowed the calculation of the number of branches (Bw), plotted by the red curve in Figure 2-14. Last but not least, the branch frequency (λ) was calculated with Equation 2-13 and plotted for each slice of the distribution (green curve).

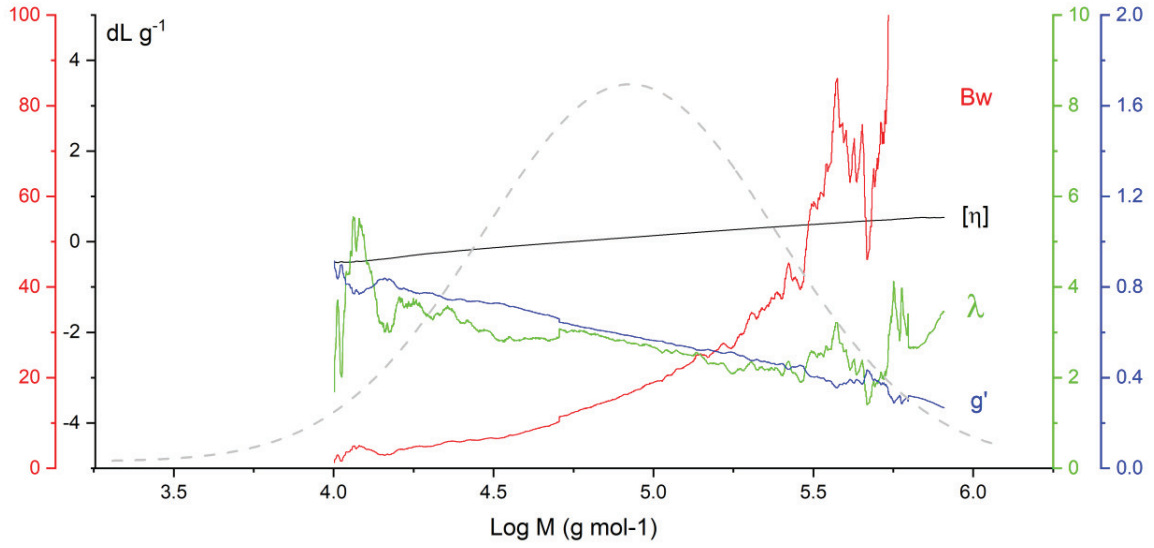


Figure 2-14: Molar mass distribution (grey dash) and viscometer parameters calculated with MHS equations for sample LDPE2.

We observe that the number of branches (Bw, red curve) is not constant in the molar mass distribution; it increases with the molar mass of the chains. When the chains are longer, they are more branched even if branch frequency decreases (λ, green curve).

The λ value obtained for the certified branched polymer (1.6 branches for 1,000 C) is quite similar to the certified value (1.4 branches for 1,000 C) which validates the method. The branch frequency is calculated close to zero for the HDPE sample, as expected. Conversely, LDPE1, with a branch frequency of 5.5 branches for 1,000 C, is the most branched sample.

The LCB frequency was calculated by comparing the viscosity of a branched polymer with that of a linear one using the Zimm–Stockmayer methodology. The HT-SEC with the viscometer detector is a powerful technique capable of obtaining the molar masses distribution and structural information at the same time. The method was applied for our LLDPE samples to determine their LCB content. Previously, the LCB amount was calculated by ^{13}C NMR to compare the results obtained by HT-SEC and validate the method.

2.4.2.3 Long chain branching calculation by ^{13}C NMR

The ^{13}C NMR spectroscopy provides another experimental technique for measuring LCB.[14] Unlike the SEC, it gives directly LCB content without using references. Three representative LLDPE models with various comonomer contents were selected to study their LCB by ^{13}C NMR (Figure 2-15).

Conventionally, the signal at about 14 ppm linked to CH_3 is used. However, this method has a limitation. When the α-olefin comonomer has more than six carbon atoms, the chemical shift detected for LCB is the same as that detected for the inserted comonomer. Recent studies have reported that it is possible to differentiate branches longer than six carbon atoms, but this requires high-resolution experiments.[49] A second and more critical restriction is that this approach cannot separate the CH_3 of branches from the CH_3 of chain ends, which cannot be negligible in the case of low levels of LCB.

Given these considerations we decided to use a CH signal at 38 ppm. The CH from the butyl branch is clearly visible at 38.0 ppm for the EC12 sample. At low comonomer content (IB10), we can observe close to this signal at 38.1 ppm another signal which we have assigned to the CH of the LCB. This signal is easy to integrate when the content of the comonomer remains low (IB10 and EC01). As the comonomer content increases, the signal from the LCB overlaps the butyl branch signal and cannot be used to calculate the LCB content. The LCB frequency was determined for three LLDPE samples with no or low comonomer content. The values, calculated with the signal at 38.0 ppm, are reported in Table 2-8.

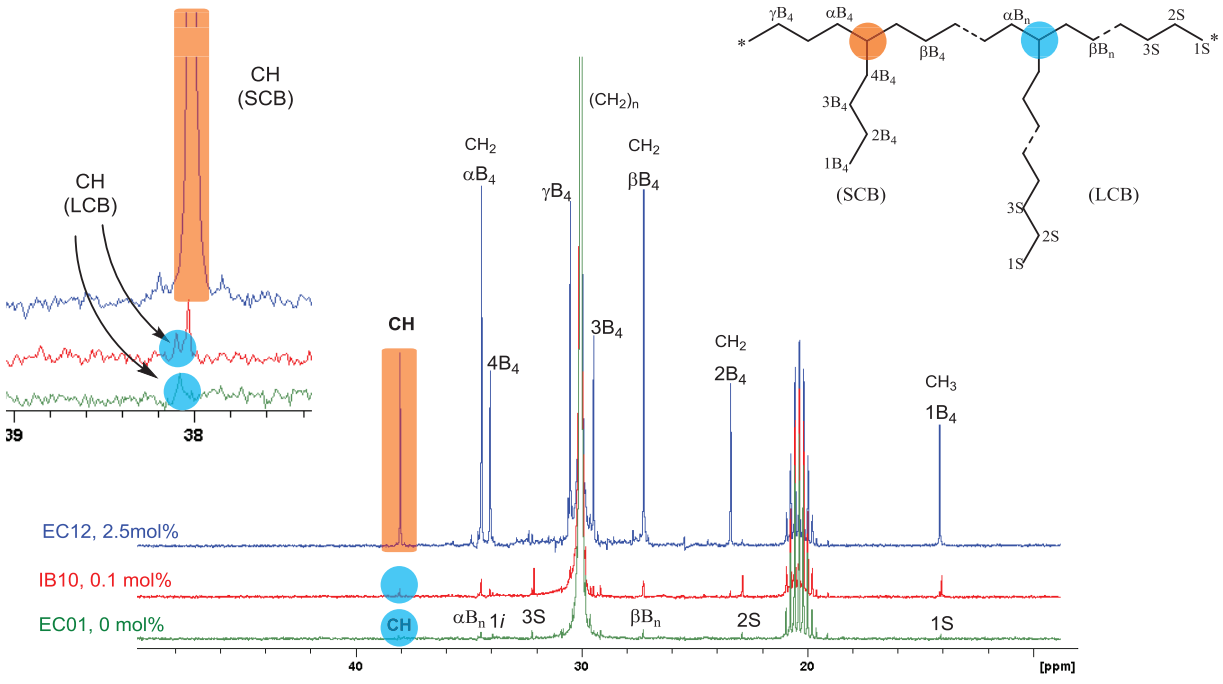


Figure 2-15: 13C NMR spectrum of an HDPE EC01 (0 mol%) and ethylene-hexene copolymer IB10 (0.1 mol% of hexene) and EC12 (2.5 mol% of hexene) in TCB/toluene-d8 at 373 K and assignments of short chain branching (SCB) and long chain branching (LCB).

2.4.2.4 Branching in our LLDPE samples

Initially, we measured the impact of LCB on the MHS plot using HDPE and LDPE. Concerning our LLDPE models containing mainly SCB, we can expect a mixed behavior in the MHS plot. According to Soares and Hamielec, few LCBs are also present in LLDPE obtained by metallocene catalysts.[31, 50] Six ethylene-hexene copolymers with various hexene contents from zero to 20.7 mol% were analyzed. Their MHS curves were plotted in Figure 2-15 and compared to the linear reference (BRPE0, black curve). The plot of the homopolyethylene sample EC01 (pink curve, Figure 2-16) attests the presence of few LCBs because the intrinsic viscosity of the sample is slightly lower than that of the linear reference, in high molar mass portion. The curves follow a straight line that can be described by the MHS coefficients (α and K). Nevertheless, unlike LCB, SCB did not affect the slope of the curve but the K parameters. Figure 2-15 shows that the MHS plot for various LLDPE shifts downwards as the comonomer content increases. All curves are linear in the low molar mass portion of the distribution and tend to curve slightly for samples EC01 and

EC12 in the high molar mass portion, highlighting that LCBs are prevalent in high molar mass chains for these samples.

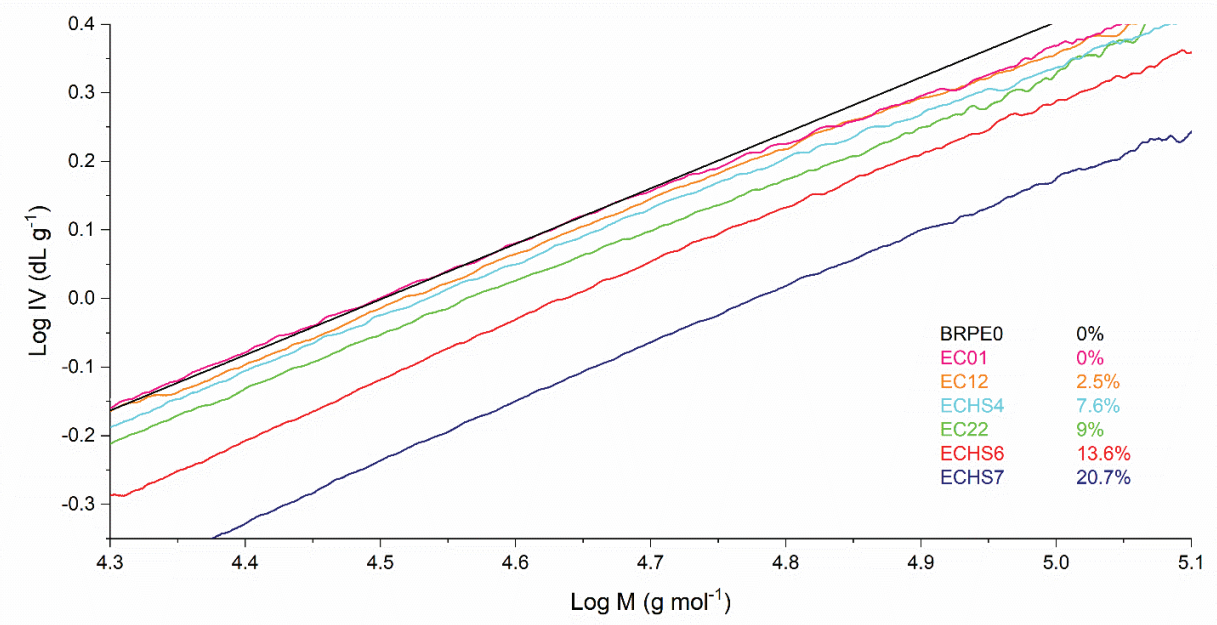


Figure 2-16: Mark-Houwink-Sakurada plot for six LLDPE samples with a linear PE reference (black line). [η] is the intrinsic viscosity in dL g^{-1}, and M is the molar mass of the polymer.

K and α values were calculated and are reported in Table 2-8.

Table 2-8: Determination of Mark-Houwink-Sakurada parameters and the branching frequency for several samples.

Sample	**Comonomer** (mol%)	**[η]**[a] (dL g^{-1})	**α**	**Log K**	**λ_{SEC}**[b] (CH_3/1000C)	**λ_{NMR}**[c] (CH_3/1000C)
BRPE0	0	1.0	0.71	-3.20		
EC01	0	1.1	0.70	-3.19	0.25	0.17
IB10	0.1	1.1	0.71	-3.18	0.62	0.73
EC12	2.5	1.0	0.72	-3.18	0.09*	-
ECHS4	7.6	0.97	0.70	-3.26	0.02*	
EC22	9	0.94	0.71	-3.76	<0.02*	
ECHS6	13.6	0.99	0.72	-3.84	<0.02*	
ECHS7	20.7	0.98	0.72	-4.08	<0.02*	

The samples were analyzed consecutively in the same sequence, and the data were processed with the same calibration. [a]Intrinsic viscosity value. The average number of branch points per 1,000 carbon atoms

(branching frequency) determined by [b]HT-SEC using Zimm-Stockmayer equations and [c]NMR (BBO probe of 10 mm in TCB/toluen-d8 3/1 at 100°C) using the signal at 38 ppm (method described in the previous part). *calculated value of LCB using a SCB correction as described below.

For samples EC01 and IB10, Table 2-8 shows that the values obtained with the HT-SEC measurements agree well with the values of the ^{13}C NMR. These results demonstrated the high sensitivity of this method to very low levels of LCB. Since the viscometer detector is very sensitive to high molar masses, we obtained high-quality data from this part of the distribution and thus high sensitivity.

However, for the other samples with higher comonomer contents, the Zimm-Stockmayer equations could not be used to calculate the LCB due to the presence of a non-negligible amount of SCB. Indeed, the presence of SCB in the copolymers affected the viscosity of the sample. Their LCB contents could not be measured before the SCB effect was corrected. Since the low molar mass part of the distribution was not affected by LCB but only by SCB, we use this part to determine the α and k values impacted only by SCB. These values were used as a virtual linear reference to calculate the LCB content for the whole distribution by applying the Zimm-Stockmayer equations.

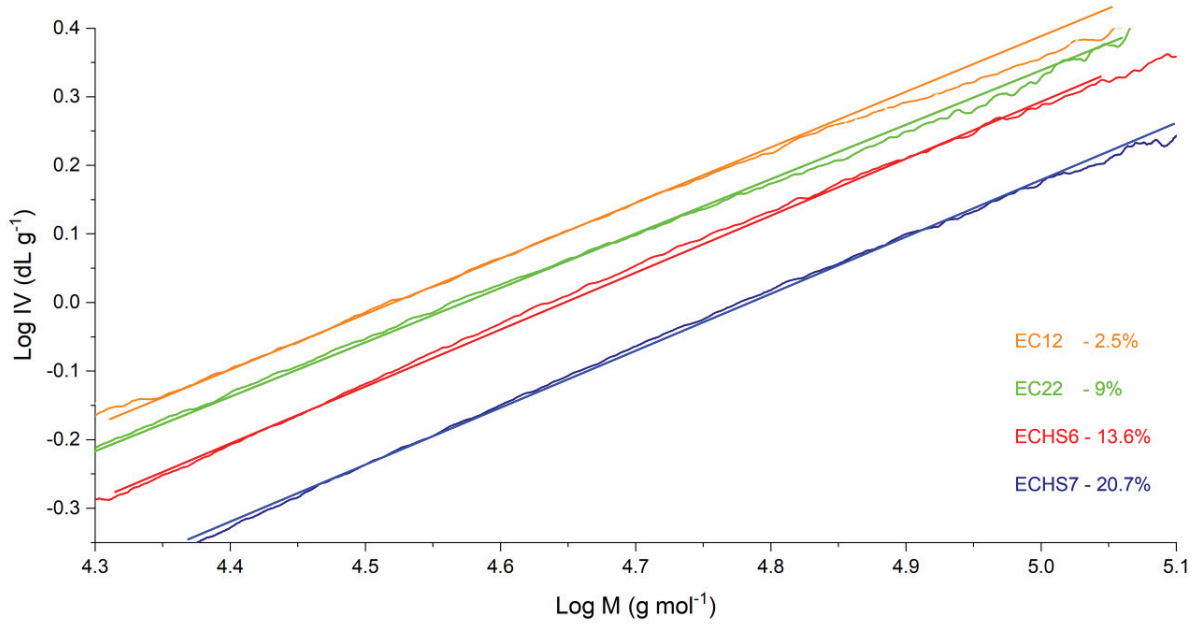


Figure 2-17: Correction of SCB impact on viscosity. The curve simulates a linear reference without LCB, fitted with the value of viscosity in the low molar masses part of the distribution and extrapolated for high molar masses. For the sake of clarity, all the samples are not plotted in the figure.

For each sample, a linear curve depicting a virtual reference without LCB, was constructed using the low molar mass portion (M < Log 4.8). These linear curves were used to determine the intrinsic viscosity over

the entire molar mass distribution that a polymer without LCB would have. We can therefore calculate g' (Equation 2-9) with the new values of $[\eta]_l$ and determine the LCB content with the Zimm-Stockmayer equations. With this method, the SCB content did not affect the LCB calculation. The values obtained are reported in Table 2-8.

The linear curves of the virtual references are all parallel to that of the linear control (BRPE0). The slopes of these curves were found to be similar and equal to 0.71±0.01. These curves and the calculated values (with an asterisk in Table 2-8) show that the LCB content is low and decreases when the comonomer content increases in LLDPE samples. No curvature on the high molar mass portion of the MHS plots was observed for the samples with high comonomer content, which confirmed the absence or low level of LCB.

Deslauriers and co-workers have described an alternative LCB determination method by multiangle light scattering.[51] They have also established a similar method to correct SCB effects using infrared and NMR results. Yau and co-workers have also proposed a new approach to correct the SCB in the measurement of LCB for LDPE samples.[52]

We clearly observed, from the results in Table 2-8, the decrease in the Log K value with increasing comonomer level in the copolymer. The variation of Log K with the comonomer content was plotted in Figure 2-18 and a calibration curve using a first order polynomial that fits the experimental data was drawn.

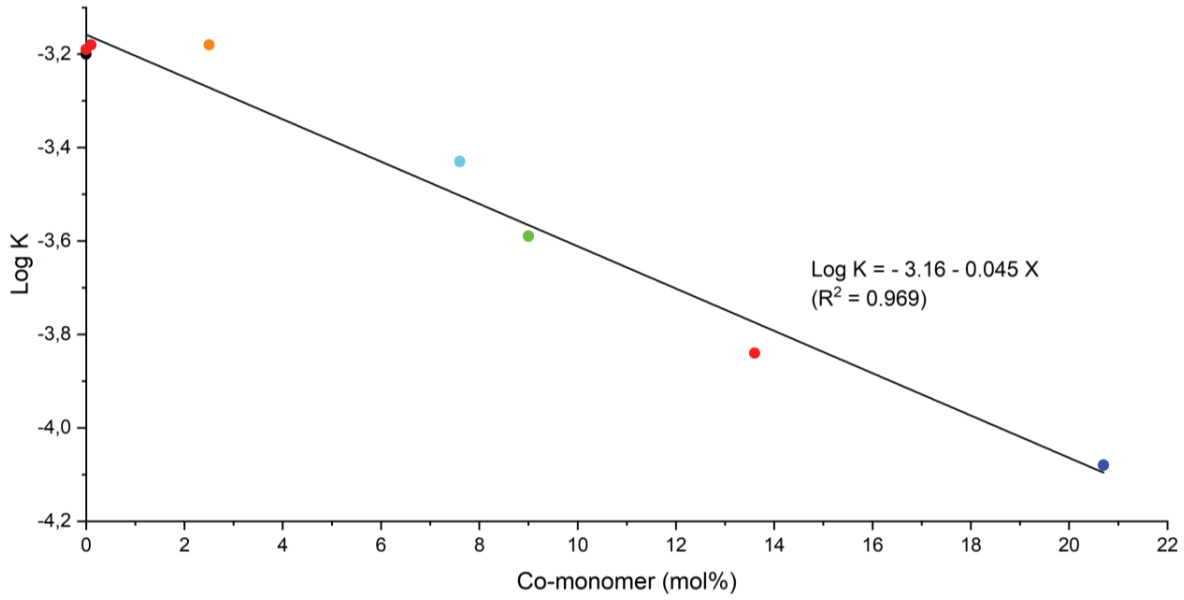


Figure 2-18: Log K measured with the viscometer detector versus comonomer content (hexene) in mol%.

In conclusion, the Mark-Houwink-Sakurada plot gives clear insights about the branching of PE. We can measure the impact of LCBs, in high molar mass portion of the distribution, with the local slope of the curves which is related to the α value of Mark-Houwink-Sakurada. In an original approach, we proved that the influence of short chain branching (comonomer content) is transcribed on the K value of Mark-Houwink-Sakurada. Using the plot in Figure 2-18, we can generate a calibration curve that can be applied to unknown PE samples to measure the comonomer content by using Log K value obtained by HT-SEC:

$$\text{Comonomer content (mol\%)} = 44.22 + 38.12 \log K + 7.91 (\log K)^2 \qquad (2\text{-}16)$$

With R-Square = 0.987

2.5 CONCLUSION

Eighty-eight LLDPE samples were obtained through the copolymerization of ethylene with various sort of α-olefines using metallocene-type catalyst. The rac-Et(Ind)$_2$ZrCl$_2$ and (nBuCp)$_2$ZrCl$_2$ complexes were used and lead in homogeneous samples both in molar masses and in chemical composition. The resulting copolymers constitute a wide range of LLDPE with varying amounts of comonomers and different types of comonomers. They constituted our standards for the following parts. They are also representative of industrial LLDPEs that can be found in daily life.

The copolymer models have been characterized. First and foremost, the comonomer content was determined by ^{1}H NMR and ^{13}C NMR. The calculation methods adapted to each comonomer have been described in this part.

Furthermore, the molar masses were measured by HT-SEC showing similar values between samples and, as expected, narrow distributions for all of them. The values are reported in Appendix 1.

Lastly, the viscometer detector and the Zimm-Stockmayer equations were also involved to measure the LCB in our copolymer. The results were compared with NMR measurements. Since elution in fractionation techniques can be influenced by LCB, it is necessary to measure their content in our models beforehand. This study demonstrated the low content of LCB. Based on these results, we assumed that LCB would have a negligible effect to the elution of samples when analyzed by fractionation techniques.

REFERENCES - CHAPTER II

[1] F. Prades, J.-P. Broyer, I. Belaid, O. Boyron, O. Miserque, R. Spitz, C. Boisson, *ACS Catal.* **2013**, *3*, 2288.

[2] P. Lehmus, O. Härkki, R. Leino, H. J. G. Luttikhedde, J. H. Näsman, J. V. Seppälä, *Macromolecular Chemistry and Physics* **1998**, *199*, 1965.

[3] T. Uozumi, K. Soga, *Die Makromolekulare Chemie* **1992**, *193*, 823.

[4] C. Lehtinen, B. Löfgren, *European Polymer Journal* **1997**, *33*, 115.

[5] F. Malz, H. Jancke, *Journal of Pharmaceutical and Biomedical Analysis* **2005**, *38*, 813.

[6] Q. Wu, A. García-Peñas, R. Barranco-García, M. L. Cerrada, R. Benavente, E. Pérez, J. M. Gómez-Elvira, *Polymers* **2019**, *11*, 1266.

[7] V. Busico, R. Cipullo, N. Friederichs, H. Linssen, A. Segre, V. Van Axel Castelli, G. van der Velden, *Macromolecules* **2005**, *38*, 6988.

[8] A. Carvill, L. Zetta, G. Zannoni, M. C. Sacchi, *Macromolecules* **1998**, *31*, 3783.

[9] A. Albrecht, R. Brüll, T. Macko, H. Pasch, *Macromolecules* **2007**, *40*, 5545.

[10] M. Kakugo, T. Miyatake, Y. Naito, K. Mizunuma, *Macromolecules* **1988**, *21*, 314.

[11] V. Busico, R. Cipullo, G. Monaco, G. Talarico, M. Vacatello, J. C. Chadwick, A. L. Segre, O. Sudmeijer, *Macromolecules* **1999**, *32*, 4173.

[12] B. Zhang, Q. Dong, Z. Fu, Z. Fan, *Polymer* **2014**, *55*, 4865.

[13] J. C. Randall, *Journal of Polymer Science: Polymer Physics Edition* **1973**, *11*, 275.

[14] J. C. Randall, *Journal of Macromolecular Science, Part C* **1989**, *29*, 201.

[15] T. Hayashi, Y. Inoue, R. Chujo, T. Asakura, *Polymer* **1988**, *29*, 1848.

[16] Z. Zhou, R. Kümmerle, J. C. Stevens, D. Redwine, Y. He, X. Qiu, R. Cong, J. Klosin, N. Montañez, G. Roof, *Journal of Magnetic Resonance* **2009**, *200*, 328.

[17] C. H. Bergström, B. R. Sperlich, J. Ruotoistenmäki, J. V. Seppälä, *Journal of Polymer Science Part A: Polymer Chemistry* **1998**, *36*, 1633.

[18] G. B. Galland, R. F. de Souza, R. S. Mauler, F. F. Nunes, *Macromolecules* **1999**, *32*, 1620.

[19] "High-Temperature SEC and Rheological Connections", in *Modern Size-Exclusion Liquid Chromatography*, p. 434.

[20] Z. Grubisic, P. Rempp, H. Benoit, *Journal of Polymer Science Part B: Polymer Letters* **1967**, *5*, 753.

[21] L. Rayleigh, *The London, Edinburgh, and Dublin Philosophical Magazine and Journal of Science* **1899**, *47*, 375.

[22] P. Debye, *The Journal of Physical and Colloid Chemistry* **1947**, *51*, 18.

[23] P. Debye, E. A., *Journal of Applied Physics* **1944**, *15*, 338.

[24] B. H. Zimm, *The Journal of Chemical Physics* **1945**, *13*, 141.

[25] B. H. Zimm, *The Journal of Chemical Physics* **1948**, *16*, 1093.

[26] B. H. Zimm, S. R. S., D. P. M., *The Journal of Chemical Physics* **1948**, *16*, 1099.

[27] P. J. Wyatt, *Analytica Chimica Acta* **1993**, *272*, 1.

[28] E. Kokko, A. Malmberg, P. Lehmus, B. Löfgren, J. V. Seppälä, *Journal of Polymer Science Part A: Polymer Chemistry* **2000**, *38*, 376.

[29] A. Santamaria, *Materials Chemistry and Physics* **1985**, *12*, 1.

[30] J. F. Vega, A. Muñoz-Escalona, A. Santamaría, M. E. Muñoz, P. Lafuente, *Macromolecules* **1996**, *29*, 960.

[31] E. Kolodka, W. J. Wang, P. A. Charpentier, S. Zhu, A. E. Hamielec, *Polymer* **2000**, *41*, 3985.

[32] P. J. Flory, T. G. Fox, *Journal of the American Chemical Society* **1951**, *73*, 1904.

[33] T. G. Scholte, N. L. J. Meijerink, *British Polymer Journal* **1977**, *9*, 133.

[34] B. H. Zimm, W. H. Stockmayer, *The Journal of Chemical Physics* **1949**, *17*, 1301.

[35] B. H. Zimm, R. W. Kilb, *Journal of Polymer Science* **1959**, *37*, 19.

[36] P. J. Flory, "*Principles of polymer chemistry*", Cornell University Press, 1953.

[37] W.-J. Wang, S. Kharchenko, K. Migler, S. Zhu, *Polymer* **2004**, *45*, 6495.

[38] R. Kuhn, H. Krömer, *Colloid & Polymer Science* **1982**, *260*, 1083.

[39] A. M. Striegel, M. R. Krejsa, *Journal of Polymer Science Part B: Polymer Physics* **2000**, *38*, 3120.

[40] G. Foster, A. Hamielec, T. MacRury, "The Molecular Weight and Branching Distribution Method", ACS Publications, 1980.

[41] P. M. Wood-Adams, J. M. Dealy, A. W. deGroot, O. D. Redwine, *Macromolecules* **2000**, *33*, 7489.

[42] S. T. Balke, T. H. Mourey, C. P. Lusignan, *International Journal of Polymer Analysis and Characterization* **2006**, *11*, 21.

[43] L. Wild, R. Guliana, *Journal of Polymer Science Part A-2: Polymer Physics* **1967**, *5*, 1087.

[44] R. N. Shroff, H. Mavridis, *Macromolecules* **1999**, *32*, 8454.

[45] A. Striegel, W. W. Yau, J. J. Kirkland, D. D. Bly, "*Modern size-exclusion liquid chromatography: practice of gel permeation and gel filtration chromatography*", John Wiley & Sons, 2009.

[46] T. G. Scholte, N. L. J. Meijerink, H. M. Schoffeleers, A. M. G. Brands, *Journal of Applied Polymer Science* **1984**, *29*, 3763.

[47] H. L. Wagner, *Journal of Physical and Chemical Reference Data* **1985**, *14*, 611.

[48] V. R. Raju, G. G. Smith, G. Marin, J. R. Knox, W. W. Graessley, *Journal of Polymer Science: Polymer Physics Edition* **1979**, *17*, 1183.

[49] L. Hou, G. Fan, M. Guo, E. Hsieh, J. Qiao, *Polymer* **2012**, *53*, 4329.

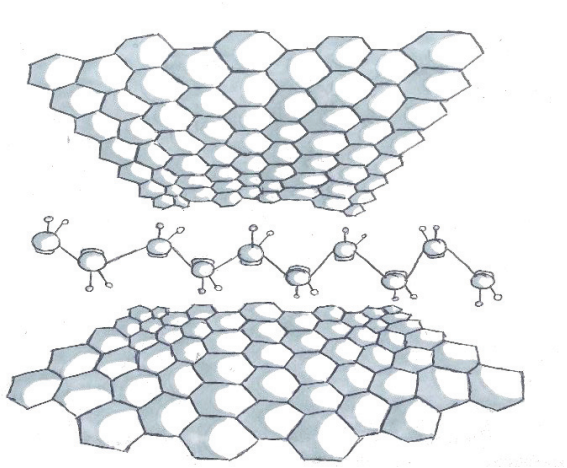
[50] J. B. P. Soares, A. E. Hamielec, "Semicrystalline Polyolefins - Narrow MWD and Long Chain Branching: Best of Both Worlds", in *Metallocene Catalyzed Polymers*, G.M. Benedikt and B.L. Goodall, Eds., William Andrew Publishing, Norwich, NY, 1998, p. 103.

[51] Y. Yu, P. J. DesLauriers, D. C. Rohlfing, *Polymer* **2005**, *46*, 5165.

[52] T. Pathaweeisariyakul, K. Narkchamnan, B. Thitisuk, W. Yau, *Journal of Applied Polymer Science* **2015**, *132*.

CHAPTER III

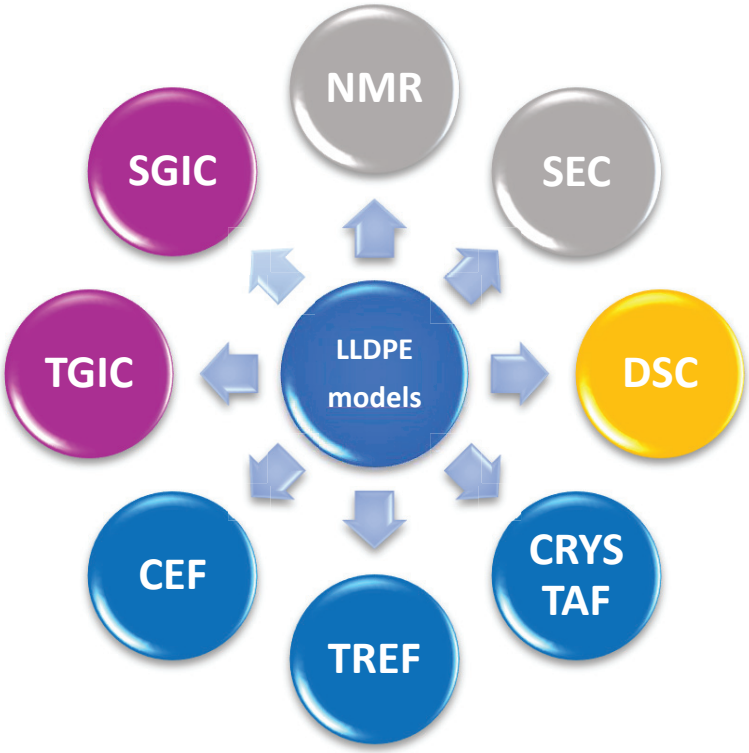
USE OF LLDPE TO CALIBRATE THERMAL FRACTIONATION TECHNIQUES



Polyethylene interacting with the graphene of the TGIC column, artist's view

Before using our LLDPE as standards for calibrating fractionation techniques, we studied them by differential scanning calorimetry (DSC). Like certain thermal fractionation techniques, the principle of DSC is also based on the crystallization capacity of polymers, but in the solid state for DSC. For the fractionation techniques, the separation occurs in a solvent that allows the behavior of each chain to be separated individually.

Thus, DSC characterization is the first approach used to understand the thermal behavior of our copolymer samples. These samples also provide the opportunity to calibrate a simple technique that is well-known and commonly used in research laboratories. The effect of α-olefin incorporation on polymers properties can be assessed by measuring crystallinity, melting temperature and crystallization temperature.



After the DSC approach, we used our copolymer models to calibrate the thermal fractionation techniques that are installed in our laboratory. Prior to this work, these techniques were used only as comparison techniques with which samples profiles were qualitatively compared with each other. This work will allow quantitative measurements of the comonomer content through the establishment of calibrations.

3.1 ROLE OF COMONOMERS IN THERMAL BEHAVIOR OF LLDPE BY DSC

Various properties of polymers can be quantitatively determined using thermoanalytical techniques. Differential scanning calorimetry (DSC) is frequently employed to characterize the physical properties of polymers via the measurement of their thermal properties. [1-3] The instrument measures the heat flow that occurs in a sample when it is heated or cooled. The physical transitions frequently determined for polymers are:

- Melting temperature and enthalpy of melting,
- Crystallization temperature and enthalpy of crystallization,
- Glass transition temperature for the amorphous fraction of a polymer.

The instrument consists of two heat flow sensors, one is used for the unknown sample and the second is used as a reference, which is an empty crucible. The instrument measures the difference of the heat flow between both sensors as a function of temperature during a temperature program. DSC is applied to detect and measure any change in heat capacity caused by glass transition and any change in enthalpy caused by melting and crystallization. DSC is used to obtain information on chemical composition; various advanced methods can be used such as stepwise isothermal segregation (SIST),[4] successive self-nucleation annealing (SSA)[5] and step crystallization.[6]

The advantage of DSC is easy sample preparation which does not need dissolution in solvent at high temperature. However, DSC suffers not only from low resolution but also from co-crystallization effects related to the low mobility of the chain in the molten state.

3.1.1 EQUIPMENT AND ANALYTICAL CONDITIONS

Thermal characterization was performed with a Mettler Toledo DSC3 apparatus (FRS5 DSC sensor). Samples were weighed (around 10 mg) and sealed in 40 µL aluminum pans. Aluminum is largely inert. The pans were pierced with a fine needle by the sample changer directly before measurement. They were heated with an empty aluminum pan as reference from -20 °C to 180 °C at 10°C min^{-1}. This value is important to mention because the heating and cooling rates have an impact on the crystallization and melting of PE, as reported by Schick.[7] Two successive heating and cooling stages were performed and only the second run was considered. Dry nitrogen with a flow rate set at 50 mL min^{-1} was used as the purge gas. The melting temperature was obtained from the top of the peak values. The crystallinity of samples was calculated in the second heating step using the expression:[1]

$$X = \Delta H_f / \Delta H_{fo} \times 100 \qquad (3\text{-}1)$$

where ΔH_f (J g^{-1}) is the melting heat of the sample and ΔH_{f0} (= 293 J g^{-1}) the melting heat of a 100% crystalline polyethylene.

3.1.2 TEMPERATURE AND HEAT FLOW CALIBRATION

Calibration for the temperature scale and the heat flow were performed using metallic standards, In and Zn, and water. It was carried out following the instrument supplier's instructions and ASTM E967-18, suggesting the calibration of the temperature and enthalpy with the values reported in Table 3-1.

Table 3-1: Melting temperature and enthalpy of standards used for the calibration.

Reference substance	Temperature (°C)	Enthalpy (J g^{-1})
Water	0 (± 0.5)	334.5 (± 16.7)
Indium	156.6 (± 0.3)	28.5 (± 0.6)
Zinc	419.5 (± 0.7)	107.5 (± 3.8)

Sample preparation: indium and zinc pellet, pressed flat, pre-melted.

The DSC curves (Figure 3-1) show the melting of water, indium and zinc, which are compared to the defined temperature. The melting points were taken at the onset of the melting process which is defined as the temperature given by the intercept of the extrapolated slope of the melting curve and the base line.

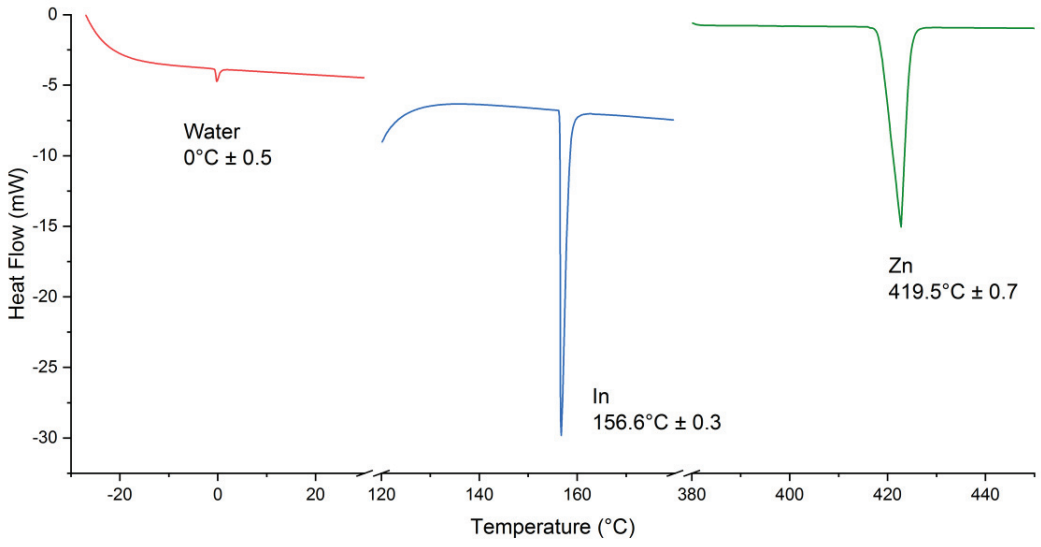


Figure 3-1: Typical water, indium and zinc DSC thermograms used for the heat flow and temperature calibrations.

3.1.3 EFFECT OF MOLAR MASS ON DSC PROFILES

DSC was used to measure the effect of comonomer content on LLDPE thermal behavior. Firstly, this part investigates the influence of the molar mass of the copolymers on the melting temperature and enthalpy, expressed in term of crystallinity according to Equation 3-1, measured by DSC. It aims at correlating the thermal behavior of copolymers with their variation of molar mass. Commercial samples of HDPE from Polymer Standard Service (PSS, Germany), certified for molar mass with a narrow dispersity (around 1.1) usually used to calibrate our HT-SEC instrument, were analyzed. They ranged from 750 to 7300 g mol^{-1}. Melting temperatures and melting enthalpies were calculated for all the samples.

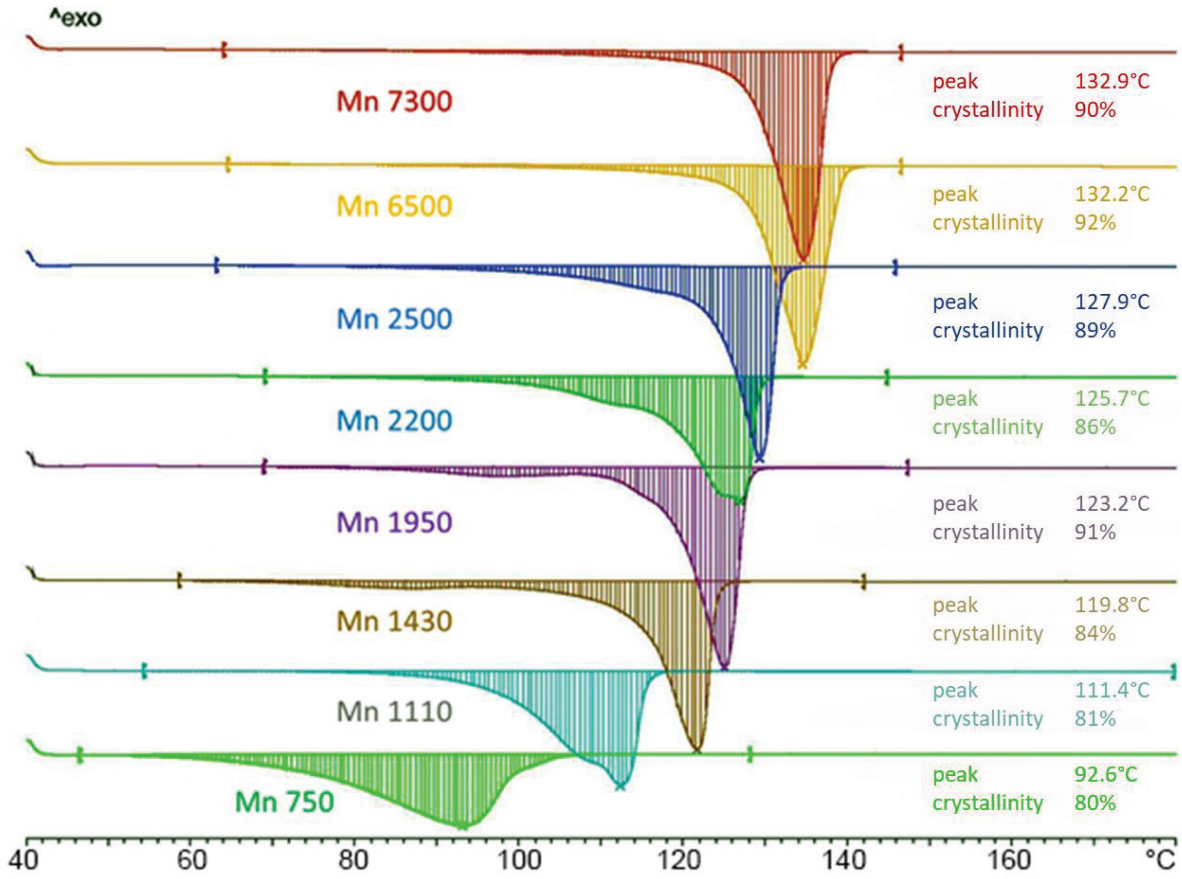


Figure 3-2: Effect of molar mass on the melting temperature of HDPE with various molar masses from 750 g mol^{-1} to 7 300 g mol^{-1}. DSC thermogram during the second heating with a rate of 10°C min^{-1} under nitrogen atmosphere.

As shown in Figure 3-2, the melting temperature of the samples clearly increases with their molar mass whereas the melting enthalpy (reported as crystallinity) is less impacted in this range of mass. The measured crystallinity varies from 80% to 90% which corresponds to enthalpies of 234 to 264 J g^{-1}. These

values show that the PEs with low molar masses have a particularly high crystallinity. Indeed, for our copolymer model, with higher molar masses, enthalpies were measured around 190 J g^{-1} for the highest (crystallinity of 65%). Small chains can easily organize into a crystalline lamella (Figure 1-14) without folding up on themselves and without disrupting the lamellar growth. Therefore, the amorphous part is reduced, and the crystallinity is increased.

Some peaks show shoulders or even a second melting peak indicating that the samples are crystallized in various kinds of lamella. This behavior was also observed for our copolymer samples.

When the molar mass increases beyond 5,000 g mol^{-1} the value of the melting temperature is less impacted and reaches 133 °C for a mass of 7 300 g mol^{-1}. For our homo PE samples with a mass around 20,000 g mol, we obtained a plateau around 137 °C (±1 °C) which seems to be the maximum value of the melting temperature of PE. This behavior was interpreted by assuming that chains with shorter lengths crystallize as extended chains.[8-11] The chains of greater lengths crystallize in the form of folded chains, increasing the melting temperature. We will see in a further part that this temperature can be sharply increased in the case of PEs with very high molar masses (UHMWPE) and greatly exceed 140 °C. For the following work we will estimate that the molar masses higher than 10,000 g mol^{-1} (this is the case for our copolymers) will not impact the melting temperatures.

The relation between the melting temperature and the chain length in polyethylene has been investigated by various researchers. In particular, we considered two equations which link the melting temperature to the length of the chain. Garner and coworkers proposed the following equation:[12]

$$T_m = \frac{0.6085\mathrm{n} - 1.75}{0.001491\mathrm{n} + 0.00404} \qquad (3\text{-}2)$$

with T_m as the melting temperature and n the number of carbons in the polymer chain.

However the best-known relationship can be reported in the following form:[8]

$$T_m = T_0 \frac{\mathrm{n} + \mathrm{a}}{\mathrm{n} + \mathrm{b}} \qquad (3\text{-}3)$$

with T_0, a and b are constant

Broadhurst and co-workers obtained their best fit with experimental values using T_0 = 414.3 °K, a=-1.5 and b=5.0.

This equation was formulated and determined with samples of paraffins with a carbon number varying from 44 to 100. The extrapolation of the equation for PE samples, with molar masses higher than paraffins, should be used with caution. Nevertheless, the authors reported that the crystal mesh of paraffins is also orthorhombic, like those observed for PE samples. The crystallization of short chains like the paraffins shown here does not occur in folded form. This is the complete olefin chain which is organized with other chains that form the crystal mesh. The organization is quite different for PE samples, for which each chain is organized in folded form. However, we compare in Table 3-2 the value measured for our sample and that obtained by Equations 3-2 and 3-3 from Garner and Broadhurst and their co-workers.

Table 3-2: Experimental melting temperature values compared to theoretical values obtained with Garner and Broadhurst equations, respectively.

$\bar{M}_n$ g mol^{-1}	N[a]	Tm experimental °K	Tm calulated Garner °K	Δ Tm[b]	Tm calulated Broadhurst °K	Δ Tm[b]
7300	521	405.1	403.8	-1.4	409.2	4.1
6500	464	405.3	403.2	-2.1	408.6	3.2
2500	178	401.1	395.5	-5.5	399.6	-1.4
2200	157	398.8	393.8	-5.0	397.7	-1.1
1950	139	396.3	392.0	-4.3	395.6	-0.7
1430	102	393.0	386.3	-6.6	389.1	-3.8
1110	79	384.5	380.3	-4.3	382.3	-2.2
750	53	365.8	367.5	1.8	368.2	2.5

[a]number of carbons in the polymer chain, [b]deviation between the calculated value and the experimental melting temperature.

The values are quite similar. However, we can note some explanations for the variations. The value of the melting temperature is affected by the heating rate. To avoid this effect, it would be interesting to create new equations based on the onset of melting temperature which is not impacted by the heating rate. Apart from the measurement errors, the dispersity of the polymer is not considered in the equation but doubtless also affects the shape of the peak and then the temperature at the top of the melting peak.

3.1.4 EFFECT OF COMONOMER CONTENT ON DSC PROFILES

All the copolymer models were analyzed by DSC using the analytical conditions detailed in 3-1-1. Because the molar masses of our copolymer models were higher than 10,000 g mol^{-1}, the measured melting temperatures were only affected by the comonomer content. Their thermal parameters (temperature and enthalpy of melting, temperature and enthalpy of crystallization, percent crystallinity) are reported in Appendix 1. Several thermograms of the various types of copolymers are plotted in Figure 3-3.

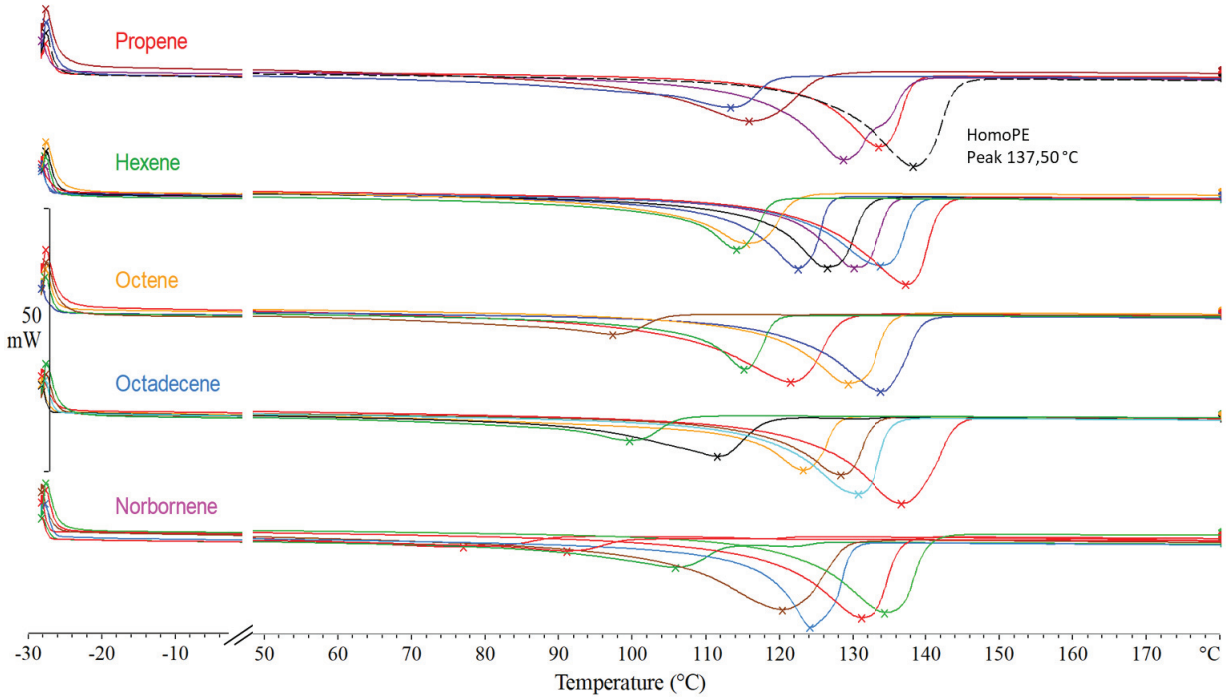


Figure 3-3: DSC thermograms of the second heating with a rate of 10°C min^{-1} under nitrogen atmosphere for LLDPE with various comonomer contents.

The obtained melting peaks are unimodal and quite narrow, showing that the copolymers are homogeneous in chemical composition. For all types of copolymers the melting temperature decreases as the comonomer content increases in the backbone.

During crystallization polymer chains fold back into crystalline lamellae in an ordered pattern. This behavior and therefore the crystallinity of polyethylene will be affected by the insertion of short chain branching (comonomer). They reduce the overall crystallinity of the polymer and the size of the lamellae as illustrated in Figure 3.4. According to the Gibbs-Thomson relationship (Equation 1-1), the size of the lamella is directly related to the melting temperature measured by DSC.

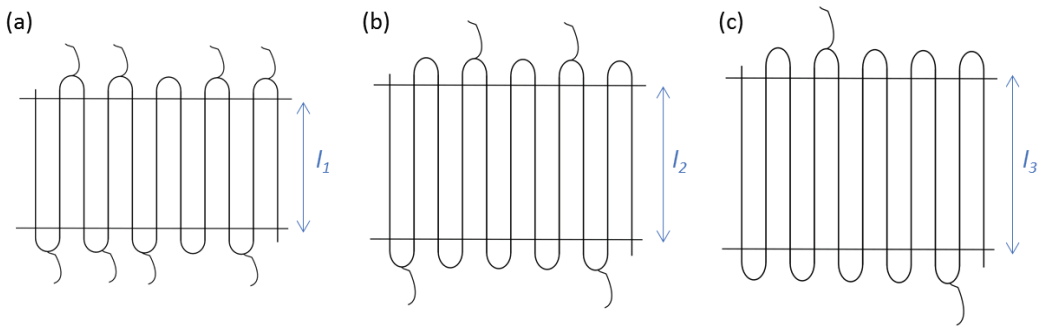


Figure 3-4: LLDPE with three different comonomer contents (the branches are represented as incurved vertical lines) resulting in three lamellar thicknesses l_1, l_2, and l_3. High comonomer content (a), medium comonomer content (b) and low comonomer content (c).

The evolution of the melting peak (top of the peak) was plotted, in Figure 3-5, as a function of the comonomer content expressed in mole percentage (a) and mass percentage (b) for the different types of copolymers.

We observed an almost linear response for all types of copolymers. Although ethylene-hexene and ethylene-octene copolymers have a similar calibration curve (when expressed in mole percentage, Figure 3-5a), for the others, the slope of the curve is different. The melting temperatures are affected not only by the number of branches but also by the length and type of branches (or comonomer). For this reason, we have also chosen to plot the graphs as a function of mass percentage instead of mole percentage.

For ethylene-propylene and ethylene-octadecene copolymers which represent the two extremes in terms of branching length the slopes are surprisingly similar in the graph expressed in mole percent. When we convert to mass percentage, they become radically different.

Conversely, for the ethylene-norbornene copolymers, the slope is the lowest in both plots. The greater steric hindrance of the norbornene molecule explains the lower melting temperature for the same comonomer content than for an ethylene-hexene copolymer. In the following part, to better understand their thermal behavior, crystallization and enthalpy exchanges will also be studied for these ethylene-norbornene copolymers.

The very short branches due to propylene have little effect on the crystallized capacity of the copolymer and therefore have less impact on the melting temperatures than branches due to hexene or octene comonomer.

Regarding octadecene, it is quite surprising that the melting is so little impacted with respect to other α-olefins. Perhaps the octadecene branches, longer than those of the other comonomers, have the ability to crystallize with their neighbors and the ethylene backbone and thus less decreased the melting temperature. Investigations by X-ray scattering techniques could bring some clarification. The mass representation for this copolymer seems particularly suitable as the value of R^2 increases.

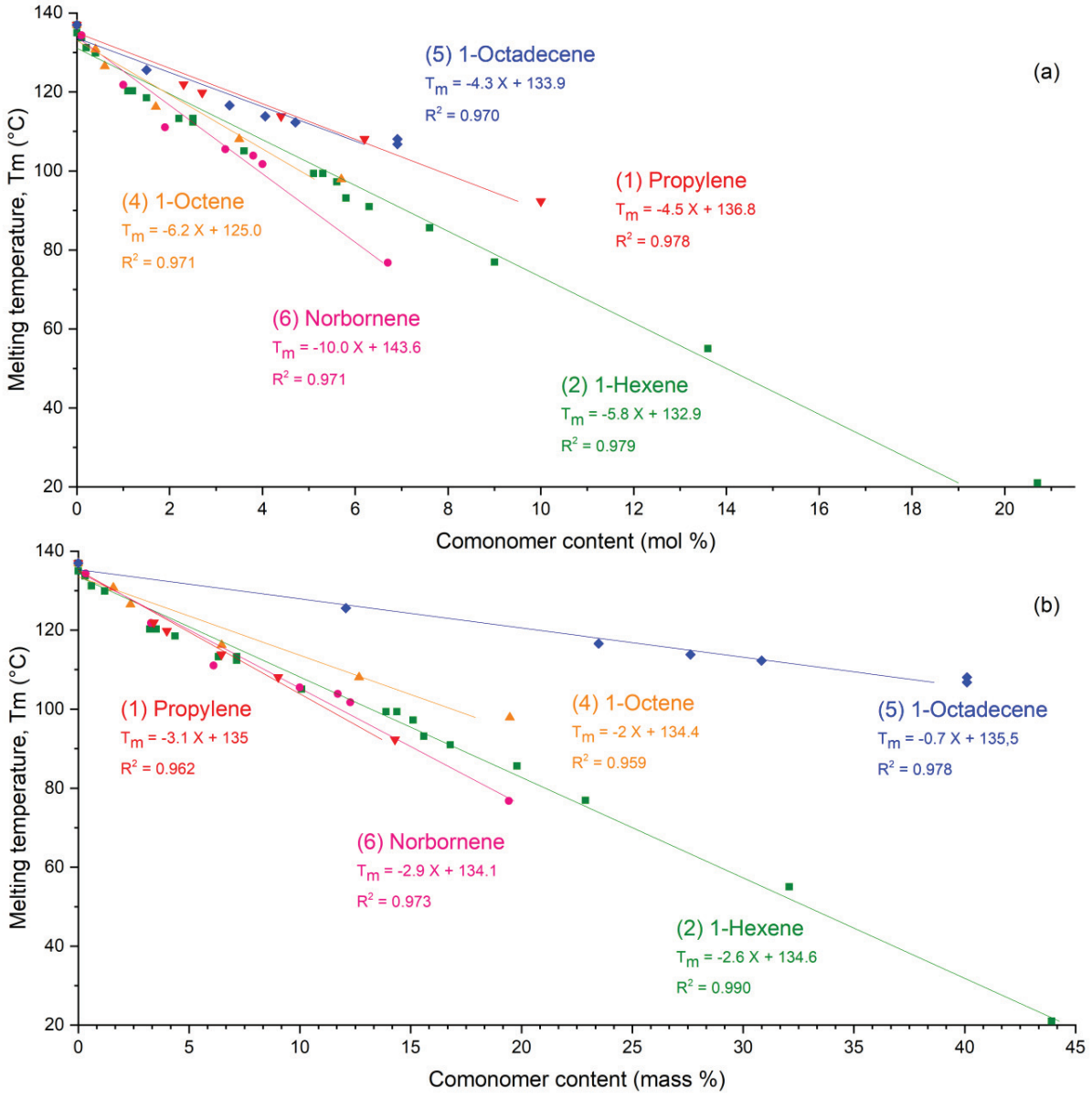


Figure 3-5: Temperature of the melting peak obtained by DSC during the second heating for different comonomer contents expressed in mole percent (a) and mass percent (b) for different types of comonomers. Heating rate of 10°C min^{-1} under nitrogen atmosphere.

The sample that contains 20 mol% of hexene has a low crystallinity and displays a broad peak in the DSC thermogram. The peak temperature (Figure 3-5a) is above the linear fit curve, 21°C instead of 18°C, which means that the crystallinity is higher than expected. When using a mass representation (Figure 3-5b) it appears that this point is better included into the linear fit.

The DSC technique, which is available in many research and control laboratories, provides an easy and rapid way to determine the comonomer content in LLDPE. In order to use it to determine the molar percentage of comonomer in LLDPE from the melting temperature we inverted the previous curves and obtained the following plots (Figure 3-6).

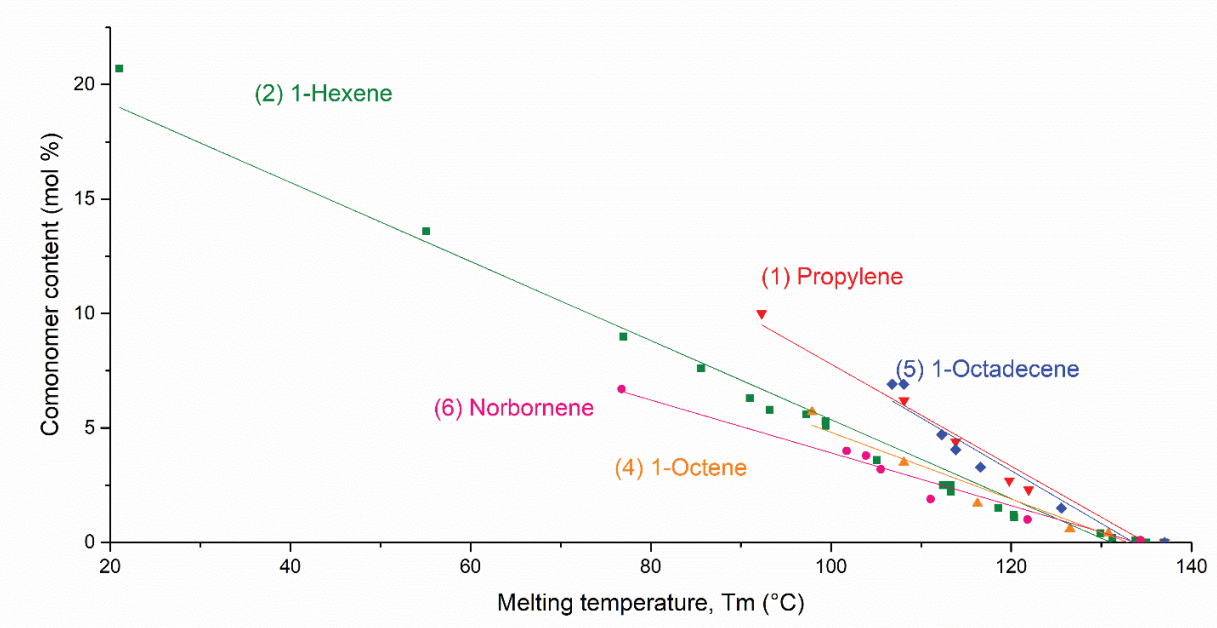


Figure 3-6: Calibration curves based on temperature of the melting peak obtained by DSC during the second heating for different comonomer contents expressed in mole percent for different types of comonomers. Heating rate of 10°C min^{-1} under nitrogen atmosphere.

The relationships between thermal parameters and comonomer content were calculated and are reported in Table 3-3. These equations are only suitable for LLDPEs obtained with metallocene catalysts. For polyethylenes produced with Ziegler-Natta multisite catalysts, the chains are heterogeneous in composition, so there are comonomer-rich fractions that are not or poorly represented by the melting peak. For these copolymers obtained with ZN catalysts, there are also equations proposed by Hosoda.[15]

3.2 MELTING AND CRYSTALLIZATION ENTHALPY

A thorough thermal analysis was performed for ethylene-norbornene (Figure 3-7) and ethylene-hexene (Figure 3-8) copolymers. The other thermal parameters were also investigated: crystallization temperature, melting and crystallization enthalpy, and the melting temperature onset peak.

3.2.1 ETHYLENE-NORBORNENE COPOLYMERS

The insertion of norbornene into the PE backbone reduces crystallinity and melting temperature, and the crystallization temperature decreases as the insertion of the comonomer increases. As seen in Figure 3-7, the insertion of norbornene decreases the melting and crystallization enthalpies.

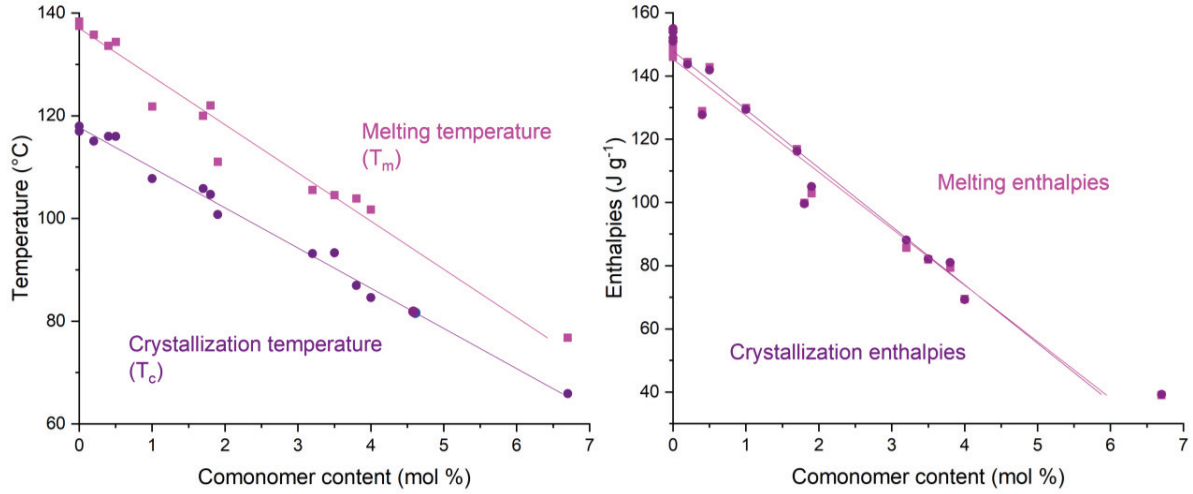


Figure 3-7: Temperature and enthalpies of melting and crystallization of ethylene-norbornene copolymers with various norbornene content (mol%). Second run, heating rate of 10°C min^{-1} under nitrogen atmosphere.

The "inverted" melting and crystallization equations resulting from the calibration curves, which correlate comonomer content with temperatures and enthalpies, are given in Table 3-3. Using these calibrations, we can evaluate the norbornene content in unknown ethylene-norbornene copolymers by various ways, up to 6 mol% and for molar masses above 10,000 g mol^{-1}.

3.2.2 ETHYLENE-HEXENE COPOLYMERS - EFFECT OF LOW COMONOMER CONTENT

Various works report a linear evolution of the melting temperature with the comonomer content, as noted previously. Nevertheless, we observed that for low comonomer contents the variation of melting temperature with the comonomer content was not linear. We decided to investigate behavior for low

comonomer content and produced additional ethylene-hexene copolymers with very low comonomer contents (< 1 mol%) to complete the initial linear calibration curve. The plots reported in Figure 3-8 show that an empiric calibration using a third order polynomial fils well the experimental data. It is even more necessary to have a good fit for low comonomer content portion and for the calibrations of melting and crystallization enthalpy.

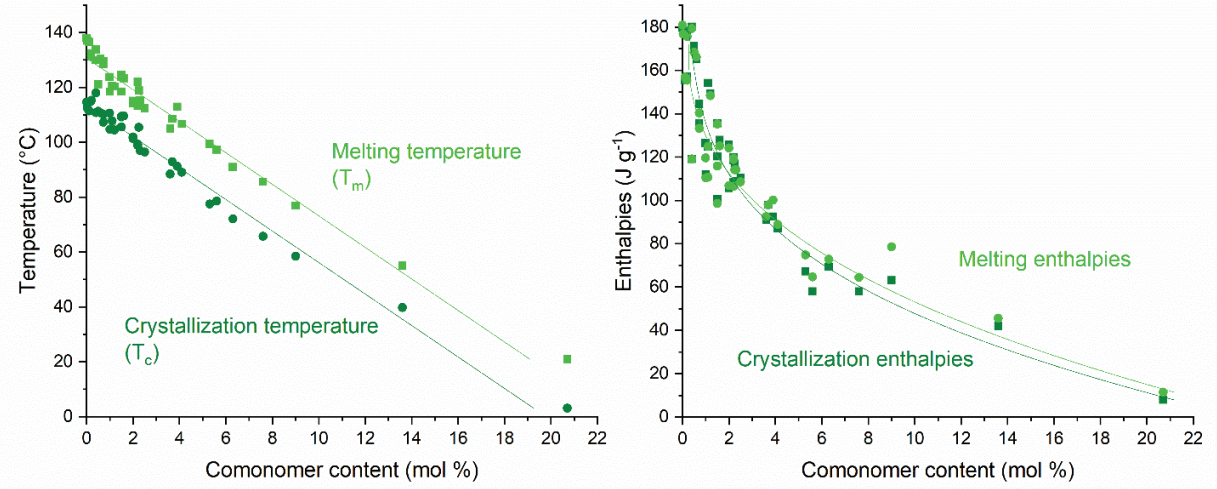


Figure 3-8: Temperature and enthalpies of melting and crystallization of ethylene-hexene copolymers with various hexene content (mol%). Second run, heating rate of 10°C min^{-1} under nitrogen atmosphere.

The resulting "inverted" equations from the calibration curves, which correlate the comonomer content with temperature and enthalpies, are given in Table 3-3. Using these calibrations, we can evaluate the hexene content in unknown ethylene-hexene copolymers by various ways, up to 21 mol% and for molar masses above 10,000 g mol^{-1}.

3.2.3 ETHYLENE-HEXENE COPOLYMERS - ONSET MELTING TEMPERATURE

The onset of melting temperature ($T_{m\ onset}$) is another representation of the melting temperature (Figure 3-9). It was also used to study the melting temperature and hexene content relationship. The onset melting temperature corresponds to the value given by the intersection between the baseline and the tangent at the inflection point. The value of the onset peak is known to be independent of the heating rate[16] and probably provides greater robustness to the measurement. In any case, it is an additional measure that can be added to the others.

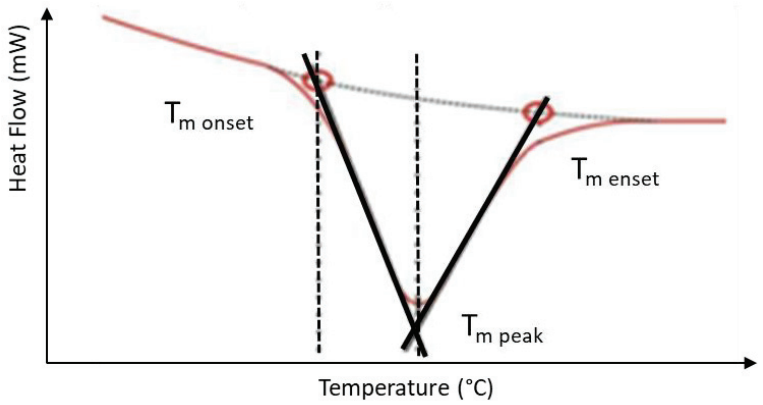


Figure 3-9: Illustration of the temperature at the top of the peak (T_m), the onset and the endset temperature during a heating step.

The onset of melting temperature was calculated for various ethylene-hexene copolymers and an additional equation was established and is reported in Table 3-3. The method using the onset of melting temperature is not better than the others since the value of R-squared is a little lower than that of the other equations. However, it is interesting to use it as an additional assessment of hexene content, as this method does not require another measurement and can be carried out at the same time as that of the temperature of the melting peak. The choice of the temperature onset is however more problematic in the case of copolymers that present several populations of chemical composition. The value will be representative of a single family but not of the whole polymer.

The equations that correlate the melting and crystallization peak temperatures (T_m, T_c) and the melting and crystallization enthalpies (ΔHc, ΔHm) to the comonomer content for various copolymers are all summarized in Table 3-3. These equations can be easily used to determine the comonomer content for an unknown LLDPE with a classical DSC analysis. These equations were replicated many times during this doctoral work and have always been constant, proving the robustness of the method. They depend only on the heating rate which must be set at 10°C min^{-1}. For good accuracy, the quantity of the sample weighed must be around 10 mg, and an aluminum pan of 40 µl must be used. The most important parameter to be observed is the use of two heating steps and the calculation of the melting temperature must be carried out during the second step. The profile obtained during the first step of DSC depends on the storage conditions of the sample and on its thermal history and should not be used for the calculation. The first step of the DSC experiment permits melting and crystallizing the sample under controlled conditions. The result will thus reflect the real chemical composition of the polymer.

Table 3-3: Equation to calculate the comonomer content using melting and crystallization parameters obtained by DSC.

Comonomer	Melting and crystallization temperature	Melting and crystallization enthalpies
propene	$30.1-0.22xT_m$	
	(0.978)	
hexene	$22.6-0.17xT_m$	
	(0.979)	
	$23.69 -0.12xT_m-0.0016xT_m^2+8.6E-6xT_m^3$	$23.97-0.38x\Delta H_m+0.002x\Delta H_m^2-4.0E-6x\Delta H_m^3$
	(0.989)	(0.946)
	$21.37-0.19xT_c-5.8E-4xT_c^2+5.8E-6xT_c^3$	$25.02-0.35x\Delta H_c +0.0015x\Delta H_c^2-1.6E-6x\Delta H_c^3$
	(0.991)	(0.924)
	$14.2-0.112xT_{m\ onset}$	
	(0.973)	
octene	$20.0-0.16xT_m$	
	(0.972)	
octadecene	$30.8-0.23xT_m$	
	(0.980)	
norbornene	$14.36-0.10xT_m$	$8.13-0.056x\Delta H_m$
	(0.985)	(0.982)
	$15.04-0.13xT_c$	$8.00-0.054x\Delta H_c$
	(0.991)	(0.954)

where T_m is the melting temperature at the top of the peak, $T_{m\ onset}$ is the melting temperature at the onset of the peak, Tc the crystallization temperature, ΔH_m and ΔH_c the enthalpy of melting and crystallization, and R-Square in brackets.

3.3 CALIBRATION OF THERMAL FRACTIONATION TECHNIQUES



3.3.1 ANALYTICAL CONDITIONS

Firstly, the temperature rising elution fractionation (TREF) and the crystallization temperature analysis fractionation (CRYSTAF) techniques were carried out to characterize our LLDPE samples in terms of chemical composition distribution (CCD). A CRYSTAF-TREF 300 model manufactured by Polymer Char S.A. (Valencia, Spain) was used. Secondly, crystallization elution fractionation (CEF) and thermal gradient interaction chromatography (TGIC) experiments were performed using a CEF/TGIC instrument from PolymerChar (Valencia, Spain). Afterwards, our copolymer models were employed to calibrate an innovative solvent gradient interaction chromatography (SGIC) method in the framework of a collaboration with the Fraunhofer Institute for Structural Durability and System Reliability, Plastics Division, Department of Materials Analytics, Darmstadt, Germany. The analytical conditions are described in the following parts.

3.3.1.1 TREF analytical conditions

Experimentally, about 80 mg of the sample was dissolved at high temperature (150 °C) in 20 mL of 1,2,4-trichlorobenzene (1,2,4-TCB) stabilized with 2,6-di(tertbutyl)-4-methylphenol. 0.5 ml of the sample solution was loaded into the TREF column of 9 mm i.d. and 15 cm length at 120 °C. The temperature was slowly decreased to 35 °C at a rate of 0.5 °C min^{-1} to allow the polymer to crystallize. A second cycle was used to quantify those fractions by pumping solvent while the temperature was being increased (1 °C min^{-1}). The eluent dissolved fractions of increasing crystallinity.

The polymer solution concentration was monitored with an infrared detector measuring total CH absorption in the 2700–3000 cm^{-1} range.

3.3.1.2 CRYSTAF analytical conditions

20 mg of the sample was dissolved at 150 °C in 30 mL of 1,2,4-TCB stabilized with 2,6-di(tertbutyl)-4-methylphenol. After the dissolution of the sample, the temperature of the solution was stabilized at 110 °C and then decreased at a rate of 0.1 °C min^{-1} to 25 °C. At regular intervals, a part of the solution is sent to the IR detector thermostatically controlled at 150°C to follow the concentration of the soluble part.

CRYSTAF technique has been patented by The Dow Chemical Company and manufactured and marketed by PolymerChar. The different parts of the instrument, which can also be used in TREF mode, are shown in Figure 3-10.



Figure 3-10: CRYSTAF-TREF instrument overview. CRYSTAF and TREF methods can be performed in the same instrument. CRYSTAF analyzes the sample during the crystallization step and TREF during the dissolution step.

3.3.1.3 CEF analytical conditions

The samples at a concentration of 2 mg mL^{-1} were dissolved in 10 mL vials in 1,2,4-TCB at 160°C for 1 hour. At the end of the dissolution period, the samples were transferred to the injection loop (200 µL) and injected into the CEF column using an isocratic pump. The samples were fractionated according to their crystallization ability using two temperature cycles (Figure 3-11). During the crystallization step, the column temperature was decreased to 35°C, at a rate of 2°C min^{-1}, under continuous 1,2,4-TCB flow (0.05 mL min^{-1}). During the elution step, the fractions deposited were gradually dissolved as the temperature increased to 130 °C at 4°C min^{-1} using a continuous 1,2,4-TCB flow (1 mL min^{-1}).

The infrared detector measured the concentration of the eluted fractions to obtain the CEF profile.

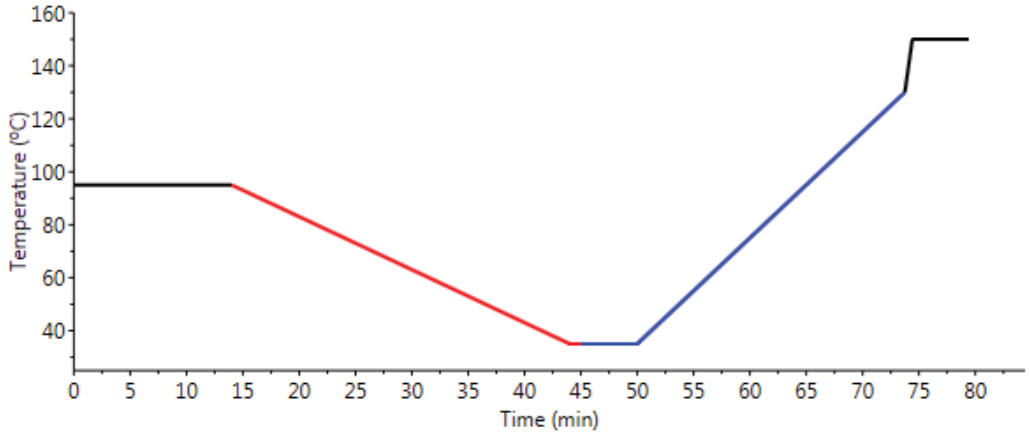


Figure 3-11: Temperature program applied to the CEF method.

3.3.1.4 TGIC analytical conditions

The instrument was equipped with a Hypercarb column from Thermo Scientific containing particles of graphitic carbon (average particle size 5 µm, pore size of 250 Å). The dimensions of the column were 100×4.6 mm^2 (LxID). The samples at a concentration of 1 mg mL^{-1} were dissolved in 10 mL vials for 1 h at 150 °C with 1,2,4-TCB containing 300 ppm of BHT and purged with nitrogen to protect the polymer against oxidative degradation. 200 µL of the sample solution was injected into the column at 160 °C. This technique requires a cooling (adsorption) and a heating (desorption) step (Figure 3-12). A cooling ramp of 20 °C min^{-1} to 40 °C was applied to promote polymer adsorption. Elution began isothermally at 40 °C for 5 min at a flow rate of 0.5 mL min^{-1}, followed by a heating ramp at 2 °C min^{-1} to desorb the polymer. An infrared detector was used to monitor the components' concentrations and compositions when the chains were eluted from the column. The main operating conditions are reported in Table 3-4.

Table 3-4: Summary of operating conditions.

Parameters	**Symbol**	**Values**	**Unit**
Cooling rate	Cr	20	°C min^{-1}
Cooling cycle		150 - 40	°C
Cooling flow rate	Fc	0	ml min^{-1}
Heating rate	Hr	2	°C min^{-1}
Elution flow rate	Fe	0.5	ml min^{-1}

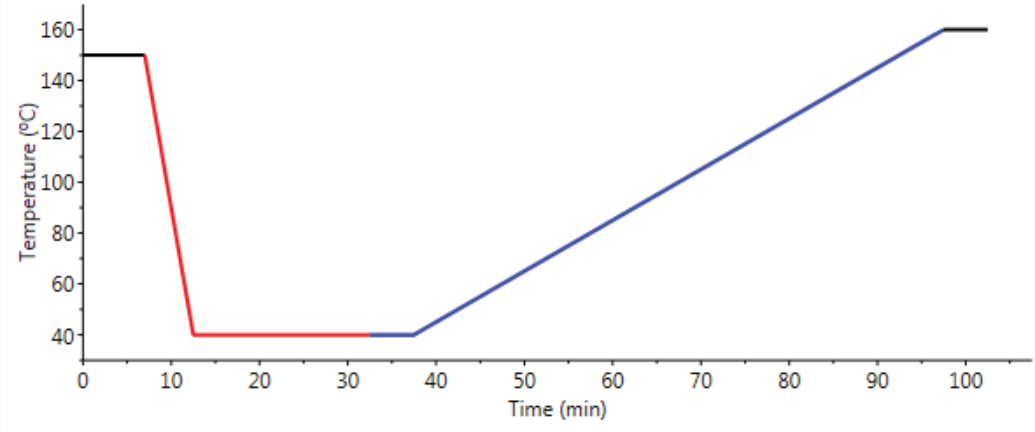


Figure 3-12: Temperature program applied to the TGIC method.

3.3.1.5 SGIC analytical conditions

The device consisted of a combination of an Agilent high temperature chromatography system (PL XT-220), a high pressure binary gradient pump and an evaporative light scattering detector (PL-ELS 1000) from Polymer Laboratories.

The system was equipped with a Hypercarb column from Thermo Scientific containing particles of porous graphitic carbon (average particle size 5 µm, surface area of 120 $m^2 g^{-1}$, pore size of 250 Å). The dimensions of the column were 100×4.6 mm^2 (LxID). The samples were dissolved for 2h to 5h in 2-ethyl-1-hexanol at 160 °C. 50 µL of the sample solution at a concentration of 1-2 mg mL^{-1} was injected into the column at 160 °C. This technique first requires an adsorption step. The polymer was absorbed onto the column due to the effect of the solvent which caused the polymer to stay on the column. The sample adsorbed was then progressively desorbed by a linear gradient, starting with alcohol and ending by *o*-DCB. 2-ethyl-1-hexanol is an adsorption promoting solvent, and *o*-DCB is a desorption promoting solvent.

An evaporative light scattering detector was used to monitor the components' concentrations when the chains were eluted from the column according to their compositions.

Calibration

The incorporation of comonomers into the polymer chains induces a decrease in the crystallinity of the sample. Polymer crystallizing at a lower temperature will also elute at a lower temperature for thermal fractionation techniques based on crystallization (TREF and CEF). Separation by TGIC and SGIC also leads to a similar behavior, the more branched chains are eluted first followed by less and less branched ones which increasingly interact with the Hypercarb column. An overall representation of the separation for all the techniques is shown schematically in Figure 3-13.

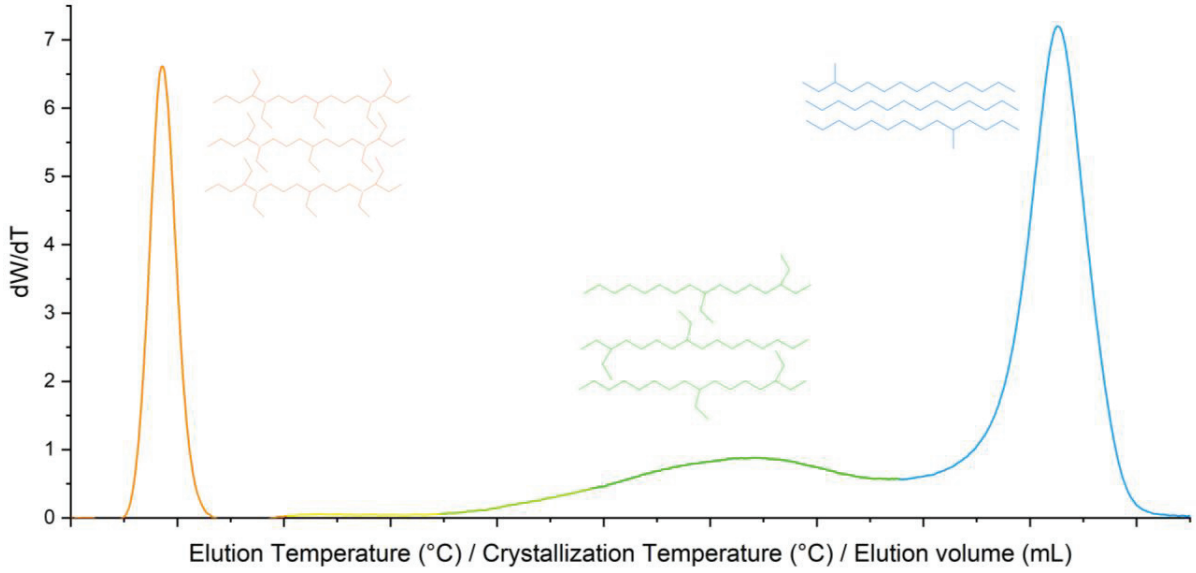


Figure 3-13: Principle of polymer chain fractionation according to their comonomer content for TREF, CRYSTAF, CEF, TGIC and SGIC. These techniques aim to measure the CCD in polyolefins.

This part will focus on the methods developed and implemented in our laboratory using these various and original thermal fractionation instruments. Our copolymer models obtained with metallocene catalysts and characterized by HT-SEC, DSC and NMR can be used to establish robust calibration equations. They indicate the elution temperatures, the crystallization temperatures, and the elution volumes as a function of the comonomer content. A review of these equations is given at the end of this part as a tool to characterize future synthesized polymers in the laboratory.

3.3.2 FRACTIONATION TECHNIQUES BASED ON CRYSTALLIZATION.

TREF, CRYSTAF and CEF are separative analytical techniques allowing the fractionation of semi-crystalline polymers according to the differences in crystallizability of the polymer chains.

3.3.2.1 TREF

Figure 3-14 shows various measurement profiles obtained by TREF which illustrate the evolution of the elution temperature of copolymers as a function of comonomer content.

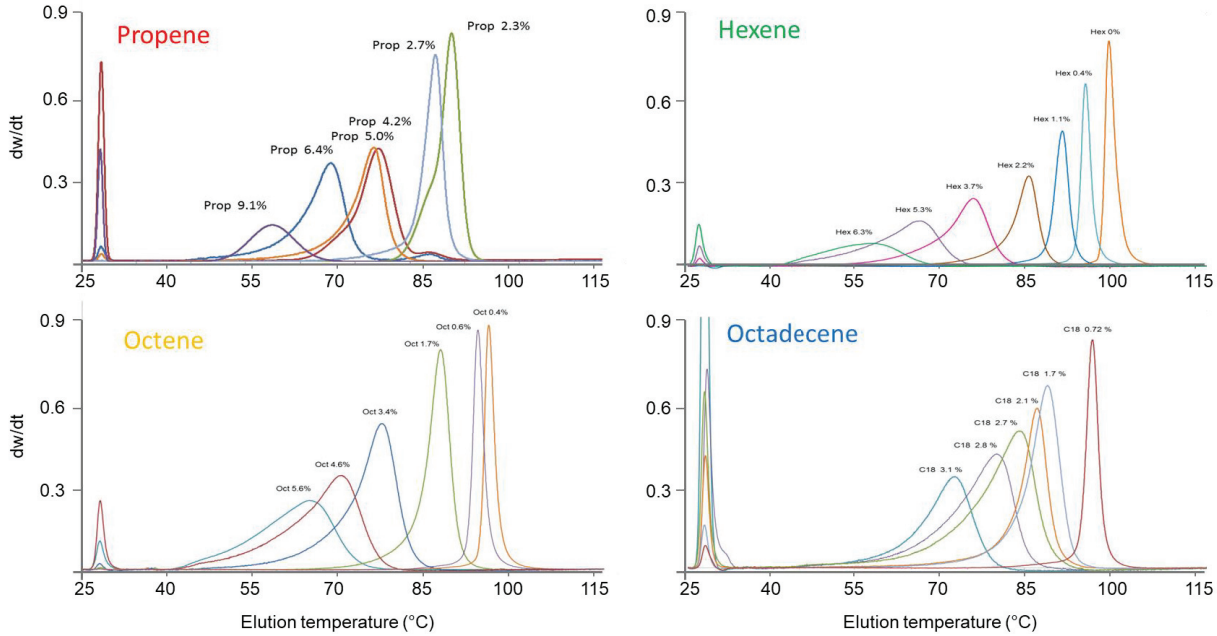


Figure 3-14: TREF profiles of individual copolymer models with various comonomer contents. Experimental conditions: cooling rate = 0.5°C min^{-1}, heating rate = 1°C min^{-1}, solvent = 1,2,4-TCB.

As expected, as the comonomer content increases in the sample, the elution temperature decreases. The broadness of the peak is related to the chemical composition homogeneity of the sample. Most of them were unimodal, which means that the polymerization was carried out under homogeneous conditions. The peak shape for samples with high comonomer contents shows that polymerization in these conditions was more difficult to control. As reported by Soares and coworkers[17] we observed the broadening of the peaks as the comonomer content increased.

The peak that elutes around 30°C is due to the soluble chains that cannot crystallize in these conditions, and its area is directly proportional to the amount of amorphous chains. This peak area rises dramatically when the comonomer content increases.

For each series, a linear regression was performed and correlation coefficients higher than 0.99 were obtained. The equations are reported in Table 3-9.

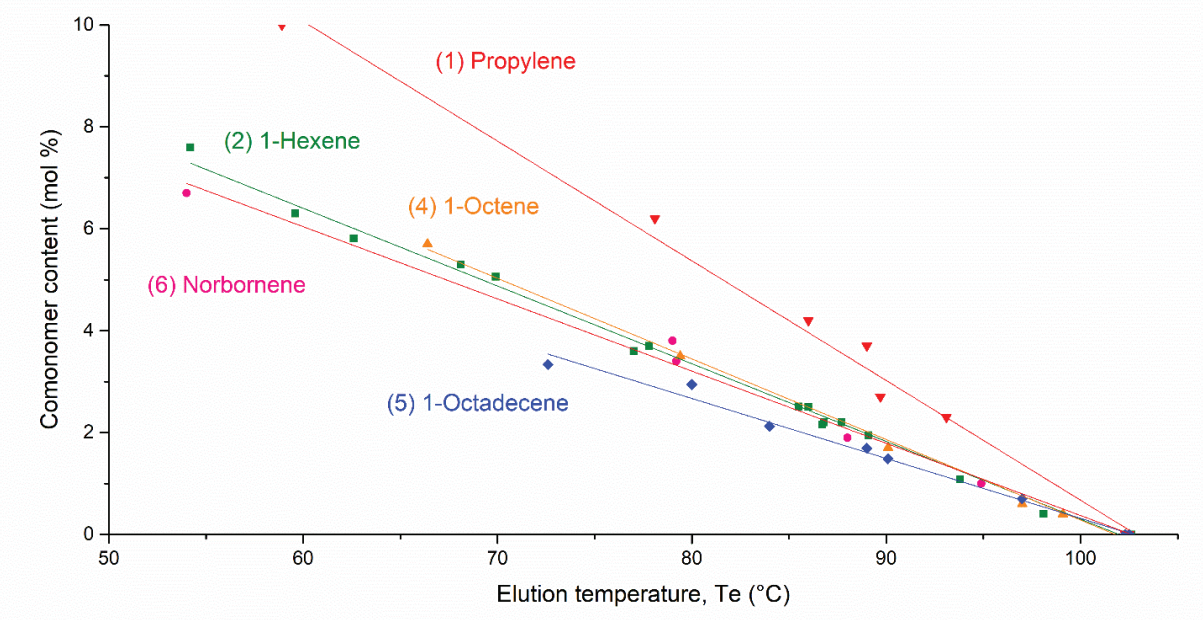


Figure 3-15: TREF calibration curves for the different series of copolymers. Experimental conditions: cooling rate = 0.5°C min^{-1}, heating rate = 1°C min^{-1}, solvent = 1,2,4-TCB.

The superposition of the curves of the four series of copolymers presented in Figure 3-15 allows making the following observations:

- The ethylene-propylene copolymers behave very differently from the other copolymers because the effective volume occupied by the methyl groups is much lower. This behavior was also observed for DSC. The samples remain more crystalline due to the short methyl branches.
- For ethylene-norbornene and ethylene-octadecene copolymers the hindrance of the branching was more marked compared to octene or hexene branches and had more impact on elution time. Consequently, these classes of copolymer required their own calibration curve. The behavior of ethylene-octadecene copolymers changes more considerably in solution (for TREF) than in the molten state (for DSC). The long branches of octadecene decrease the crystallinity and increase the solubility of the polymer when it is in solution.
- The ethylene-hexene and ethylene-octene copolymers led to very similar calibration lines. A common calibration for both these comonomers was therefore possible.
- The ethylene-hexene copolymers showed the same characteristics on the TREF profile whatever the catalysts used for their preparation. It was therefore possible to use the same curve for various metallocene catalysts in the range of zero to eight mol% of comonomer. This study should also be continued with other metallocene catalysts in order to generalize these conclusions. If the catalyst or

the polymerization conditions favor the creation of ethylene or comonomer sequences, crystallization could be affected, making the calibration inappropriate.

Variation in analytical conditions

In the literature we found various analytical conditions. An exploration of different analytical parameters was carried out on our device by various Master students, whom I supervised. Here, we will discuss only a part of this work.

During the crystallization step, the polymer fractions with chains of different compositions are separated. This is the most important step in the TREF experiment. We therefore had to optimize this step. The analysis with two crystallization rates and with cryo-accessories were compared. Cryo-TREF analysis was performed by Alberto Ortin from the PolymerChar company using our copolymer models. In this condition, sub-ambient analyses (-20°C) were performed using liquid nitrogen to decrease the temperature limit of the instrument. *Ortho*-dichlorobenzene (*o*-DCB) was used as solvent because of its lower melting temperature (-17°C) than that of 1,2,4-TCB. The calibration curves for each condition are plotted and overlayed in Figure 3-16.

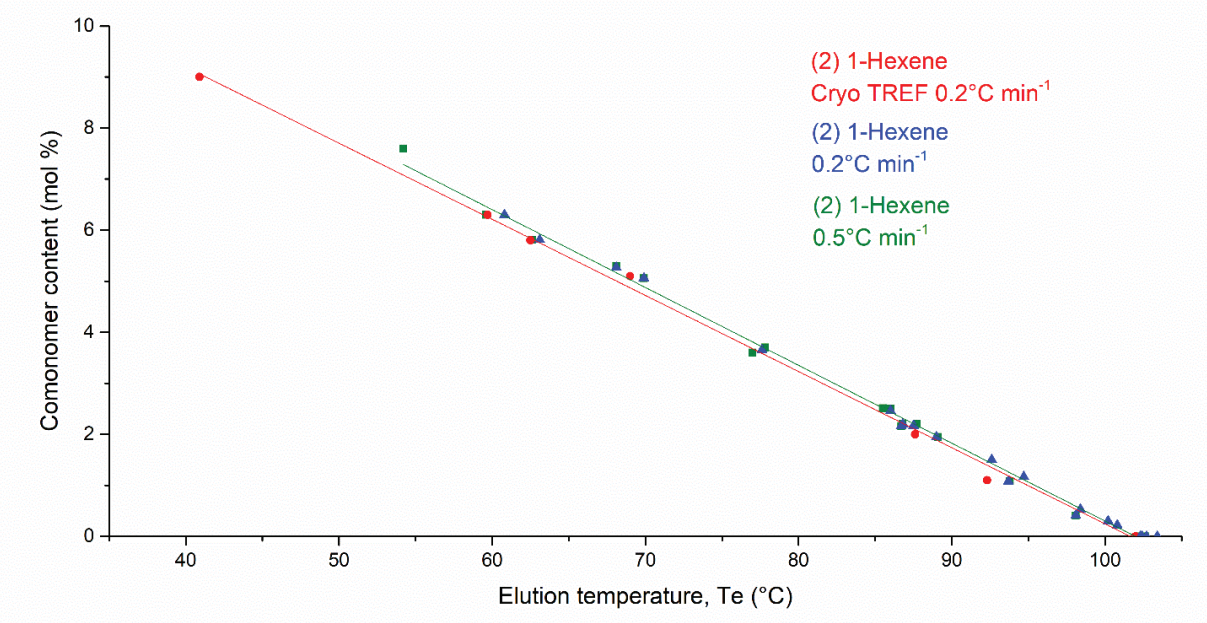


Figure 3-16: Comparison of cooling rate effect during crystallization step. Experimental conditions: cooling rate = 0.5°C min^{-1} and 0.2°C min^{-1}, heating rate = 1°C min^{-1}, Cryo TREF = sub-ambient analyses (-20°C) using liquid nitrogen and *o*-DCB.

The related equations for each experiment, reported in Table 3-5, are similar; a crystallization rate of 0.5 and 0.2 will give comparable results. However, at 0.2 °C min, the slope of the curve decreases slightly, showing a slightly better resolution but significantly increasing the analysis time. The cryo accessory shows that is able to analyze a wider range of branched copolymers up to 9 mol% for hexene.

Table 3-5: Calibration equation for ethylene-hexene copolymers for the various analytical conditions.

Analytical conditions	**Equation**
Cr 0.5 (°C min)	Hexene (mol%) = -0.153xTe+15.55
Cr 0.2 (°C min)	Hexene (mol%) = -0.151xTe+15.47
Cryo TREF[a] - Cr 0.2 (°C min)	Hexene (mol%) = -0.151xTe+15.26

[a]sub-ambient analyses (-20°C) using liquid nitrogen and *o*-DCB (melting point -17.00 °C) as solvent, Cr cooling rate during the crystallization step (°C min), Te elution temperature (°C). Experimental conditions: heating rate = 1°C min^{-1}.

3.3.2.2 CRYSTAF

As described previously, TREF has been widely used to measure the chemical composition distribution of LLDPE samples. It requires two temperature cycles. The fractionation in CRYSTAF needs only one temperature cycle. During the decrease in temperature, the concentration of the polymer in solution (the soluble part) is monitored by the IR detector, and a cumulative curve is obtained. The first derivative of the data provides the CRYSTAF distribution as a function of crystallization temperature. The first derivative is plotted for various LLDPE copolymers in Figure 3-17. The sample profiles obtained were very similar to the TREF profiles. The square at 30°C represents the soluble part of the sample. This part is bigger when the comonomer content increases as observed in TREF. The crystallization temperature is expected to be lower than the melting temperature as observed in DSC and this is even more true in solution. It would be even more interesting here to further decrease the temperature (as in the cryo-TREF experiments).

Like TREF, CRYSTAF separation reveals a linear relationship between the crystallization temperature and the comonomer content (Figure 3-18). A lower resolution and a lower analytical range were observed for CRYSTAF than for TREF. For instance, the sample with 6.3 mol% of hexene is not well resolved and a large part of the sample appeared in the amorphous fraction. This sample was better resolved with TREF. CRYSTAF is, therefore, a rapid analysis technique which allows the simultaneous measurement of several samples for a fairly short time, but it does not reach the resolution and the range of the TREF.

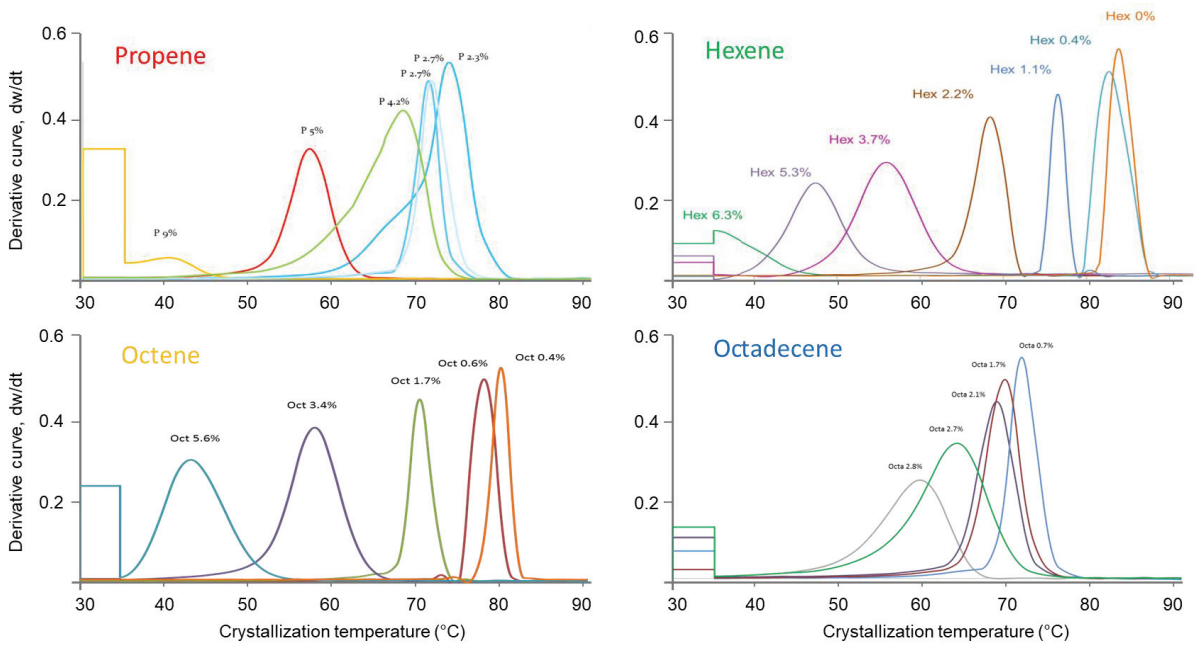


Figure 3-17: CRYSTAF profiles of individual copolymer models with various comonomer contents. Experimental conditions: cooling rate = 0.1°C min^{-1}, solvent = 1,2,4-TCB.

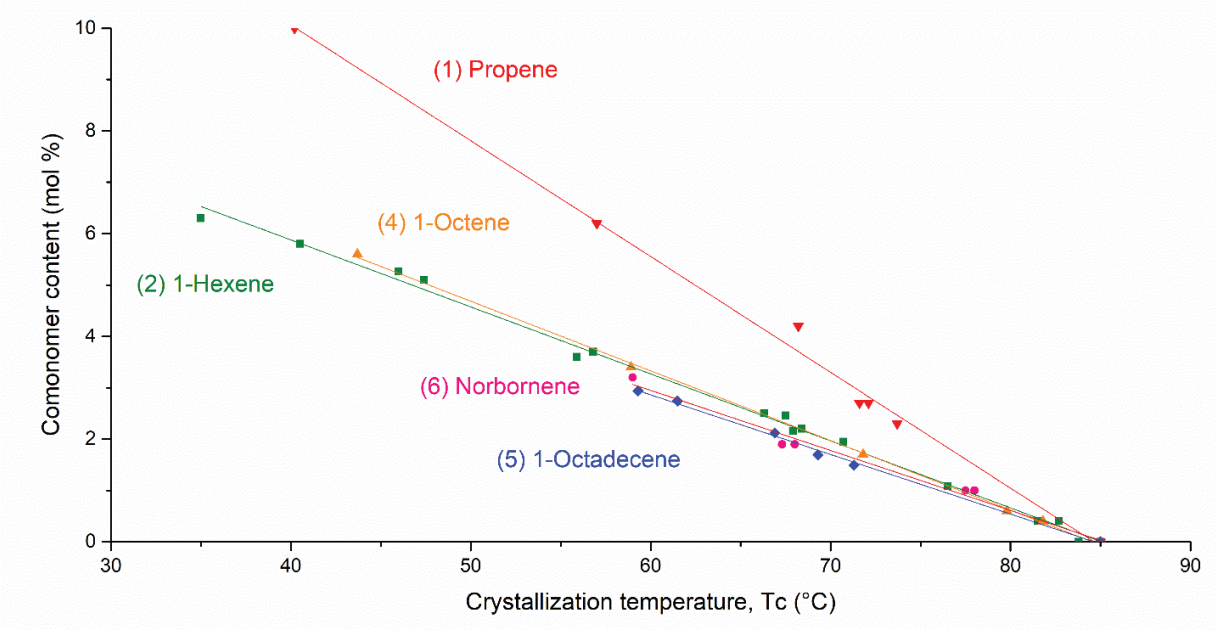


Figure 3-18: CRYSTAF calibration curves for the different series of copolymers. Experimental conditions: cooling rate = 0.1°C min^{-1}, solvent = 1,2,4-TCB.

3.3.2.3 CEF

The effects of co-crystallization, widely studied by Soares and co-workers,[18, 19] weakens the resolution of TREF and CRYSTAF. This effect occurs when polymer chains of distinct compositions tend to crystallize simultaneously and result in a broadening of peaks. This effect can be minimized by the operating conditions. A slow cooling rate is necessary to minimize the co-crystallization but increases the analysis time. The CEF method enables faster analysis, compared to TREF and CRYSTAF, by applying dynamic crystallization during the first step (Table 3-6). The approach minimizes co-crystallization effects by segregating crystallites inside the column. Therefore, the analysis offers a high resolution in a shorter time. In this part our LLDPE models were used to construct calibration curves for our CEF, recently installed in our laboratory.

Table 3-6: Duration of an analysis by fractionation techniques for one sample.

Technique	TREF	CRYSTAF	CEF	TGIC
Duration (min)	260	260	80	120

Setting of instrument parameters

Before starting the analysis, some instrumental constants have to be determined. The CEF and TGIC analysis were done with the same device, so the calibration process was similar. Several instrumental parameters must be adjusted:

- The solvent signal to be subtracted from the signal of the sample,
- The constants of the infrared detector and the viscometer: K_{IR} and K_{IV}
- The volume between the column and the detector: $K_{col\text{-}det}$
- The volume between the detectors: $K_{det\text{-}det}$
- The composition (CH_3/1000C) measured with the IR detector.

To calibrate the above parameters, several experiments are necessary:

- First, the analysis of 1,2,4-TCB stabilized with 2,6-di(ter-butyl)-4-methylphenol (200 mg L^{-1}) was performed with the same method used to analyze the sample. It will be subtracted from the signal of the succeeding samples.

- Next, a standard sample, whose intrinsic viscosity was known, was prepared carefully to know the concentration injected. The NBS1475 served as a reference material for this calibration step. It is a high-density polyethylene having a molar mass: $\overline{M}_w$ = 52 kg mol^{-1} and $\overline{M}_n$ = 18 kg mol^{-1} and an intrinsic viscosity of 1.01 dl g^{-1} in 1,2,4-TCB. This experiment allowed the calibration of the following parameters: K_{IR}, K_{IV}, $K_{det-det}$, $K_{col-det}$. The values obtained for each coefficient are reported in Table 3-7.

K_{IR} is the response factor for the IR and allowed measuring the concentration of the sample according to the Beer-Lambert law:

$$A = \varepsilon l C = K_{IR} C \qquad (3\text{-}4)$$

Where A is the infrared absorbance, ε is the molar attenuation coefficient, ℓ is the optical path length of the cell, c is the concentration of the sample.

Table 3-7: CEF and TGIC calibration constants.

Infrared	**Viscometer**	**Column CEF**	**Column TGIC**	**Inter-detector**
K_{IR}	K_{IV}	$K_{col-det}$	$K_{col-det}$	$K_{det-det}$
0.436 ± 0.006	0.0886 ± 0.0008	3.315 ± 0.005	1.329 ± 0.005	0.187± 0.005

Calibration of methyl/methylene ratio for IR detector

The infrared detector (IR5) is equipped with two cells. One sensor is sensitive to the stretching vibrations in the C-H bonds of methyl groups (CH_3 at 2960 cm^{-1}) and the second sensor is sensitive to the C-H bonds in the methylene groups (CH_2 at 2920 cm^{-1}). Since methyl groups indicate branches, it is possible to determine their number by using the IR detector directly. To quantify the methyl content in unknown samples for the calculation of the comonomer content, it is necessary to calibrate the IR detector with standards of known methyl content.

We used ethylene-butene copolymers provided by the PolymerChar company and some of our ethylene-hexene copolymers as standards to calibrate the IR detector. For this calibration, the mol% of the comonomer was translated into a methyl number for 1000C (CH_3/1000C) according to Equation 3-5. In these conditions the methyl chain ends were neglected.

$$CH_3/1000C = \frac{1000 \times mol\%}{mol\% \times (C_n) + (1 - mol\%) \times 2} \qquad (3\text{-}5)$$

With CH_3/1000C is the methyl number for 1000C, mol% is the comonomer content, C_n is the number of carbons in the α-olefin comonomer.

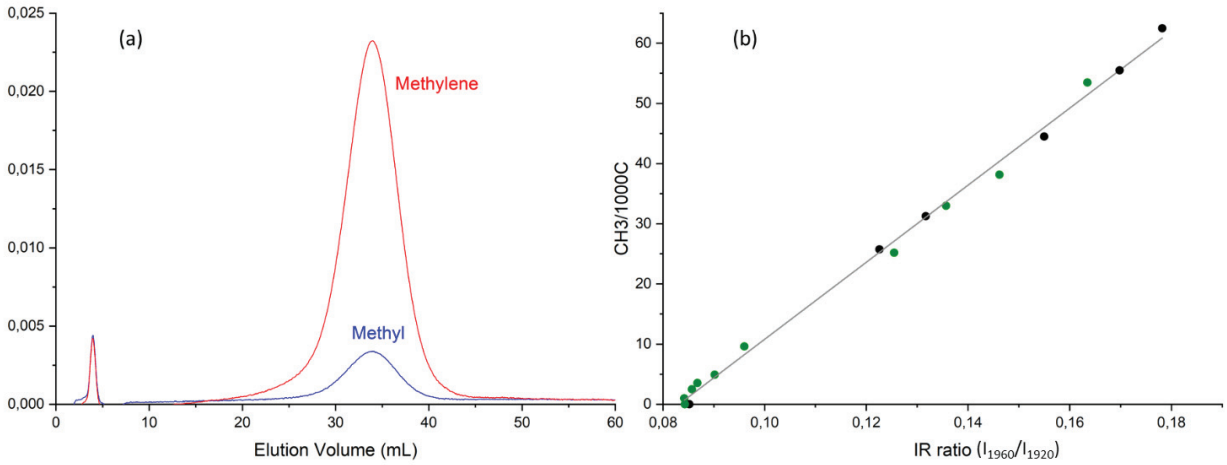


Figure 3-19: Results of the detection of the content of methylene (CH_2) as well as methyl (CH_3) in an ethylene-hexene sample (a). Calibration of the IR detector with ethylene-butene (black points) and ethylene-hexene copolymers (green points) (b).

The IR band ratio (methyl over methylene absorbance, I_{1960}/I_{1920}) was calibrated to methyl groups frequency (CH_3/1000C) using LLDPE standards. During this thesis work the equation was calculated several times and the error estimated (in brackets) could be evaluated. The equation (3-6) obtained is given below:

$CH_3/1000C = 640.2\ (\pm\ 11.3) \times IR_{ratio} - 53.2\ (\pm\ 1.4)$ (3-6)

R-square = 0.996

Therefore, there are two ways to measure the comonomer content, with elution time (calibrated in % of comonomer, Figure 3-21) and with the IR ratio (calibrated in CH_3/1000C, Figure 3-19).

The measurement of methyl groups frequency (CH_3/1000C) by IR has the advantage of being universal and can be used for various ethylene/α olefin copolymers. For unknown samples measured in this way, we can reverse the calculation of the corresponding mol% value depending on the comonomer type with Equation 3-5.

Use of viscometer

The CEF and TGIC system is equipped with a viscometer detector. It is useful to determine the molar masses of the copolymer analyzed. The Mark-Houwink-Sakurada relationship [20, 21] links the intrinsic viscosity, measured by the device, to the molar masses of the polymers thanks to the K and α coefficients.

$$[\eta] = K \times M^{\alpha} \qquad (3\text{-}7)$$

with [η] being the intrinsic viscosity of the compound (mL mol-1), M is the molar mass of the compound (g mol-1), K (mL g-1) and α are the characteristic coefficients of the polymer/solvent couple at a given temperature (for PE in 1,2,4-TCB at 150 °C, K = 73.6 x10-6 L g-1 and α = 0.67).

For each fraction separated by chemical composition, the viscometer can access the intrinsic viscosity making it possible to link the molar masses to a fraction of comonomer content.

Calibration of CEF with copolymer models

After adjusting the instrumental constants, our copolymer samples were analyzed by CEF (Figure 3-20).

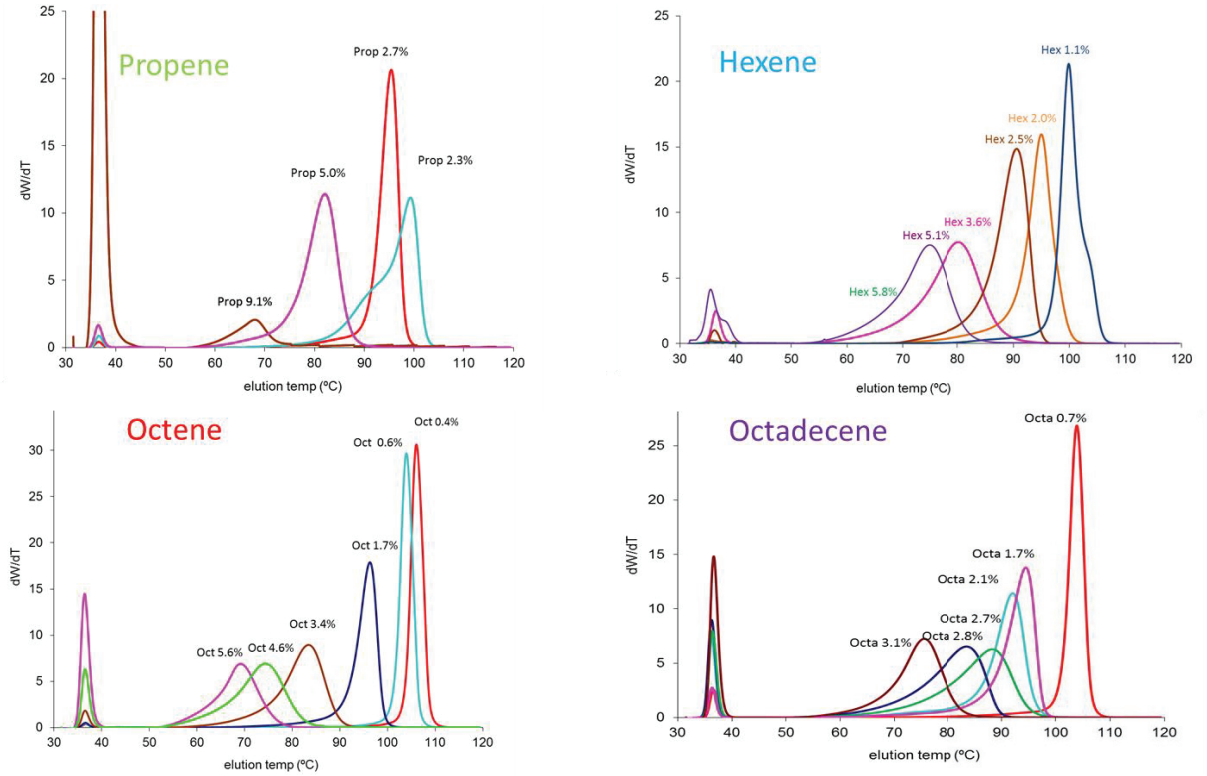


Figure 3-20: CEF profiles of individual copolymer models with various comonomer contents. Experimental conditions: cooling rate = 2°C min^{-1}, cooling flow = 0.05 mL mn^{-1}, heating rate = 4°C min^{-1}, heating flow = 1 mL min^{-1}, solvent = 1,2,4-TCB.

Similar behaviors and profiles from TREF were observed. As expected, the analysis time was significantly reduced by a factor of 3 for the same resolution. The ethylene-propylene sample with 2.3 mol% of propylene shows a clear shoulder in its CEF profile. For this sample, the polymerization conditions probably drifted during the synthesis, resulting in a second population of chemical compositions. CEF can thus, be a powerful and precise tool for controlling synthesis conditions.

We plotted the elution peak temperature obtained by CEF as a function of the comonomer content. The calibration curves for the five series of copolymers are traced and overlayed in Figure 3-21:

- The ethylene-propylene copolymers have a specific behavior compared to the other copolymers because of the capacity of incorporation of the methyl groups in the crystallites. This behavior was also observed for TREF and DSC.
- For ethylene-norbornene and ethylene-octadecene copolymers, the steric hindrance of the branches affects the elution time. Therefore, these copolymers require their own calibration curve as observed for TREF.
- A common calibration for ethylene-hexene and ethylene-octene copolymers can be used since the calibration lines are comparable.

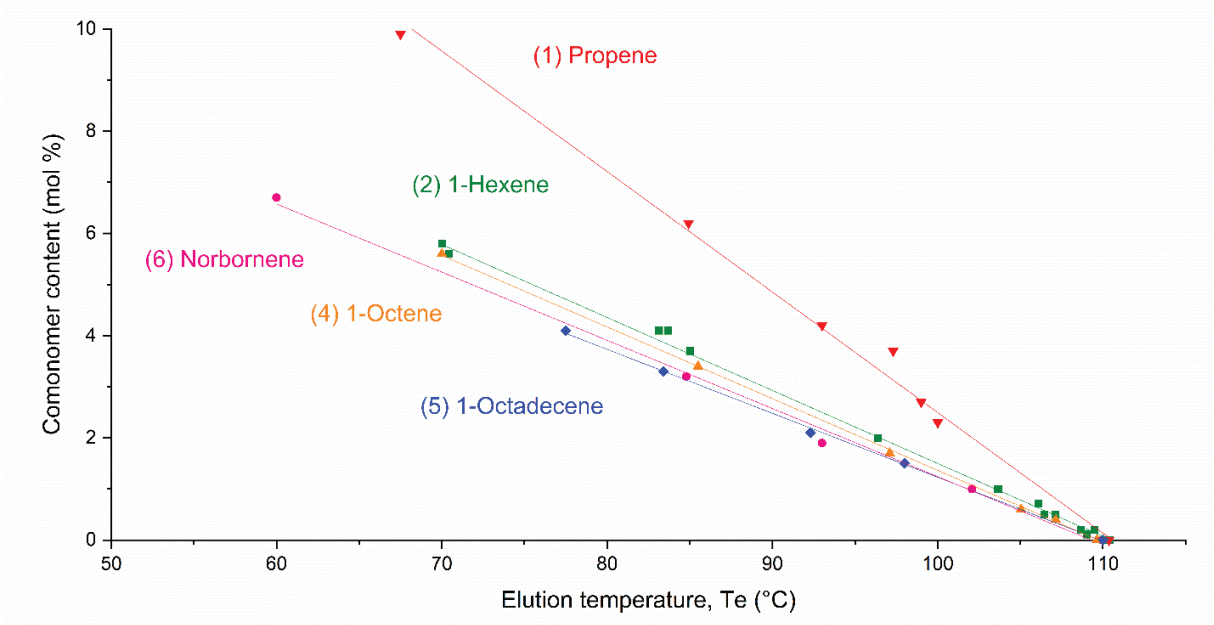


Figure 3-21: CEF calibration curves for the different series of copolymers. Experimental conditions: cooling rate = 2°C min^{-1}, cooling flow = 0.05 mL mn^{-1}, heating rate = 4°C min^{-1}, heating flow = 1 mL min^{-1}, solvent = 1,2,4-TCB

3.3.3 FRACTIONATION TECHNIQUES BASED ON INTERACTION

Fractionation techniques based on crystallization have several limitations when characterizing ethylene copolymers. Two innovative techniques have been developed to improve the measurement of comonomer contents: solvent gradient interaction chromatography and thermal gradient interaction chromatography (SGIC and TGIC). With these methods, co-crystallization is reduced, and amorphous polymers can finally be analyzed. These techniques combine separation by crystallization and by adsorption on the surface of the column stationary phase.

3.3.3.1 TGIC

A new and original technique developed by Cong and commercialized by PolymerChar was installed in our laboratory. The TGIC separation is based on the interaction of the sample with the column and therefore can also be applied for non-crystalline polymers. We used this instrument to investigate its capacity to separate highly branched copolymers and other kinds of ethylene copolymers such as ethylene-butadiene and ethylene/vinyl acetate copolymers. Although they were analyzed by TGIC, the results will not be discussed here. This part is focused to the analyses by TGIC of our copolymer models: profiles of ethylene-hexene copolymers in Figure 3-22 and profiles of ethylene-norbornene copolymers in Figure 3-23.

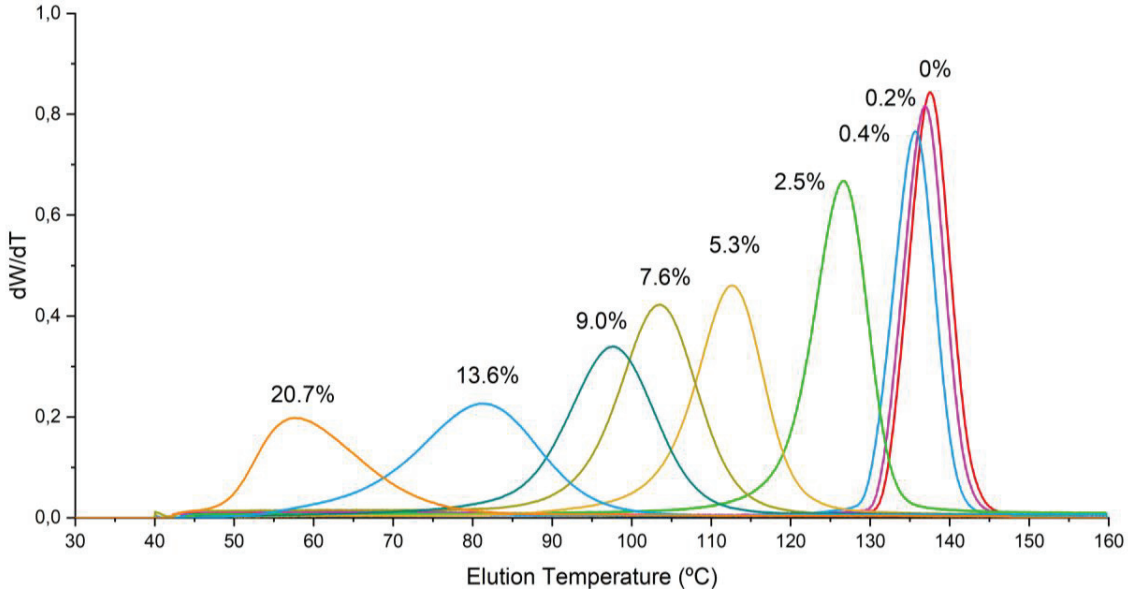


Figure 3-22: TGIC profile of individual ethylene-hexene copolymer models with various comonomer contents. Experimental conditions: cooling rate = 20°C min^{-1}, cooling flow = 0 mL min^{-1}, heating rate = 2°C min^{-1}, heating flow = 0.5 mL min^{-1}, solvent = 1,2,4-TCB.

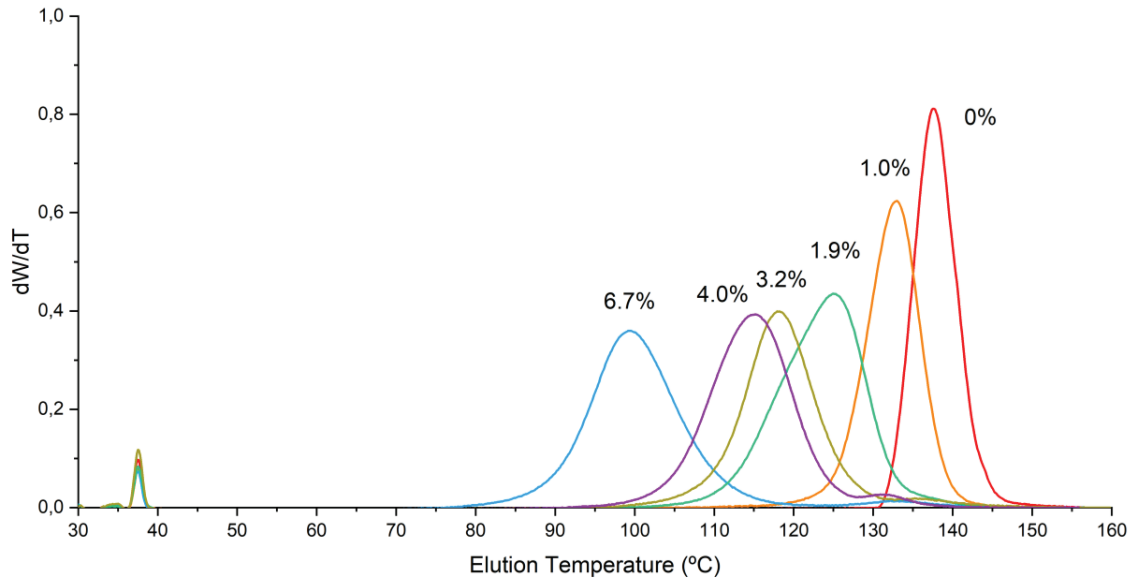


Figure 3-23: TGIC profile of individual ethylene-norbornene copolymer models with various comonomer contents. Experimental conditions: cooling rate = 20°C min^{-1}, cooling flow = 0 mL min^{-1}, heating rate = 2°C min^{-1}, heating flow = 0.5 mL min^{-1}, solvent = 1,2,4-TCB.

The other families of copolymers (ethylene-propylene, ethylene-octene, and ethylene-octadecene) were also analyzed. We plotted the temperature of the elution peak obtained by TGIC as a function of the comonomer content. The set of calibration curves obtained are compared in Figure 3-24.

- For TGIC, the behaviors of ethylene-propylene copolymers and ethylene-norbornene copolymers are similar to those observed for other crystallization-based techniques (TREF, CRYSTAF, CEF). However, the calibration curve for ethylene-propylene copolymers is very different from the other curves. It reveals that the CH_3 groups are less disruptive to the interactions between the backbone and the column than the other bulkier groups.
- For octadecene, the behavior is quite different from that observed with crystallization-based techniques. It is also slightly different from the other copolymers; the slope of the curve is significantly higher than that of ethylene-hexene copolymers. This means that the branches are long enough to interact by themselves with the hypercarbon column, which leads to an increase in the elution temperature.
- As expected, the working range of ethylene-hexene copolymers is broader than for all other fractionation techniques. Indeed, we efficiently separated ethylene-hexene copolymers up to 21 mol% of hexene. With CEF and the other techniques the limit was around 7 mol% of hexene.

- An order of one or even an order of three can be used for a better fit of data points at high comonomer contents. In this case (> 20mol%) the polymer is mainly amorphous and the crystallization mechanism is not involved. The significance of the elution temperature is then very different, as it combines both polymer/column interaction and dissolution. This could also explain why the elution temperature does not follow a simple linear rule and a deviation is observed for high comonomer content.

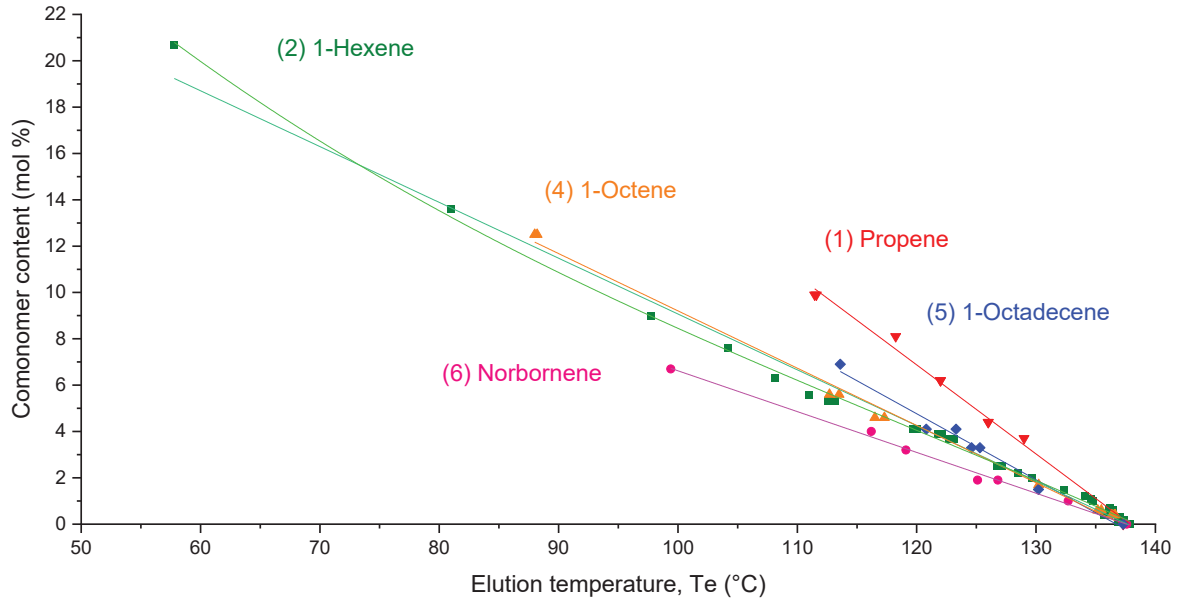


Figure 3-24: TGIC calibration curves for the different series of copolymers. Experimental conditions for TGIC: cooling rate = 20°C min^{-1}, cooling flow = 0 mL min^{-1}, heating rate = 2°C min^{-1}, heating flow = 0.5 mL min^{-1}, solvent = 1,2,4-TCB.

Variation in analytical conditions

Many variations of TGIC parameters were tested by Soares and co-workers.[22, 23] Our optimal analytical conditions were selected using their conclusions. However, inspired by the CEF method, we decided to test the impact of adding a flow of the solvent during the cooling step (cooling flow) in the method. For CEF, this adjustment allowed increasing the resolution.

The comparison was therefore carried out between the classical analytical method named "TGIC-a" and the proposed method with a cooling flow named "TGIC-b". The analytical conditions for these two methods are detailed and compared in Table 3-8.

Table 3-8: Detailed parameters for methods TGIC-a and TGIC-b.

Analytical parameters	Symbol	Units	Values TGIC-a	Values TGIC-b
Cooling rate	Cr	°C min^{-1}	20	5
Cooling flow	Fc	mL min^{-1}	0	0,02
Crystallization start temperature		°C	150	150
End crystallization temperature		°C	35	35
Heating rate	Hr	°C min^{-1}	2	3
Elution flow	Fe	mL min^{-1}	0.5	0.5
Analysis time		min	120	120

Solvent: 1,2,4-TCB.

For this comparison, six ethylene-hexene samples with various hexene contents were analyzed by the two methods and the profiles obtained are plotted in Figure 3-25.

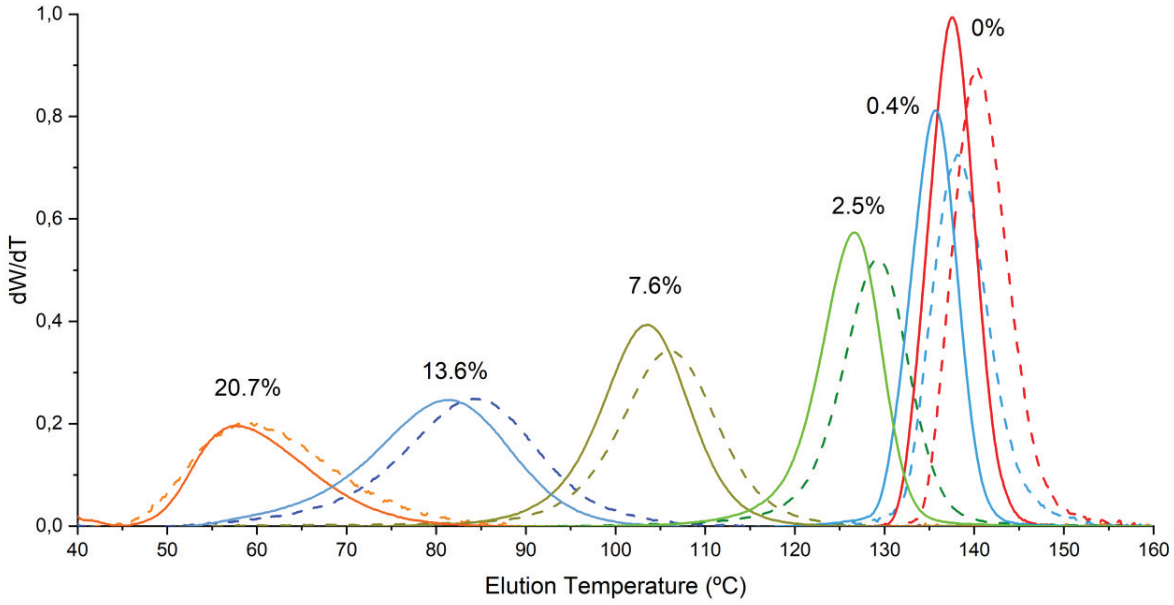


Figure 3-25: Profiles of ethylene-hexene copolymers with various contents of hexene (in mol%) measured by the classic method (TGIC-a) shown by the solid line and by the method with the cooling flow (TGIC-b) by the dashed line. Solvent: 1,2,4-TCB.

The efficiency and resolution of both methods were compared. We observed a shift of 1 °C in the elution temperature, without a change in the shape of the peaks. Regarding the result we cannot consider an increase in resolution between the peaks. It can be concluded that there was no significant variation regardless of the used method. It is therefore advisable to use the classical method without a cooling flow.

TGIC's broad range of separation, reaches 50 mol% of octene.[5] This range is better than other techniques based on crystallization, but it is still narrower than that of SGIC, which covers the full range of comonomer incorporation. The latter technique was also applied to our copolymer models in the next section.

3.3.3.2 SGIC

Tibor Macko and co-workers have recently developed an innovative SGIC. To complete the calibration of all the fractionation techniques available, we proposed our copolymer samples to Tibor Mack to perform an original calibration dedicated to SGIC. Ethylene-propylene, ethylene-hexene, ethylene-octene and ethylene-octadecene copolymers were injected into the SGIC instrument after optimizing the analytical conditions. The elution profiles obtained are plotted in Figure 3-26.

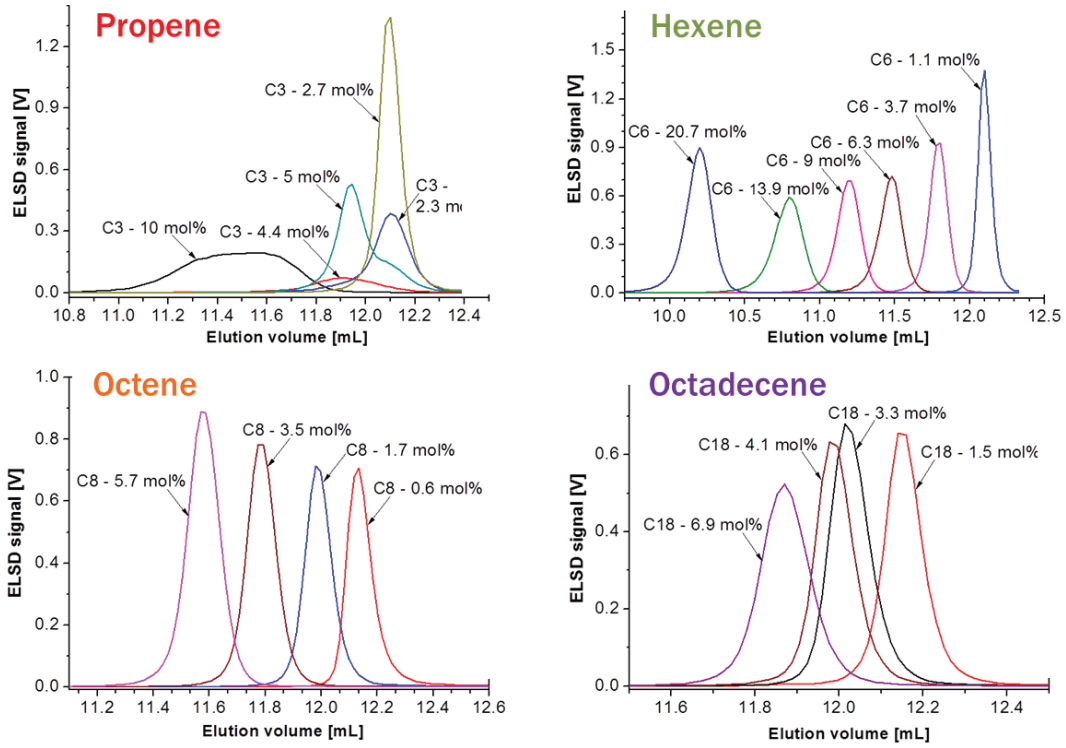


Figure 3-26: SGIC profiles of individual copolymer models with various comonomer content. Experimental conditions: temperature = 160°C, flow rate = 1 ml min^{-1}, mobile phase = 2-ethyl-1-hexanol to 1,2,4-TCB, Hypercarb column from Thermo Scientific (average particle size 5 µm).

The analysis of our copolymer samples was used to construct calibration curves to correlate the comonomer content versus the elution volume at the top of the peak (Figure 3-27). The elution volume is directly proportional to the comonomer content as with all the other fractionation techniques and it is also affected by the length of the branches.

The calibration curves showed good linearity, proving the considerable interest of this technique. The analytical range is wide, ethylene-hexene copolymers up to 20 mol% were efficiently separated by the method.

Various analytical conditions were assessed: type of mobile phase, temperature, solvent, etc. This work, focusing on the variation of analytical conditions for improving the separation of our copolymers, was published in Macromolecular Chemistry and Physics. This publication is a subsequent part of this chapter.

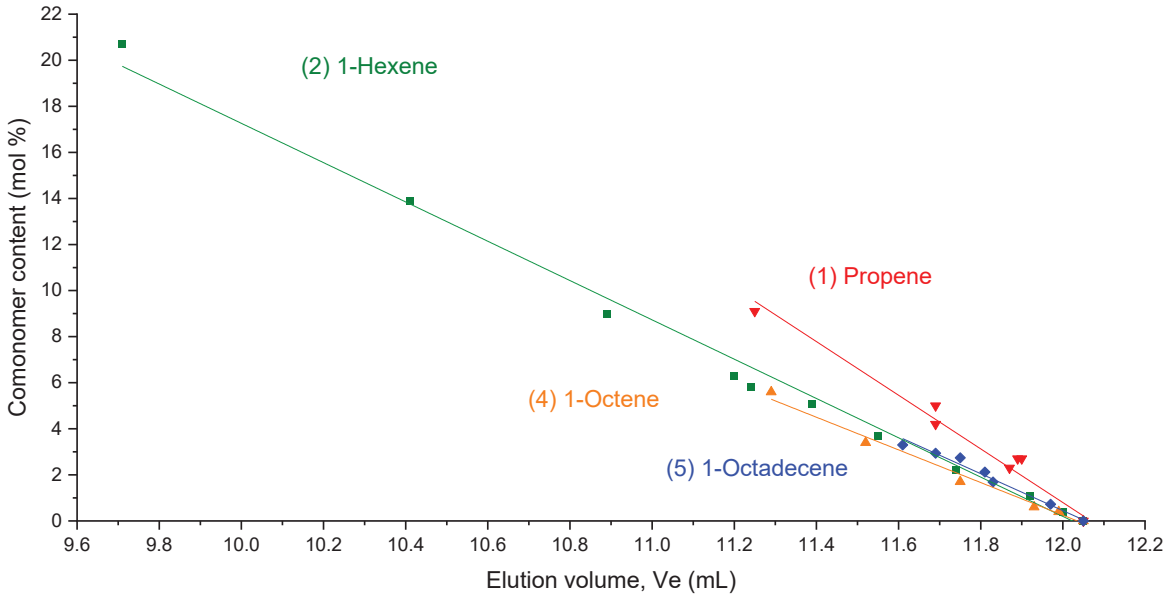


Figure 3-27: SGIC calibration curves for the different series of copolymers. Experimental conditions: temperature = 160°C, flow rate = 1 ml min^{-1}, mobile phase = 2-ethyl-1-hexanol to 1,2,4-TCB, Hypercarb column from Thermo Scientific (average particle size 5 µm).

3.3.4 COMPARISON OF TECHNIQUES (CEF AND TGIC)

It is agreed that CEF can effectively replace thermal fractionation techniques based on crystallization (TREF and CRYSTAF), the following part will be devoted to the comparison of this technique with the TGIC technique. In particular, their separation efficiency, their working range and the impact of molar masses on the separation of these two techniques were confronted.

Three LLDPE industrial samples of unknown composition were characterized by CEF and TGIC to illustrate the information that can be obtained by these techniques. The Figure 3-28 shows a representation of comonomer content distribution obtained using the calibration equation constructed with our copolymer models. The x-axis corresponding to the elution volumes on the chromatogram is thus transformed into the amount of comonomer. This is the chemical composition distribution curve.

The analytical range (in mol% of comonomer) for TGIC is wider than that for CEF; in TGIC amorphous samples can be separated. However, with CEF a better resolution is obtained as can be seen in Figure 3-28. Indeed, the blue and orange samples showed two peaks, indicating the presence of two families with various comonomer contents in CEF and a third peak characteristic of the amorphous part. All these fractions can be easily quantified by CEF. Conversely, a broader elution peak is observed on the TGIC profiles with a drag towards the region where the second peak is expected. Obviously, CEF leads to better separation for complex samples.

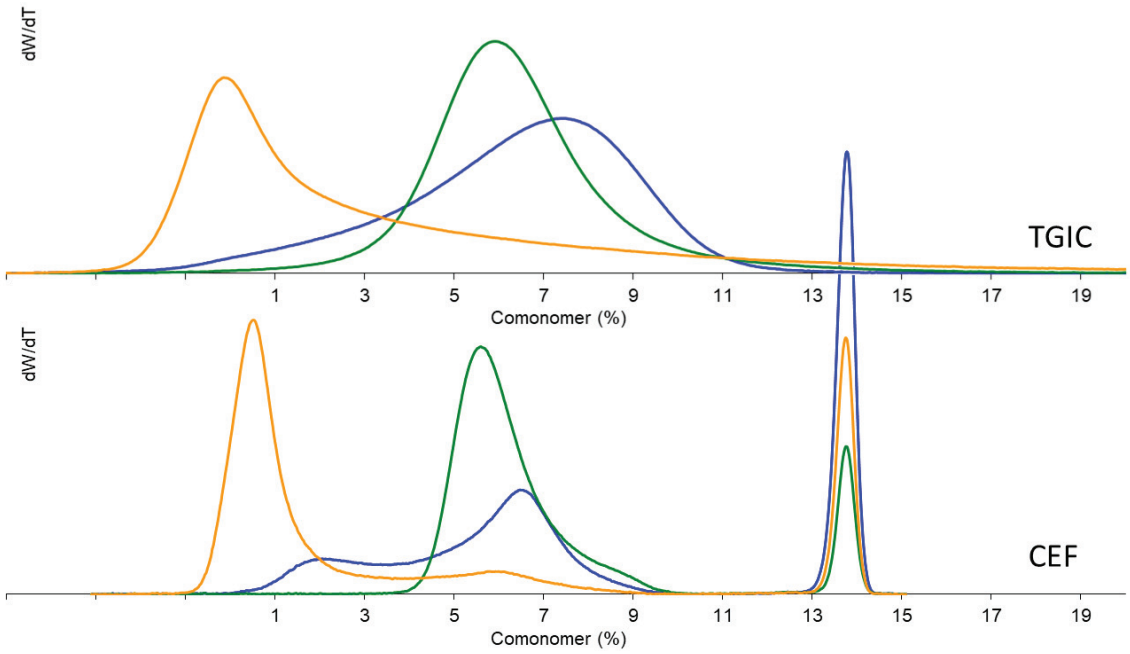


Figure 3-28: Comonomer distribution of unknown industrial samples analyzed by TGIC and CEF. Comonomer distributions were obtained using the calibration curve for ethylene-hexene copolymers from Table 3-9. Experimental conditions for CEF: cooling rate = 2°C min^{-1}, cooling flow = 0.05 mL mn^{-1}, heating rate = 4°C min^{-1}, heating flow = 1 mL min^{-1}, solvent = 1,2,4-TCB. Experimental conditions for TGIC: cooling rate = 20°C min^{-1}, cooling flow = 0 mL min^{-1}, heating rate = 2°C min^{-1}, heating flow = 0.5 mL min^{-1}, solvent = 1,2,4-TCB.

The comparison of TGIC and TREF for a series of ethylene-octene copolymers has been reported[17], demonstrating that resolution with TREF is slightly better than with TGIC for medium density resins. TREF and other crystallization techniques are also more appropriate for industrial LLDPE materials with low comonomer content. However, since the separation mechanism is not based on polymer crystallization, TGIC covers a wider compositional range down to the amorphous region, which crystallization techniques cannot reach. In addition, TGIC requires shorter analysis times because adsorption/desorption mechanism is faster than crystallization.

3.3.5 ULTRA-HIGH MOLECULAR WEIGHT POLYETHYLENE (UHMWPE)

3.3.5.1 Impact of molar mass on elution temperature

Molar mass is a parameter that influences the elution temperature of the copolymer. Indeed, Soares and coworkers[23] determined that the molar mass of the polymers studied had no impact on separation if $\bar{M}_n$ is higher than 25 kg mol^{-1}. In order to determine our own detection limit and the linear range of our apparatus, various homo-PE samples of known and certified molar masses were injected. The elution temperature peaks as a function of the molar mass are plotted in Figure 3-29.

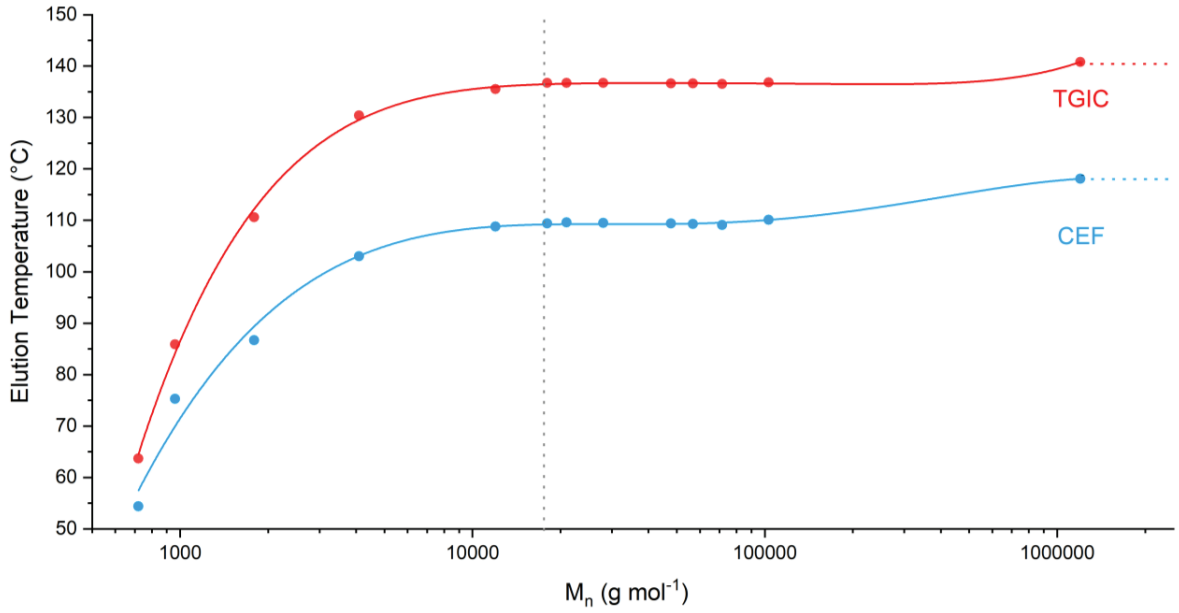


Figure 3-29: Impact of molar mass on the elution temperature of homo-PE for CEF and TGIC. Experimental conditions for CEF: cooling rate = 2°C min^{-1}, cooling flow = 0.05 mL mn^{-1}, heating rate = 4°C min^{-1}, heating flow = 1 mL min^{-1}, solvent = 1,2,4-TCB. Experimental conditions for TGIC: cooling rate = 20°C min^{-1}, cooling flow = 0 mL min^{-1}, heating rate = 2°C min^{-1}, heating flow = 0.5 min^{-1}, solvent = 1,2,4-TCB.

For both techniques, a minimum molar mass of 720 g mol^{-1} is necessary in order to observe a peak outside the soluble fraction. A plateau is reached at 110 °C for CEF and at 138 °C for TGIC for samples having molar masses greater than 17 Kg mol^{-1}. The limit announced by previous works is therefore slightly higher than that obtained in our conditions.

Nevertheless, the last polymer in Figure 3-29 has a very high molar mass ($\overline{M}_n$ = 1 200 Kg mol^{-1} and Đ = 1.8) and shows an unusual behavior both in CEF and in TGIC. The polymer elutes at higher temperatures than usual (115 °C against 110 °C for CEF and 139 °C instead of 138 °C for TGIC). Polymers of high molar mass seem to crystallize in a different way for CEF and thus are eluted at high temperature. The elution temperatures obtained for high molar mass PE are significantly higher than that obtained for our synthetized homo-PE. This behavior has not yet been discussed in the literature, and it seems important to study it more precisely. This is the subject of the following part.

3.3.5.2 UHMWPE melting process (DSC)

Ultra-high molecular weight PE (UHMWPE) is a class of high-performance polymers with unique properties such as Dyneema® fiber of DSM. They paved the way for new applications to obtain materials that are both ultra-strong and ultra-light. This type of PE is more and more studied in our laboratory and therefore we were also interested in its behavior when analyzed by thermal fractionation techniques. Further investigations were performed with polymers synthesized by Astrid Cordier during her thesis work in our laboratory. Several UHMWPE samples obtained with a single phenoxy-imine-methoxy (SFI) catalyst were analyzed by DSC (Figure 3-30) and also characterized by CEF and TGIC (Figure 3-32).

For UHMWPE we observed an elevated melting temperature measured by DSC, up to 144°C, during the first heating step. However, a lower melting temperature and crystallinity were observed for the second heating step after a 5-minutes isotherm at 180°C followed by a cooling at a rate of 10°C min^{-1}.

Similar results were reported by Rastogi and co-workers who investigated the melt behavior of UHMWPE by DSC.[26-29] They proposed that the higher temperature peak (144°C) obtained in the first step could be attributed to the polymer chains which are disentangled and producing exceptionally large crystalline lamellae than those usually observed. The use of homogeneous single-site catalyst makes possible to obtain a disentangled UHMWPE. Indeed, in this system, the active sites are dispersed and distant from each other. During the propagation reaction, the chains being far apart, they are unlikely to get entangled (Figure 3-31 a).

In the DSC experiment, upon crystallization from the melt state, most of the entanglements are trapped in the solid leading to a lower melting temperature (136 ° C) in the second melting step.

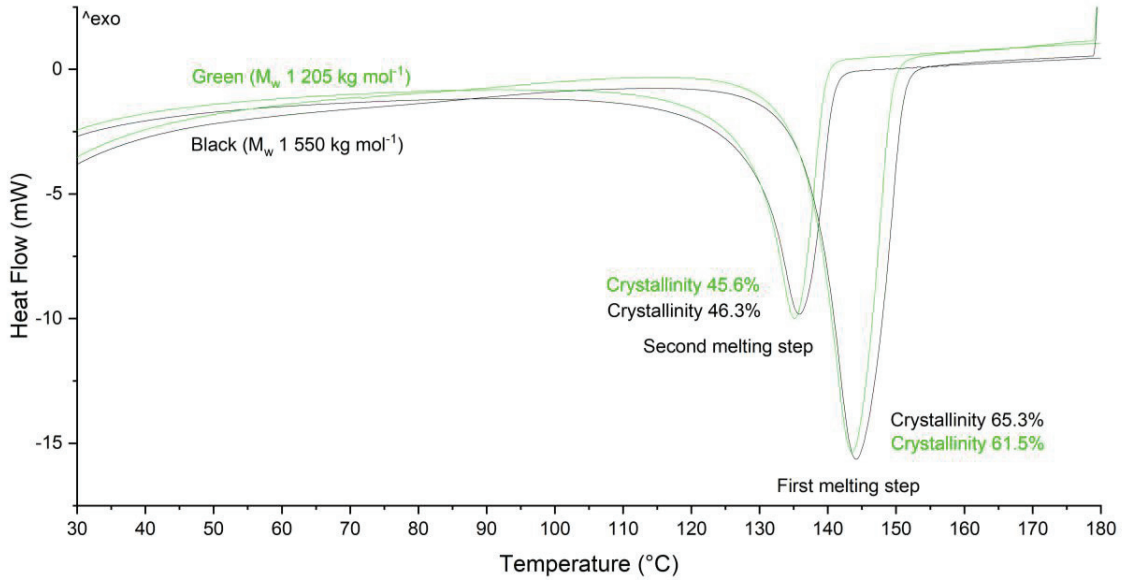


Figure 3-30: DSC curve acquired on the first and second heating runs on two disentangled UHMWPE (>1,200 kg mol^{-1}). Heating rate of 10°C min^{-1} under nitrogen atmosphere. Similar DSC curves were observed for different molar masses.

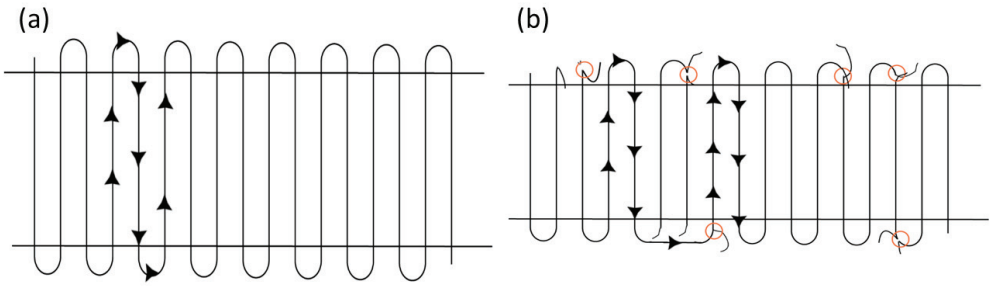


Figure 3-31: Schematic model of the folded crystal structure of (a) a nascent disentangled sample and (b) a nascent entangled sample. The entanglements are circled in red.

To follow the UHMWPE melting process, Rastogi et al. studied the effect of annealing below the melting temperature. A heating step on the annealed samples showed two distinct melting peaks, proving the existence of two types of crystallites. The peak with a higher melting temperature (144°C) suggests a crystalline enhancement obtained with disentangled chains (Figure 3-31 a). The lower endothermic peak (135°C) is independent of the annealing parameters and indicates imperfect crystals obtained with entangled chains (Figure 3-31 b). In this case, the thickness of the lamella is smaller.

3.3.5.3 UHMWPE elution process (CEF)

In the present work, similar behavior was observed for CEF with two elution temperature peaks at 110°C and 115°C, respectively (Figure 3-32).

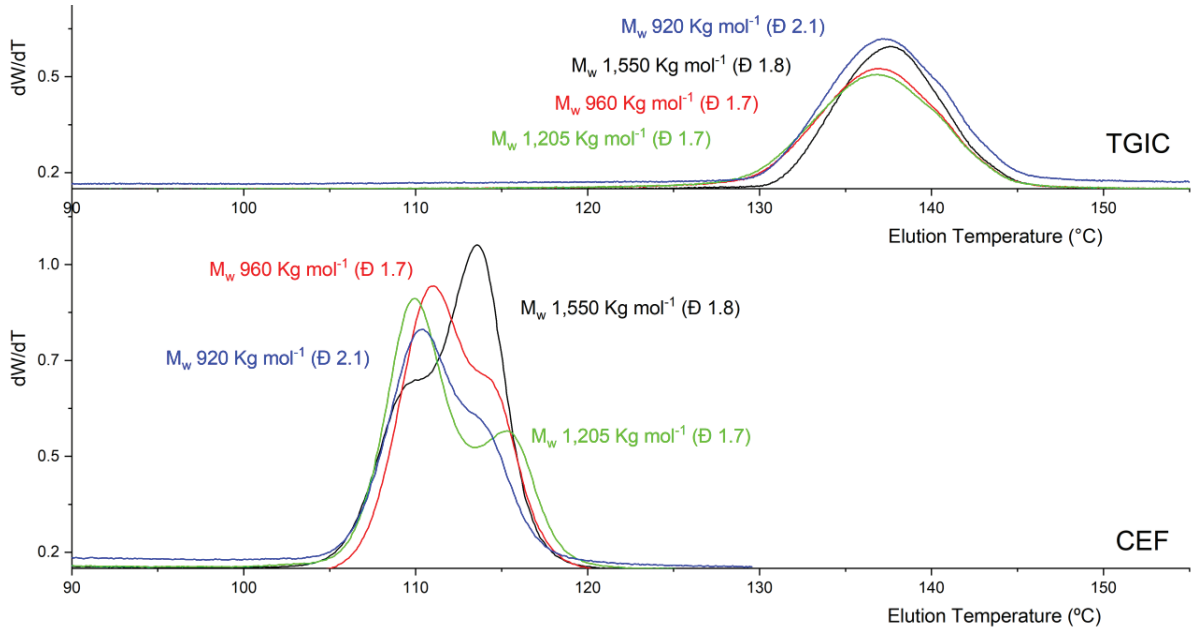


Figure 3-32: Comparison of TGIC and CEF profiles for UHMWPE synthetized with a phenoxy-imine (SFI) catalyst. Experimental conditions for CEF: solubilization temperature = 160°C for 2h, cooling rate = 2°C min^{-1}, cooling flow = 0.05 mL mn^{-1}, heating rate = 4°C min^{-1}, heating flow = 1 mL min^{-1}, solvent = 1,2,4-TCB, concentration = 2 mg ml^{-1}. Experimental conditions for TGIC: solubilization temperature = 160°C for 2h, cooling rate = 20°C min^{-1}, cooling flow = 0 mL min^{-1}, heating rate = 2°C min^{-1}, heating flow = 0.5 mL min^{-1}, solvent = 1,2,4-TCB, concentration = 1 mg ml^{-1}.

Concerning the CEF experiments of our UHMWPEs (Figure 3-32), we observed a peak at 110°C as expected for homo-PE and as the molar mass of the samples increased, a shoulder at high elution temperature was clearly visible in the profile. The intensity of the shoulder increased with the molar mass; it even became the major peak of the sample with the highest molar mass (black profile in Figure 3-32). The CEF profile suggests the presence of two types of crystallites as observed in DSC annealing experiments.

As Rastogi et al showed by DSC, UHMWPEs have the ability to crystallize at high temperature forming large lamellae when conditions allow. These chains are eluted at higher temperature. The peak at 115°C corresponds to these disentangled chains. Perhaps the conditions are not totally favorable to disentanglement and we observe a second peak at lower temperature due to entangled chains.

These entangled chains can appear for two reasons:

1- depending on their distance from the stationary phase of the column, which acts as a nucleating agent and favors the creation of small lamellae (110°C). If the distance between the chain and the surface of the column increases, it has less effect on the chains. They crystallize into lamellae of larger thicknesses that melt at higher temperatures (115°C). A test, described in the following section, was performed in DSC to measure the crystallization, and melting temperature in solvent condition but without a support (column).

2- depending on the local concentration of the polymer chains. If the concentration is below the critical concentration, the chains do not interact with each other and do not entangle; if the concentration is higher, the chains can interact and entangle. Both conditions can be observed in the CEF. Large lamellae can be created when the chains in solution are far apart. They can crystallize slowly in the same way as disentangled chains produced with a homogeneous single-site catalyst. A small-angle X-ray scattering (SAXS) study will be conducted to follow the crystal lattice of these high molar mass PE as a function of temperature under solvent conditions (1,2,4-TCB). This study will probably clarify the understanding of the second peak formation.

This high-molar mass effect is less observed in TGIC analysis. It can be justified by the different separation in TGIC since it is not only based on crystallization.

The lower limit given by Soares and co-workers is therefore not the only one to be considered for the samples. We can conclude that samples between 17 Kg mol^{-1} and 1 million Kg mol^{-1} can be compared with each other. The only effect of separation is the length and content of branching. Below or beyond this limit, the molar mass of the polymer will impact its elution.

CEF is also a means of identifying the presence of very high-molar mass chains in a sample when an elution peak appears around 115°C.

3.3.5.4 UHMWPE melting and dissolution process (DSC)

To better understand the behavior of UHMWPE in CEF further investigations were carried out. DSC experiments were conducted under solvent condition on a medium molar mass HDPE (30 kg mol^{-1}) as a reference and a UHMWPE (6,000 Kg mol^{-1}). To be as close as possible to the concentration required in CEF a quantity of 0.1 mg of sample was added in 100 µl of 1,2,4-TCB in a 120 µl medium pressure crucible. A

temperature program identical to that of CEF was used: dissolution at 150°C, cooling to 25°C at a rate of 2°C min^{-1} and heating at 4°C min^{-1} to 130°C.

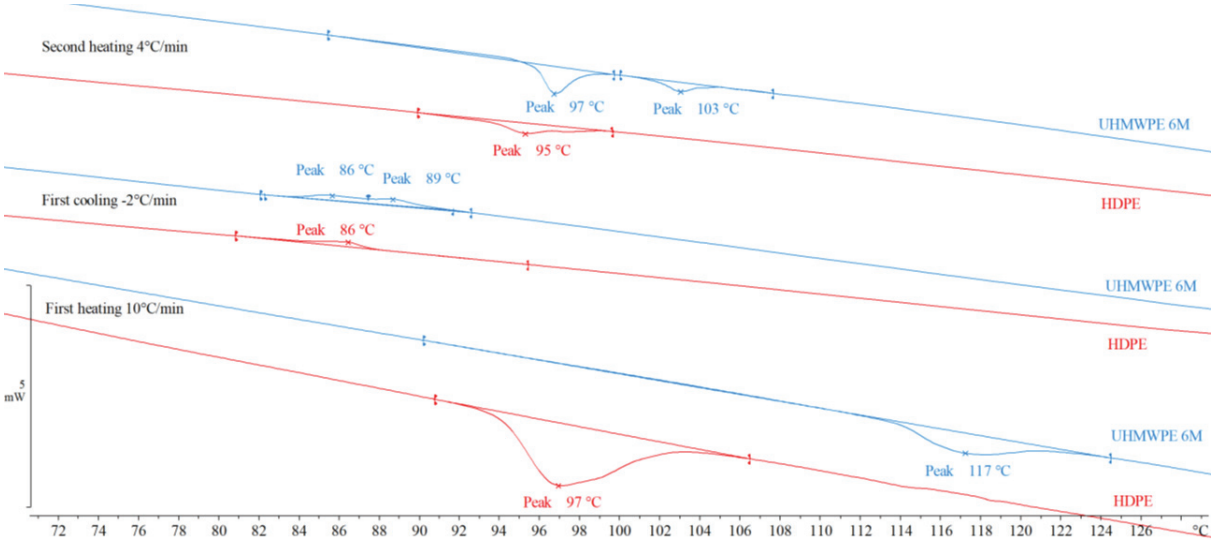


Figure 3-33: DSC curves acquired on an UHMWPE (6,000 kg mol^{-1}) and an HDPE (30 kg mol^{-1}) with a first heating rate at 10°C min^{-1} to 130°C, a cooling rate at 2°C min^{-1} and a second heating rate at 4°C min^{-1} under nitrogen atmosphere. Similar DSC curves were observed for different UHMWPE.

For UHMWPE, during the first heating, a melting peak at high temperature (117°C) appears. This peak increases with the molar mass of the UHMWPE sample. For a UHMWPE of 2,000 Kg mol^{-1} it was observed a little below at 115°C. The thickness of the lamellae seems to be linked to molar mass.

During low-rate cooling (-2°C min-1), two peaks appear for UHMWPE. The one at low temperature (86°C) is similar to that observed for a conventional HDPE of medium molar mass. This value is similar to that obtained by CRYSTAF for HDPE samples (Figure 3-17). The presence of a second peak is not usually observed in DSC under bulk (solvent-free) conditions. Under solvent and low-velocity cooling conditions, UHMWPE can crystallize as a long lamella in the disentangled mode. A second fraction, which probably corresponds to entangled chains, crystallizes at lower temperatures.

During the second heating, corresponding to the elution in the CEF experiment, two peaks were observed. The temperature of the lower peak, at 97°C, is similar to that of HDPE. The second peak is 6°C higher in temperature. This behavior is similar to that observed previously in the CEF experiments. We can assume that the higher peak is related to disentangled chains and the lower one to entangled chains. The conditions of low polymer concentration in solution promote the emergence of the peak at high temperature.

A column filled with inert beads is used in CEF to promote crystallization of chains. By being able to crystallize at higher temperature than in DSC they are solubilized or eluted at higher temperature: 110 and 115°C in CEF instead of 86 and 89°C in DSC.

3.4 CONCLUSION

Over the past 10 years, driven by the development of increasingly controlled synthesis methods and of polymers with increasingly better-defined structures, many developments have been achieved regarding the characterization of polyolefins. Several novel and original fractionation techniques were invented and developed, and we had the opportunity of installing some of them in our laboratory to improve the analytical capability of our team.

The proficiency, in our laboratory, of controlled synthesis methods via the use of metallocene catalysts for the polymerization of olefins allowed us to conceive copolymer models and to calibrate all the fractionation techniques used to characterize the main industrial ethylene-α-olefin copolymers. The calibration equations that can now be used in industrial and academic laboratories, and in control and research services, are summarized in Table 3-9.

Table 3-9: Calibration equation for various thermal fractionation techniques.

Comonomer	TREF	CRYSTAF	CEF	TGIC	SGIC
Propene	-0.23xTe+24.2	-0.22xTc+19.1	-0.24xTe+26.1	-0.38xTe+53.0	-11.6xVe+140.5
R^2	(0.991)	(0.993)	(0.994)	(0.991)	(0.980)
Hexene	-0.15xTe+15.5	-0.13xTc+11.1	-0.14Te+15.8	-0.24xTe+33.2	-8.5xVe+102.6
R^2	(0.997)	(0.996)	(0.997)	(0.992)	(0.993)
Octene	-0.16xTe+16.1	-0.13xTc+11.5	-0.14xTe+15.4	-0.25xTe+33.9	-7.1xVe+85.3
R^2	(0.997)	(0.999)	(0.997)	(0.994)	(0.987)
Octadecene	-0.12xTe+12.1	-0.12xTc+9.8	-0.12xTe+13.7	-0.28xTe+38.9	-8.0xVe+96.7
R^2	(0.990)	(0.996)	(0.998)	(0.990)	(0.985)
Norbornene	-0.14xTe+14.5	-0.12xTc+9.9	-0.13xTe+14.6	-0.18xTe+24.2	
R^2	(0.990)	(0.987)	(0.996)	(0.993)	

Te: elution temperature, Tc: crystallization temperature, Ve: elution volume, R^2: R-squared, the square of the sample correlation coefficient ranges from zero to one.

To illustrate the use of these equations, two industrial samples were characterized by CEF (Figure3-33).

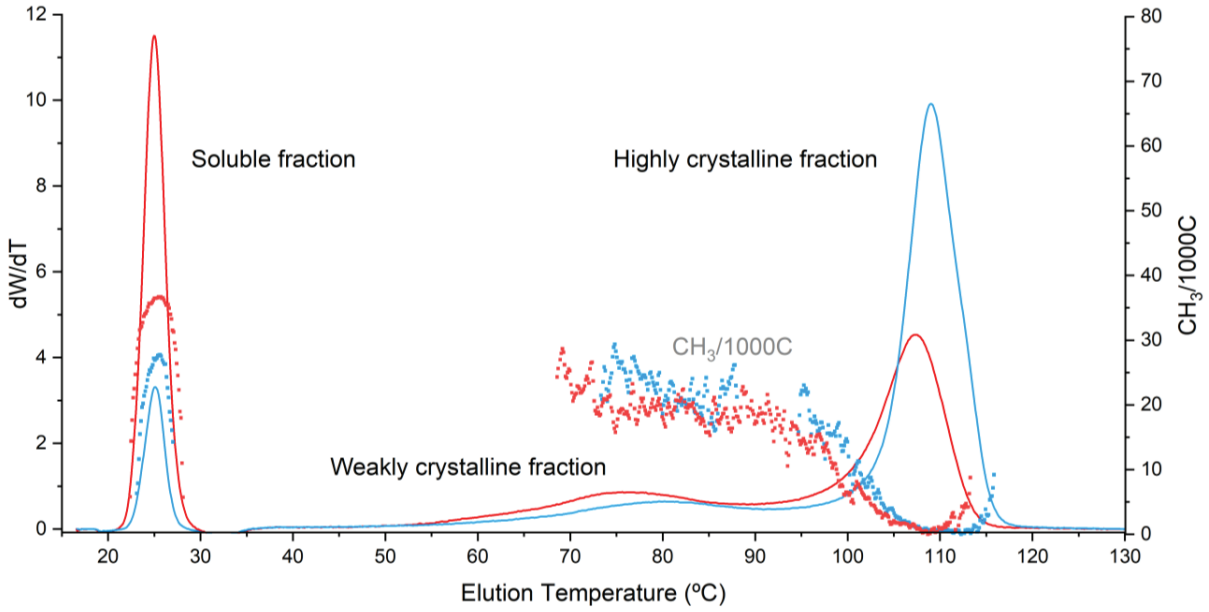


Figure 3-34: CEF profiles for two industrial samples. Experimental conditions: cooling rate = 2°C min^{-1}, cooling flow = 0.05 mL mn^{-1}, heating rate = 4°C min^{-1}, heating flow = 1 mL min^{-1}, solvent = 1,2,4-TCB.

The analysis shows the presence of three families of polyethylene chains: a soluble fraction (25°C) with high comonomer content, the semi-crystalline fraction (60 to 90°C) with medium comonomer content and the highly crystalline fraction (100 to 115°C) with low comonomer content. The CEF measurement allowed us to measure the molar comonomer content of each of these families and their weight proportion. The ratio of each family has a strong impact on the mechanical properties of the final material.

Table 3-10: Quantitative results for Blue and Red samples obtained by CEF experiments.

Fraction	**Soluble**		**Weakly crystalline**		**Highly crystalline**	
	Blue[a]	**Red[a]**	**Blue**	**Red**	**Blue**	**Red**
Wt Fraction[b]	10%	34%	15%	21%	75%	45%
IV (dL g^{-1})[c]	1.0	1.1	1.5	2.4	2.0	2.9
CH_3/1000C[d]	50	70	21	24	1	2
Comonomer content (mol %)	>9%	>9%	4.6%	5.3%	0%	0%

[a]Blue and Red samples corresponding to CEF profiles in Figure 3-33, [b]weight fraction of each family, [c]the intrinsic viscosity which can give the molar mass information via the Mark-Houwink-Sakurada parameters, [d]number of CH_3 groups per 1000 carbons.

As shown the CEF analysis (like TREF, CRYSTAF, TGIC or SGIC) enabled the measurement of:

- the distribution of the different families (% by mass of soluble fraction, weakly and highly crystalline fraction),
- the composition in terms of branching of each fraction (CH_3/1000C and the mol% of hexene content) with the use of the calibration curve constructed previously,
- the viscosimetric average molar masses on each fraction when a viscometer is used.

However, a difficulty persists if we do not know the comonomer inserted in an unknown LLDPE, i.e. we cannot choose a suitable calibration method and must restrict ourselves to measuring the number of CH3/1000C. It was therefore important to extend this thesis work to develop methods for identifying the comonomer inserted in the LLDPE or, in other words, measuring the length of the branching.

The following part attempts to tackle this subject by proposing two different and innovative strategies. The first method used the ability of FTIR to provide a broad range of information about the structure of LLDPE through all the wavelengths absorbed in medium IR and near IR. The finesse of this information can only be fully exploited using chemometric tools. FTIR coupled with chemometrics was then developed to rapidly obtain access to chemical composition.

The second strategy employs mass spectrometry, widely used in analytical laboratories but difficult to apply to polymers. In order to make it usable for understanding the structure of our copolymers, we coupled it to thermogravimetric analysis (TGA). This coupling made it possible to split the copolymers into very specific fragments which could be identified and quantified by mass spectrometry. The method has been shown to be effective in identifying the type of comonomer used during the synthesis of a LLDPE sample.

All of this work is described in three publications that constitute the whole of Chapter 4 of this thesis.

In order to enhance these developments and to extend the exploitation of these techniques and the understanding of their separation mechanism, three papers have been published. The first one presents and details the calibration of the TREF instrument using the LLDPE models; the second highlights the advantages and disadvantages of the SGIC techniques versus CRYSTAF; the last one is focused on the fractionation mechanisms in TGIC.

The first publication, titled "Homogeneous copolymers of ethylene with α-olefins synthesized with metallocene catalysts and their use as standards for TREF calibration", was published to describe the DSC and TREF calibration. Various co-authors were involved in this project. Emilie Cossoul was the student I supervised to produce copolymer samples and perform characterizations. Laetitia Baverel characterized the samples by HT-SEC. Elsa Martigny was the PhD student who produced the heterogeneous samples with a classical Ziegler-Natta catalyst to illustrate the method. We had valuable discussions with Tibor Macko from the Fraunhofer Institute for Structural Durability and System Reliability, Plastics Division, Department of Materials Analytics, Darmstadt, Germany. My contribution, assisted by Christophe Boisson, was to organize the experiments, interpret the data, and write and submit the article.

The second work was performed in the framework of a collaboration with Tibor Macko from the Fraunhofer Institute for Structural Durability and System Reliability, in Germany. For this work, I provided the LLDPE samples that were well-characterized in chemical composition and in molar masses which are used as standards. Rajeh chitta, Tibor Macko and Robert Brull completed the work with SGIC experiments and the optimization of the separation conditions. Finally, novel calibration fields for SGIC were established for the study of different ethylene-α-olefin copolymers.

The third publication, titled "Molecular dynamic simulation of ethylene-hexene copolymer adsorption onto graphene: new insight into thermal gradient interaction chromatography", was published with Fabrice Brunel, a researcher in our group. This work aims at understanding the fractionation mechanism and interactions that occur in a graphene column with LLDPE chains during TGIC experiments. These adsorption mechanism of copolymers on the graphene surface of the column was studied by molecular dynamics simulation. Fabrice Brunel performed simulations and my work focused on TGIC experiments to strengthen and validate the model.

Dear Mr. Olivier Boyron,

Thank you for placing your order through Copyright Clearance Center's RightsLink® service.

Order Summary

Licensee:	CNRS
Order Date:	Jan 21, 2021
Order Number:	4993691212633
Publication:	Macromolecular Symposia
Title:	Homogeneous Copolymers of Ethylene with α-olefins Synthesized with Metallocene Catalysts and Their Use as Standards for TREF Calibration
Type of Use:	Dissertation/Thesis
Order Total:	0.00 USD

42 | *Macromol. Symp.* **2013**, 330, 42–52 DOI: 10.1002/masy.201300022

Homogeneous Copolymers of Ethylene with α-olefins Synthesized with Metallocene Catalysts and Their Use as Standards for TREF Calibration

Emilie Cossoul,[1] *Laetitia Baverel,*[1] *Elsa Martigny,*[1] *Tibor Macko,*[2] *Christophe Boisson,**[1] *Olivier Boyron**[1]

Summary: A range of crystalline copolymers of ethylene with α-olefins (propene, hexene, octene and octadecene) were prepared using the complexes $Et(Ind)_2ZrCl_2$ and $(nBuCp)_2ZrCl_2$ activated with MAO. The average composition of the copolymers was measured using ^1H- and ^{13}C-NMR. Then the samples were characterized by High Temperature SEC and DSC. These investigations showed that polymers are homogeneous in composition and consequently were suitable to be used as standards for TREF. This work provided calibrations curves for TREF that can be used on a wide range of α-olefin contents. Finally, these calibrations curves were used to characterize heterogeneous copolymers of ethylene/hexene synthesized using a conventional Ziegler-Natta catalyst.

Keywords: CRYSTAF; DSC; LLDPE; metallocene; TREF

Introduction

LLDPE is a copolymer of ethylene with a α-olefin (typically hexene or octene). One of its main advantage is that its structure and consequently its properties are easily adjustable by variation of the co-monomer content (short chain branching). It is thus of high interest to determine the chemical composition of LLDPE. The average composition is measured by spectroscopy techniques *i.e.* infrared (IR) or nuclear magnetic resonance (NMR). However conventional Ziegler-Natta catalysts are multi-sites. Besides, it is well known that if some active sites insert the comonomer efficiently other sites have a bad response to the α-olefin. Consequently, in addition to a broad molecular weight, a broad chemical composition distribution is obtained for LLDPE. The investigation by differential scanning calorimetry (DSC) of the evolution of the melting temperature with respect to the α-olefin content provides little information since the top peak observed corresponds to the fraction of high molar mass with low α-olefin content. This peak does not evolve significantly enough with the α-olefin content in the copolymer. The Temperature Rising Elution Fractionation (TREF) separation technique has been developed in the late 1970s to analyze the chemical composition distribution (CCD) of semi-crystalline polymers which give a good representation of the real structure of the polymer.[1–5] Monrabal modified TREF and has developed crystallization analysis fractionation (CRYSTAF)[6,7] and more recently Crystallisation Elution Fractionation (CEF).[8,9] Since the main parameter that affects the crystallinity and solubility of ethylene/α-olefin copolymers is the co-monomer content, these techniques gave access to the chemical composition distribution of semi-crystalline polyolefins.[10–12]

[1] Université de Lyon, Univ. Lyon 1, CPE Lyon, CNRS UMR 5265, Laboratoire de Chimie Catalyse Polymères et Procédés (C2P2), Equipe LCPP, Bat 308F, 43 Bd du 11 Novembre 1918, F-69616, Villeurbanne, France
E-mail: boisson@lcpp.cpe.fr; boyron@lcpp.cpe.fr

[2] Fraunhofer Institute for Structural Durability and System Reliability, Division Plastics, Department of Materials Analytics, Schlossgartenstr. 6, 64289, Darmstadt, Germany

Copyright © 2013 WILEY-VCH Verlag GmbH & Co. KGaA, Weinheim

Macromol. Symp. **2013**, 330, 42–52

The present study aims to establish a calibration of the TREF to get quantitative information about the CCD of LLDPE. Moreover it provides the analyses of a wide range of copolymers. Since no commercial standards of ethylene/α-olefin copolymers (propene, hexene, octene and octadecene) are available, metallocene catalysts have been used to prepare polymer standards with homogeneous chemical compositions. Eventually, the use of calibrations for investigation of chemical composition of heterogeneous copolymers obtained with conventional Ziegler Natta catalyst is also reported.

Experimental Part

Materials

All syntheses were performed under pure and dry argon, using the standard Schlenk techniques and a glove box. 1-hexene was distilled over CaH_2 prior to use. Toluene and n-heptane were dried on 3 Å molecular sieves. Methyl-aluminoxane (MAO) 10% wt. in toluene was purchased from Aldrich and triethylaluminium ($AlEt_3$) was purchased from Albemarle and used as heptane solution (1 M). Ethylene (99.5%) from Air Liquide was purified by passing on three successive columns containing respectively molecular sieves, alumina and a copper catalyst. The metallocene complexes *rac*-Et $(Ind)_2ZrCl_2$ and $(n$BuCp$)_2ZrCl_2$ were purchased from Sigma-Aldrich. Homemade conventional Ziegler-Natta precatalysts were implemented to get reference LLDPE.

Polymerization Procedures

Metallocene Catalysts

Polymerizations were performed in a 500 mL glass reactor equipped with a stainless steel blade stirrer and an external water jacket for temperature control. MAO (0.3 mL) and the required amounts of co-monomer (1-hexene, 1-octene, 1-octadecene) were introduced in a flask containing 300 mL of heptane. The mixture was transferred in the reactor under a stream of argon. The argon was then pumped out before introducing the ethylene or a mixture of ethylene/propene. Temperature and pressure were then progressively increased up to 80 °C and 3.8 bars. 100 μL of a solution (1.5 mM in toluene) of *rac*-Et$(Ind)_2ZrCl_2$ (or $(nBuCp)_2ZrCl_2$) were then introduced in the reactor under 4 bars of ethylene to start the polymerization. The pressure was kept constant at 4 bars during the polymerization. After 30 minutes of reaction, the polymerization was stopped. The resulting mixture was poured in 400 mL of methanol. The polymer was collected by filtration, washed with methanol and dried under vacuum.

Classical Ziegler-Natta Catalysts

A 1 L stainless steel reactor equipped with a stainless steel blade was used to polymerize ethylene. $AlEt_3$ (3 mM), hexene (35%wt) and the precatalyst were respectively introduced in a flask containing 300 mL of heptane. The mixture was introduced at room temperature into the reactor under a stream of ethylene. Then, 1 bar of hydrogen was injected into the reactor followed by ethylene. The temperature was adjusted to 80 °C and the total pressure to 7 bars. The total pressure of the reactor was kept constant at 7 bars during the entire reaction by continuous ethylene feed. Polymerisations were stopped when about 20 g of polymer are produced. After the desired reaction time, the reactor was cooled and the gas pressure released. The polymer was then filtered off from the polymer suspension, washed with methanol then dried under vacuum for 1 hour at 100 °C.

Characterization of Synthesized Polymer Samples

NMR

Co-monomer contents of copolymers were determined by NMR using a Bruker Avance III 400 spectrometer operating at 400 MHz for ^{1}H-NMR and 100.6 MHz for

Copyright © 2013 WILEY-VCH Verlag GmbH & Co. KGaA, Weinheim

^{13}C-NMR. ^{1}H-NMR spectra were obtained with a 5 mm QNP probe at 373 K and the ^{13}C-NMR spectra were obtained with a 10 mm PA-SEX probe at 373 K. A 3:1 volume mixture of 1,2,4-trichlorobenzene and toluene-d8 was used as solvent. Chemical shifts were measured in ppm using for ^{1}H-NMR the reference of toluene (CHD_2 at 2.185 ppm) and for ^{13}C-NMR the resonance of polyethylene ("PE" at 30.06 ppm) as internal references.

The ^{1}H-NMR analyses was used to determine the α-olefin content in copolymers. The spectrum is composed of two main signals. The signals of CH_2 and CH protons of the polyethylene chain at 1.3 ppm and the signal of methyl branches at 0.9 ppm (Figure S1). Since high molar mass copolymers ($> 20\,kg.mol^{-1}$) were prepared, methyl chain ends were neglected. However at low content of comonomer (< 1 mol%), the resolution of ^{1}H-NMR appears not suitable. In this case, the ^{13}C-NMR spectra (Figure S2 and S3) were used for the determination of α-olefin content. The assignment of signals and the notation of carbons are based on the article of Galland et al..[13] Details of calculation of olefin content based on ^{1}H- and ^{13}C-NMR data are given in ESI.

DSC

Thermal characterizations were performed with a differential scanning calorimetry, Mettler Toledo DSC 1, equipped with an auto-sampler and a 120 thermocouple sensor. The temperature and the heat flow of the equipment were calibrated with an indium standard. All samples were accurately weighed (between 5 to 10 mg) and sealed in aluminium pans. They were heated from −20 °C to 180 °C at 10 °C. min^{-1} with an empty aluminium pan as reference. Two successive heating and cooling were performed and only the second run was considered. Dry nitrogen with a flow rate set at 50 mL.min^{-1} was used as the purge gas. The melting temperature (T_m) was measured at the top of the endothermic peak. The STAR^e thermal analysis software is used to calculate the melting temperature and the crystallinity of the copolymers: $X = \Delta H_f/\Delta H_{f0}$ where ΔH_f ($J.g^{-1}$) is the melting heat of the sample and ΔH_{f0} ($= 293\,J.g^{-1}$) the melting heat of a 100% crystalline polyethylene.[14]

HT-SEC

High temperature Size Exclusion Chromatography (HT-SEC) analyses were performed using a Viscotek system (from Malvern Instruments) equipped with three columns (PLgel Olexis 300 mm × 7 mm I. D. from Agilent Technologies). 200 μL of sample solutions with concentration of $5\,mg \cdot mL^{-1}$ were eluted in 1,2,4-trichlorobenzene using a flow rate of $1\,mL \cdot min^{-1}$ at 150 °C. The mobile phase was stabilized with 2,6-di(tert-butyl)-4-methylphenol ($200\,mg \cdot L^{-1}$). Online detection was performed with a differential refractive index detector and a dual light scattering detector (LALS and RALS) for absolute molar mass measurement. The OmniSEC software was used for the calculations.

TREF

Temperature Rising Elution Fractionation (TREF) technique was carried out for the characterization of polymers in terms of Chemical Composition Distribution (CCD) with a CRYSTAF-TREF 300 model manufactured by Polymer Char S.A. The fractionation in TREF is based on layers deposition of polymers of decreasing crystallinity on an inert support within the TREF column. The polymer is thus segregated in layers of different chemical compositions. Experimentally, about 80 mg of sample were dissolved at high temperature (150 °C) in 20 mL of 1,2,4-trichlorobenzene stabilized with 2,6-di(tert-butyl)-4-methylphenol. 0.5 ml of the sample solution is automatically loaded into the TREF column of 9 mm *i.d.* and 15 cm length at 120 °C. The temperature was slowly decreased down to 35 °C at a rate of

Copyright © 2013 WILEY-VCH Verlag GmbH & Co. KGaA, Weinheim

Macromol. Symp. **2013**, 330, 42–52

$0.5\,°C \cdot min^{-1}$ to allow the polymer to crystallize. A second cycle was used to quantify those fractions by pumping solvent meanwhile the temperature is being increased ($1\,°C \cdot min^{-1}$). The eluent dissolved fractions of increasing crystallinity. The polymer solution concentration was monitored with an infrared detector measuring total CH absorption in the 2700–3000 cm^{-1} range and operating at 150 °C.

Results and Discussion

Metallocene catalysts obtained by combination of complexes $Et(Ind)_2ZrCl_2$ **(1)** and $(nBuCp)_2ZrCl_2$ **(2)** with MAO were used for preparing a series of homogeneous copolymers of ethylene with respectively propene, hexene, octene and octadecene. Results are summarized in Table 1.

Chemical Composition Characterization by NMR

The α-olefin content in copolymers was determined by ^{1}H-NMR and ^{13}C-NMR. The ^{1}H-NMR analysis is reliable since the molar masses (Mn) of the polymers are high enough to neglect the terminal methyl groups when the comonomer content is higher than 1 mol%. At low content of α-olefin the composition was measured by ^{13}C-NMR (see ESI).

Molar Mass Characterization by SEC

Copolymer samples were analyzed by high temperature SEC. The molar mass distribution of the samples was unimodal and narrow, which is characteristic of polymers synthesized with metallocene catalysts. Nieto et al. reported[15] that molar masses lower than $18\,kg \cdot mol^{-1}$ have a significant effect on crystallization temperature of polymers. M_n values reported in Table 1 are higher than $20\,kg \cdot mol^{-1}$, consequently that samples can be used as standards for the TREF calibration.

Thermal Properties Characterization by DSC

The results of DSC analyses are summarized in Table 1. As expected, the increase of α-olefin content leaded to a decrease of the melting temperature and melting enthalpy of copolymers (see also DSC thermogram in Figure S4, S5, S6, S7, S8).[16] The influence of the comonomer content on the melting peak temperature of copolymers has been plotted for each α-olefin sample (Figure 1). A linear regression for each co-monomer was used to determine the lines of best fit leading to calibration. The resulting equations are given in Table 2. Nevertheless, the melting temperature of homopolyethylenes and of copolymers with low α-olefin content (less than 0.4 mol%) are out of the line; these samples were not used to perform the calibration. Consequently, the calibration curve should be only used for copolymers incorporating at least 0.4 mol% of a α-olefin. It appears difficult to explain the difference of crystallization properties of copolymers bearing low content of α-olefins. However, we can underline that linear homopolyethylenes crystallize at higher temperature than copolymers at heating rate of $10\,°C \cdot min^{-1}$ (run 1, $Tm = 138\,°C$).

The catalytic systems based respectively on the complexes $Et(Ind)_2ZrCl_2$ and $(nBuCp)_2ZrCl_2$ used for the preparation of ethylene/hexene samples showed no influence on the calibration curve. Indeed this class of metallocene catalysts has a low hexene reactivity ratio.[17] Even if the ethylene reactivity ratios are different since the catalyst **1**/MAO has a better hexene response ($r_E = k_{EE}/k_{EH}$ of 26 and 55 for respectively **1**/MAO and **2**/MAO were measured using ^{13}C-NMR) similar comonomer distribution are expected at low hexene content. Consequently, the linear calibration curves reported here will be used for crystalline copolymers incorporating at least 0.4 mol% of α-olefin and without propensity to form long α-olefin sequences.

As expected, propene and octadecene units exhibited a different influence on thermal properties of copolymers than hexene or octene units. In the case of propene, this behavior can be explained by

Copyright © 2013 WILEY-VCH Verlag GmbH & Co. KGaA, Weinheim

Table 1.
Polymerization conditions and characterization data for ethylene/α-olefin copolymers.

Runs	Met.	α-olefin	Content[a] mol%	Activity $g \cdot mol^{-1} h^{-1}$	Mn (PDI)[b] $kg \cdot mol^{-1}$	Tm (Xc)[c] °C (%)	Tp[d] °C	Tw[d] °C
1	**1**	Hexene	0	8.5E+7	60.2 (2.9)	138 (65)	101.8	101.8
2	**1**	Hexene	0.4	1.1E+8	49.8 (2.7)	131 (55)	97.4	99.1
3	**1**	Hexene	1.1	8.2E+7	40.4 (2.6)	121 (51)	94.0	95.1
4	**1**	Hexene	2.0	7.5E+7	35.2 (1.8)	117 (49)	88.6	86.3
5	**1**	Hexene	2.2	1.5E+8	40.2 (2.0)	114 (48)	86.6	84.2
6	**1**	Hexene	3.7	1.2E+8	33.4 (1.8)	106 (39)	77.3	72.9
7	**1**	Hexene	5.3	1.5E+8	29.5 (1.8)	98 (32)	68.1	62.6
8	**1**	Hexene	5.8	1.2E+8	29.7 (1.9)	93 (29)	63.2	57.5
9	**1**	Hexene	6.3	1.4E+8	28.7 (1.8)	91 (27)	59.6	52.1
10	**2**	Hexene	0	1.5E+8	74.2 (2.7)	136 (62)	102.5	104.0
11	**2**	Hexene	0.2	3.5E+7	48.7 (3.0)	130 (58)	100.2	103.1
12	**2**	Hexene	0.5	7.2E+7	24.4 (3.4)	126 (56)	97.7	98.2
13	**2**	Hexene	1.2	1.2E+8	55.6 (3.1)	121 (50)	94.3	94.1
14	**2**	Hexene	1.5	5.9E+7	52.1 (3.1)	119 (49)	91.9	88.9
15	**2**	Hexene	2.0	7.2E+7	34.6 (2.3)	115 (48)	87.3	87.7
16	**1**	Octene	0.4	1.0E+8	48.4 (2.4)	130 (59)	98.1	97.3
17	**1**	Octene	0.6	1.4E+8	41.0 (2.6)	127 (58)	96.2	94.3
18	**1**	Octene	1.7	1.1E+8	32.4 (1.8)	117 (50)	89.5	86.8
19	**1**	Octene	3.4	7.3E+7	32.1 (1.8)	108 (39)	78.7	75.9
20	**1**	Octene	5.6	7.0E+7	32.2 (1.8)	98 (30)	66.4	61.1
21	**1**	Propene	2.3	1.5E+8	33.1 (1.9)	122 (59)	93.1	88.7
22	**1**	Propene	2.7	5.0E+7	31.2 (1.8)	120 (49)	89.3	88.4
23	**1**	Propene	4.2	6.1E+7	33.0 (1.8)	115 (46)	85.0	75.3
24	**1**	Propene	5.0	4.1E+7	26.2 (2.0)	109 (47)	78.1	74.8
25	**1**	Propene	6.4	3.9E+6	26.7 (1.8)	101 (38)	70.4	67.7
26	**1**	Propene	9.1	1.3E+8	29.5 (1.7)	92 (26)	58.9	41.0
27	**1**	Octadecene	0.7	1.1E+8	26.0 (2.5)	126 (47)	97.0	93.5
28	**1**	Octadecene	1.7	5.0E+7	35.8 (2.6)	117 (38)	89.0	84.1
29	**1**	Octadecene	2.1	6.4E+7	38.8 (1.9)	114 (23)	87.1	76.7
30	**1**	Octadecene	2.7	1.2E+8	26.1 (2.3)	110 (31)	84.0	71.4
31	**1**	Octadecene	2.9	2.5E+8	25.6 (2.3)	106 (21)	80.0	65.1
32	**1**	Octadecene	3.3	7.7E+7	43.2 (1.9)	96 (16)	72.6	57.1

Polymerization conditions: 80 °C, 30 min, 4 bars. [a] Determined by ^{1}H- and ^{13}C-NMR. [b] Determined by HT-SEC using a dual light scattering detector. [c] Determined by DSC. [d] Determined by TREF. PDI: polydispersity index.

the fact that long branches are excluded from the crystallites of the polymer, whereas a small olefin like propene produces short branches that can be incorporated into the crystallites and therefore decrease the crystallization temperature by a lower extent.[18,19] Longer branches resulting of octadecene units showed a higher impact on polymer crystallization than C4 or C6 branches.

Chemical Composition Characterization by TREF

Before performing the calibration, a study of the repeatability of TREF analyses was performed using 12 runs of the same ethylene/hexene copolymer sample. It showed that the peak elution temperature is repeatable to ± 0.4 °C and the weight average temperature to ± 1.8 °C (Table S1).

Results of TREF analyses of ethylene/α-olefin copolymers are reported in Table 1. T_{peak} is defined as the top peak elution temperature. T_w as defined by Monrabal[7] is the weight-average elution temperature calculated according to Equation 1:

$$T_w = \Sigma C_i{}^{*}Ti / \Sigma C_i \quad (1)$$

where C_i is the concentration of the polymer in solution at the *i*th data point and T_i is the temperature at the *i*th data point (°C).

This value is calculated using the whole TREF profile and consequently is related to the average composition of the sample.

Copyright © 2013 WILEY-VCH Verlag GmbH & Co. KGaA, Weinheim

Macromol. Symp. **2013**, 330, 42–52

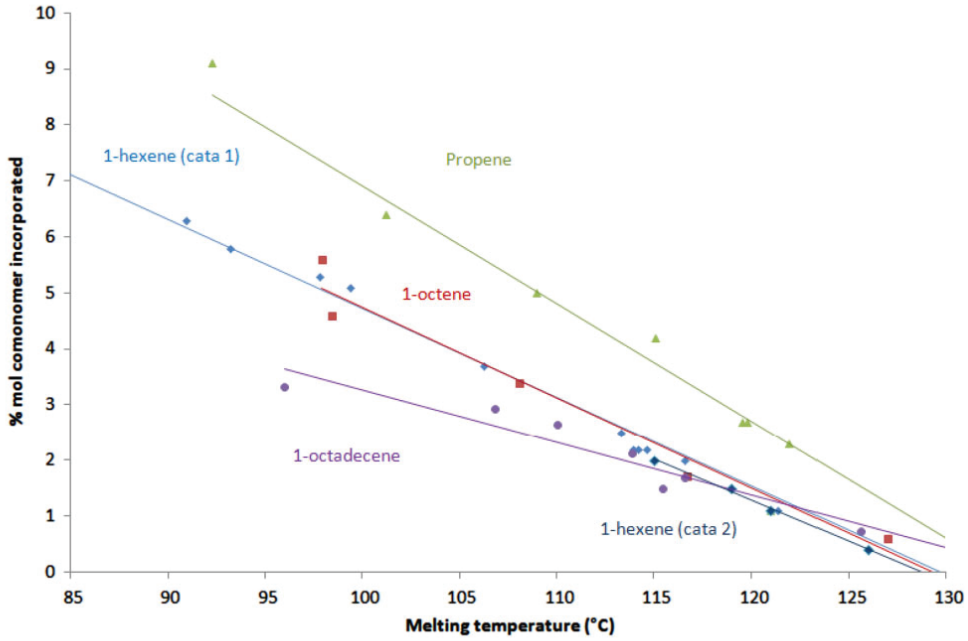


Figure 1.
Calibration curves mol% of co-monomer incorporated in function of the melting temperature measured by DSC for ethylene/propene, ethylene/hexene, ethylene/octene and ethylene/octadecene copolymers.

Table 2.
DSC calibration curve equations for each series of copolymers.

Complex	Co-monomer	Calibration curve equation	R^2
1	Hexene	$\% = -0.16 \times T_m + 21.0$	0.99
2	Hexene	$\% = -0.15 \times T_m + 19.0$	0.99
1	Octene	$\% = -0.16 \times T_m + 20.9$	0.97
1	Propene	$\% = -0.21 \times T_m + 27.9$	0.96
1	Octadecene	$\% = -0.094 \times T_m + 12.7$	0.92

The TREF profiles of ethylene/hexene copolymers shown in Figure 2 confirmed that all the polymer samples have monomodal distribution of chemical composition, as expected with single-site catalysts. The peak elution temperature decreased when increasing the co-monomer content (see also Figures S9, S10, S11, S12).

The influence of the α-olefin content on the elution peak temperature (Figure 3) has been plotted. No significant difference of behavior between copolymers containing respectively hexene or octene was observed together with any influence of the used catalyst. Consequently, only one linear calibration curve was determined for both ethylene/hexene and ethylene/octene copolymers (Table 3). Calibration curves are given for each co-monomer and according to the used catalyst in supporting information (Table S2). The results are in agreement with previous works using CRYSTAF analyses.[10,20] Soares et al.. have also shown that the crystallization rate is a major operation parameter.[21] In order to investigate this parameter, TREF analyses of ethylene/hexene copolymers were recorded using a lower crystallization rate ($0.2\,°C \cdot min^{-1}$). Similar calibration equations were determined at respectively 0.2 and $0.5\,°C \cdot min^{-1}$ (Table 3). However, it was of interest to perform these

Copyright © 2013 WILEY-VCH Verlag GmbH & Co. KGaA, Weinheim

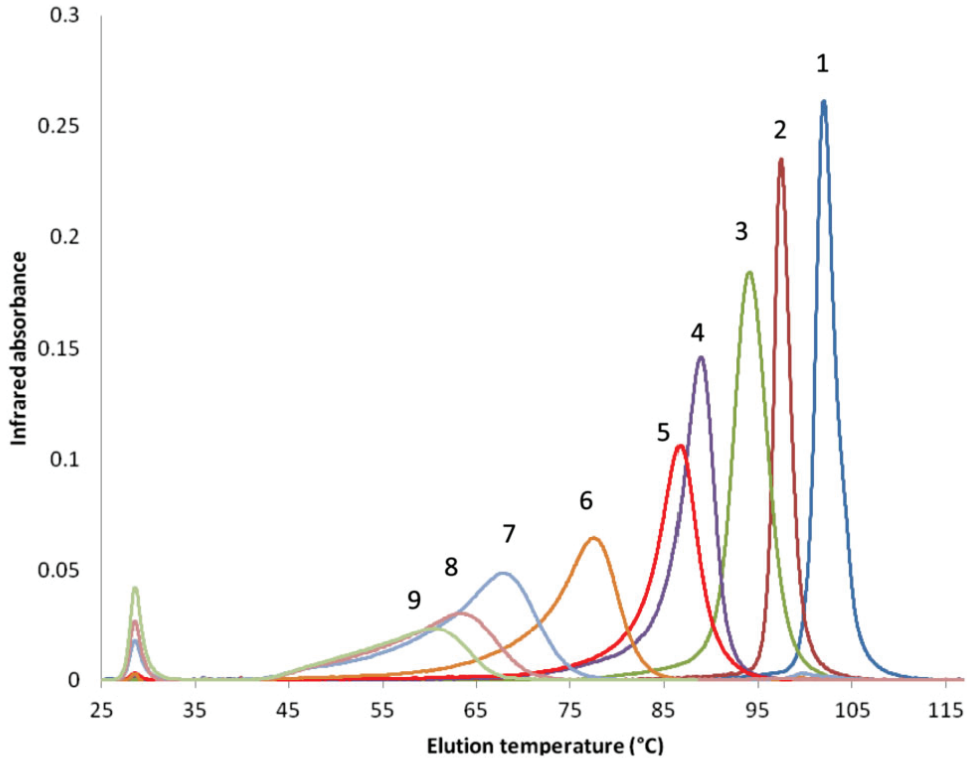


Figure 2.
TREF profile of ethylene/hexene copolymers synthesized using 1/MAO catalyst - Crystallization rate = 0.5 °C · min^{-1}.

measurements since low crystallization rate are useful in the case of mixture of polymers where co-crystallization can occur (see below).

In TREF, the same trends than in the case of DSC analyses were observed concerning the effect of the co-monomer except that in the present case point alignments were also obtained for copolymers containing low α-olefin contents (lower than 0.4%). It is possible to conclude that TREF calibration equation can be used on a larger range of compositions than DSC calibration.

Analysis of Blends of Homogeneous Polymers

Two blends of homogeneous polymers were analyzed by TREF. The first blend (blend 1) was a mix (50/50 w/w) of two ethylene/hexene copolymers (respectively 0.4 mol% and 3.7 mol% of hexene - runs 2 and 6). The second blend (blend 2) was a mix (50/50 w/w) of a homopolyethylene (run 1) with an ethylene/hexene copolymer (1.1% mol. of hexene - run 3).

The first blend gave two temperature elution peaks which are superimposable with the peak of each copolymer analyzed separately (Figure 4).

The analysis of the second blend, consisting of two polymers with close chemical composition, showed a broad elution peak with two shoulders as shown in Figure 5. The deconvolution of the TREF distribution corresponding to blend 2 using Origin software (Gaussian distribution) showed three peaks (Figure S13). Two peaks correspond more or less to the polymers used to prepare the blend (respectively at 94.9 °C and 102.7 °C compared to 94 °C and 102 °C) and one peak is observed at an intermediate temperature (99.1 °C). This last peak is ascribed to the co-crystallization of the polymers.[21,22]

Copyright © 2013 WILEY-VCH Verlag GmbH & Co. KGaA, Weinheim

Macromol. Symp. **2013**, 330, 42–52

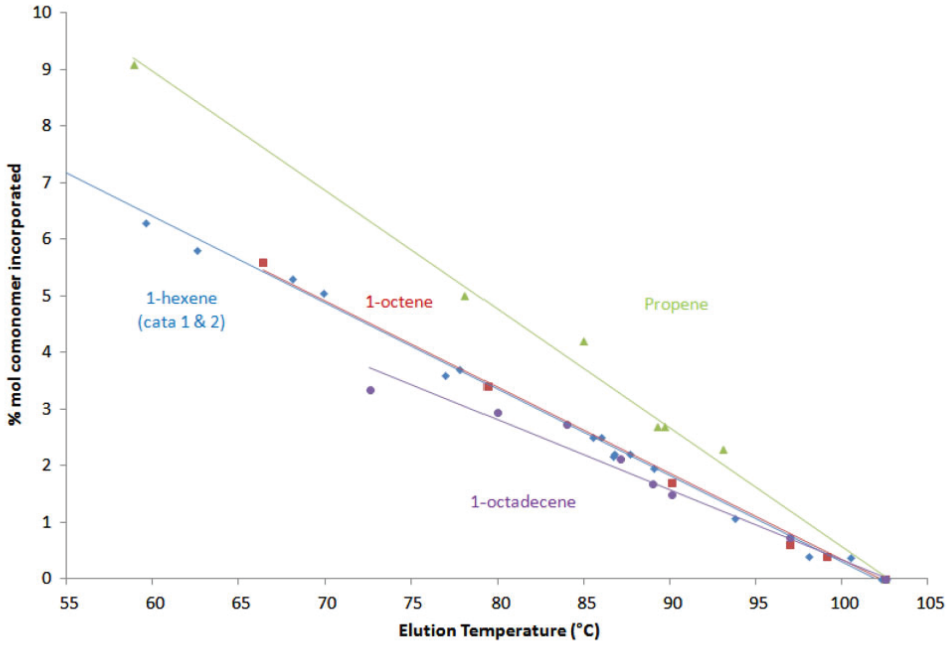


Figure 3.
TREF calibration curves using the top peak temperature. Crystallization rate = 0.5 °C · min^{-1}.

Table 3.
TREF calibration curve equations.

Complex	Co-monomer	Rate °C · min^{-1}	Calibration curve equation	R^2
1 or 2	Hexene, octene	0.5	$\% = -0.152xT_{peak} + 15.5$	0.997
			$\% = -0.132xT_w + 13.4$	0.990
1 or 2	Hexene, octene	0.2	$\% = -0.153xT_{peak} + 15.6$	0.998
			$\% = -0.127xT_w + 13.0$	0.995
1	Propene	0.5	$\% = -0.210xT_{peak} + 21.6$	0.996
			$\% = -0.158xT_w + 16.3$	0.978
1	Octadecene	0.5	$\% = -0.124xT_{peak} + 12.7$	0.980
			$\% = -0.065xT_w + 7.0$	0.954

Use of the TREF Calibration Curve to Determine Chemical Composition of Heterogeneous Ethylene/Hexene Copolymers

Ethylene/hexene copolymers were synthesized with conventional Ziegler Natta catalysts showing various hexene responses. The co-monomer content was determined by NMR analyses which gave the average composition of α-olefin. The polymer were then analyzed by DSC and TREF and the results investigated on the basis of calibration curves established in this work. Results are summarized in Table 4.

DSC analyses showed only one broad peak. The use of the DSC calibration curve leads to the determination of average co-monomer content for each sample. The obtained values are lower than that determined by NMR. The main reason is that the melting transition peak observed is related to the polymer fraction corresponding to active sites with the lowest co-momoner response. In addition, the low crystalline fraction has a weaker response in DSC.

TREF analyses underlined the heterogeneous chemical composition distribution of the samples which results in a main peak

Copyright © 2013 WILEY-VCH Verlag GmbH & Co. KGaA, Weinheim

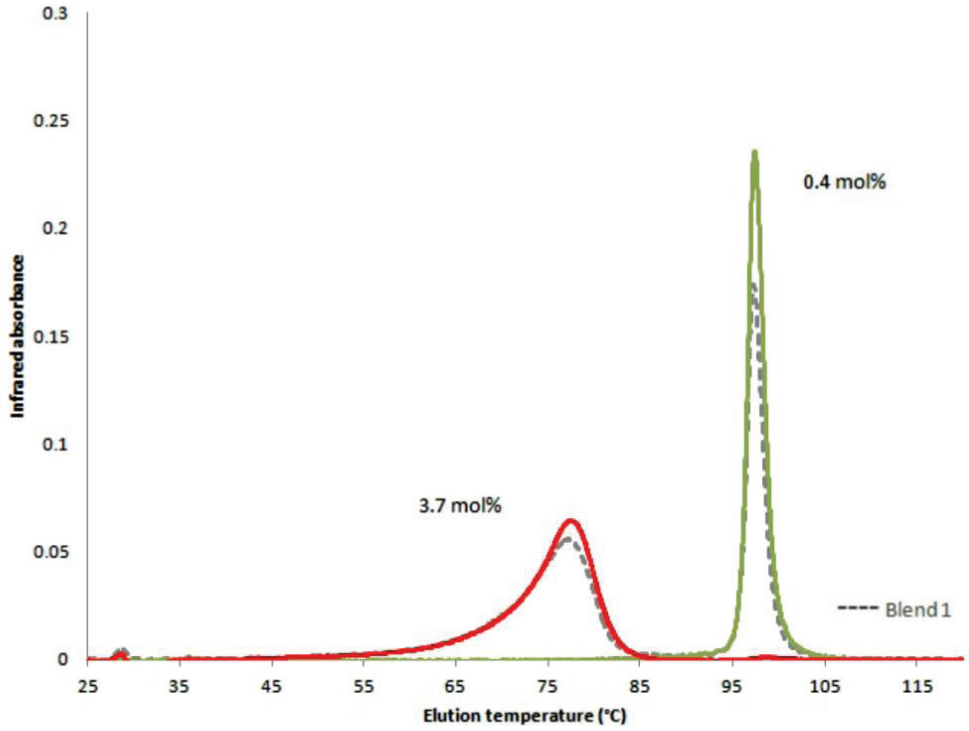


Figure 4.
TREF profile of blend 1 and of copolymers containing respectively 0.4 mol% and 3.7 mol% of hexene. Crystallization rate = 0.5 °C · min^{-1}.

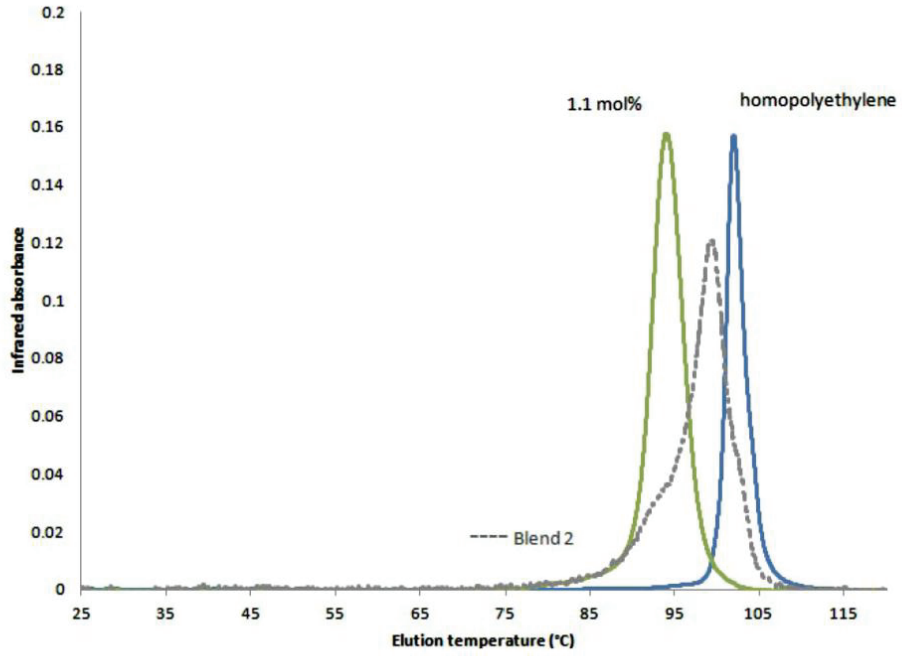


Figure 5.
TREF profile blend 2, of a homopolyethylene and of a copolymer containing at 1.1 mol% of hexene. Crystallization rate = 0.5 °C · min^{-1}.

Copyright © 2013 WILEY-VCH Verlag GmbH & Co. KGaA, Weinheim

Macromol. Symp. **2013**, 330, 42–52

Table 4.
Determination of chemical composition of heterogeneous ethylene/hexene copolymers synthesized using conventional Ziegler Natta catalysts by DSC and TREF.

run	Hexene average composition					Two main fractions	
	NMR	DSC		TREF		TREF	
	mol %	Tm (°C)	mol %	Tw (°C)	mol%	Tpeak (°C)	mol%
27	1.0	127	0.7	93	1.2	85.0	2.5
						100.0	0.2
28	0.8	127	0.7	96	0.8	86.7	2.2
						100.2	0.2
29	0.9	128	0.5	95	0.9	86.7	2.2
						100.1	0.2
30	0.5	130	0.2	99	0.4	89.5	1.9
						100.3	0.2

and a broad poorly resolved peak as shown in Figure 6. The calibration curve established with the T_W value gave an average chemical composition in good agreement with the NMR results. In addition the chemical composition distribution showed three fractions, a main fraction with low hexene content, a broad peak related to a fraction with higher hexene content and a low amount of a soluble fraction. A Tpeak value was determined for crystalline fractions which permitted to evaluate hexene content for these fractions. The most crystalline fraction contains around 0.2 mol% of hexene whatever the catalyst used while the second fraction shows different response to hexene (1.9–2.5 mol %). Note that the main fraction showed a bimodal shape which certainly results from different active sites of the catalysts. As

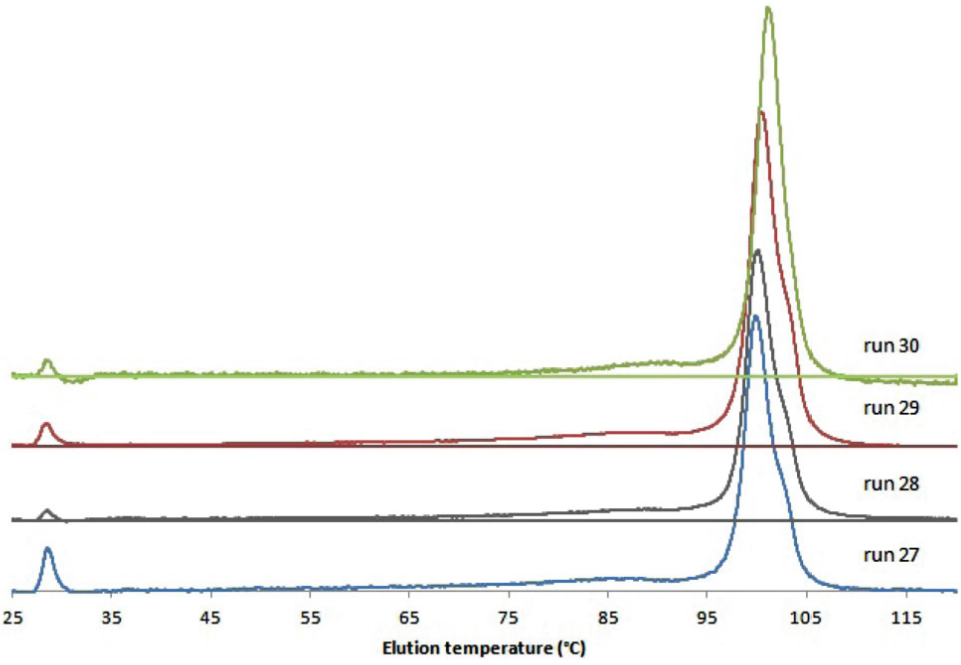


Figure 6.
TREF analysis of the heterogeneous ethylene/hexene copolymers synthesized using Ziegler Natta catalysts. Runs 27 to 30 from down to up. Crystallization rate of 0.5 °C · min^{-1}.

Copyright © 2013 WILEY-VCH Verlag GmbH & Co. KGaA, Weinheim

illustrated TREF is a very useful analytical method which provides unique information on CCD for that kind of complex heterogeneous polymers.

Conclusion

A range of homogeneous ethylene/α-olefin copolymers were prepared and used as standards for calibration of both DSC and TREF techniques. TREF calibration curves are suitable for a determination of olefin content in homogeneous crystalline copolymers obtained with single-site catalysts such as metallocenes. Interestingly TREF can be used in a larger range of olefin content. In addition TREF analyses provide more information than DSC on the chemical composition of heterogeneous copolymers prepared with conventional Ziegler-Natta catalysts. However TREF can only be used for crystalline polymers and some co-crystallisation effects are an issue for the analysis of complex mixture of polymers. Recently, separation techniques for polyolefins based on interactive liquid chromatography have been developed and have attracted a great interest.[23–25] In particular, these techniques enable selective separation of amorphous as well as semi-crystalline polyolefins. Subsequent to the present study a broader range of standards was prepared and investigated by Chitta et al. using a HPLC system. This work will be reported in a next paper.

Acknowledgements: The authors thank Alberto Ortin and João B. P. Soares for valuable discussions. The NMR Polymer Service in Lyon and Mettler Toledo are acknowledged for their technical support.

Electronic Supplementary Information (ESI) available: determination of the comonomer content by NMR, Figure S1 to S13, Table S1 and S2.

[1] L. Wild, T. R. Ryle, D. C. Knobeloch, I. R. Peat, *J. Pol. Sci., Polym. Phys. Ed.* **1982**, *20*, 441.
[2] L. Wild, *Adv. Polym. Sci.* **1991**, *98*, 1.
[3] L. Wild, C. Blatz, *New Adv. Polyolefins*, Ed. T. Chung, Plenum Press, New York **1993**, 147.
[4] J. B. P. Soares, A. E. Hamielec, in: *Modern Techniques for Polymer Characterization*; R. A., Pethrick, D. V. Dawkins, Eds; Wiley, New York **1999**, 15.
[5] S. Anantawaraskul, J. B. P. Soares, P. M. Wood-Adams, *Adv. Polym. Sci.* **2005**, *182*, 1.
[6] B. Monrabal, *J. Appl. Polym. Sci.* **1994**, *52*, 491.
[7] B. Monrabal, "TREF and CRYSTAF technologies for polymer characterization" in *Encyclopedia of Analytical Chemistry*, John Wiley & Sons **2000**.
[8] B. Monrabal, J. Sancho-Tello, N. Mayo, L. Romero, *Macromol. Symp.* **2007**, *257*, 71.
[9] B. Monrabal, L. Romero, N. Mayo, J. Sancho-Tello, *Macromol. Symp.* **2009**, *282*, 14.
[10] B. Monrabal, J. Blanco, J. Nieto, J. B. P. Soares, *J. Polym. Sci., A Polym. Chem.* **1999**, *37*, 89.
[11] I. Bruaseth, J. B. P. Soares, E. Rytter, *Polymer* **2004**, *45*, 7853.
[12] D. M. Sarzotti, J. B. P. Soares, A. Penlidis, *J. Polym. Sci., B Polym. Phys.* **2002**, *40*, 2595.
[13] G. B. Galland, R. F. De Souza, R. S. Mauler, F. F. Nunes, *Macromolecules* **1999**, *32*, 1620.
[14] B. Wunderlich, *Thermal analysis*. Academic Press, **1990**, 417.
[15] I. Nieto, T. Oswald, F. Blanco, J. B. P. Soares, B. Monrabal, *J. Polym. Sci., B Polym. Phys.* **2001**, *39*, 1616.
[16] A. Lustiger, J. B. P. Soares, C. L. P. Shan, *Annual Technical Conference - Society of Plastics Engineers* **2001**, *59th*, 1835.
[17] G. B. Galland, P. Quijada, R. Santos Mauler, S. C. De Menezes, *Macromol. Rapid Commun.* **1996**, *17*, 607.
[18] R. Alamo, R. Domszy, L. Mandelkern, *J. Phys. Chem.* **1984**, *88*, 6587.
[19] J. B. P. Soares, S. Anantawaraskul, *J. Polym. Sci., B Polym. Phys.* **2005**, *43*, 1557.
[20] R. Brull, H. Pasch, H. G. Raubenheimer, R. Sanderson, A. J. van Reenen, U. M. Wahner, *Macromol. Chem. Phys.* **2001**, *202*, 1281.
[21] S. Anantawaraskul, J. B. P. Soares, P. M. Wood-Adams, *J. Polym. Sci., B Polym. Phys.* **2003**, *41*, 1762.
[22] S. Anantawaraskul, J. B. P. Soares, P. M. Wood-Adams, *Macromol. Chem. Phys.* **2004**, *205*, 771.
[23] T. Macko, R. Bruell, Y. Zhu, Y. Wang, *J. Sep. Sci.* **2010**, *33*, 3446.
[24] T. Macko, H. Pasch, *Macromolecules* **2009**, *42*, 6063.
[25] R. Cong, W. de Groot, A. Parrott, W. Yau, L. Hazlitt, R. Brown, M. Miller, Z. Zhou, *Macromolecules* **2011**, *44*, 3062.

Copyright © 2013 WILEY-VCH Verlag GmbH & Co. KGaA, Weinheim

Dear Mr. Olivier Boyron,

Thank you for placing your order through Copyright Clearance Center's RightsLink® service.

Order Summary

Licensee:	CNRS
Order Date:	Jan 21, 2021
Order Number:	4993701208875
Publication:	Macromolecular Chemistry and Physics
Title:	Characterization of the Chemical Composition Distribution of Ethylene/1-Alkene Copolymers with HPLC and CRYSTAF —Comparison of Results
Type of Use:	Dissertation/Thesis
Order Total:	0.00 USD

Full Paper

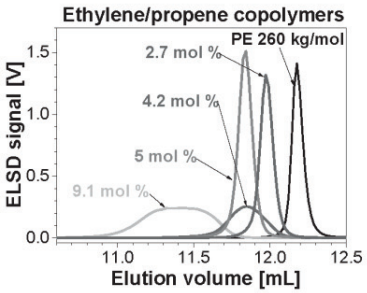
Macromolecular Journals

Macromolecular Chemistry and Physics

Characterization of the Chemical Composition Distribution of Ethylene/1-Alkene Copolymers with HPLC and CRYSTAF—Comparison of Results

Rajesh Chitta, Tibor Macko, Robert Brüll,* Christophe Boisson, Emilie Cossoul, Olivier Boyron

A series of copolymers of ethylene with propene, 1-hexene, 1-octene, and 1-octadecene is characterized by size-exclusion chromatography (SEC), nuclear magnetic resonance spectroscopy (NMR), crystallization analysis fractionation (CRYSTAF), and high-temperature interactive liquid chromatography. Four different solvent pairs are used as the mobile phase, while porous graphite is used as the column packing. The elution volumes of the polymer samples do not correlate with their average molar mass (SEC); however, they correlate with the average chemical composition (NMR). High performance liquid chromatography (HPLC) enables separation of the copolymers over the full range of their composition and independent of their crystallinity. Dependence between the elution volume and the average chemical composition distribution (CCD) of the copolymer is linear and it is a function of the length of branches as well as the type of the mobile phase. The CCDs of copolymers derived from HPLC profiles are similar to, yet broader than the CCDs obtained with CRYSTAF.



1. Introduction

Polyolefins are industrially, by far, the largest scale of produced synthetic polymers. They are used for manufacturing a wide range of products due to their excellent cost/performance value, easily available raw materials, recyclability, and processability.[1] However, to obtain polymers with defined macroscopic properties, it is essential to understand the structure ↔ property relationships. Polymer analysis provides information about the molecular structure, which builds a bridge between macroscopic properties of the polymer and the polymerization conditions.[2] The distributions with regard to molar mass distribution (MMD) and chemical composition distribution (CCD) are important characteristics. They can be used to impart predetermined physical properties to a final product. High-temperature size-exclusion chromatography (SEC) is the conventional method to characterize the MMD of polyolefins,[3] and the information from SEC can be further enhanced by coupling SEC with specific detectors: Thus, using a light scattering or a viscometric detector, the absolute molar mass may be determined,[3,4] with FTIR detection short-chain branching[4–9] or with NMR

Dr. R. Chitta, Dr. T. Macko, Dr. R. Brüll
Fraunhofer Institute for Structural Durability and System Reliability, Division Plastics, Group Material Analytics
Schlossgartenstr. 6, 64289 Darmstadt, Germany
E-mail: Robert.Bruell@lbf.fraunhofer.de
Dr. C. Boisson, Dr. E. Cossoul, Dr. O. Boyron
Université de Lyon, Univ. Lyon 1, CPE Lyon, CNRS, UMR 5265
Laboratoire de Chimie Catalyse Polymères et Procédés (C2P2)
LCPP Team, Bat 308F, 43 Bd. du 11 novembre 1918,
F-69616 Villeurbanne, France

© 2015 WILEY-VCH Verlag GmbH & Co. KGaA, Weinheim

DOI: 10.1002/macp.201400490

Macromolecular
Chemistry and Physics

www.mcp-journal.de

the microstructure or the chemical composition along the MMD.[10]

The CCD of polyolefins is routinely evaluated by temperature rising elution fractionation (TREF) or crystallization analysis fractionation (CRYSTAF). These techniques are based on the crystallization of polymer chains from diluted hot solution. The incorporation of comonomer units interrupts the chain regularity, and consequently the ability of the polymer chains to orient into a crystal will be lower. Thus, copolymers vary in their crystallizability, and the crystallization temperature is related to the comonomer content. Both TREF and CRYSTAF have been widely used to characterize polyethylene (PE), polypropylene (PP), and their copolymers.[11–19] Fractions collected using preparative TREF can be used for further characterization by SEC, NMR, differential scanning calorimetry (DSC), or Fourier transform infrared spectroscopy (FTIR).[19–22] Stepwise DSC (self-nucleation annealing thermal fractionation, SSA[24]) and solvent/nonsolvent fractionation[25] have been less often applied to analyze the CCD of polyolefins.

The application of TREF and CRYSTAF as well as SSA is limited to semicrystalline polymers, i.e., these techniques fail to fractionate amorphous samples. Other limitations are long analysis time and co-crystallization. Solvent/non-solvent fractionation is also time consuming; moreover, the fractionation is substantially influenced by molar mass of the analyzed samples.

Interactive liquid chromatography is an emerging alternative technique to fractionate polyolefin samples according to their chemical heterogeneity. A selective chromatographic adsorption and desorption of polyolefins was first demonstrated by Macko et al. on porous graphitic carbon (Hypercarb) using a solvent gradient 1-decanol→1,2,4-trichlorobenzene (TCB).[26,27] The sorbent Hypercarb was developed by Knox et al.[28] and shows a unique chromatographic behavior. The carbon atoms are arranged in hexagonally flat structures, which can interact with non-polar analytes due to dispersive interactions, as well as with polar ones via induced dipoles.[29] Moreover, the highly ordered nature of the surface imparts structure selectivity for particular features of an analyte and strong affinity towards molecules, which can orientate themselves on the carbon surface in a planar conformation. Owing to that, porous graphitic carbon separates linear PE from PP, discriminates the stereoisomers of PP,[26,30] and separates copolymers of ethylene or propylene with 1-alkenes[31–35] as well as EP rubbers[36,37] and EPDM terpolymers[38] according to their comonomer content.

So far, interactive high performance liquid chromatography (HPLC) of polyolefins has mostly been realized using 1-decanol→TCB as mobile phase and Hypercarb as graphitic stationary phase. An important question that has not been answered is how the combination of adsorption and desorption promoting solvents in the mobile phase affects the elution behavior of ethylene/1-alkene copolymers from the graphitic stationary phase. Also the influence of the length of short-chain branches on the elution behavior of ethylene/1-alkene copolymers has not yet been compared. In this study, we want to probe these questions, using well defined, with regard to composition and molar mass narrowly distributed ethylene/1-alkene copolymers. The results from HPLC will be compared with results from CRYSTAF and correlated with data from both SEC and NMR.

2. Experimental Section

2.1. Polymer Samples

The polymer samples were synthesized using the catalyst system *rac*-Et(Ind)$_2$ZrCl$_2$/MAO (Al/Zr = 3000) in toluene (300 mL, 4 bars, 80 °C).[39] The average chemical compositions were measured using ^{1}H and ^{13}C NMR and the average molar masses were determined by HT-SEC. The results are summarized in Table 1.

2.2. Solvents

1-Decanol, 2-octanol, 2-ethyl-1-hexanol, 1,2-dichlorobenzene (ODCB), and TCB, all of synthesis quality (Merck, Darmstadt, Germany), were used as components of the mobile phases. ODCB and TCB were distilled before use, while the other solvents were used as delivered.

2.3. High-Temperature Chromatograph PL XT-220

A high-temperature chromatograph PL XT-220 (Polymer Laboratories, Agilent Inc., Church Stretton, England) equipped with a robotic sample handling system PL-XTR (Polymer Laboratories) for injection of the samples was used. A high-pressure binary gradient pump is a part of this chromatograph. The temperature of the sample block, the injection needle, the injection port, and the transfer line between the auto sampler and the column compartment was set at 160 °C. An evaporative light-scattering detector (ELSD, model PL-ELS 1000, Polymer Laboratories, Church Stretton, England) was used for detection. The following parameters were used for the ELSD: gas flow rate 1.5 L min^{-1}, nebulizer and evaporator temperatures 160 and 260 °C, respectively. The flow rate of the mobile phase was 1 mL min^{-1}. The polymers were dissolved for 2–5 h in 1-decanol, 2-ethyl-1-hexanol, or 2-octanol at a concentration of 1–2 mg mL^{-1} and a temperature of 160 °C. 50 µL of the polymer solution was injected into a Hypercarb column (Thermo Scientific, Dreieich, Germany) containing particles of porous graphitic carbon (average particle size 5 µm, surface area of 120 m^2 g^{-1}, pore size of 250 Å). The dimensions of the column were 100 × 4.6 mm^2 L x ID. After the injection of a sample, the adsorption promoting liquid (alcohol) was pumped for 3 min. The adsorbed sample was then desorbed by a linear gradient, starting with the alcohol and ending with TCB or

Macromolecular Journals

Macromol. Chem. Phys. **2015**, *216*, 721–732

© 2015 WILEY-VCH Verlag GmbH & Co. KGaA, Weinheim

Table 1. Weight-average molar mass (M_w), dispersity (D), and average chemical composition of the ethylene/1-alkene copolymers.

Comonomer	Comonomer content[a] [mol%]	M_w[b] [kg mol^{-1}]	D
Propene (EP)	2.3	62.9	1.9
	2.7	56.2	1.8
	2.7	72.0	2.3
	5.0	52.4	2.0
	4.2	59.4	1.8
	9.1	50.3	1.7
1-Hexene (EH)	0	174.6	2.9
	0.4	134.5	2.7
	1.1	105.0	2.6
	2.2	80.4	2.0
	3.7	60,1	1.8
	5.1	43.5	2.1
	5.8	56.4	1.9
	6.3	51.7	1.8
	9.0	55.2	2.2
	13.9	111.2	2.0
	20.7	60.7	2.3
1-Octene (EO)	0.4	116.2	2.4
	0.6	106.6	2.6
	1.7	58.3	1.8
	3.4	57.8	1.8
	5.6	57.9	1.8
1-Octadecene (EOD)	0.7	65.0	2.5
	1.5	64.1	1.8
	1.7	93.1	2.6
	2.1	73.7	1.9
	2.7	60.0	2.3
	2.9	58.9	2.3
	3.3	82.1	1.9

[a]Determined by ^{1}H and ^{13}C NMR; [b]Determined by HT-SEC using a dual-angle light-scattering detector.

ODCB in 10 min. Thereafter, pure TCB or ODCB were pumped for 2 min, and then the column was purged for 20 min with the pure alcohol in order to establish a new adsorption equilibrium in the column before injecting the next sample.

2.4. CRYSTAF

A CRYSTAF apparatus, model 200, manufactured by PolymerChar SA (Valencia, Spain) was used. 20 mg of the sample was dissolved in 30 mL of ODCB at 160 °C. After dissolution of the sample, the temperature of the solution was stabilized at 110 °C and after that decreased at a rate of 0.1 °C min^{-1} to 25 °C. The concentration of the polymer in the solution was monitored by an IR-detector operating at 150 °C and a wavelength of 3.5 µm.

3. Results and Discussion

3.1. CRYSTAF

The first derivative of the CRYSTAF traces, dw/dT, of ethylene/1-alkene copolymers is shown in Figure 1. The temperature of the peak maximum decreases with increasing comonomer content as expected. At low content of 1-alkene, the CRYSTAF profiles are almost symmetrical and become broader and less symmetrical when the content increases. Moreover, some samples contain fractions, which remain in the solution at 20 °C. The peak maximum crystallization temperature, T_c, from CRYTAF is a linear function of the average chemical composition, and the length of branches does not play a role, if the branch is longer than a methyl group (Figure 2), i.e., it is excluded from the crystal lattice and no side-chain crystallization takes place. The scattering of the points around the straight lines in Figure 2 is caused by the fact that the average chemical composition of the copolymers is correlated with the temperature, which corresponds to the top of the peaks. The average chemical composition, however, corresponds to this temperature only if a CRYSTAF peak is symmetrical. This means that asymmetry of the crystallization profiles, due to inhomogeneous comonomer incorporation, as well as the presence of an amorphous part, which many samples contain, has been neglected. Despite this, the trends observed in Figure 2 are in agreement with data from DSC and CRYSTAF for random copolymers of ethylene with various 1-alkene comonomers.[6,7,40] Moreover, the independence of the melting (DSC) and crystallization temperature (CRYSTAF) on the length of the branches was found also by Brüll et al. for random copolymers of propene with various 1-alkene comonomers.[41,42]

3.2. High-Temperature HPLC

3.2.1. TCB as Desorption Promoting Solvent

An interesting question is how the adsorption promoting strength of the alcohol and the desorption strength of the good solvent affect the elution behavior. To probe this, the elution behavior of the samples was analyzed using 1-decanol, 2-ethyl-1-hexanol, and 2-octanol as adsorption promoting solvent, and TCB or ODCB as desorption promoting solvent. Representative chromatograms are shown in Figure 3.

© 2015 WILEY-VCH Verlag GmbH & Co. KGaA, Weinheim

Macromolecular
Chemistry and Physics
www.mcp-journal.de

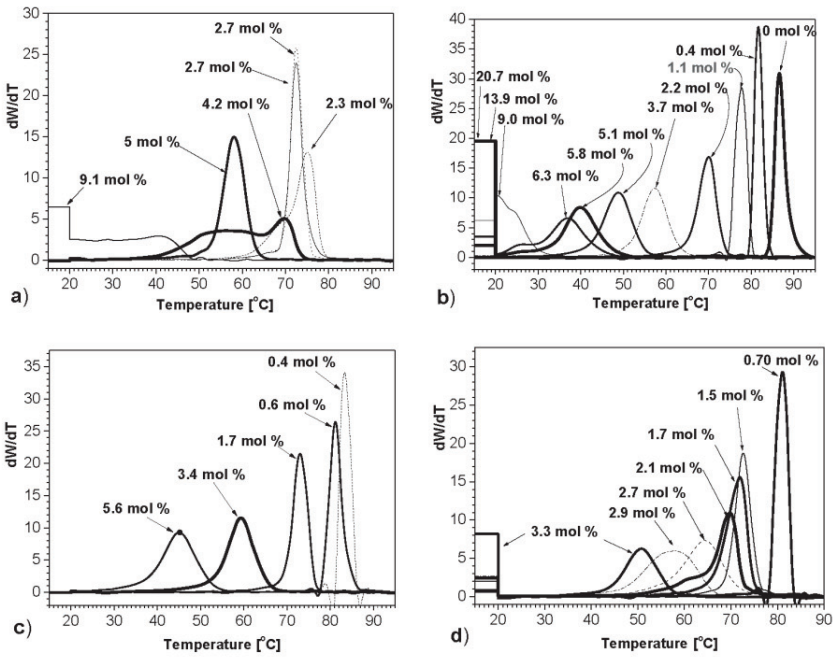


Figure 1. Overlay of profiles obtained with CRYSTAF for ethylene/1-alkene copolymers for a) EP; b) EH; c) EO; d) EOD.

Similarly symmetrical peaks as shown in Figure 3, however, with different elution volumes, were recorded in all tested mobile phases. The elution volume at peak maximum, V_e, is plotted as a function of comonomer content in Figure 4.

The elution volume at peak maximum linearly decreases with increasing comonomer content for all comonomers and in all tested HPLC systems. It is assumed that the SCB decreases the probability of orientation of the macromolecules in a flat conformation on the graphite surface, i.e., SCB interrupts the methylene sequences, which interact with the surface of Hypercarb. As a consequence, the retention of the copolymers decreases with increasing comonomer content.

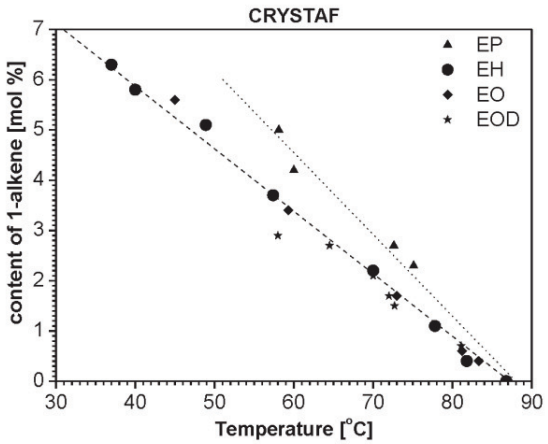


Figure 2. Correlation between the average comonomer content and the peak maximum crystallization temperature, T_c (Figure 1) measured by CRYSTAF for a) EP; b) EH; c) EO; d) EOD.

It is necessary to notice that the top of the peaks has been correlated with the average chemical composition as determined by NMR, i.e., in case a peak is asymmetrical, the average composition does not correspond to the top of a peak. As a consequence, in such cases, the points are scattered around the straight lines in Figure 4.

The results in Figure 4, which were obtained with four different mobile phases, indicate that the EP copolymers elute with the largest elution volumes, consecutively followed by the EH and EO copolymers. The line corresponding to the EOD copolymers falls (for four mobile phases) between the lines, which correspond to the EH and the EO copolymers. The differences in the retention of linear low density polyethylene (LLDPE) with different type of comonomer are, however, small, hence, the type of comonomer other than the propene cannot be distinguished with reasonable accuracy.

It is supposed that the longer the side chain length, the less the interaction of the polymer backbone

Macromolecular Journals
Macromol. Chem. Phys. **2015**, *216*, 721–732
© 2015 WILEY-VCH Verlag GmbH & Co. KGaA, Weinheim

Macromolecular Chemistry and Physics

www.mcp-journal.de

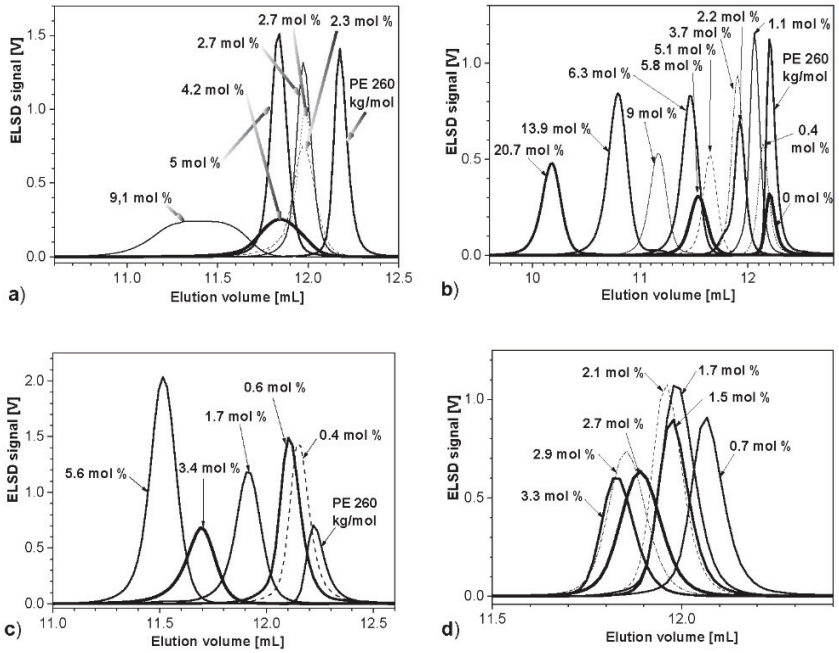


Figure 3. Overlay of chromatograms of a) EP; b) EH; c) EO; d) EOD in Hypercarb/2-ethyl-1-hexanol → TCB. The average content of the respective 1-alkene is indicated in the figure.

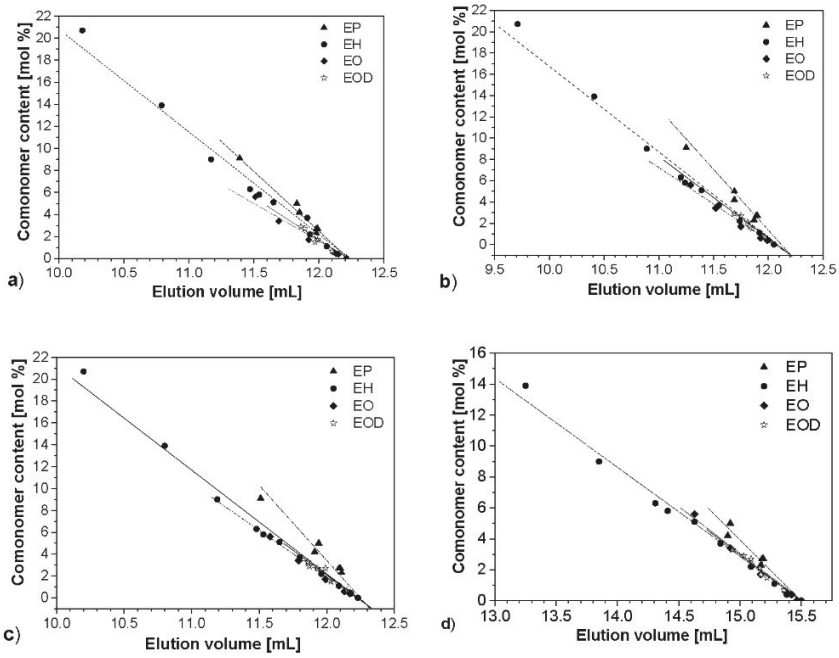


Figure 4. Correlation between V_e and the comonomer content of the ethylene/1-alkene copolymers for the mobile phase: a) 2-ethyl-1-hexanol→TCB; b) 1-decanol→TCB; c) 2-octanol→TCB; d) 2-octanol→ ODCB.

Macromol. Chem. Phys. **2015**, *216*, 721–732

© 2015 WILEY-VCH Verlag GmbH & Co. KGaA, Weinheim

Macromolecular
Chemistry and Physics
www.mcp-journal.de

with the graphitic surface is, i.e., the retention of a macromolecule decreases. However, EOD copolymers are retained to a slightly larger extent than the EO- (Figure 4a,b,c) or EH- (Figure 4d) copolymers with an equivalent content of branches. This indicates that the C16-branches are also partially adsorbed and thus contribute to the retention. Similarly, adsorption of C12 and C16 branches was observed previously for copolymers of propene with 1-dodecene and 1-hexadecene in Hypercarb/1-decanol→TCB.[32]

The experimentally found linear dependences (Figure 4) indicate that the retention of the copolymers is controlled mainly by the chemical composition of the samples, which, in turn, means that the profile of the chromatograms may be considered as the CCD of the samples. The profiles obtained with CRYSTAF (Figure 1) as well as the HPLC chromatograms (Figure 3, as well as in all other tested mobile phases) indicate a trend, namely that the width of the peaks, i.e., CCD of the samples, increases with increasing the average comonomer incorporation (Table 2).

Especially, broad CCD can be observed for the EP sample containing 9.1% of propene (Figure 3a). The same trend is observed with CRYSTAF (Figure 1a) where, however, the amorphous fractions of the samples are not selectively separated (Figure 1) and, thus, the results of HPLC may be more informative.

The CRYSTAF profile for the EP sample containing 4.2 mol% of propene is much broader than that for EP with 5 mol% (Figure 1a, Table 2). The difference in broadness of the peaks is significantly smaller (Figure 3a) in HPLC. However, the reason for this is not yet clear.

The majority of the copolymers elutes in narrow peaks what indicates their narrow CCD. Such polymer samples are suitable to calibrate both used separation methods, CRYSTAF and HPLC.

CRYSTAF is especially sensitive to the crystalline polymers, i.e., usually with 0–6 mol% of 1-alkene. For example, temperature 91.8 °C and 77.8 °C corresponds in CRYSTAF to the EH copolymers with 0.4 mol% and 1.1 mol% 1-hexene, respectively. For obtaining this sensitivity, small changes in temperature (temperature gradient in 14 h) are necessary in CRYSTAF. On the other hand, HPLC separates copolymers from 0% to 100% alkene and the used solvent gradient, (i.e., changing the composition of the mobile phase from 0% to 100% TCB) required—in contrast to the temperature gradient in CRYSTAF—only 10 min. For example, the EH copolymers with 0.4 mol% and 1.1 mol% 1-hexene eluted with elution volume 12.14 and 12.06 mL, respectively (Figure 3b). Prolonging the time for the gradient (for example, from 0% to 100% TCB in 100 min) may increase distance between the separated peaks and this topic will be covered in another paper in the future.

Table 2. Width of peaks obtained with CRYSTAF (Figure 1) and HPLC (Figure 3) for ethylene/1-alkene copolymers, as measured at the baseline.

Comonomer	Comonomer content [mol%]	Width of peak in CRYSTAF [°C]	Width of peak in HPLC [mL]
Propene (EP)	2.3	19	4.5
	2.7	13	4.6
	2.7	10	4.7
	4.2	34	5.9
	5.0	17	4.3
	9.1	*	10.0
1-Hexene (EH)	0	10	3.2
	0.4	7	3.6
	1.1	7	3.9
	2.2	15	4.5
	3.7	18	4.9
	5.1	20	4.6
	5.8	25	5.0
	6.3	28	5.8
	9.0	*	6.3
	13.9	*	7.5
	20.7	*	6.6
1-Octene (EO)	0.4	6	4.6
	0.6	9	4.1
	1.7	13	5.0
	3.4	21	5.0
	5.6	24	5.4
1-Octadecene (EOD)	0.7	7	2.7
	1.5	15	2.8
	1.7	14	3.1
	2.1	23	3.6
	2.7	24	3.4
	2.9	26	3.5
	3.3	*	3.2

*Not determined due to amorphous part of the sample.

3.2.2. ODCB as Desorption Promoting Solvent

Elution volume and selectivity of an HPLC separation depend on the nature of the adsorption promoting solvent as well as the desorption promoting solvent. Only two desorption promoting solvents for PE in Hypercarb are known at the moment, namely TCB and ODCB.

The difference in retention volumes for an identical copolymer sample shows that the sample elutes

Macromolecular Journals
Macromol. Chem. Phys. **2015**, *216*, 721–732
© 2015 WILEY-VCH Verlag GmbH & Co. KGaA, Weinheim

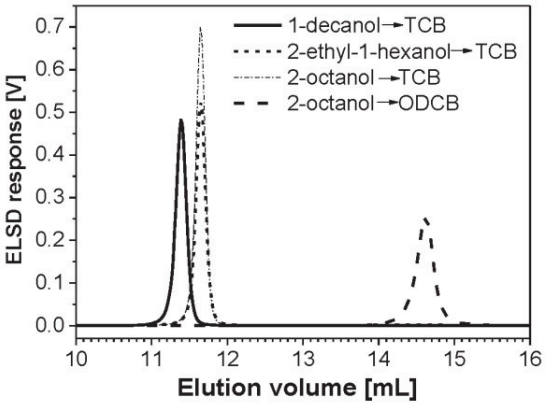


Figure 5. Overlay of chromatograms of the EH copolymer with 5.1 mol% 1-hexene in different mobile phases.

at larger elution volume, if ODCB is used instead of TCB (Figure 5), i.e., that ODCB is not as strong desorption promoting solvent as TCB. As a consequence, peaks eluted in alcohol→ODCB are slightly broader than peaks eluted in alcohol→TCB.

3.2.3. Relation Between Chemical Composition, Molar Mass, and Elution Volume of Ethylene/1-Alkene Copolymers in Four Mobile Phases

The elution volumes of the ethylene/1-alkene copolymers in four mobile phases do not at all correlate with the corresponding values of their average molar mass (Figure 6). The molar masses varied in the range 50–72 kg mol^{-1} (Figure 6a), 43–134 kg mol^{-1} (Figure 6b), 57–116 kg mol^{-1} (Figure 6c), and 65–82 kg mol^{-1} (Figure 6d). The evidence that the molar mass does not play a significant role in these HPLC systems is important with regard to the orthogonality of the separation in 2D liquid chromatography.

The same findings have been reported recently for different series of LLDPE in Hypercarb/1-decanol→TCB,[33] which implies that the elution behavior of these copolymers in HPLC is primarily determined by the chemical composition. Moreover, there are linear correlations between the content of 1-alkene in the copolymers and their elution volume (Figure 6).

Let us discuss first the mobile phases with TCB: According to the values of the elution volume, the copolymers are strongest retained from 2-octanol and 2-ethyl-1-hexanol

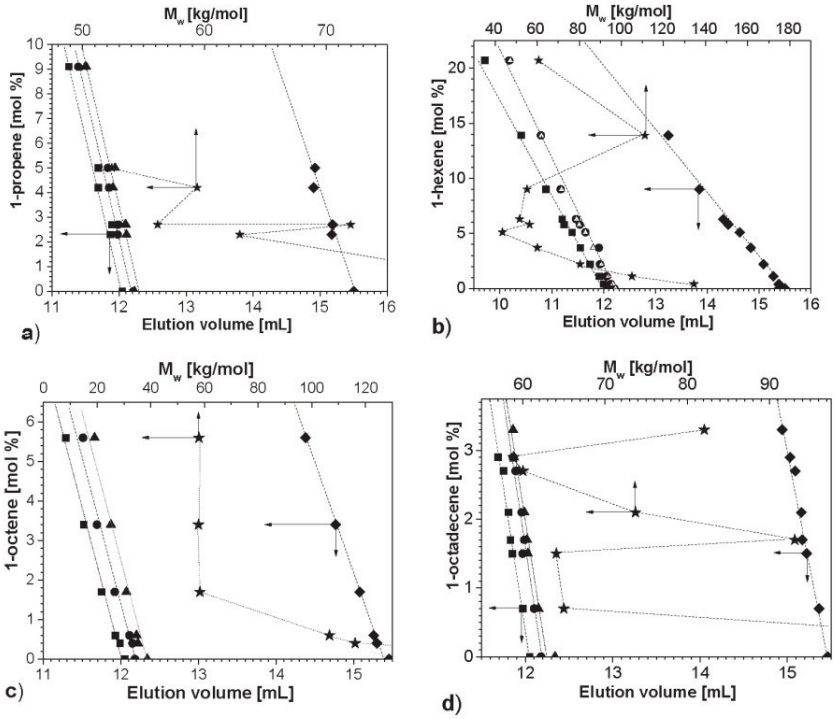


Figure 6. Dependence of the elution volume on the content of 1-alkene for a) EP; b) EH; c) EO; d) EOD in different mobile phases. Symbols: ★ – M_w of a sample. Mobile phase: ■ – 1-decanol→TCB; ● – 2-ethyl-1-hexanol→TCB; ▲ – 2-octanol→TCB; ♦ – 2-octanol→ODCB. Notice: The elution volume does not correlate with the average molar mass of the copolymers.

© 2015 WILEY-VCH Verlag GmbH & Co. KGaA, Weinheim

Macromolecular
Chemistry and Physics

www.mcp-journal.de

and then follows 1-decanol (Figure 6). These three adsorption promoting liquids have different polarity (dipole moment: 1-decanol = 1.60 D, 2-octanol = 1.71 D, 2-ethyl-1-hexanol = 1.74 D[43] and differ in their solvation quality for PE (cloud points of PE[44]: 1-decanol = 138 °C, 2-octanol = 145 °C, 2-ethyl-1-hexanol = 150 °C). According to the polarity of molecules and the cloud point values, the strongest adsorption could be expected from the most polar and, therefore, thermodynamically poorest solvents, i.e., in the order 2-ethyl-1-hexanol, 2-octanol, 1-decanol. In fact, the copolymers are the least retained from 1-decanol and more or similarly from 2-octanol and 2-ethyl-1-hexanol.

Extrapolating the straight lines to 100 mol% of ethylene coincides with the experimentally determined elution volume of the linear PE standard 260 kg mol^{-1}.

Figure 6 shows that the calibration dependencies for the copolymers are similar when TCB is applied as desorption promoting liquid, which means that the samples are adsorbed/desorbed from these alcohols to a similar extent. Using ODCB, the calibration is shifted to much larger elution volumes, which indicates that ODCB is a weaker desorption promoting solvent.

The dependence of the elution volume on the content of 1-alkene is linear for all ethylene/1-alkene copolymers in all tested solvents (Table 3). The quotients and the slopes of equations in Table 3 are different for different types of copolymers and for different mobile phases, because the extent of adsorption and desorption is function of both type of comonomer and the nature of the mobile phase. Equations from Table 3 will be applied for

Table 3. Equations obtained from experimental data of ethylene/1-alkene copolymers.

		EP	
Method		**Equation**[a)]	R^2
CRYSTAF	**ODCB**	Cont = 13.552–0.149 T_c	0.988
HPLC	1-Decanol→TCB	Cont = 131.624–10.874 Ve	0.971
	2-Ethyl-1-hexanol→TCB	Cont = 136.864–11.198 Ve	0.984
	2-Octanol→TCB	Cont = 146.244–11.893 Ve	0.960
	2-Octanol→ODCB	Cont = 119.434–7.700 Ve	0.946
		EH	
Method	**Mobile phase**	**Equation**[a)]	R^2
CRYSTAF	ODCB	Cont = 11.116–0.128 T_c	0.996
HPLC	1-Decanol→TCB	Cont = 104.706–8.731 V_e	0.992
HPLC	2-Ethyl-1-hexanol→TCB	Cont = 121.987–10.024 V_e	0.989
HPLC	2-Octanol→TCB	Cont = 122.479–10.062 V_e	0.991
HPLC	2-Octanol→ODCB	Cont = 92.350–5.977 V_e	0.990
		EO	
Method	**Mobile phase**	**Equation**[a)]	R^2
CRYSTAF	ODCB	Cont = 11.116–0.128 T_c	0.995
HPLC	1-Decanol→TCB	Cont = 86.936–7.229 V_e	0.984
HPLC	2-Ethyl-1-hexanol→TCB	Cont = 92.056–7.549 V_e	0.967
HPLC	2-Octanol→TCB	Cont = 100.404–8.158 V_e	0.954
HPLC	2-Octanol→ODCB	Cont = 80.031–5.186 V_e	0.971
		EOD	
Method	**Mobile phase**	**Equation**[a)]	R^2
CRYSTAF	ODCB	Cont = 11.116–0.128 T_c	0.995
HPLC	1-Decanol→TCB	Cont = 100.578–8.347 V_e	0.980
HPLC	2-Ethyl-1-hexanol→TCB	Cont = 111.015–9.118 V_e	0.968
HPLC	2-Octanol→TCB	Cont = 84.949–6.910 V_e	0.940
HPLC	2-Octanol→ODCB	Cont = 101.830–6.586 V_e	0.979

[a)]Cont = content of 1-alkene in a copolymer in mol%; T_c in °C; V_e in mL.

Macromolecular Journals

Macromol. Chem. Phys. **2015**, *216*, 721–732
© 2015 WILEY-VCH Verlag GmbH & Co. KGaA, Weinheim

Materials Views
www.MaterialsViews.com

calculation of CCD from CRYSTAF profile as well as for calculation of CCD from shape of the HPLC peak of a polymer sample in the next chapter. Namely, the temperature in CRYSTAF and the elution volume in HPLC are functions of the chemical composition of the copolymers; heights of a CRYSTAF profile or a HPLC peak reflect the concentration of copolymers.

3.3. Comparison of Data from HPLC with Those from CRYSTAF

Both, CRYSTAF and HPLC are based on measuring different physical properties: CRYSTAF evaluates the concentration of a polymer in solution at defined temperatures, i.e., it responds to differences in crystallinity of macromolecules in one solvent. On the contrary, solvent gradient HPLC is based on selective adsorption and desorption of macromolecules at a constant temperature above the melting point of the analyzed polymer, i.e., it is based on differences in interactions between macromolecules and a sorbent in two solvents. As a consequence, CRYSTAF fails to fractionate olefin copolymers when the comonomer content exceeds 6 mol% (see Figure 1b), while HPLC enables fractionation of all components of a comonomer, i.e., amorphous as well as semicrystalline ones. Moreover, CRYSTAF does not discriminate between branches of different length (except for EP copolymers, Figure 3).[8,40] In contrast, the retention in HPLC is a function of the length of SCB (Figure 4,6).

An advantage of both CRYSTAF and HPLC is that they offer a linear dependence between the content of 1-alkene and temperature T_c (CRYSTAF, Figure 2) and between the content of 1-alkene and the elution volume (HPLC, Figure 6). The corresponding equations of the linear dependencies are summarized in Table 3. These equations are considered as calibrations of CRYSTAF and HPLC systems and may be used, when the CCD of a sample from these series of samples is of interest. To use these calibrations for calculation of CCD of an unknown copolymer sample (prepared by using a different catalyst or under different conditions of polymerization) would be premature, because microstructural arrangement of monomers also plays a role in elution behavior.

With the aim to compare the separation of an ethylene/1-alkene copolymer (for example, with 5.1 mol% 1-hexene) with CRYSTAF and HPLC, the content of 1-hexene was calculated to each value of temperature T_c (CRYSTAF, Figure 1b) and to each elution volume V_e (HPLC, Figure 5) using the corresponding equation in Table 3. The height of peaks obtained with an IR-detector or ELSD is proportional to the concentration of the sample in the mobile phase. With the aim to compare the response of both detectors, the detector signals have been normalized. The described procedure was used to calculate the CCD of a polymer sample (with 5.1 mol% 1-hexene) from

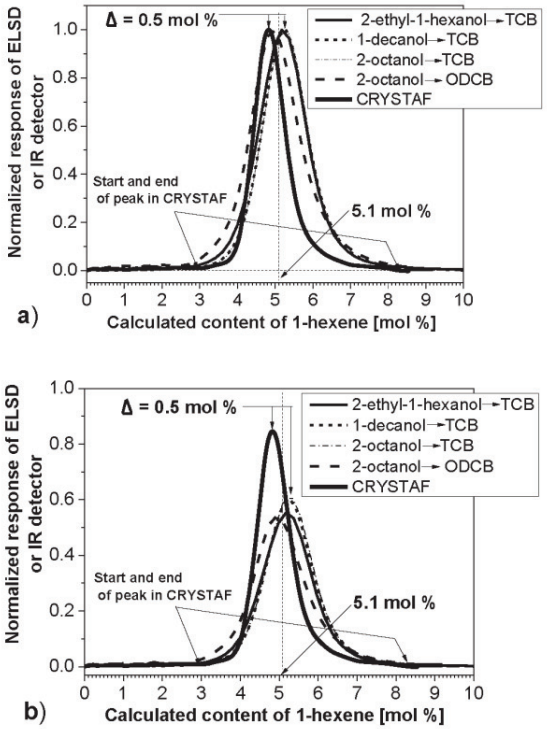


Figure 7. CCD of the EH copolymer with 5.1 mol% 1-hexene calculated from experimental HPLC and CRYSTAF data. Solvent pairs, used as the mobile phase in HPLC are indicated in the figure. a) The height of peaks was normalized (i.e., the maximum height of all peaks is the same). b) The area of peaks was normalized (i.e., the areas of all peaks are identical).

the elution profiles obtained from CRYSTAF and HPLC. An example of the calculated CCD is shown in Figure 7. The calculated content of 1-hexene is presented on the *x*-axis and the *y*-axis shows the relative concentration of polymer.

The calculated CCDs of the EH sample with 5.1 mol% 1-hexene obtained from HPLC with alcohols→TCB are almost identical (Figure 7), which indicates that the interactions between the polymers and graphite in alcohol/TCB-mixtures are comparable. On the other hand, the CCD obtained with alcohol→ODCB is the broadest one, and its maximum is slightly shifted. The CCD obtained from CRYSTAF is narrower than the corresponding CCD obtained by HPLC (Figure 7). It could be expected that a polymer sample has in CRYSTAF a narrow peak and has in HPLC a broader peak, because the amorphous part (which elutes in CRYSTAF at 20 °C, Figure 1a,b,d) has not been taken account in the CRYSTAF profile of the considered sample, while the amorphous and semicrystalline part elute in HPLC together in one peak. However, the CCD calculated from the HPLC chromatograms is broader

© 2015 WILEY-VCH Verlag GmbH & Co. KGaA, Weinheim

Macromolecular
Chemistry and Physics

www.mcp-journal.de

than the CCD calculated from the CRYSTAF profiles for all copolymer samples, i.e., including samples without an amorphous part in the CRYSTAF.

HPLC separation is more sensitive to the length of branching in comparison with CRYSTAF, which is illustrated in Figure 2 and 4. This selectivity in HPLC depends on the selected sorbent/solvents system.

We conclude that there are differences between the CCD determined from CRYSTAF and HPLC, because both methods are based on different principles (crystallization/dissolution contra adsorption/desorption) and as a consequence, each method reflects specifically the CCD and microstructure of a copolymer sample. HPLC is, however, applicable in full range of the LLDPE composition, while CRYSTAF is limited to semicrystalline components of a polymer sample.

3.4. Peculiarities of Adsorption of PE and Ethylene/1-Alkene Copolymers on Graphite

A lot of experience exists with HPLC of small molecules using porous graphite[33] (see review[29]). According to literature references, the surface of the porous graphite is crystalline and is composed of flat sheets of hexagonally arranged carbon atoms. Such specific structure substantially influences its adsorption capabilities: The strength of interactions depends on the molecular area of a solute in contact with the surface of graphite. Thus, structural planarity of chemically comparable solutes correlates with selectivity of their separation, i.e., two solutes differ in their elution volumes, if they differ in their planar conformations; it was found that retention of bulky, nonplanar compounds was unfavorable on the graphite.

In series of experimental works and theoretical calculations,[45–50] it was shown that long-chain alkanes (e.g., C_{60}^{48}) adopt a regular zigzag conformation on the planar surface of graphite upon adsorption from a solution, where each carbon with two atoms of hydrogen is placed on specific position in a hexagon (Figure 8). Such an arrangement is assumed also for PE.[49] Analogue arrangements of carbon atoms on the planar surface of graphite have been observed for n-alkanes using scanning-tunneling-microscopy[45,46] and derived from data of neutron and X-ray diffraction[50] or were supposed from studying the adsorption isotherms.[51]

Morishige et al.[47] expressed the opinion that the scanning-tunneling microscopy images reflect the real arrangement of the molecules adsorbed on graphite: The molecules are adsorbed in a monomolecular layer. Magonov et al.[48] found, using atomic force microscopy, that nanocrystals of n-alkane C_{60} melted around 95 °C, while the epitaxial layers of n-C_{60} formed on graphite from xylene were observed to melt at temperatures up to 140 °C. This means that the interactions between the adsorbed n-alkane and graphite and the corresponding orientations of methylene groups on the sorbent surface are stable even above the crystallization temperature of the PE oligomers. It may be supposed that such regular conformations exist on a graphitic surface at conditions used for HPLC of polyolefins.

The results from HPLC of polyolefins are in agreement with the rules derived from HPLC of small molecules: Linear macromolecules of PE are strongly retained and incorporation of alkyl branches into linear chains decreases their retention in the HPLC column. The length of alkyl groups influences the retention of ethylene-alkene copolymers, as it is illustrated in this paper. The

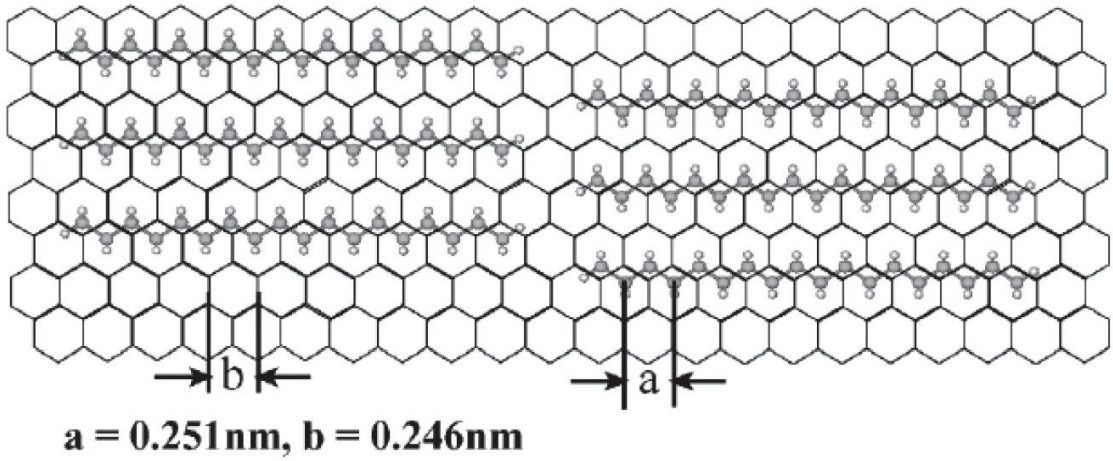


Figure 8. Schematic diagram of alkane molecules ($C_{18}H_{38}$) adsorbed on graphite.[45] The length of the C–C–C zig-zag is 0.251 nm. The hollow distance of the graphite lattice is $b = 0.246$ nm.[45]

Macromolecular Journals

Macromol. Chem. Phys. **2015**, *216*, 721–732

© 2015 WILEY-VCH Verlag GmbH & Co. KGaA, Weinheim

Materials Views
www.MaterialsViews.com

mutual orientation of alkyl groups relative to the main chain (i.e., tacticity) may influence the retention behavior of polyolefins, for example, isotactic, atactic, and syndiotactic PP are retained (adsorbed/desorbed) to a different extent on the surface of graphite from 1-decanol.[26]

Naturally, the adsorption of a polymer is a function of the nature of the solvent used. Full adsorption of PE is observed also at temperature as high as 160 °C from various polar and nonpolar solvents.[26,27,31–36] PE is adsorbed on graphite at 100 °C even from ODCB and TCB, i.e., from thermodynamically very good solvents,[52] which underlines that pronounced interactions exist between the PE and the sorbent surface. On the other hand, PE is fully desorbed by ODCB and TCB at 160 °C.

Similarly, like in HPLC of small molecules, the variability of solvents used for adsorption and desorption enables to tune the chromatographic separations.

4. Conclusion

A series of ethylene/1-alkene random copolymers (ethylene/1-propene, 1-hexene, 1-octene, 1-octadecene) was analytically characterized with traditional methods, i.e., SEC, NMR, and CRYSTAF and with an emerging method for analytical separation of polyolefins–interactive gradient liquid chromatography. The chromatographic measurements were realized in four different mobile phases using a chromatographic column packed with porous graphite, Hypercarb. The chromatographic separation was based on adsorption of the polymers from 1-decanol, 2-ethyl-1-hexanol, or 2-octanol at 160 °C. The adsorbed polymers were desorbed after addition of TCB or ODCB into the mobile phase.

It was found that the crystallization temperatures (CRYSTAF) and the elution volumes (HPLC) of the copolymers depend linearly on their average chemical composition (NMR). The crystallization temperatures (CRYSTAF) and the elution volumes (HPLC) of the copolymers decrease with increasing concentration of branches (methyl, butyl, hexyl, hexadecyl) in the copolymers.

CRYSTAF profiles were partially tailing and some profiles contained fractions, which did not crystallize at 20 °C. In contrast, the copolymer samples were fully adsorbed and desorbed, and the peaks of the copolymers recorded with HPLC were more or less symmetrical. Moreover, the retention of ethylene-propene copolymers and, to a smaller extent also the retention of ethylene/1-hexene, 1-octene, 1-octadecene copolymers with equivalent concentration of branches in HPLC was different, while in CRYSTAF these copolymers (except EP copolymers) cannot be differentiated. These differences in HPLC are, however, small, hence, type of comonomer other than propene is difficult to distinguish with reasonable accuracy.

Both analytical techniques, CRYSTAF and HPLC, reflect the CCD of the copolymer samples and thus enable their comparison. The CCD profiles derived from HPLC data are, however, broader that the CCD obtained with CRYSTAF. The physical principles underlying both methods are different—CRYSTAF is based on crystallization and HPLC on adsorption/desorption of polymers. As a result, HPLC is applicable over the full range of the LLDPE composition (even in range 0%–100% of ethylene[37], while CRYSTAF and TREF are limited on semicrystalline components.

It is known that the average molar mass determined with SEC-RI does not coincide fully with the molar mass determined with SEC-MALS or SEC-VIS and the average chemical composition determined with NMR often not fully coincide with values obtained with IR spectroscopy. Even results from TREF do not coincide fully with results from CRYSTAF for an identical analyzed sample.

HPLC of polyolefins with porous graphite as column packing, started in 2009.[26] Thus, HPLC of polyolefins is a young method, which still has an undiscovered potential and possibilities for improvements. The particular advantage of HPLC of polyolefins in comparison to CRYSTAF and TREF is the fact that HPLC may selectively separate partially as well as fully amorphous polyolefin samples. Moreover, HPLC measurement requires much smaller amounts of samples and less time for obtaining experimental data.

Acknowledgements: This research forms part of the research programme of the Dutch Polymer Institute (DPI), project Nr. 750. The financial support by Deutsche Forschungsgemeinschaft (DFG) (project MA 4348/1-1) is gratefully acknowledged.
Note: Academic titles for all authors were added on April 22, 2015, after initial publication online.

Received: September 22, 2014; Revised: December 17, 2014; Published online: February 4, 2015; DOI: 10.1002/macp.201400490

Keywords: adsorption; chemical composition distribution; ethylene/1-alkene copolymers; liquid chromatography

[1] W. Kaminsky, *Macromol. Chem. Phys.* **2008**, *209*, 459.
[2] W. W. Yau, D. Gillespie, *Polymer* **2001**, *42*, 8947.
[3] A. Striegel, W. W. Yau, J. J. Kirkland, D. D. Bly, *Modern Size Exclusion Liquid Chromatography*, Wiley-VCH, New York **2009**.
[4] P. J. DesLauriers, D. C. Rohlfing, E. T. Hsieh, *Polymer* **2002**, *43*, 159.
[5] A. Faldi, J. B. P. Soares, *Polymer* **2001**, *42*, 3057.
[6] R. Alamo, R. Domszy, L. Mandelkern, *J. Phys. Chem.* **1984**, *88*, 6587.
[7] S. M. Graf, R. Brüll, H. Pasch, U. M. Wahner, *e-Polymers* **2003**, *3*, 51
[8] C. Piel, A. Albrecht, C. Neubauer, C. W. Klampfl, J. Reussner, *J. Anal. Bioanal. Chem.* **2011**, *400*, 2607.
[9] A. Ortin, E. Lopez, B. Monrabal, J. R. Torres-Lapasio, M. C. Garcia-Alvarez-Coque, *J. Chromatogr. A* **2012**, *1257*, 66.

© 2015 WILEY-VCH Verlag GmbH & Co. KGaA, Weinheim

[10] W. Hiller, H. Pasch, T. Macko, M. Hofmann, J. Ganz, M. Spraul, U. Braumann, R. Streck, J. Mason, F. van Damme, *J. Magn. Reson.* **2006**, *183*, 290.
[11] B. Monrabal, *J. Appl. Polym. Sci.* **1994**, *52*, 491.
[12] R. Brüll, V. Grumel, H. Pasch, H. G. Raubenheimer, R. Sanderson, U. M. Wahner, *Macromol. Symp.* **2002**, *178*, 81.
[13] H. Pasch, R. Brüll, U. Wahner, B. Monrabal, *Macromol. Mater. Eng.* **2000**, *279*, 46.
[14] H. Nakatani, H. Matsuoka, S. Suzuki, T. Taniike, B. Liu, M. Terano, *Macromol. Symp.* **2007**, *257*, 112.
[15] N. Aust, I. Beytollahi-Amtmann, K. Lederer, *Int. J. Polym. Anal. Charact.* **1995**, *1*, 245.
[16] A. Ortin, B. Monrabal, J. Sancho-Tello, *Macromol. Symp.* **2007**, *257*, 13.
[17] C. Gabriel, D. Lilge, *Polymer* **2001**, *42*, 297.
[18] I. Nishiyama, B. Liu, H. Matsuoka, H. Nakatani, M. Terano, *Macromol. Symp.* **2003**, *193*, 71.
[19] C. Li Pi Shan, J. B. P. Soares, A. Penlidis, *Polymer* **2002**, *43*, 767.
[20] B. Monrabal, *Adv. Polym. Sci.* **2013**, *257*, 203.
[21] M. Gahleitner, P. Jääskeläinen, E. Ratajski, C. Paulik, J. Reussner, J. Wolfschwenger, W. Neißl, *J. Appl. Polym. Sci.* **2005**, *95*, 1073.
[22] W. J. Wang, E. Kolodka, S. Zhu, A. E. Hamielec, L. K. Konstanski, *Macromol. Chem. Phys.* **1999**, *200*, 2146.
[23] M. A. Matsko, L. G. Echevskaya, M. P. Vanina, M. I. Nikolaeva, T. B. Mikenas, V. A. Zakharov, *J. Appl. Polym. Sci.* **2012**, *126*, 2017.
[24] S. M. M. Mortazavi, H. Arabi, G. Zohuri, S. Ahmadjo, M. Nekoomanesh, M. Ahmadi, *Polym. Int.* **2010**, *59*, 1258.
[25] M. A. Matsko, L. G. Echevskaya, V. A. Zakharov, M. I. Nikolaeva, T. B. Mikenas, M. P. Vanina, *Macromol. Symp.* **2009**, *282*, 157.
[26] T. Macko, H. Pasch, *Macromolecules* **2009**, *42*, 6063.
[27] T. Macko, H. Pasch, Y. Wang, *Macromol. Symp.* **2009**, *282*, 93.
[28] J. H. Knox, K. K. Unger, H. Mueller, *J. Liq. Chromatogr.* **1983**, *6*, 1.
[29] L. Pereira, *J. Liq. Chromatogr. Rel. Technol.* **2008**, *31*, 1687.
[30] T. Macko, F. Cutillo, V. Busico, R. Brüll, *Macromol. Symp.* **2010**, *298*, 182.
[31] T. Macko, R. Brüll, Y. Wang, B. Coto, I. Suarez, *J. Appl. Polym. Sci.* **2011**, *122*, 3211.
[32] T. Macko, R. Brüll, R. G. Alamo, Y. Thomann, V. Grumel, *Polymer* **2009**, *50*, 5443.
[33] T. Macko, R. Brüll, R. G. Alamo, F. J. Stadler, S. Losio, *Anal. Bioanal. Chem.* **2011**, *399*, 1547.
[34] M. D. Miller, A. W. deGroot, J. W. Lyons, F. A. van Damme, B. L. Winniford, *J. Appl. Polym. Sci.* **2012**, *123*, 1238.
[35] A. Roy, M. D. Miller, M. D. Meunier, W. A. deGroot, W. L. Winniford, F. A. Van Damme, R. J. Pell, J. W. Lyons, *Macromolecules* **2010**, *43*, 3710.
[36] R. Chitta, T. Macko, R. Brüll, G. van Doremaele, L. C. Heinz, *J. Polym. Sci., Part A: Polym. Chem.* **2011**, *49*, 1840.
[37] T. Macko, A. Ginzburg, K. Remerie, R. Brüll, *Macromol. Chem. Phys.* **2012**, *213*, 937.
[38] R. Chitta, A. Ginzburg, G. van Doremaele, T. Macko, R. Brüll, *Polymer* **2011**, *52*, 5953.
[39] E. Cossoul, L. Baverel, E. Martigny, T. Macko, C. Boisson, O. Boyron, *Macromol. Symp.* **2013**, *330*, 42.
[40] N. Luruli, V. Grumel, R. Brüll, A. du Toit, H. Pasch, A. J. van Reenen, H. G. Raubenheimer, *J. Polym. Sci., Polym. Chem.* **2004**, *42*, 5121.
[41] R. Brüll, N. Luruli, H. Pasch, H. G. Raubenheimer, E. Rotimi Sadiku, R. Sanderson, A. J. van Reenen, U. M. Wahner, *e-Polymers* **2003**, *3*, 785.
[42] R. Brüll, H. Pasch, H. G. Raubenheimer, R. Sanderson, A. J. van Reenen, U. M. Wahner, *Macromol. Chem. Phys.* **2001**, *202*, 1281.
[43] *CRC Handbook of Chemistry and Physics* (Ed: D. R. Lide), 85th ed., CRC Press, Boca Raton, Florida, **2005**.
[44] T. Macko, R. Brüll, H. Pasch, *Chromatographia* **2003**, *57*, 539.
[45] Q. Chen, H. J. Yan, C. J. Yan, G. B. Pan, L. J. Wan, G. Y. Wen, D. Q. Zhang, *Surf. Sci.* **2008**, *602*, 1256.
[46] S. De Feyter, F. C. De Schryver, *Chem. Soc. Rev.* **2003**, *32*, 139.
[47] K. Morishige, Y. Takami, Y. Yokota, *Phys. Rev. B* **1993**, *48*, 8277.
[48] S. N. Magonov, N. A. Yerina, *Langmuir* **2003**, *19*, 500.
[49] T. Yang, S. Berber, J. F. Liu, G. P. Miller, D. Tomanek, *J. Chem. Phys.* **2008**, *128*, 124701.
[50] T. Arnold, C. C. Dong, R. K. Thomas, M. A. Castro, A. Perdigon, S. M. Clarke, A. Inaba, *Phys. Chem. Chem. Phys.* **2002**, *4*, 3430.
[51] A. J. Groszek, *Proc. Roy. Soc. Lond. A* **1970**, *314*, 473.
[52] R. Chitta, T. Macko, R. Brüll, M. Miller, R. Cong, W. A. deGroot, *J. Separ. Sci.* **2013**, *101*, 2063.

© 2015 WILEY-VCH Verlag GmbH & Co. KGaA, Weinheim

Dear Mr. Olivier Boyron,

Thank you for placing your order through Copyright Clearance Center's RightsLink® service.

Order Summary

Licensee:	CNRS
Order Date:	Jan 21, 2021
Order Number:	4993700983111
Publication:	Macromolecular Chemistry and Physics
Title:	Research Engineer
Type of Use:	Dissertation/Thesis
Order Total:	0.00 USD

Dear Mr. Olivier Boyron,

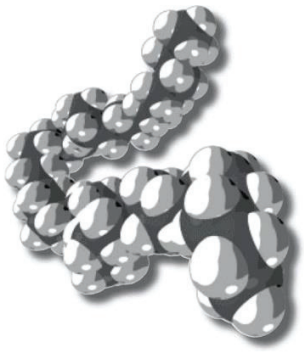
Thank you for placing your order through Copyright Clearance Center's RightsLink® service.

Order Summary

Licensee:	CNRS
Order Date:	Jan 21, 2021
Order Number:	4993710071902
Publication:	Wiley Books
Title:	Research Engineer
Type of Use:	Dissertation/Thesis
Order Total:	0.00 USD

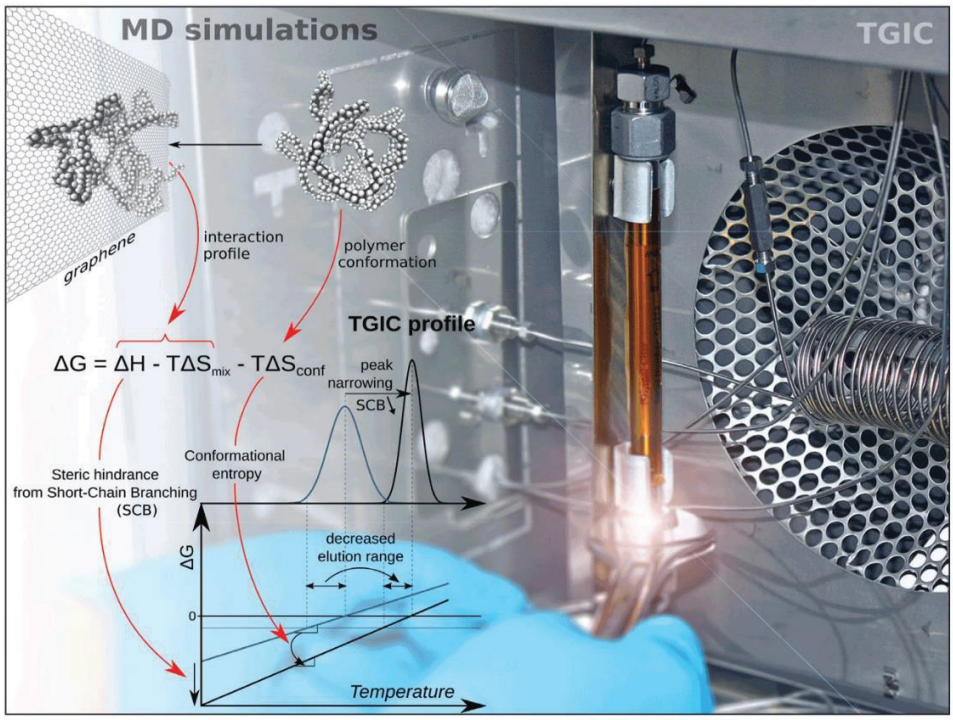
Volume 220 • Number 8 • April 18, 2019

www.mcp-journal.de



Macromolecular Chemistry and Physics

Founded by Hermann Staudinger



8/2019

WILEY-VCH

FULL PAPER

Copolymer Adsorption

Macromolecular Chemistry and Physics
www.mcp-journal.de

Molecular Dynamics Simulation of Ethylene/Hexene Copolymer Adsorption onto Graphene: New Insight into Thermal Gradient Interaction Chromatography

Fabrice Brunel, Olivier Boyron, Arnaud Clement, and Christophe Boisson*

Crystallization-based fractionation techniques are powerful methods for the analysis of short-chain branching (SCB) in linear low-density polyethylene. Recently, thermal gradient interaction chromatography (TGIC) has been developed for SCB determination of semi-crystalline and amorphous polyolefins. In TGIC, the fractionation mechanism relies on the interaction of polyolefin chains with a graphite surface upon temperature change for a given solvent strength. Using molecular dynamics simulations, both the enthalpic and entropic contributions responsible for the separation of short-chain branched polyethylene are estimated. A new thermodynamic framework for understanding the fractionation mechanism of TGIC is proposed. It is confirmed that at high SCB content, the decrease of the adsorption enthalpy is mostly due to the increased steric hindrance of short branches. However, for low chain branching density, strong increase of the persistence length observed during adsorption decreases the conformational entropy of the polymer and thus counter-balances the favorable adsorption enthalpy. This entropic contribution may also explain the narrowing of the peak observed experimentally with low short-chain branching density at high elution temperature.

1. Introduction

Linear low-density polyethylene (LLDPE), is a copolymer of ethylene with α-olefins produced by either Ziegler–Natta[1,2] or metallocene catalysts.[3–7] LLDPE has gained importance in the packaging industry due to its outstanding mechanical properties; namely a higher tensile strength and a higher impact and puncture resistance than low-density polyethylene.[8–11] These properties are a result of the short-chain branched molecular structure and its distribution.[12] Hence, the characterization of LLDPE with respect to molar masses and short chain branches by new and improved analytical techniques is of great interest.[13] A well-established method is the analytical temperature rising elution fractionation technique (TREF) that fractionates semicrystalline polymer according to crystallizability. It has been widely used for the characterization of LLDPE with respect to short-chain branching.[14–19] The fractionation procedure of TREF involves a slow crystallization step of the polymer loaded into a column and a subsequent elution step during which the temperature is raised causing elution of the polymer as a function of its branching structure. A faster method is the crystallization analysis fractionation (CRYSTAF) where the distribution of short-chain branching is investigated only during the crystallization procedure which is performed similarly to TREF. In CRYSTAF, the analysis is carried out in stirred crystallization vessels with no support, by monitoring the polymer solution concentration, through the crystallization process, while decreasing temperature.[20–23] More recently, crystallization elution fractionation (CEF) has been developed by combining the separation power obtained in the crystallization cycle (equivalent to CRYSTAF), with that obtained in the elution melting cycle (equivalent to TREF). CEF can achieve rapid and extended separations.[24–26] All these techniques are based on the ability of polyolefin chains to crystallize in a dilute solution upon temperature change. LLDPEs with elevated comonomer content are unable to crystallize in the presence of a good solvent, like 1,2,4-trichlorobenzene or orthodichlorobenzene. Co-crystallization further complicates the separation of multiple-component systems with poor precision and accuracy.[27] Therefore, thermal gradient interaction chromatography (TGIC) has been adapted in order to determine the chemical composition of polyolefins.[28] TGIC separates the polymer molecules according to their adsorption on a graphite column upon a temperature change.[29]

The HT-TGIC analysis consists of the following steps: 1) the polymer solution is loaded into a heated graphitized carbon column; 2) then the polymer chains are retained within the column by reducing column temperature (cooling step); 3) finally, the polymer is eluted by raising the column temperature (elution step). During the cooling step, polymer chains with lower α-olefin fractions (longer ethylene segments) adsorb at the highest temperatures. Inversely, during the heating step polymer chains with higher α-olefin fractions (shorter ethylene

Dr. F. Brunel, O. Boyron, A. Clement, Dr. C. Boisson
Chemistry, Catalysis
Polymers and Processes (C2P2)
UMR 5265, CNRS, CPE Lyon, Université Lyon 1, 43 Bvd. du 11 Novembre 1918, F-69615, Villeurbanne, France
E-mail: fabrice.brunel@univ-lyon1.fr

The ORCID identification number(s) for the author(s) of this article can be found under https://doi.org/10.1002/macp.201800496.

DOI: 10.1002/macp.201800496

 © 2019 WILEY-VCH Verlag GmbH & Co. KGaA, Weinheim

ADVANCED SCIENCE NEWS
www.advancedsciencenews.com

Macromolecular Chemistry and Physics
www.mcp-journal.de

segments) are eluted at lower temperature. Note that the polymer can crystallize during the cooling process at a temperature above the adsorption temperature, in the case of polypropylene, for example. During the heating step, the polymer will elute at the TREF dissolution temperature, which must be higher than the desorption temperature of such a branched molecule.[30] The elution profile is measured by concentration detectors at the outlet of the column. A calibration curve relating elution temperature to average α-olefin content calculates the chemical composition of the ethylene/α-olefin copolymer. Cong et al. have shown that TGIC calibration curves (i.e., elution peak temperatures as a function of α-olefin mole fractions) are linear.[28] However, the lower slopes of TGIC calibration curves compared to crystallization-based techniques evidence the poorer resolution of this technique. The TGIC's main advantage over the crystallization-based technique is its ability to separate ethylene/α-olefin copolymers over a wider compositional range. The separation is also faster and free of co-crystallization effects which hampers TREF, CRYSTAF, and CEF.[31]

Monrabal and co-workers showed that any packing material having atomically flat surface provided the same separation as graphitic column. They suggested that the adsorption strength depends on the available surface area of the molecule (i.e., the length of the ethylene segments) in contact with the flat support surface.[32,33] The adsorption is based on weak van der Waals forces interaction between nonpolar polyolefin and an atomic level flat surface. Increasing the α-olefin fractions (i.e., shortening the ethylene segments) hinders this interaction thus lowering the desorption temperature.[32] They have also reported that the elution temperature is independent of the polymer molar mass above a 25 000 g mol^{-1} threshold.[24] Soares and co-workers have studied the impact of the column type (particle sizes and column length) as well as various elution parameters (solvent type, sample injection volume, the heating/cooling rate, and the elution flow rate...). They have shown that o-dichlorobenzene slightly increases resolution compared to 1,2,4-trichlorobenzene and that smaller injection volumes can reduce co-adsorption/co-desorption effects. The cooling rate had no significant effect on the shape and position of TGIC peaks whereas the heating rate and the elution flow rate strongly impact the TGIC profiles. Increasing heating rate leads to higher elution temperature (the temperature of the column will rise faster between the moment the polymer is desorbed and the moment it reaches the detector). Decreasing the elution rate results in higher elution temperature and broaden the TGIC profile probably due to an increased residence time in the column.[34–36]

One of the key features of the TGIC profile is the broadening of the peaks at high α-olefins content. A similar feature was observed with TREF and it was attributed to the Stockmayer bivariate distribution of the copolymer chemical composition.[37] However, in the case of TGIC, experimental peaks are broader than the ones predicted by Stockmayer's distribution. The authors suggest that the difference could be the result of axial dispersion which is the main contributor to peak broadening in conventional chromatographic techniques.[36] This enhanced peak broadening of TGIC profile compared to Stockmayer's distribution was recently confirmed by Arndt et al.[38] In this work, we suggest a complementary explanation for this peak broadening. TGIC experiments were conducted for a series of ethylene/hexene copolymers (synthesized with metallocene catalysts) and compared to a series of simulations (using the GROMACS package). Our results point out an entropic contribution similar to a size exclusion effect as previously suspected.[36] This work could help to better understand separation mechanisms that occur during TGIC analysis and enhance its resolution which could further widen the applications of this interesting fractionation technique.

2. Experimental Section

2.1. Polymerization Procedures

Syntheses were realized under dry argon, using a glove box and Schlenk techniques. The comonomer, 1-hexene, was distilled over CaH_2 before use. The solvents, toluene and n-heptane, were dried on 3 Å molecular sieves. Methylaluminoxane (MAO) 10% wt. in toluene was purchased from Aldrich. Ethylene (99.5%) from Air Liquide was purified by passing on three successive columns containing respectively molecular sieves, alumina, and a copper catalyst. The metallocene complex rac-Et(Ind)$_2$ZrCl$_2$ was purchased from Sigma-Aldrich.

The polymerizations were carried out in a 500 mL glass reactor equipped with a stainless steel paddle stirrer and an external water jacket for temperature control. The required amounts of comonomer were added to a flask containing 0.3 mL of MAO in 300 mL of heptane. The mixture was transported to the reactor under a stream of argon. Before introducing ethylene, argon was pumped out of the reactor. Temperature and pressure were then gradually increased up to 80 °C and 3.8 bar. 100 µL of a rac-Et(Ind)$_2$ZrCl$_2$ solution (1.5 mM in toluene) was then introduced into the reactor under 4 bar of ethylene to initiate the polymerization. A constant pressure of 4 bars was kept during all the polymerization. After 30 min of reaction, the polymerization was stopped. The product of the reaction was then transferred into methanol to precipitate the polymer. The polymer was recuperated by filtration, washed with methanol and finally dried under vacuum.

2.2. Nuclear Magnetic Resonance

Comonomer contents of copolymers were determined by Nuclear Magnetic Resonance (NMR) using a Bruker Avance III 400 spectrometer operating at 400 MHz for ^{1}H NMR and 100.6 MHz for ^{13}C NMR. ^{1}H NMR spectra were obtained with a 5 mm QNP probe at 373 K and the ^{13}C NMR spectra were obtained with a 10 mm PA-SEX probe at 373 K. A 3:1 volume mixture of 1,2,4-trichlorobenzene and toluene-d8 was used as solvent. Chemical shifts were measured in ppm using the resonance of toluene (CHD_2 at 2.185 ppm) or polyethylene ("PE" at 30.06 ppm) as internal references for ^{1}H-NMR and for ^{13}C-NMR respecively. ^{1}H NMR spectrum was used to measured the comonomer content. Since high molar mass copolymers (>20 kg mol^{-1}) were prepared, methyl chain ends were

© 2019 WILEY-VCH Verlag GmbH & Co. KGaA, Weinheim

ADVANCED SCIENCE NEWS
www.advancedsciencenews.com

Macromolecular Chemistry and Physics
www.mcp-journal.de

neglected. However, at low content of comonomer (<1 mol%), the resolution of ^{1}H NMR appears not proper. In this case, the ^{13}C NMR spectra were used for the determination of α-olefin content. The assignment of signals and the calculation of olefin content were based on the article of Galland et al.[39]

2.3. High Temperature Size Exclusion Chromatography

High temperature size exclusion chromatography (HT-SEC) analyses were performed using a Viscotek system (from Malvern Instruments) equipped with three columns (PLgel Olexis 300 mm × 7 mm I.D. from Agilent Technologies). 200 µL of sample solutions with concentration of 5 mg mL^{-1} were eluted in 1,2,4-trichlorobenzene using a flow rate of 1 mL min^{-1} at 150 °C. The mobile phase was stabilized with 2,6-di(tert-butyl)-4-methylphenol (200 mg L^{-1}) to avoid polymer degradation. Online detection was performed with a differential refractive index detector and a dual light scattering detector (LALS and RALS) for absolute molar mass measurement. The OmniSEC software was used for the calculations.

2.4. TGIC

TGIC experiments were performed using a CEF instrument from PolymerChar (Valencia, Spain). The instrument was equipped with a Hypercarb column from Thermo Scientific to be used as TGIC instrument. The samples were dissolved in 10 mL vials for 1 h at 150 °C with 1,2,4 trichlorobenzene (TCB) containing 300 ppm of BHT and purge with nitrogen. 200 µL of sample solution at a concentration of 1 mg mL^{-1} were injected into the column at 150 °C. A cooling ramp of 20 °C min^{-1} down to 40 °C was applied to promote polymer adsorption. Elution begins isothermally at 40 °C for 5 min at a flow rate of 0.5 mL min^{-1} followed by a heating ramp at 2 °C min^{-1} to desorb the polymer. An infrared detector was used to monitor the components' concentration and composition when the chain was eluted from the column.

2.5. Molecular Dynamics Simulations

Molecular Dynamics (MD) simulations were carried out using the GROMACS package, version 5.1.4.[40–43] Force field from the OPLS-AA parameter set were applied to all species in the simulated system.[44] Short-range non-bonded interactions were cut off at 1.4 nm, with long-range electrostatics calculated using the particle mesh Ewald (PME) algorithm.[45] Dispersion correction was applied to energy and pressure terms to account for truncation of Van der Waals terms.[46] Periodic boundary conditions were applied in all directions.

2.6. Umbrella Sampling

MD simulations were carried out for three polymer systems having a degree of polymerization (DP) of 350 with an hexene content of 0, 3.7, and 13 mol%. The molar mass of these copolymers ($M_n \approx 10000$ g mol^{-1}) corresponds to the lower limit for TGIC separation (see Figure S1 and Table S1, Supporting Information). The hexene monomers were introduced randomly and the effects of the comonomer distribution are not studied here. First, a fully extended PE chain (linear and branched) was collapsed into a globule in vacuum. This globular PE chain was then placed in a cubic box of 1,2,4-trichlorobenzene. Following steepest descents minimization, each of the PE systems was equilibrated in two steps. The first simulation phase was conducted under a constant volume (NVT) ensemble for 50 ps. Temperature was maintained at 310 K using the Berendsen weak coupling method. Following NVT equilibration, 50 ps of constant-pressure (NPT) equilibration was then performed, also using weak coupling to maintain pressure isotropically at 1.0 bar. Production MD simulations were conducted for 20 ns with position restraints applied to the carbon atoms of the graphene sheet. For this data collection period, the Nose–Hoover thermostat was used to maintain temperature, and the Parrinello–Rahman barostat was used to isotropically regulate pressure. During all steps, position restraints were applied to all graphene atoms. Structures from the end of each of these trajectories were used as starting configurations for pulling simulations. The polymer structures were placed in the center of a cubic box with a graphene sheet placed at $z = 0$ and 1,2,4-trichlorobenze was used as a solvent. Equilibration was performed for 100 ps under an NPT ensemble, using the

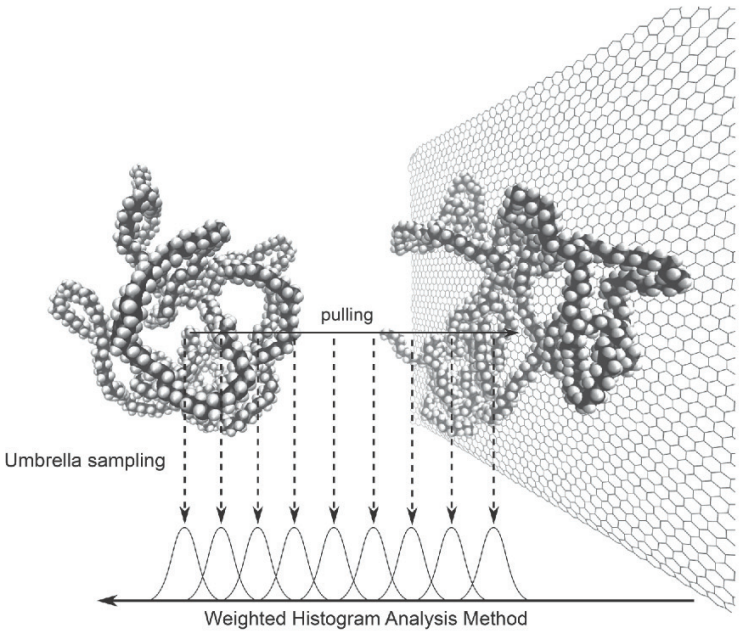


Figure 1. Illustration of the umbrella sampling simulation/weighted histogram analysis method.

© 2019 WILEY-VCH Verlag GmbH & Co. KGaA, Weinheim

ADVANCED SCIENCE NEWS
www.advancedsciencenews.com

Macromolecular Chemistry and Physics
www.mcp-journal.de

same methodology described above. The PE chain was pulled forward to the graphene sheet along the *z*-axis over 500 ps, using a spring constant of 1000 kJ mol^{-1} nm^{-2} and a pull rate of 0.01 nm ps^{-1}. From these trajectories, snapshots were taken to generate the starting configurations for the umbrella sampling (cf. **Figure 1**). A distribution of sampling windows was used with regular spacing of the umbrella sampling windows of 0.2 nm. In each window, 5 ns of MD was performed for a total simulation time of about 60 ns utilized for umbrella sampling. An analysis of the results was performed with the weighted histogram analysis method (WHAM) implemented in the gromacs package.[47] The persistence length was calculated from the gromacs tools *gmx polystat*. The persistence length is defined as number of bonds where the average cosine of the angles between carbon bonds of the polymer backbone reaches a value of 1/e, the odd pairs are not used, because straight polymer backbones are usually all trans and therefore only every second bond aligns. The number of contact points was determined by measuring the distance between the center of mass of ethylene monomers and the carbon atoms of the graphene sheet. An ethylene monomer is considered to be in contact with the graphene sheet when the distance between the ethylene center of mass and any graphene atom is inferior to the cut-off distance of the Van der Waals interaction.

3. Results and Discussion

3.1. TGIC

Eight different ethylene-hexene copolymers, in a range from 0.11 to 20.7 mol% of hexene, plus one ethylene homopolymer, were prepared with a zirconium metallocene catalyst to obtain copolymers with homogeneous chemical composition distribution. All LLDPE samples were characterized by HT-SEC. The molar mass distributions were narrow as expected for a metallocene catalyst. The molar mass reported in **Table 1** were higher than 20 kg mol^{-1} and then are high enough to avoid an effect on the TGIC elution temperature.[48] The hexene content was determined by ^{1}H NMR for high content of hexene and by ^{13}C NMR for low content as reported in Table 1. The TGIC profiles of LLDPE are given, in **Figure 2**. A nearly symmetric peak confirms that all polymers were unimodal in composition. As observed by Soares, Cong, and Monrabal copolymers elute in the order of decreasing hexene content.[26,28,32] The elution temperature of the nine copolymers were plotted against hexene mol% (see the inset in Figure 2). A linear calibration curve was obtained in good agreement with the scientific literature cited above. Based upon this linear regression, the elution temperature was calculated and reported in Table 1.

Table 1. Characterization data for ethylene hexene copolymer.

Runs	Hexene content[a] [mol%]	M_n (Đ)[b] [kg mol^{-1}]	Elution peak[c] [°C]	Elution peak[c] [K]
1	0	53.6 (2.8)	137.5	410.7
2	0.1*	46.4 (2.9)	136.9	410.1
3	0.4*	49.8 (2.7)	135.7	408.9
4	2.5	39.7 (1.9)	126.7	399.9
5	5.3	29.5 (1.8)	112.7	385.9
6	7.6	27.3 (1.9)	103.5	376.7
7	9.0	25.8 (1.8)	97.6	370.8
8	13.6	24.8 (1.9)	80.9	354.1
9	20.7	20.9 (2.0)	57.5	330.7

[a]Hexene content determined by ^{1}H NMR and ^{13}C NMR*; [b]Number average molar mass and dispersity determined by HT-SEC using light scattering detector; [c]Elution peak temperature obtained by TGIC.

3.2. Free Energy Profiles

Figure 3 shows the free energy profile between ethylene/hexene copolymers and a graphene sheet, obtained from umbrella sampling simulation using the weighted histogram analysis method at three temperatures (350, 375, and 400 K)

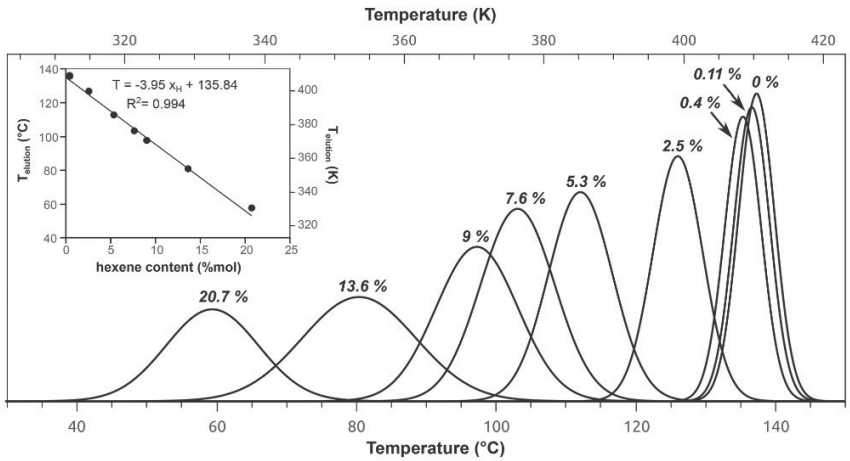


Figure 2. TGIC profiles of a series of ethylene/1-hexene copolymers ranging from 0 to 20.7 mol% of hexene and the corresponding calibration curve.

© 2019 WILEY-VCH Verlag GmbH & Co. KGaA, Weinheim

ADVANCED SCIENCE NEWS
www.advancedsciencenews.com

Macromolecular Chemistry and Physics
www.mcp-journal.de

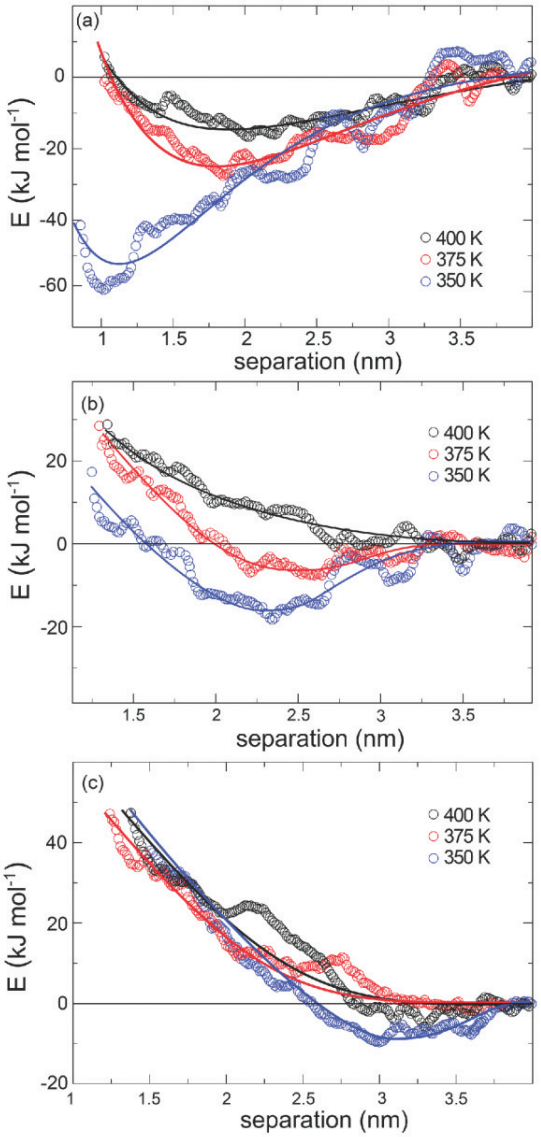


Figure 3. a–c) Potential of mean force (E) curves for ethylene/hexene copolymers at various temperatures (350, 375, and 400 K for black, red, and blue dots, respectively). Hexene content = 0, 3.7, and 13 mol% for (a), (b), and (c) respectively.

for a hexene content of 0, 3.7, and 13 mol%, respectively. With 3.7 and 13 mol% hexene, the energy profile (see Figure 3b,c) clearly shows the transition of the PE–graphene interaction from attractive ($\Delta E < 0$) to repulsive ($\Delta E > 0$). This transition happens in the 350–375 K range for 13 mol% hexene and in the 375–400 K range for 3.7 mol% hexene. This evolution of the adsorption free energy as a function of the temperature can be well compared with the elution temperature determined from the TGIC linear calibration curve: 394 and 358 K for 3.7 and 13 mol% hexene, respectively (cf. Figure 2 and Table 2).

Table 2. Adsorption energies and elution temperature of PE having various hexene content.

Hexene content [mol%]	ΔH_{ads} [kJ mol^{-1}]	ΔS_{mix} [kJ mol^{-1}]	T[a)] [K]	T[b)] [K]
0	−180	0.4	450	409
3.7	−160	0.4	400	394
13	−150	0.4	375	358

[a)]Elution temperature determined from the zero-crossing point of the $\Delta E = f(T)$ curves in Figure 7; [b)]TGIC elution peak temperature determined for the linear regression of Figure 2.

At a low temperature, this attractive interaction causes the polymer to adsorb onto the surface; then, with increasing temperature, the transition to a repulsive interaction leads to the desorption of the polymer into the solvent. Finally, surprisingly strong adsorption free energy is observed with the 0 mol% hexene polymer at 350 K; see Figure 3a. At this temperature, a very deep energy well is observed and appears to be shifted very close to the graphene surface (≈1 nm). This is caused by the crystallization of PE chain onto the graphene surface which can act as a nuclei leading to a rapid crystallization rate characteristic of an heterogeneous crystallization kinetic.[49,50] Careful observation of this simulation snapshot shows strongly folded PE chains onto the graphene surface (see **Figure 4**). Furthermore, these folded segments lead to multilayer adsorption of PE chains, forming a protocrystalline phase. Therefore, the strong free energy observed with linear PE at low temperature is very likely due to the crystallization of the polymer onto the graphene surface. At a higher temperature, the adsorption free energy decreases but, in this case, remains relatively high (i.e., favorable to the adsorption) even at the highest temperature. This result is discussed in the next section.

3.3. Thermodynamic Model

The adsorption free energy, ΔE, can be estimated as the depth of the energy well and are reported in Table 2. For all copolymers, the adsorption free energy increases linearly with increasing temperature. Excluding the ΔE value from the 0 mol% polymer at 350 K due to the presence of a peculiar crystallization event, all curves exhibit a very similar slope. Our goal here is not to obtain a precise value of the adsorption energies but merely to build a qualitative model of thermodynamic processes involved in the TGIC fractionation. From the look of the $\Delta E = f(T)$ curves in Figure 7, one can suggest a thermodynamic explanation of the evolution of the adsorption free energy as a function of the temperature. We theorize that this adsorption free energy is the result of a competition between an enthalpy term favourable to the adsorption (ΔH_{ads}) and the entropy of mixing of the polymer between the bulk and the surface (ΔS_{mix}).

$$\Delta E = \Delta H_{ads} - T\Delta S_{mix} \quad (1)$$

From this equation, adsorption enthalpy (ΔH_{ads}), mixing entropy (ΔS_{mix}) were estimated and are reported in Table 2. The obtained values of adsorption enthalpy and mixing entropy are

© 2019 WILEY-VCH Verlag GmbH & Co. KGaA, Weinheim

ADVANCED SCIENCE NEWS
www.advancedsciencenews.com

Macromolecular Chemistry and Physics
www.mcp-journal.de

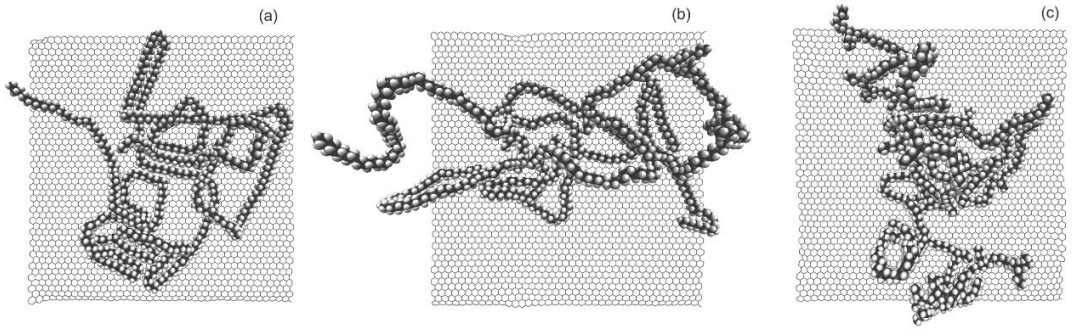


Figure 4. a–c) Snapshots of the adsorbed ethylene/hexene copolymer onto the graphene surface (separation = 1 nm) at 350 K. Hexene content = 0, 3.7, and 13 mol% for (a), (b), and (c) respectively.

in the same order of magnitude when compared to the literature. Using sum-frequency vibrational spectroscopy, Su et al. found an adsorption free energy of about 42 kJ mol^{-1} for a short alkane chain having only 60 ethylene units.[51] Inwong et al. proposed a theoretical model based on population balances in non-equilibrium, multi-stage adsorption/desorption process which gives values of the enthalpy of adsorption between 50 and 100 kJ mol^{-1} and an entropic term of about 0.4 kJ mol^{-1}.[52] We found higher enthalpy values but very similar entropic terms. From our thermodynamic model, the theoretical elution temperature (i.e., desorption of the polymer for $\Delta E \approx 0$) were also estimated (cf. Table 2). The copolymer having 3.7 mol% hexene shows good agreement between theoretical and experimental elution temperature. However, for high hexene content (13 mol%), the theoretical elution temperature was found to be slightly superior ($\Delta T \approx 15$ K) to the TGIC elution peak temperature. One should note that, with this copolymer, the estimation of the elution temperature must be taken with caution since only one value of the adsorption free energy could be determined at 350 K, at a higher temperature, the energy profile becomes purely repulsive. Finally, the ethylene homopolymer (0 mol% hexene) reveals important discrepancy between elution temperature determined from either TGIC or MD ($\Delta T \approx 40$ K) which is discussed in the next section.

3.4. Adsorption Enthalpy and Steric Effect

Our thermodynamic model suggest a constant entropic term but a strong variation of the adsorption enthalpy with the hexene content. In other words, the TGIC fractionation appears to be an enthalpy-driven phenomenon as suggested by Monrabal et al.[32] The authors suggested that the adsorption strength of ethylene/α-olefin copolymers on graphite was proportional to the available contact surface area of the polymer chain. A sample with no or few α-olefin interacts strongly with the support because it has longer ethylene sequences and a larger contact surface area. Such a sample will desorb from the surface at higher temperatures than a sample having many α-olefin and shorter ethylene sequences. Therefore, we measured the number of contacts between ethylene/hexene copolymer and the graphene surface for all umbrella simulations (cf. **Figure 5**). The values displayed in Figure 5 are the average of three umbrella simulations carried out at different temperatures with the corresponding standard deviation. Judging by the low error bars, the number of contact points appears to be independent of the temperature. However, a clear decrease of the number of contacts between ethylene/hexene copolymer and the graphene surface with increasing hexene density is observed. This result confirms that the steric hindrance from hexene residue reduces the number of contacts between ethylene and the graphene and therefore the overall adsorption enthalpy. This enthalpy-driven phenomenon is particularly important at low degree of hexene as suggested by the large drop of ΔE from 0 to 3.7 mol%.

3.5. Entropic Conformation

MD simulation optimizes the potential energy, rather than the free energy of the polymer, meaning that all conformational entropies of the polymer chain are neglected. Therefore, we decided to have a closer look at the conformational entropies of polymers. **Figure 6** shows the persistence length of the

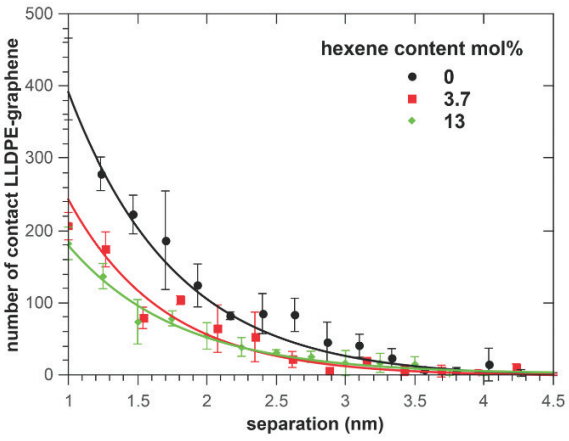


Figure 5. Number of contacts between ethylene/hexene copolymer and the graphene surface as a function of the separation (i.e., the distance between the polymer center of mass and the graphene sheet). Average values and standard deviation are calculated from umbrella sampling simulations at three different temperatures (350, 375, and 400 K).

© 2019 WILEY-VCH Verlag GmbH & Co. KGaA, Weinheim

ADVANCED SCIENCE NEWS
www.advancedsciencenews.com

Macromolecular Chemistry and Physics
www.mcp-journal.de

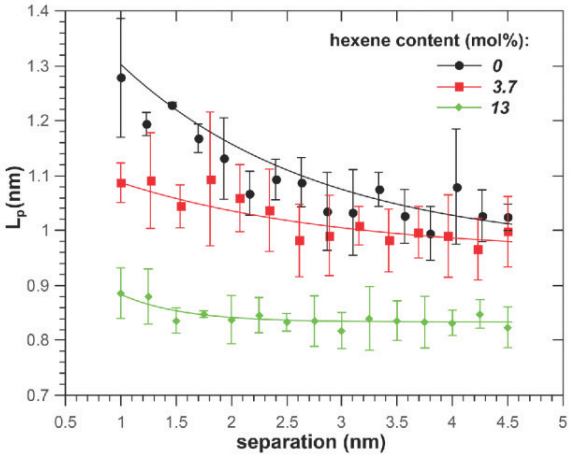


Figure 6. Persistence length (L_p) of ethylene/hexene copolymer having various hexene content as a function of the separation between the center of mass of the copolymer and the graphene sheet. Straight lines are exponential decay fit. Average values and standard deviation are calculated from umbrella sampling simulations at three different temperatures.

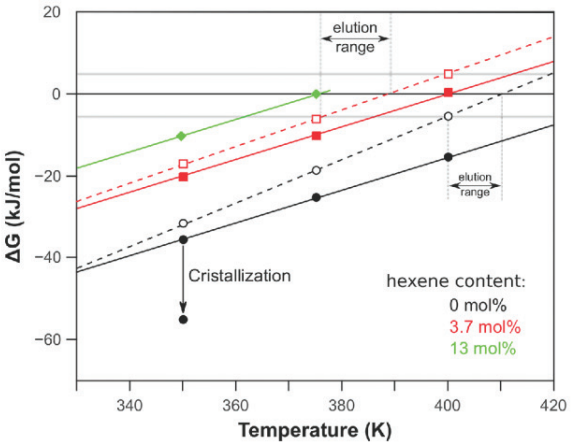


Figure 7. Illustration of the thermodynamic adsorption model. The adsorption free energy (ΔG_{ads}) contained three parts of contributions: adsorption enthalpy (ΔH_{ads}), mixing entropy (ΔS_{mix}) for the full line, and additional conformational entropy (ΔS_{conf}) for the dashed line.

three polymers as a function of the distance between the graphene sheet and the polymer center of mass. The persistence length increases when the polymer is adsorbed, especially with decreasing hexene. The polymer can be considered as an equivalent chain with N segments of length (L_p) which can randomly orient in any direction. Thus, the increased persistence length observed during the adsorption of the 0 mol% hexene polymer led to a decrease of the number segments. Less segments results in a lower number of configuration and thus a decrease of the conformational entropy of polymer due to the adsorption. This effect could counter-balance the adsorption enthalpy and explain why 0 mol% hexene polymer is in fact eluted around 400 K. The overall conformation of the chain was estimated from the numbers of possible arrangement of the chain segment in the 3D space (diamond lattice). In the lattice model, a polymer chain consists of monomers sitting on the grids and bonds connecting them. Here, each bond corresponding to a segment of length L_p. In three dimensions, a cubic lattice is frequently used as well as a diamond lattice to a lesser extent. Thus the total number of the arrangement (Ω) of the chain segments is roughly N^{Z-1}. The lattice coordinate Z refers to the number of nearest neighbours for a lattice point. Where $Z = 4$ for a diamond (tetrahedral) lattice which proved to be a suitable model for polyethylene chains.[53–55] The conformational entropy is estimated from the numbers of possible arrangement:

$$S = k_B \times ln(\Omega) = k \times ln\left(N^{Z-1}\right) \quad (2)$$

where k_B is the Boltzmann constant ($k_B = 1.38 \times 10^{-23}$ J K^{-1}). Here, the gas constant, R, was used to calculate these energies in kJ mol^{-1} ($R = \mathcal{N}_A \times k_B = 8.314$ kJ mol^{-1}). The variation of conformational entropy (ΔS_{conf}) resulting from the polymer adsorption is given by:

$$\Delta S_{conf} = S_{adsorbed} - S_{solution}$$

The calculation yields conformational entropies of around −30 and −40 J mol^{-1} for 3.7 and 0 mol% of hexene respectively. Introducing this new entropic term in the calculation of the total free energy (ΔG_{ads}) (dashed curves on **Figure 7**) gives a free energy close to zero at 400 K for homopolyethylene. The conformational entropy can thus explain the discrepancy observed above. Furthermore, the decrease of entropy of the low hexene content polymer during adsorption could also explain the narrowing of the peak observed experimentally for such polymer. At high hexene content, the decrease of the adsorption enthalpy is mostly due to the increased steric hindrance which shifts the $\Delta G_{ads} = f(T)$ curves vertically (straight line in Figure 7). On the other hand, this additional conformational entropy modified the slope of the $\Delta G_{ads} = f(T)$ curve (dashed line on Figure 7) for polymers having a low short chain branching density. From these curves, one can estimate the elution range of a given polymer: the difference between the temperature where the polymer start to elute ($\Delta G_{ads} \lesssim 0$; i.e., the beginning of the elution peak) and the temperature where the PE is rapidly released ($\Delta G_{ads} \gtrsim 0$; i.e., the maximum of the elution peak). Increasing the slope of the $\Delta G_{ads} = f(T)$ would logically reduce this temperature range and therefore lead to a narrowing of the elution peaks.

4. Conclusion

Using umbrella sampling and WHAM algorithm we calculated the adsorption free energy of various LLDPE samples onto graphene at different temperatures. The values of the adsorption free energies confirmed that the steric hindrance from hexene residues reduces the number of contacts between ethylene and graphene and therefore the overall adsorption enthalpy. With low chain branching density measured adsorption free energy remains negative (favorable to adsorption) above the polymer elution temperature. However, for this polymer, a strong increase of the persistence length is observed during

© 2019 WILEY-VCH Verlag GmbH & Co. KGaA, Weinheim

ADVANCED SCIENCE NEWS
www.advancedsciencenews.com

Macromolecular Chemistry and Physics
www.mcp-journal.de

adsorption. The increase in persistence length would decrease the conformational entropy of the polymer and thus counterbalance the favorable adsorption free energy. This entropic contribution could contribute to the peak narrowing observed experimentally with a low short-chain branching density at a high elution temperature. This model accurately reproduced the elution temperature measured by HT-TGIC with ethylene/hexene comonomers. Furthermore, it could also qualitatively explain the shape of the HT-TGIC profile. Finally, we can reasonably assume that this entropic mechanism will depend on the molar mass of the copolymer and thus induce a size-exclusion separation in the graphite column. Such size-exclusion effects could induce a broadening of all peaks due to the molar mass distribution of the polymer which could explain the discrepancy observed between the experimental TGIC profile and the Stockmayer's distribution. However, further work is needed to better understand the interplay between the entropic effect and comonomer distribution.

Umbrella sampling method and the WHAM algorithm are commonly used to obtain energy landscape for ligand-protein binding energy[56–60] and to generate free energy profiles for the conformational transition of protein molecules.[61–64] Current findings suggest that it can also be used for studying polymer adsorption. In the case of LLDPE adsorption onto graphene, this method has proven very useful and led to the discovery of a new mechanism approach for the TGIC separation. This could be of great importance toward developing advanced analytical tools for the characterization of complex polymer architecture and understanding some fundamental aspects of polymer adsorption.

Supporting Information

Supporting Information is available from the Wiley Online Library or from the author.

Acknowledgements

The authors thank Mr. Claude Bonura and Mr. Nicolas Fuller from the Centre Commun Informatique et Réseau CCIR (ICBMS - UMR 5246) for providing computational resources and technical support.

Conflict of Interest

The authors declare no conflict of interest.

Keywords

adsorption, molecular dynamics, polyethylene

Received: November 14, 2018
Published online:

[1] K. Ziegler, E. Holzkamp, H. Breil, H. Martin, *Angew. Chem., Int. Ed.* **1955**, *67*, 541.
[2] G. Natta, I. Pasquon, *Adv. Catal.* **1959**, *11*, 1.
[3] J. R. Severn, J. C. Chadwick, *Tailor-Made Polymers: Via Immobilization of Alpha-Olefin Polymerization Catalysts*, John Wiley & Sons, New York **2008**.
[4] P. S. Chum, K. W. Swogger, *Prog. Polym. Sci.* **2008**, *33*, 797.
[5] R. Mülhaupt, *Macromol. Chem. Phys.* **2003**, *204*, 289.
[6] M. C. Baier, M. A. Zuideveld, S. Mecking, *Angew. Chem., Int. Ed.* **2014**, *53*, 9722.
[7] D. W. Sauter, M. Taoufik, C. Boisson, *Polymers* **2017**, *9*, 185.
[8] R. K. Krishnaswamy, M. J. Lamborn, *Polym. Eng. Sci.* **2000**, *40*, 2385.
[9] A. O. Ogah, J. N. Afiukwa, *Int. J. Eng. Manage. Sci.* **2012**, *3*, 85.
[10] M. Chanda, S. K. Roy, *Plastics Technology Handbook*, Vol. 72, CRC Press, Boca Raton, FL **2006**.
[11] K. W. Doak, *Encyclopedia of Polymer Science and Engineering*, Vol. 6, WileyInterscience, New York **1985**.
[12] A. Todo, N. Kashiwa, *Macromol. Symp.* **1996**, *101*, 301.
[13] A. Roy, M. D. Miller, D. M. Meunier, A. W. Degroot, W. L. Winniford, F. A. Van Damme, R. J. Pell, J. W. Lyons, *Macromolecules* **2010**, *43*, 3710.
[14] T. Usami, Y. Gotoh, S. Takayama, *Macromolecules* **1986**, *19*, 2722.
[15] L. Wild, G. Glöckner, *Separation Techniques Thermodynamics Liquid Crystal Polymers*, Springer, Berlin, **1991**, pp. 1–47.
[16] L. Wild, *Adv. Polym. Sci.* **1991**, *98*, 1.
[17] S. Anantawaraskul, J. Soares, P. Wood-Adams, *Polymer Analysis Polymer Theory*, Springer, Berlin **2005**, pp. 686–686.
[18] J. B. P. Soares, A. E. Hamielec, *Polymer* **1995**, *36*, 1639.
[19] E. Cossoul, L. Baverel, E. Martigny, T. Macko, C. Boisson, O. Boyron, *Macromol. Symp.* **2013**, *330*, 42.
[20] B. Monrabal, *J. Appl. Polym. Sci.* **1994**, *52*, 491.
[21] B. Monrabal, *Macromol. Symp.* **1996**, *110*, 81.
[22] D. M. Sarzotti, J. B. P. Soares, A. Penlidis, *J. Polym. Sci., Part B: Polym. Phys.* **2002**, *40*, 2595.
[23] J. B. P. Soares, S. Anantawaraskul, *J. Polym. Sci., Part B: Polym. Phys.* **2005**, *43*, 1557.
[24] B. Monrabal, J. Sancho-Tello, N. Mayo, L. Romero, *Macromol. Symp.* **2007**, *257*, 71.
[25] B. Monrabal, L. Romero, N. Mayo, J. Sancho-Tello, *Macromol. Symp.* **2009**, *282*, 14.
[26] A. A. Alghyamah, J. B. P. Soares, *Macromol. Symp.* **2012**, *312*, 43.
[27] S. Anantawaraskul, J. B. P. Soares, P. Jirachaithorn, *Macromol. Symp.* **2007**, *257*, 94.
[28] R. Cong, W. Degroot, A. Parrott, W. Yau, L. Hazlitt, R. Brown, M. Miller, Z. Zhou, *Macromolecules* **2011**, *44*, 3062.
[29] T. Macko, H. Pasch, *Macromolecules* **2009**, *42*, 6063.
[30] B. Monrabal, L. Romero, *Macromol. Chem. Phys.* **2014**, *215*, 1818.
[31] B. Monrabal, N. Mayo, R. Cong, *Macromol. Symp.* **2012**, *312*, 115.
[32] B. Monrabal, E. López, L. Romero, *Macromol. Symp.* **2013**, *330*, 9.
[33] B. Monrabal, *Macromol. Symp.* **2015**, *356*, 147.
[34] A. Z. Al-Khazaal, J. B. P. Soares, *Macromol. Chem. Phys.* **2014**, *215*, 465.
[35] A. Alghyamah, J. B. P. Soares, *Macromol. Chem. Phys.* **2015**, *216*, 38.
[36] A. Z. Al-Khazaal, J. B. P. Soares, *Macromol. Chem. Phys.* **2017**, 218.
[37] J. B. P. Soares, A. E. Hamielec, *Macromol. Theory Simul.* **1995**, *4*, 305.
[38] J.-H. Arndt, R. Brüll, T. Macko, P. Garg, J. C. J. F. Tacx, *Polymer* **2018**, *156*, 214.
[39] G. B. Galland, R. F. de Souza, R. S. Mauler, F. F. Nunes, *Macromolecules* **1999**, *32*, 1620.
[40] H. J. C. Berendsen, D. van der Spoel, R. van Drunen, *Comput. Phys. Commun.* **1995**, *91*, 43.
[41] B. Hess, C. Kutzner, D. Van Der Spoel, E. Lindahl, *J. Chem. Theory Comput.* **2008**, *4*, 435.
[42] S. Pronk, S. Páll, R. Schulz, P. Larsson, P. Bjelkmar, R. Apostolov, M. R. Shirts, J. C. Smith, P. M. Kasson, D. van der Spoel, B. Hess, E. Lindahl, *Bioinformatics* **2013**, *29*, 845.

 © 2019 WILEY-VCH Verlag GmbH & Co. KGaA, Weinheim

ADVANCED SCIENCE NEWS
www.advancedsciencenews.com

Macromolecular Chemistry and Physics
www.mcp-journal.de

[43] S. Pall, M. J. Abraham, C. Kutzner, B. Hess, E. Lindahl, *Tackling Exascale Software Challenges in Molecular Dynamics Simulations with GROMACS*, Springer, Berlin **2014**.
[44] W. L. Jorgensen, J. Tirado-Rives, *J. Am. Chem. Soc.* **1988**, *110*, 1657.
[45] T. Darden, D. York, L. Pedersen, *J. Chem. Phys.* **1993**, *98*, 10089.
[46] U. Essmann, L. Perera, M. L. Berkowitz, T. Darden, H. Lee, L. G. Pedersen, *J. Chem. Phys.* **1995**, *103*, 8577.
[47] J. S. Hub, B. L. De Groot, D. Van Der Spoel, *J. Chem. Theory Comput.* **2010**, *6*, 3713.
[48] J. Nieto, T. Oswald, F. Blanco, J. B. P. Soares, B. Monrabal, *J. Polym. Sci., Part B: Polym. Phys.* **2001**, *39*, 1616.
[49] A. Tracz, I. Kucińska, J. K. Jeszka, *Macromolecules* **2003**, *36*, 10130.
[50] J. Nakamura, M. Tsuji, A. Nakayama, A. Kawaguchi, *Macromolecules* **2008**, *41*, 1358.
[51] Y. Su, H.-L. Han, Q. Cai, Q. Wu, M. Xie, D. Chen, B. Geng, Y. Zhang, F. Wang, Y. R. Shen, *Nano Lett.* **2015**, *15*, 6501.
[52] N. Inwong, S. Anantawaraskul, J. B. P. Soares, A. Z. Al-Khazaal, *Macromol. Symp.* **2015**, *354*, 361.
[53] I. Teraoka, *Polymer Solutions, An Introduction to Physical Properties*, John Wiley & Sons, New York **2002**.
[54] Z.-H. Duan, L. N. Howard, *J. Comput. Chem.* **1999**, *20*, 348.
[55] Z.-H. Duan, L. N. Howard, *J. Chem. Phys.* **1998**, *108*, 5608.
[56] H.-J. Woo, *Molecular Modeling of Proteins*, Springer, Berlin **2008**, pp. 109–120.
[57] T. Baştuğ, P.-C. Chen, S. M. Patra, S. Kuyucak, *J. Chem. Phys.* **2008**, *128*, 04B614.
[58] K. El Hage, P. Mondal, M. Meuwly, *Mol. Simul.* **2018**, *44*, 1.
[59] M. S. Lee, M. A. Olson, *Biophys. J.* **2006**, *90*, 864.
[60] H. Kokubo, T. Tanaka, Y. Okamoto, *J. Chem. Theory Comput.* **2013**, *9*, 4660.
[61] W. Plazinski, A. Knys-Dzieciuch, *J. Mol. Graphics Modell.* **2013**, *45*, 122.
[62] J. Higo, J. Ikebe, N. Kamiya, H. Nakamura, *Biophys. Rev.* **2012**, *4*, 27.
[63] Y. Yonezawa, *J. Comput. Chem.* **2016**, *37*, 1139.
[64] J. Wang, Q. Shao, Z. Xu, Y. Liu, Z. Yang, B. P. Cossins, H. Jiang, K. Chen, J. Shi, W. Zhu, *J. Phys. Chem. B* **2013**, *118*, 134.

 © 2019 WILEY-VCH Verlag GmbH & Co. KGaA, Weinheim

REFERENCES - CHAPTER III

[1] B. Wunderlich, Thermal Analysis, in *Thermal Analysis*, B. Wunderlich, Ed., Academic Press, 1990, p. 417.

[2] V. B. Mathot, "*Calorimetry and thermal analysis of polymers*", Hanser Publishers, 1994.

[3] G. Höhne, W. F. Hemminger, H.-J. Flammersheim, "*Differential scanning calorimetry*", Springer Science & Business Media, 2013.

[4] P. Starck, K. Rajanen, B. Löfgren, *Thermochimica acta* **2002**, *395*, 169.

[5] A. J. Müller, Z. H. Hernández, M. L. Arnal, J. J. Sánchez, *Polymer Bulletin* **1997**, *39*, 465.

[6] K. M. Drummond, J. L. Hopewell, R. A. Shanks, *Journal of Applied Polymer Science* **2000**, *78*, 1009.

[7] C. Schick, *Anal. Bioanal. Chem.* **2009**, *395*, 1589.

[8] M. G. Broadhurst, G. C. G., *The Journal of Chemical Physics* **1962**, *36*, 2578.

[9] P. J. Flory, A. Vrij, *Journal of the American Chemical Society* **1963**, *85*, 3548.

[10] T. Arakawa, B. Wunderlich, *Journal of Polymer Science Part A-2: Polymer Physics* **1966**, *4*, 53.

[11] A. Schaper, *Acta Polymerica* **1989**, *40*, 479.

[12] W. E. Garner, K. Van Bibber, A. M. King, *Journal of the Chemical Society (Resumed)* **1931**, 1533.

[13] J. C. Randall, E. T. Hsieh, *Macromolecules* **1982**, *15*, 1584.

[14] J. C. Randall, *Journal of Macromolecular Science, Part C* **1989**, *29*, 201.

[15] S. Hosoda, *Polymer Journal* **1988**, *20*, 383.

[16] K. H. Illers, *European Polymer Journal* **1974**, *10*, 911.

[17] J. B. P. Soares, A. E. Hamielec, *Polymer* **1995**, *36*, 1639.

[18] S. Anantawaraskul, J. B. P. Soares, P. M. Wood-Adams, *Journal of Polymer Science Part B: Polymer Physics* **2003**, *41*, 1762.

[19] J. B. P. Soares, S. Anantawaraskul, *Journal of Polymer Science, Part B: Polymer Physics* **2005**, *43*, 1557.

[20] I. Sakurada, "Nihon Kagakusenikenkyusho Koensyo", in *Proc. Symp. Jpn. Textile Res. Lab*, 1940, p. 5/33.

[21] H. L. Wagner, *Journal of Physical and Chemical Reference Data* **1985**, *14*, 611.

[22] A. Alghyamah, J. B. P. Soares, *Industrial & Engineering Chemistry Research* **2014**, *53*, 9228.

[23] A. Z. Al-Khazaal, J. B. P. Soares, *Macromolecular Chemistry and Physics* **2014**, *215*, 465.

[24] K. Patel, S. H. Chikkali, S. Sivaram, *Progress in Polymer Science* **2020**, *109*, 101290.

[25] S. Kurtz, "*UHMWPE biomaterials handbook: ultra high molecular weight polyethylene in total joint replacement and medical devices*", Academic Press, 2009.

[26] D. R. Lippits, S. Rastogi, S. Talebi, C. Bailly, *Macromolecules* **2006**, *39*, 8882.

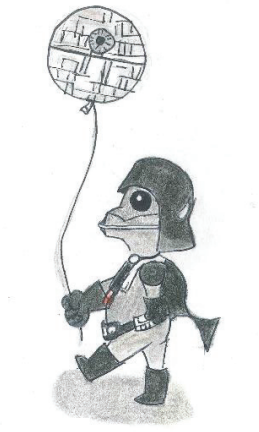
[27] S. Rastogi, D. R. Lippits, G. W. Höhne, B. Mezari, P. C. Magusin, *Journal of Physics: Condensed Matter* **2007**, *19*, 205122.

[28] A. Pandey, Y. Champouret, S. Rastogi, *Macromolecules* **2011**, *44*, 4952.

[29] S. Rastogi, Y. Yao, S. Ronca, J. Bos, J. van der Eem, *Macromolecules* **2011**, *44*, 5558.

CHAPTER IV

CHEMICAL COMPOSITION OF ETHYLENE COPOLYMERS USING SPECTROMETRY



The catalytic synthesis of ethylene copolymers has made it possible to synthesize LLDPE models with narrow distributions in chemical composition and molar mass. These polymer models have enabled us to successfully calibrate the different thermal fractionation techniques from TREF to SGIC.

We have shown that fractionation techniques are unique tools for accessing to chemical composition distribution. These separation techniques can be compared to liquid chromatography. Like the latter, they require dissolution of the samples, which for polyolefins is tricky and implies aggressive solvents and elevated temperatures. In this context of sample preparation, it is necessary to be aware both on the proper dissolution of the polymer and to avoid its degradation. Consequently, preparation and analysis times are time consuming and delicate. It is advantageous to develop also quicker techniques to reach the chemical composition.

Spectroscopy techniques are widely used by research laboratories, they can be powerful tools for measuring chemical composition. In this chapter we are interested in two techniques of spectroscopy the infrared spectroscopy (FTIR) and mass spectrometry.

FTIR has been widely used for many years for the characterization of polyolefins. The development of chemometric techniques now allows a new approach in the exploitation of the spectra obtained. Chemometrics make it possible to obtain information on polymers by observing several wavelengths connect to the information requested. We have shown that it can be applied effectively both to medium infrared and near infrared on LLDPE (first part of the chapter) but also on other types of copolymer such as ethylene-butadiene which has complex structures (second part of the chapter).

Regarding mass spectrometry, which are difficult to use in the context of polymers, we have explored the interest of a coupling with thermogravimetric instrument. This led to obtain significant fragments of the degraded copolymers that were identified by mass spectrometry.

Each of the three sections of this chapter has been published in the journal Macromolecular Chemistry and Physics. Each section has its own references. Reproduction of publications has been requested from the editor and accepted to be included in the thesis.

Dear Mr. Olivier Boyron,

Thank you for placing your order through Copyright Clearance Center's RightsLink® service.

Order Summary

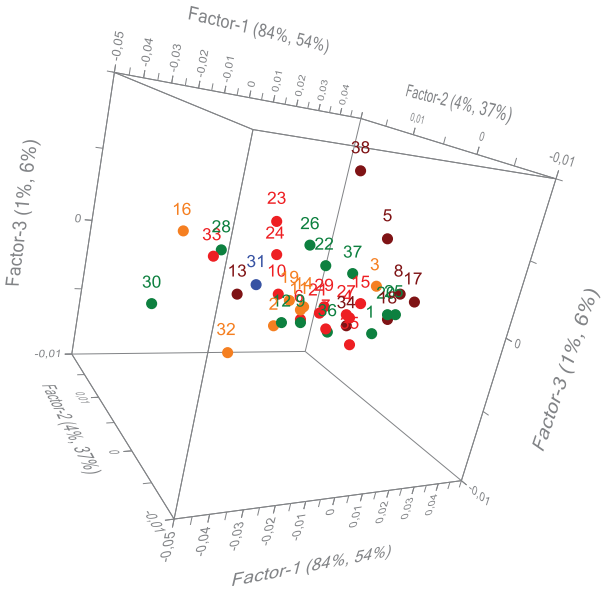
Licensee:	CNRS
Order Date:	Jan 15, 2021
Order Number:	4990250114747
Publication:	Macromolecular Chemistry and Physics
Title:	Chemical Composition of Hexene-Based Linear Low-Density Polyethylene by Infrared Spectroscopy and Chemometrics
Type of Use:	Dissertation/Thesis
Order Total:	0.00 USD

Licensee:	CNRS
Order Date:	Jan 15, 2021
Order Number:	4990250971025
Publication:	Macromolecular Chemistry and Physics
Title:	Rapid Determination of the Chemical Composition of Ethylene/Butadiene Copolymers Using FTIR Spectroscopy and Chemometrics
Type of Use:	Dissertation/Thesis
Order Total:	0.00 USD

Licensee:	CNRS
Order Date:	Jan 15, 2021
Order Number:	4990251091577
Publication:	Macromolecular Chemistry and Physics
Title:	An Advanced Technique for Linear Low-Density Polyethylene Composition Determination: TGA–IST16–GC–MS Coupling
Type of Use:	Dissertation/Thesis
Order Total:	0.00 USD

4.1 CHEMICAL COMPOSITION OF HEXENE BASED LLDPE BY IR SPECTROSCOPY AND CHEMOMETRICS

This article describes a rapid investigation method, based on a combination of mid and near infrared spectroscopy and chemometrics tools, for measuring the amount of hexene in LLDPE. We have used our well-defined copolymers to calibrate the PLS model. The processing and the assessment of the obtained regression models are discussed and show that the methods are efficient, accurate and fast.



Mid and near infrared (MIR and NIR) spectroscopy associated with the partial least squares (PLS) method makes it possible to rapidly characterize the composition of linear low-density polyethylene (LLDPE) in a large range of 1-hexene content from 0 to 21 mol%. LLDPEs are produced using zirconocene catalysts activated with methylaluminoxane. PLS regression methods for MIR and NIR are constructed from this series of LLDPEs to quantify the 1-hexene content in unknown copolymers. In this case, the PLS regression method aims to correlate the 1-hexene content in the copolymers with their IR spectra. Multivariate calibration models are constructed by the PLS algorithm on pretreated data of MIR and NIR analyses. They are tested and validated by comparing results obtained by NMR and the PLS analyses for four unknown ethylene-1-hexene copolymers.

4.1.1 INTRODUCTION

With an annual global production of approximately 100 million tons, polyethylenes (PEs) are the main commercial polymeric materials.[1, 2] They are typically classified into three main families such as high-

density polyethylene (HDPE; 0.940 to 0.970 g/cm3), low-density polyethylene (LDPE; 0.910 to 0.940 g/cm^3) and linear low-density polyethylene (LLDPE; 0.916 to 0.940 g/cm^3). HDPE has no or only a small amount of branching (SCB), LDPE contains a combination of long (>C_6) and short chain branching, while the branching in LLDPE is predominantly from short chain branching. This last one is synthetized by copolymerization of ethylene and an α-olefin which allows the insertion of a short-chain branching into the main chain and thus impacts the crystallinity of the material.[3] The frequently used α-olefins are 1-butene, 1-hexene and 1-octene.[1, 4] The crystallinity and then the physical properties of LLDPE can be adjusted using different content of comonomer.[5, 6] Consequently, it is highly relevant to quantify the amount of comonomer units incorporated into LLDPE during the polymerization process.

Various analytical techniques have been developed to quantify the short chain branching content. It has been widely investigated using spectroscopy like Fourier transform infrared (FTIR)[7-10], proton and carbon nuclear magnetic resonance (H-NMR and ^{13}C-NMR)[11-14]. Liquid chromatography based on crystallibility of polyolefins has been established by Wild, Monrabal, Soares and Pasch through temperature rising elution fractionation (TREF)[15-19] and crystallization analysis fractionation (CRYSTAF)[20, 21]. However, these techniques cannot be used for the separation of amorphous fractions of the polymers. The combination of high temperature liquid chromatography with a Hypercarb column operating with a temperature gradient [22-27] was introduced by Cong and Macko and allow the analysis of amorphous polymers. These high temperature fractionation techniques were able to determine the chemical composition distribution (CCD) of LLDPE. In addition, thermal analysis coupled with mass spectrometry[28-31] has been employed to measure the branching type and the content of α-olefins in LLDPE.

However, these approaches are time consuming due to the sample preparation (dissolution at high temperature with toxic solvent) for most techniques and the time required to record and process the data. In many instances, for example in the case of high throughput experiments or during recycling process, it is desirable to determine the polymer composition in a shorter time.

Infrared spectroscopy is a consistent and an essential analytical method for exploring polymer composition.[32, 33] More specifically, Fourier transform infrared spectroscopy in attenuated total reflection mode (ATR-FTIR)[34-36] and near infrared (NIR)[37-39] equipped with an integrating sphere might be advantageous for measuring the chemical composition of LLDPE as inexpensive sample preparation is sufficient for theses technique. While many previous studies[9, 40, 41] are based on absorbance attributable to branch type there are few publications on quantitative studies.[7, 42, 43] In work of Blitz and McFaddin,[7]

FTIR calibration for different branch type (methyl, ethyl, butyl, hexyl) in LLDPE based on absorption of only one wavelength was reported. Sano et al and Shimoyama et al described methods to predict density in LLDPE by applying chemometrics tools to Raman spectra[42] and near IR spectra[43]. In this present study we propose to calibrate IR analysis of LLDPE with a large and complete set of polymers up to 21 mol% of 1-hexene and with multiple absorption bands in order to increase the robustness and precision of the method.

Because structural changes in ethylene-1-hexene copolymers cause low modifications in MIR and NIR spectra, the use of chemometrics techniques are required to highlight differences in polymer spectra. Partial least-squares (PLS) regression is commonly used to improve the resolution in analytical signals that can be overlaid for intricate materials.[44-48] In particular, we demonstrated, in a previous work, that PLS regression can be efficiently used for quantitative determination of composition of ethylene-butadiene copolymers.[49]

This work proposes an original method based on infrared spectroscopy and chemometrics. Firstly, copolymers containing various proportions of 1-hexene were synthetized using the zirconocene catalyst.[50-52] Secondly, the average composition of the copolymers was measured using ^{1}H and ^{13}C-NMR spectroscopy. The homogeneity in molar mass and chemical composition was also controlled by high temperature size exclusion chromatography (HT-SEC) and thermal gradient interaction chromatography (TGIC). Subsequently, the copolymers were used to construct the PLS model with NIR and MIR data.

4.1.2 EXPERIMENTAL SECTION

4.1.2.1 Polymerization method

All manipulations were performed under dry argon, using standard Schlenk techniques and glovebox. 1-hexene was dried over CaH_2 prior to use. Toluene and heptane were dried on 3 Å molecular sieves. Methyl-aluminoxane (MAO) 10% wt. in toluene was purchased from Aldrich and triethylaluminium ($AlEt_3$) was purchased from Albemarle and used as heptane solution (1 M). Ethylene (99.5%) from Air Liquide was purified by passing on three successive columns containing respectively molecular sieves, alumina and a copper catalyst. The metallocene complexes rac-Et$(Ind)_2ZrCl_2$ and $(nBuCp)_2ZrCl_2$ were purchased from Sigma-Aldrich. The activating support was prepared as described in previous work.[53]

Ethylene polymerizations were performed in a 500 ml glass reactor equipped with a stainless-steel blade stirrer and an external water jacket to control the temperature. MAO and the required amounts of 1-

hexene were introduced in a flask containing 300 mL of heptane. The mixture was transferred in the reactor under a stream of argon. The argon was then pumped out before introducing the ethylene or a mixture of ethylene-propylene. Temperature and pressure were then progressively increased up to 80 °C and 3.8 x 10^5 Pa. 100 µL of a solution (1.5 mM in toluene) of rac-Et$(Ind)_2ZrCl_2$ and $(nBuCp)_2ZrCl_2$ were then introduced in the reactor under 4 x 10^5 Pa of ethylene to start the polymerization. The pressure was kept constant at 4 x 10^5 Pa during the polymerization. After 30 minutes of reaction, the polymerization was stopped by releasing the pressure and cooling down the reactor to the room temperature. The resulting mixture was poured in 400 mL of methanol. The polymer was collected by filtration, washed with methanol and dried under vacuum.

In the case of slurry polymerization using the supported rac-Et$(Ind)_2ZrCl_2$ catalyst, a similar procedure was used. However the Al(i-Bu)$_3$ (1 M solution in heptane), the activating support, the metallocene precatalyst (1 mM solution in toluene), and 1-hexene were introduced successively in the flask containing 300 mL of heptane. The mixture was transferred in the reactor and the polymerization started by pressurization of the reactor to 4 x 10^5 Pa.

4.1.2.2 Characterization

High temperature size exclusion chromatography

High temperature size exclusion chromatography (HT-SEC) analyses were performed using a Viscotek system, from Malvern Instruments, equipped with a combination of three columns (PLgel Olexis from Agilent Technologies, 300 mm × 7.5 mm, 13µm). Samples were dissolved in 1,2,4-trichlorobenzene (TCB) with a concentration of 5 mg mL^{-1} by heating the mixture for 1 h at 150°C. 200 µL of sample solutions were injected and eluted with 1,2,4-TCB using a flow rate of 1 mL min^{-1} at 150 °C. 2,6-di-tert-butyl-4-methylphenol (BHT) was added to the eluent (200 mg L^{-1}) in order to stabilize the polymer against oxidative degradation. Online detection was performed with a differential refractive-index detector and a dual light-scattering detector (LALS and RALS) for absolute molar mass determination. OmniSEC software version 5.2 was used for data acquisition and calculation.

Thermal Gradient Interaction Chromatography

TGIC experiments were performed using an instrument from PolymerChar (Valencia, Spain) to characterize the composition distribution in samples. The instrument was equipped with a Hypercarb column from Thermo Scientific. The samples were dissolved in 10 mL vials for 1 h at 150 °C with 1,2,4-trichlorobenzene

(TCB) containing 300 ppm of BHT and purge with nitrogen to protect the polymer against oxidative degradation. 200 µL of sample solution at a concentration of 1 mg mL^{-1} were injected into the column at 150 °C. This technique requires a cooling (adsorption) and a heating (desorption) step. A cooling ramp of 20 °C min^{-1} down to 40 °C was applied to promote polymer adsorption. Elution begins isothermally at 40 °C during 5 min at a flow rate of 0.5 mL min^{-1} followed by a heating ramp at 2 °C min^{-1} to desorb the polymer. An infrared detector was used to monitor the components' concentration and composition when the chains were eluted from the column.

Because TGIC separates by adsorption it has the possibility to extend the range of polymers to be analyzed towards the amorphous region which is limited by crystallization techniques (TREF, CRYSTAF). Then, LLDPE with high content of comonomer can be separated.

Nuclear magnetic resonance spectroscopy

Comonomer contents of copolymers were determined by NMR using a Bruker Avance III 400 spectrometer operating at 400 MHz for ^{1}H-NMR and 100.6 MHz for ^{13}C-NMR. ^{1}H-NMR spectra were obtained with a 5mm QNP probe at 373 K and the ^{13}C-NMR spectra were obtained with a 10 mm PA-SEX probe at 373 K. A 3:1 volume mixture of 1, 2, 4-trichlorobenzene and toluene-d8 was used as solvent. The chemical shifts were measured in ppm using for ^{1}H-NMR the reference of toluene (CHD_2 at 2.185 ppm) and for ^{13}C-NMR the resonance of the major backbone methylene carbon resonance (CH_2 at 30.00 ppm) as internal references.

Mid infrared spectroscopy

Mid infrared (MIR) spectra were recorded using a Nicolet iS50 Fourier transform infrared (FTIR) spectrometer from Thermo Fisher Scientific. The spectrometer was equipped with an attenuated total reflection (ATR) module (single-bounce diamond crystal) and a deuterated triglycine sulfate detector and KBr optics. Before each measurement, the diamond crystal was carefully cleaned with ethanol and dried in ambient air. A small amount of sample in powder state was pressed directly on the diamond crystal with a constant pressure of 7 x 10^7 Pa. Background and sample were acquired using 32 scans at a spectral resolution of 4 cm^{-1} from 4 000 to 400 cm^{-1}. Spectral data were obtained with OMNIC Software from Thermo Fisher Scientific. The ATR spectra were not corrected for pathlength. Three replicates for each sample were made and compared. If they were similar, only one spectrum was selected and used for the model. They were different for one sample and it was not used in this work.

Near infrared spectroscopy

Near infrared (NIR) spectra were collected using a Nicolet iS50 FTIR spectrometer from Thermo Fisher Scientific under nitrogen. The spectrometer was equipped with an integrating sphere (Thermo Scientific Smart NIR).

The synthetized LLDPE gives, for some of them, a heterogeneous powder agglomeration. Working on the raw samples was difficult and a second method using a solvent to dissolve samples was also performed. To obtain a homogenous solution, 40 mg of polymer in 200 µL of 1,2,4-TCB, with BHT as stabilizer, was dissolved in a 2 ml vial. Then the vials were heated up to 150 °C for 1 hour in order to entirely dissolve the sample. Since glass does not absorb in NIR the samples were analyzed directly through the vials.

Background and samples were acquired using 32 scans at a spectral resolution of 4 cm^{-1} from 11 000 to 3 800 cm^{-1}. Spectral data were obtained with OMNIC Software from Thermo Fisher Scientific.

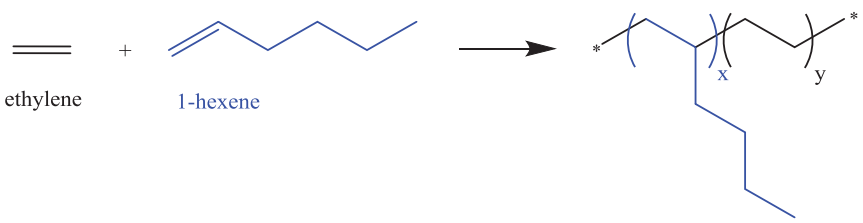
Chemometrics tools

Chemometric analyse of NIR and MIR spectra were achieved using a partial least squares (PLS) method with two different softwares. TQ Analyst software from Thermo Fisher Scientific and The Unscrambler X 10.5.1 software from Camo were used to analyze NIR and MIR data, construct the models and quantify the unknown samples.

4.1.3 RESULTS AND DISCUSSION

Chemical composition of ethylene-1-hexene copolymers

The present work was developed to determine 1-hexene content in LLDPE in a straightforward way. The copolymerization of ethylene with 1-hexene using metallocene catalysts provides polymers with various comonomer content (Scheme 1).



Scheme 4-1: Chemical structure of ethylene-1-hexene copolymers

A vast set of ethylene-1-hexene copolymers (Table 4-1) was obtained by changing comonomer content during synthesis. The catalyst used in this work led to polymers with the controlled molecular structure in molar mass and in comonomer composition. They were analysed by HT-SEC, TGIC and NMR before using them to construct the PLS models.

Table 4-1: Characterization of ethylene-1-hexene copolymers obtained with zirconocene catalyst.

Sample	Cata[a]	$\bar{M}_n$ (Đ)[a] kg.mol^{-1}	Hex[c] mol%	Tp[d] °C	Hex[d] mol%	Cw/Cn[d]
1	1	60 (2.9)	**0.0**	132.5	0.1	2.5
2	1	51 (3.2)	**0.0**	132.5	0.0	2.5
3	1	50 (3.4)	**0.0**	*nd*	*nd*	*nd*
4	1	44 (3.0)	**0.0**	*nd*	*nd*	*nd*
5	1	51 (3.1)	**0.0**	*nd*	*nd*	*nd*
6	2	49 (3)	**0.2**	132.0	0.3	3.0
7	1	41 (3.8)	**0.3**	131.7	0.3	2.0
8	1	21 (2.2)	**0.4**	130.8	0.2	1.3
9	2	24 (3.4)	**0.5**	131.0	0.4	3.0
10	3	36 (3.1)	**0.7**	*nd*	*nd*	*nd*
11	3	48 (2.6)	**0.7**	130.8	0.7	1.1
12	3	33 (4.1)	**1.0**	130.5	0.6	1.2
13	1	40 (2.6)	**1.1**	*nd*	*nd*	*nd*
14	3	29 (4.7)	**1.1**	*nd*	*nd*	*nd*
15	3	51 (2.2)	**1.2**	129.4	0.9	2.0
16	2	52 (3.1)	**1.5**	126.9	1.2	2.0
17	3	56 (2.3)	**1.5**	*nd*	*nd*	*nd*
18	1	54 (2.6)	**1.6**	*nd*	*nd*	*nd*
19	3	25 (3.7)	**1.8**	129.4	0.7	1.4
20	2	56 (3.1)	**1.9**	128.7	1.2	1.1
21	1	36 (1.8)	**2.0**	124.3	1.8	1.6
22	2	35 (2.3)	**2.0**	*nd*	*nd*	*nd*
23	1	40 (1.7)	**2.2**	123.1	2.1	1.3
24	1	40 (2)	**2.2**	*nd*	*nd*	*nd*
25	1	28 (2.2)	**2.2**	*nd*	*nd*	*nd*

26	3	42 (2.3)	**2.3**	*nd*	*nd*	*nd*
27	1	40 (1.9)	**2.5**	121.8	2.5	1.2
28	1	40 (2.2)	**2.5**	*nd*	*nd*	*nd*
29	3	56 (2.3)	**3.0**	*nd*	*nd*	*nd*
30	1	24 (2.9)	**3.0**	*nd*	*nd*	*nd*
31	3	40 (2.1)	**3.6**	114.4	4.2	1.5
32	3	26 (2.6)	**3.7**	117.8	4.0	1.4
33	3	22 (3.7)	**3.9**	116.7	3.8	1.3
34	3	24 (2.9)	**4.1**	114.7	4.1	1.1
35	1	41 (1.8)	**5.3**	107.8	5.8	1.1
36	1	46 (2)	**5.6**	105.7	6.3	1.1
37	1	37 (1.8)	**6.3**	102.7	7.0	1.1
38	1	40 (2.1)	**7.0**	98.9	7.8	1.0
39	1	60 (4.1)	**9.0**	*nd*	*nd*	*nd*
40	1	56 (2)	**13.6**	77.4	13.1	1.2
41	1	31 (1.4)	**20.7**	53.6	19.0	1.0

[a] catalytic systems based on the complexes [1] rac-Et(Ind)$_2$ZrCl$_2$ and [2] (nBuCp)$_2$ZrCl$_2$ [3] supported rac-Et(Ind)$_2$ZrCl$_2$ used for the preparation of ethylene-1-hexene samples.[b] Number average molar mass and dispersity obtained with HT-SEC, [c] 1-hexene content determined with ^{1}H NMR and ^{13}C NMR, [d]elution peak temperature, 1-hexene content and dispersity of chemical composition obtained by TGIC, [nd] not determined

4.1.3.1 Interpretation of NMR spectra

^{13}C NMR spectra was used to determine and quantify the chemical composition of homopolymers and copolymers with a 1-hexene content below 4% (Figure 4-1). The ^{13}C NMR spectra of highly branched linear low-density polyethylene is tricky and requires a detail analysis of monomer sequences.[54] In that case ^{1}H-NMR was used to provide reliable 1-hexene content since the signal of methyl chain end can be neglected. Calculation of 1-hexene content has been reported in a previous work.[18]

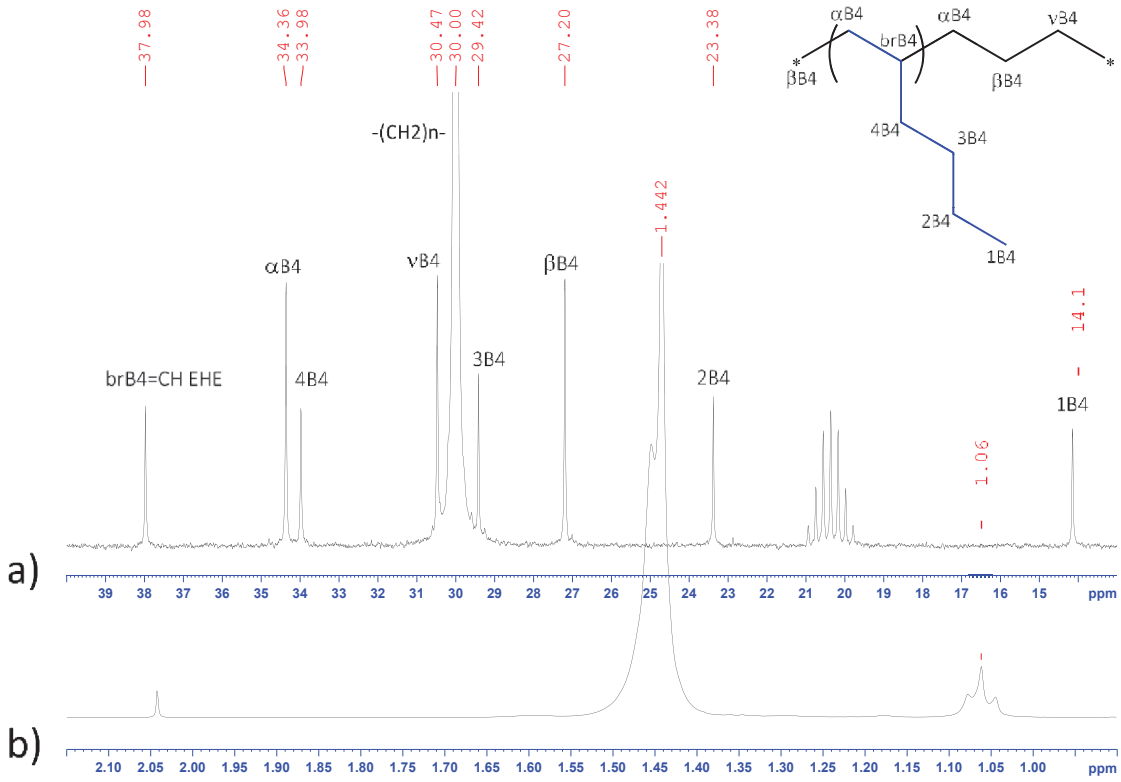


Figure 4-1: 13C NMR spectra (TCB/toluene-d8, 363 K) of sample 23 with 2,2 mol% of 1-hexene, a), resonance region of 1H NMR spectra (TCB/toluene-d8, 363 K) of sample 40 with 13,6 mol% of 1-hexene b).

4.1.3.2 Chemical composition distribution

The molar masses and the dispersity of samples are reported in Table 4-1. The SEC profiles, in Figure 4-2a, show a unimodal molar masses distribution. The TGIC peak of the samples elutes in decreasing order of comonomer content, as observed in previous works.[24, 27, 55-58] The elution temperature of 11 samples, issued from homogeneous catalyst [1, 2] and supported catalyst [3], were plotted (Figure 4-2b). The peaks are rather narrow and have a similar distribution to a Gaussian which confirms that all polymers were quite homogeneous in composition.

Quantifications of the 1-hexene content by TGIC were very similar to the values obtained by NMR. As NMR is a more conventional method, it has been chosen as the main reference method for developed models.

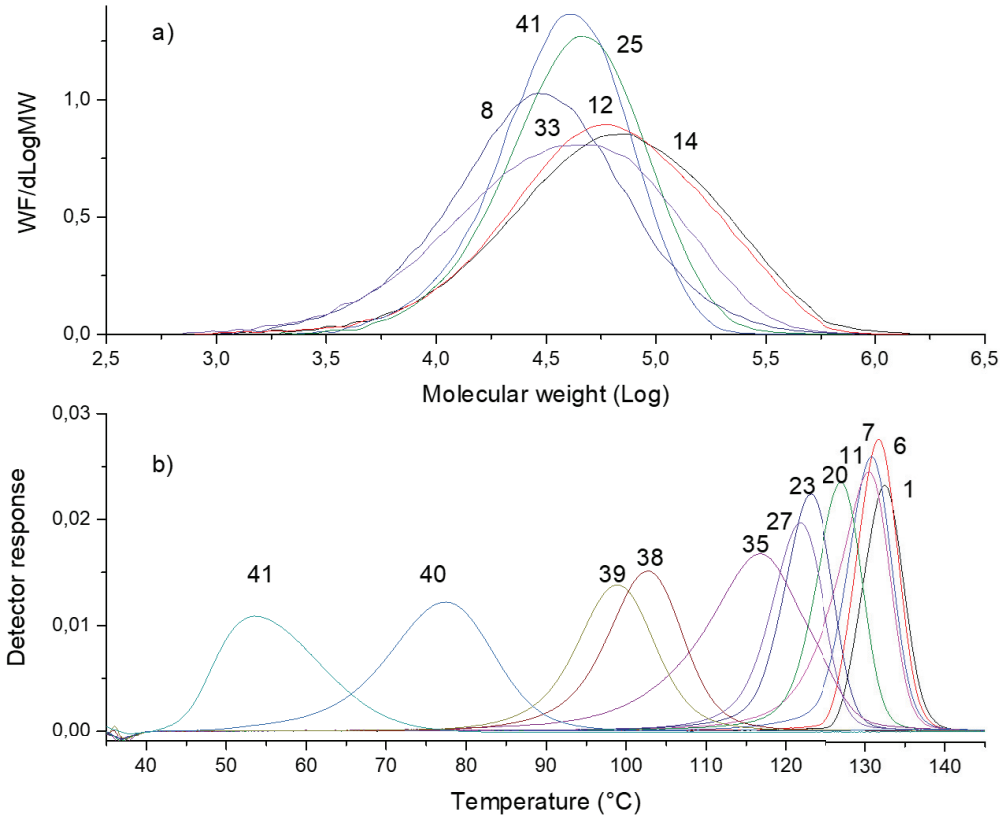


Figure 4-2: SEC a) and TGIC b) profiles of a set of ethylene-1-hexene copolymers ranging from 0 to 20.7 mol% of 1-hexene.

4.1.3.3 Interpretation of MIR spectra

The copolymer samples were analysed by MIR spectroscopy using ATR accesory. Figure 4-3 shows the comparison of FTIR spectra of a homopolyethylene and four ethylene-1-hexene copolymers.

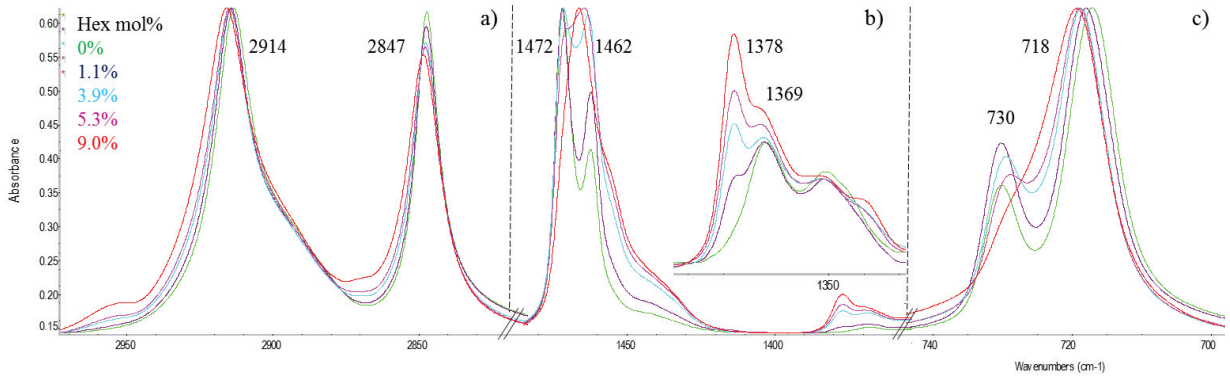


Figure 4-3: MIR spectra overlay of a polyethylene and four copolymers with various comonomer contents.

LLDPE showed a relatively simple infrared spectrum (Figure 4-3), the major absorption bands observed have been reported previously.[47, 59, 60] The IR spectra of LLDPE, containing different amounts of hexene, were found to have significant differences in four different regions. Four ratios of very close bands were studied. When the comonomer content increases in the copolymer we observed that the ratio of the peak intensity 2914 cm^{-1}/2847 cm^{-1}, 1472 cm^{-1}/1462 cm^{-1} and 1378 cm^{-1}/1369 cm^{-1} increased while the ratio of the peak intensity 730 cm^{-1} /718 cm^{-1} decreased significantly.

In Figure 4-3b, the ratio of absorption at 1378 cm^{-1} (due to methyl groups C-H deformation) versus absorption at 1369 cm^{-1} (due to methylene group C-H deformation) clearly shows a trend with the variation of 1-hexene amount in the copolymer. For the homo-polyethylene, no absorption was observed at 1378 cm^{-1} whereas as the comonomer content increased in the copolymer, the intensity of this peak increased. The splitting of absorption bands is due to semi-crystalline properties of LLDPE as described in previous work[61]. Comonomer content has a slight impact on different parts of the IR spectrum. In order to consider all these modifications on the spectrum, the chemometric analysis was applied in this study.

4.1.3.4 Interpretation of NIR spectra

The absorption spectrum of a representative sample is shown in Figure 4-4. In agreement with previous work,[62-64] the assignments of the eight main absorption bands are reported in Table 4-2.

Table 4-2: Assignments of NIR bands of ethylene-1-hexene copolymers.

NIR	Wavenumber [cm-1]	Assignment	Comments
LLDPE	8600 à 8000	second harmonic oscillation of CH, CH_2,CH_3	large, medium, gaussian look
	7300 à 6800	first harmonic oscillation of CH, CH_2, CH_3	very large, medium
	7200		medium, thin
	5800 à 4800	//	elevation of the base line
	5780	first harmonic oscillation of CH, CH_2, CH_3	very intense, thin
	5620		intense, thin
	5600 à 5400		medium, large
	4400 à 4200	combination of CH, CH_2, CH_3	very intense

NIR spectra are composed of overlapping overtones and combinations of bands originating from the MIR. They contain a wealth of information on the chemical and physical properties of the copolymers. Since it

was a considerable effort to deduce some characteristic of LLDPE microstructure from the spectra, the data were exploited using chemometric tools.

The spectrum of dissolved polymer (Figure 4-4b) were more noisy but more robust and repetitive compare to spectrum obtained with solid sample (Figure 4-4a). A PLS model was constructed with both kinds of preparation. The NIR spectrum of the solvent, used for the sample dissolution, was acquired separately (Figure 4-4c).

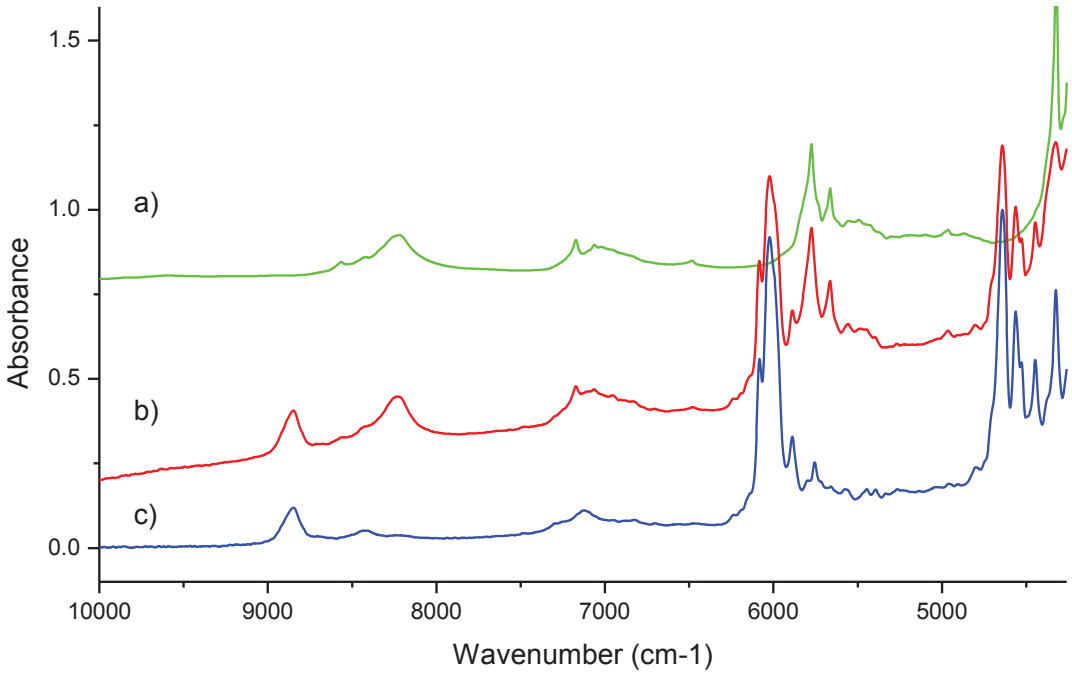


Figure 4-4: NIR spectra of a copolymer (sample 12) a) in solid state b) dissolved in 1,2,4-trichlorobenzene and c) solvent alone.

4.1.3.5 Chemometric study

The goal of this work was to obtain a robust method to determine the 1-hexene content of an unknown copolymer with MIR and NIR spectroscopy. A partial least squares regression (PLS) model[44, 45, 65] was used.

Calibration set

In order to determine composition of an unknown ethylene-1-hexene copolymer, calibration methods for MIR and for NIR were created with a set of 41 samples described above. The wide range of composition of ethylene-1-hexene copolymers, from 0% to 20.7 mol%, was particularly interesting for this purpose.

Performance index

The performance index (PI), that indicates the adequacy between the calculated polymer compositions and NMR measurements, was chosen to measure the accuracy of the method. The higher the performance index (up to 100) is, the better the agreement between calculated and NMR values are. This parameter, reported for each method in Table 4-4, allowed us to decide whether the modifications of the pre-processing data improve the accuracy of the method.

Prediction performance

The performance of the model was evaluated with the root mean square error of calibration (*RMSEC)*, the root mean square error of validation (*RMSEV)* and the correlation coefficient (r). These values were reported in Table 4-4. RMSEC (mol%) corresponds to the error calculated using the standards and was calculated with Equation 4-1.

$$RMSEC = \sqrt{\sum_{i=1}^{N}(\hat{y}_i - y_i)^2 / (N - A - 1)} \qquad (4\text{-}1)$$

RMSEV (mol%) was calculated with a cross validation method. The Kernel algorithm[46-48] was selected. It can be expected to perform well in our case with data containing many samples and few variables. A sample was removed from the calibration set and predicted with a model created with the remaining samples. The procedure was repeated by omitting each of the samples from the calibration set. RMSEV value was a measure of the average uncertainty that could be expected when predicting new samples, and was calculated with Equation 4-2:

$$\boldsymbol{RMSEV} = \sqrt{\sum_{i=1}^{N_p}(\hat{y}_i - y_i)^2 / (N_p)} \qquad (4\text{-}2)$$

N = number of samples; N_p = number of samples in prediction set; $\hat{y}_i$ = model predicted value for sample *i*; *A* = number of PLS factors in model;

- r^2: the correlation coefficient between predicted and measured value is a measure of the quality of the model. The closer to 1, the better is the model. For the calibration, r_c represents the quality of the fit. For validation, r_v characterizes the predictive ability of the model. In order to validate the model, RMSEC and RMSEV values must be low and similar and r^2 close to one.

Number of factors in PLS regression

The performance index plot was used to measure the divergence between the model and actual data. It allows the determination of the PLS factor number (Table 4-4) to be used to properly describe the variables. As the number of PLS factors increased, the performance index plot increased. When the curve reaches its maximum, this value corresponds to the optimum number of PLS factors. Including more PLS factors, the model will fit the calibration set better but can lead to an 'over-fitting' of the model and to a poorer prediction for unknown sample. The choice of four factor number in the calibration model was a balance between optimizing the explain variance and limiting the model complexity.

Preprocessing method

Several data pre-processing methods were applied. The first derivate of the NIR and MIR signals was chosen in order to reduce the baseline offset and the instrumental drift. In the derivation process, noise can increase which requires a smoothing. The Savitzky-Golay algorithm[66-68] was used for smoothing the signal and to reduce the impacts of varying baseline, variable path lengths, and high stray lights due to scatter effects. A polynomial order of 2 and a segment length of 7 points were applied. The pre-processing method was applied both to the whole spectrum and to the spectral region selection.

Scores

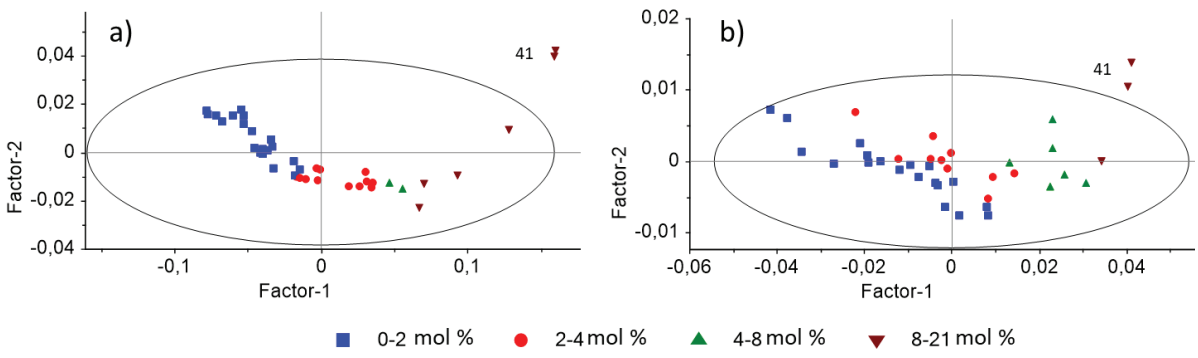


Figure 4-5: A principal component analysis (PCA) scores for factor 1 and factor 2 with confidence intervals of 95% of a) MIR and b) NIR for ethylene-1-hexene copolymers sample. Samples were disctinctly separated into four groups (blue, red, green and brown) depending of 1-hexene content (in mol%).

A principal component analysis (PCA) scores for factor 1 and factor 2, in Figure 4-5, summarized more variation in the data than any other pair of components. The closer the samples were in the score plot, the more similar they were. The plot for MIR (Figure 4-5a) and for NIR (Figure 4-5b) shows that when 1-hexene content increase, from blue to brown, the sample was clearly shifted to the right. This means that

the amount of comonomer had a real impact on the spectra and that it could be measured using PLS regression. The scores plot shows that the separation of the four regions of different hexene levels was better for the MIR model than for the NIR model. The both score plot show that the sample 41 was considered as outlier. This sample was different from the others, not because of an analytical error, but because of the high amount of hexene. It was considered a false outlier and was not removed to preserve the large range of analyses. Sample 41 was analyzed and used twice in the model to give more weight to this sample which is located alone at the end of the calibration. In addition, the sigmoid-shaped curvature of the score plots indicates that there were interactions between the predictors. Adding more factor to the model would improve it.

Spectral region selection

One approach was based on spectral region selection in which the wavelengths with low correlation were eliminated.

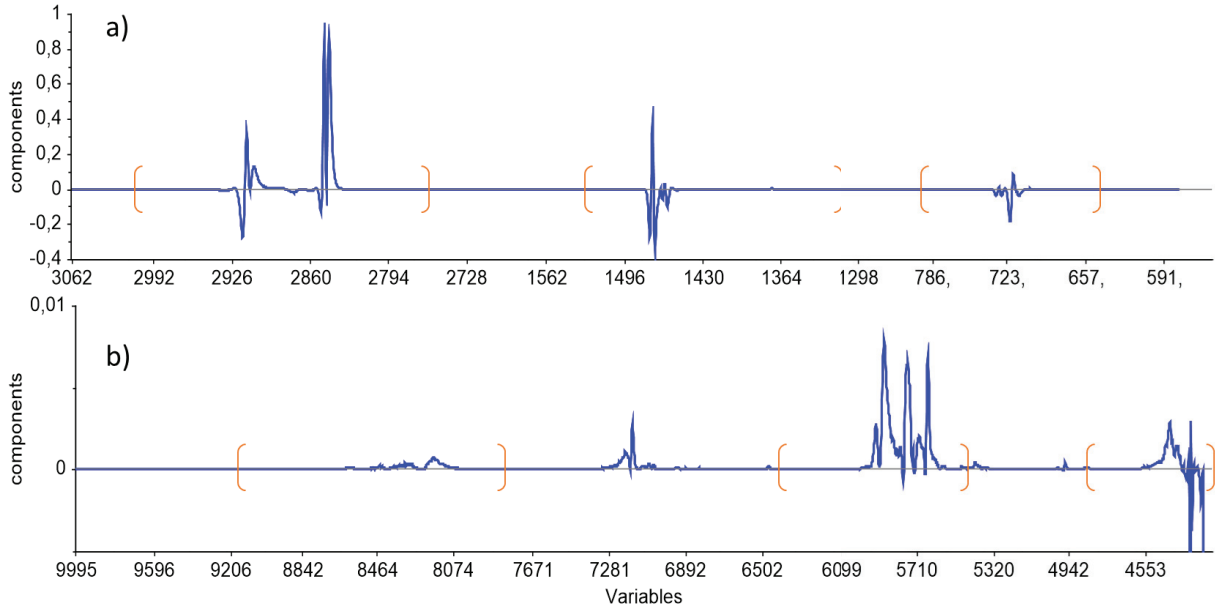


Figure 4-6: The contribution plot describes how individual variables contribute to the model, 3 spectral regions were clearly highlighted a) in MIR and b) in NIR. Variables represents the wavenumber in cm^{-1}. The brackets indicate the wavenumber ranges selected to be included in the models.

In the contribution plot for MIR (Figure 4-6a), three spectral regions contribute significantly to the discrimination. In order to improve the model and eliminate the wavenumbers likely generating noise, we decided to select only the interesting spectral region: the bands from 3000 to 2750 cm^{-1}, from 1500 to 1300 cm^{-1} and from 800 to 630 cm^{-1}. This corresponds well to the main absorption wavenumbers of

polyethylene (2914 cm^{-1}, 2847 cm^{-1}, 1472 cm^{-1}, 1462 cm^{-1}, 730 cm^{-1} and 718 cm^{-1}) indicated in previous work.[49]

For NIR, the contribution plot (Figure 4-6b) made it possible to select the bands from 9000 to 7800 cm^{-1}, from 6400 to 5400 cm^{-1} and from 4800 to 4000 cm^{-1}. Although we observed an absorption between 7500 to 6900 cm^{-1}, this range was not selected in the model. The NIR model has been improved without the use of this range mainly impacted by the solvent.

Calibration and validation

Using the samples different models were created, six of them are reported in Table 4-3. Since common industrial LLDPEs have a low 1-hexene content of up to 4 mol%, calibrations with a reduced 1-hexene range have also been designed to be more precise.

Models [c] for MIR and [f] for NIR, reported in Table 4-3, were constructed with samples ranging from 0 to 4 mol% of 1-hexene.

Table 4-3: Processing parameters of six PLS models for MIR and NIR

Model	IR	Sample[a]	Spectrum[b]	Pre-treatment[c]	Range[d] (mol%)
[a]	MIR	solid	whole	derivative SG	0-21
[b]	MIR	solid	selection	derivative SG	0-21
[c]	MIR	solid	selection	derivative SG	0-4
[d]	NIR	solid	whole	derivative SG	0-21
[e]	NIR	dissolved	whole	derivative SG	0-21
[f]	NIR	dissolved	selection	derivative SG	0-4

[a] solid or dissolved sample in 1,2,4 TCB, [b] whole spectrum or spectral region selection (3000-750, 1500-1300 and 630-800 cm^{-1} for MIR ; 9000-7800, 6400-5400 and 4800-4000 cm^{-1} for NIR), [c] first derivative and Savitzky–Golay smoothing, [d] range of the 1-hexene content in samples used for calibration.

With four factors and a spectral region selection, the performance index plot reached a maximum of 97.7% for MIR (method [b] in Figure 4-7) and a maximum of 97.2% for NIR (method [e] in Figure 4-7). It was, once again, improved for methods with a reduced 1-hexene content range (method [c] and [f]).

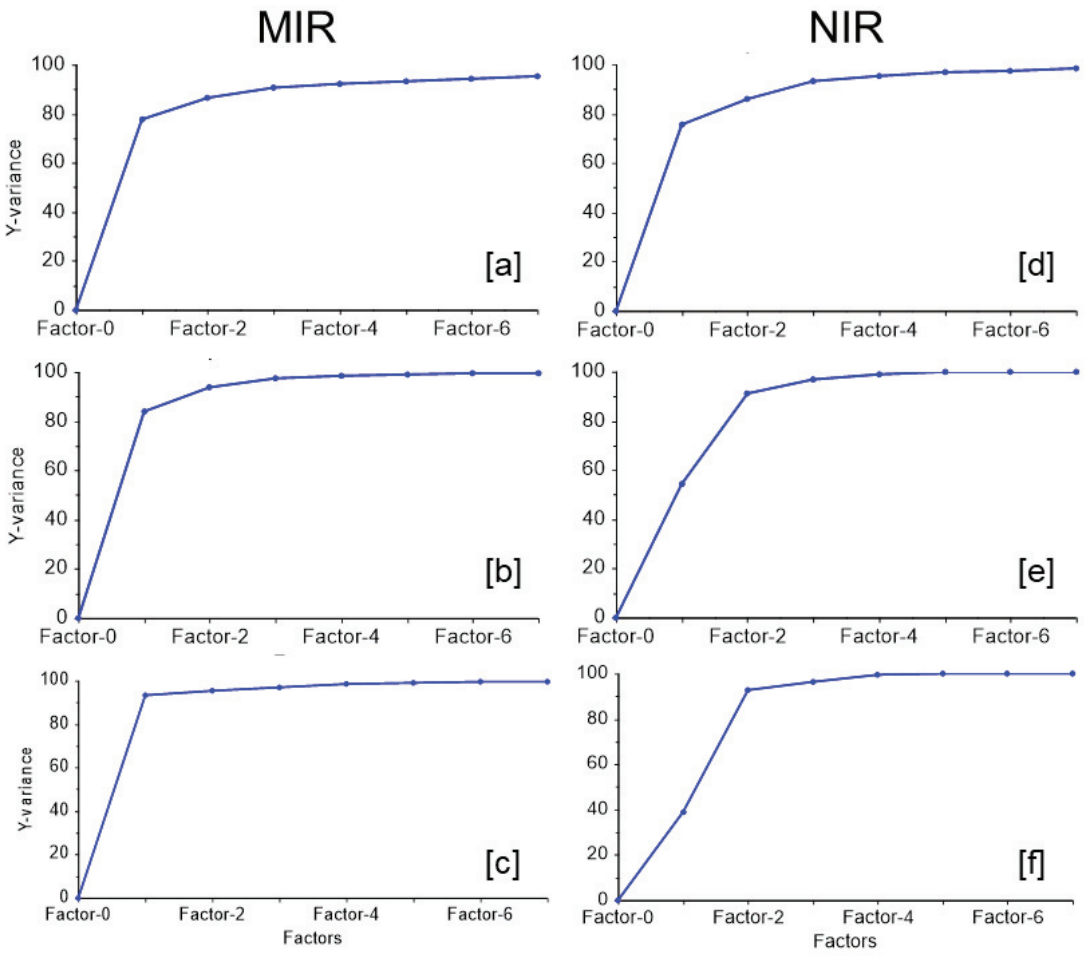


Figure 4-7: Evolution of performance index (in %) in function of the number of PLS factors for the six models reported in Table 4-3.

The numerical values of the performance index for the different tests are compared in Table 4-4. We observed that spectral region selection, with superior interpretability, significantly improved performance of the model and produced the lowest prediction error. Figure 4-8 shows the calibration curve for the quantification of 1-hexene content using different parameters detailed in Table 4-3 to construct the regression.

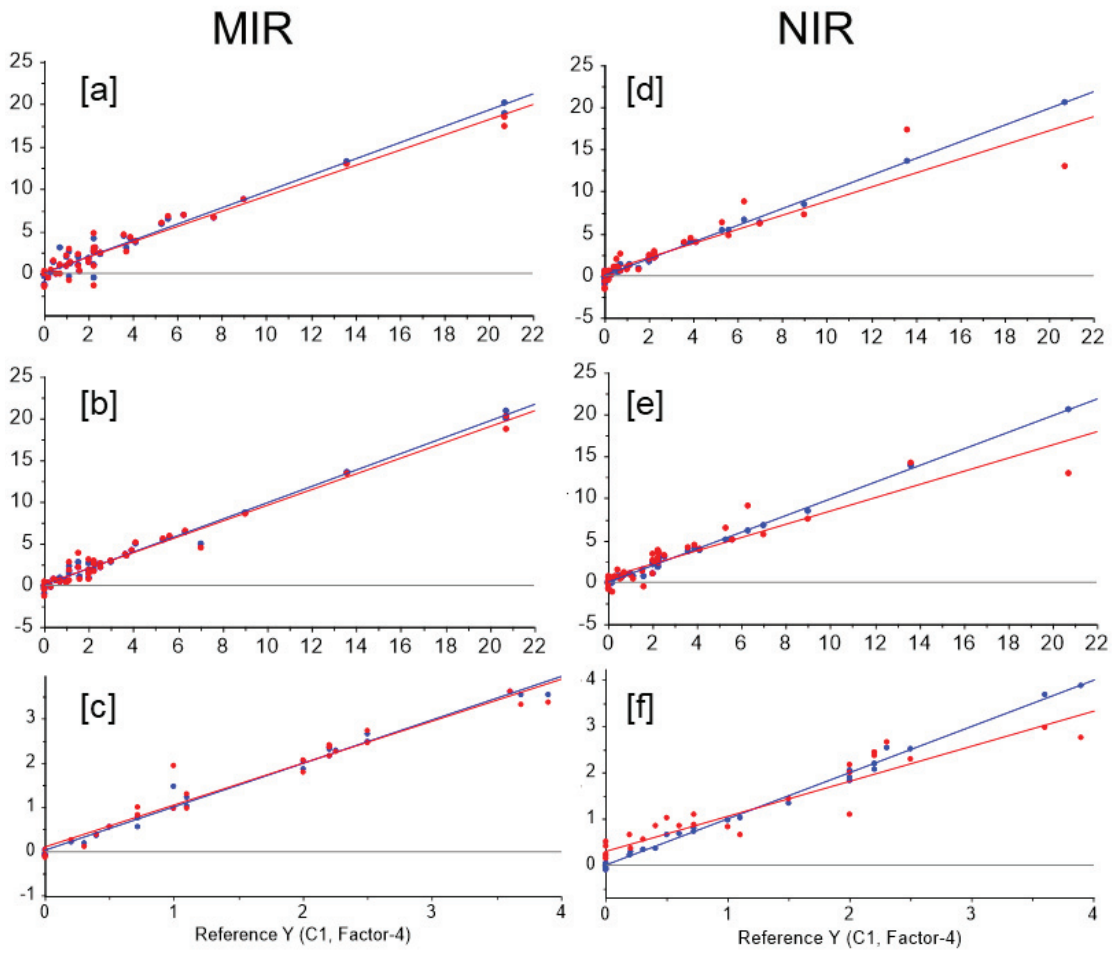


Figure 4-8: Correlation diagrams between predicted and reference values of the dataset for the six models reported in Table 4-3 (blue data for calibration and red data for validation). The axes units are expressed in mol% (1-hexene content).

The assessments of the six PLS models are summarized in Table 4-4.

Table 4-4: Assessment of the PLS models for MIR and NIR

Model	**[a] MIR**	**[b] MIR**	**[c] MIR**	**[d] NIR**	**[e] NIR**	**[f] NIR**
Number of factors	4	4	4	4	4	4
Performance index	97.4	97.7	98.5	91.8	97.2	98.2
RMSEC	0.6	0.5	0.1	1.0	0.3	0.1
r_c^2	0.98	0.99	0.99	0.96	0.99	0.98
RMSEV	0.9	0.6	0.2	1.6	1.7	0.4
r_v^2	0.97	0.98	0.97	0.86	0.85	0.84

The RMSEV values for the MIR model were slightly better than that values of NIR model. Finally, it appears that the methods [b] and [e] were reliable for the determination of the 1-hexene content in copolymers containing high comonomer content (up to 21 mol%). For lower content the methods [c] and [f] will be the most efficient and suitable. The repeatability and the validity of both methods were evaluated using new samples.

Repeatability of the model

A repeatability test for the measurement of 1-hexene content using the MIR and NIR methods ([c] and [f]) was performed. An unknown ethylene-1-hexene copolymer was measured 10 times by the same operator, in a short period of time. Afterwards, the PLS models [c] and [f] were applied to all IR spectra to quantify the 1-hexene content.

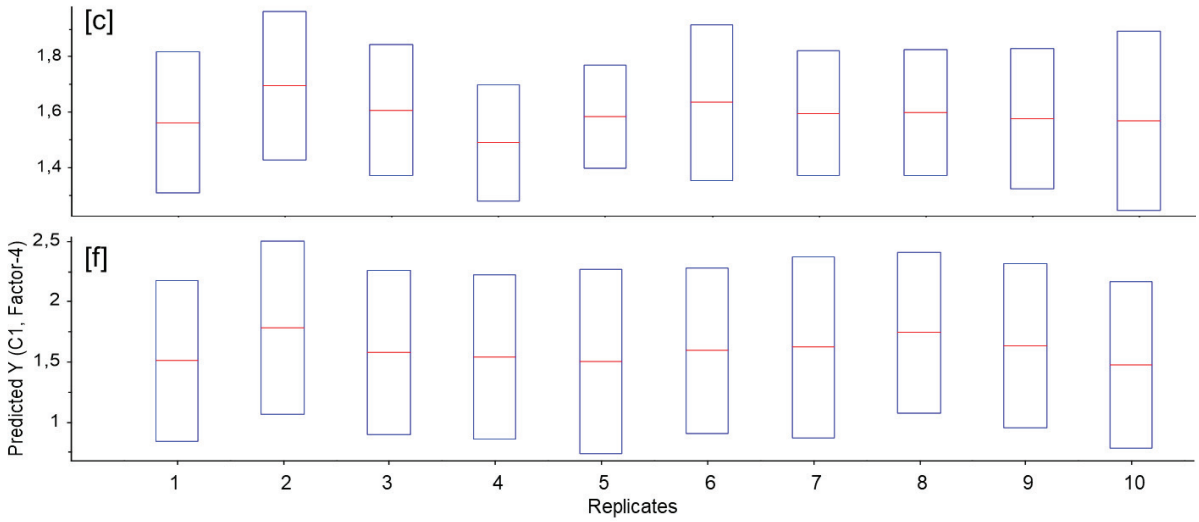


Figure 4-9: Predicted values (in red) and deviation (in blue) of a repetability test for the MIR and NIR models, quantification of 1-hexene content (in mol%) for an unknown sample with the method [c] and [f].

A good repeatability of both methods was observed based on the data plot in Figure 4-9. An average of 1.59 mol% with a standard deviation of 0.05 were obtained for MIR method [c] and an average of 1.60 mol% and standard deviation of 0.08 were obtained for NIR method [f]. Since a very similar average value for both methods and low sigma values were obtained, we concluded that the proposed models were accurate. Furthermore, the values were in good agreement with the 1.50 mol% obtained by NMR. The relative standard deviation (RSD) for each model was calculated using 10 replicates of the same sample. It is reported in Table 4-5.

Table 4-5: The relative standard deviation of each model determined with 10 replicates of one sample.

Model	**[a] MIR**	**[b] MIR**	**[c] MIR**	**[d] NIR**	**[e] NIR**	**[f] NIR**
RSD	4.9%	3.9%	3.1%	6.8%	6.1%	5.0%

Validation of the model

With all those observations it seems that the use of the method for the quantification of 1-hexene for an unknown copolymer is appropriate. In order to validate the model in real conditions, four new ethylene-1-hexene copolymers, obtained by Ziegler Natta catalyst, were analysed with both NMR and the proposed NIR and MIR models. The results are given in Table 4-6.

Table 4-6: Comparison of NMR and IR data of three unknown ethylene-1-hexene copolymers for the validation of the chemometric method.

Sample	**1-Hexene [mol%]**		
	NMR	**MIR method [b] [c]**	**NIR method [e] [f]**
A	0.6	0.7[c]	0.7[f]
B	2.2	2.7[c]	2.8[f]
C	5.3	5.6[b]	5.9[e]
D	10.2	10.1[b]	11.0[e]

[b]prediction value obtained with method [b], [c]prediction value obtained with method [c], [e]prediction value obtained with method [e], [f]prediction value obtained with method [f]

The values calculated by the models all show a bias in the same direction: the predicted results are all higher than the NMR results. This indicates that there is a small source of systematic error in the case of LLDPE obtained with Ziegler Natta catalyst and analyzed by these models. However, the predicted values obtained by IR are quite close to NMR results, which shows that the PLS model can be applied as a routine analysis. Considering this result, we can also conclude that the proposed model is reliable and accurate.

4.1.4 CONCLUSION

In this study a MIR and NIR method combined with PLS modeling was developed for a rapid determination of 1-hexene units in LLDPE. A series of 41 copolymers with a wide variety of chemical composition was synthetized. SEC profiles and TGIC profiles showed that all polymers were quite homogeneous in molar mass and composition. They were then characterized by NMR to determine 1-hexene content, and

analysed by MIR and NIR. The IR spectra obtained were exploited using chemometric tools and correlate with NMR results. The PLS method was revealed to be rapid, highly efficient and low-cost for determining the composition of copolymers even if characteristic vibrations of 1-hexene are indistinguishable in the spectrum. The proposed methodology provides also the great advantage of non-destructive measurement. The method is highly satisfactory based on its good repeatability and accurate results. This study shows that chemometric analysis of MIR and NIR spectrum is an easy and a valuable tool to understand the chemical composition of copolymers. The developed models can be applied for routine analysis of unknown samples with satisfactory results.

REFERENCES - CHAPTER 4.1

[1] R. Mulhaupt, *Macromol. Chem. Phys.* **2003**, *204*, 289.

[2] W. D. Sauter, M. Taoufik, C. Boisson, *Polymers* **2017**, *9*.

[3] M. M. Stalzer, M. Delferro, T. J. Marks, *Catal. Lett.* **2015**, *145*, 3.

[4] M. P. McDaniel, *Adv. Catal.* **2010**, *53*, 123.

[5] V. Kumar, C. R. Locker, P. J. in 't Veld, G. C. Rutledge, *Macromolecules* **2017**, *50*, 1206.

[6] S. Bensason, J. Minick, A. Moet, S. Chum, A. Hiltner, E. Baer, *J. Polym. Sci. Pol. Phys.* **1996**, *34*, 1301.

[7] J. P. Blitz, D. C. McFaddin, *J. Appl. Polym. Sci.* **1994**, *51*, 13.

[8] L. H. Cross, R. B. Richards, H. A. Willis, *Faraday Discuss.* **1950**, *9*, 235.

[9] T. Usami, S. Takayama, *Polym. J.* **1984**, *16*, 731.

[10] C. France, P. J. Hendra, W. F. Maddams, H. A. Willis, *Polymer* **1987**, *28*, 710.

[11] J. C. Randall, *J. Polym. Sci. Pol. Phys.* **1973**, *11*, 275.

[12] D. E. Dorman, E. P. Otocka, F. A. Bovey, *Macromolecules* **1972**, *5*, 574.

[13] W. Liu, P. L. Rinaldi, L. H. McIntosh, R. P. Quirk, *Macromolecules* **2001**, *34*, 4757.

[14] M. E. A. Cudby, A. Bunn, *Polymer* **1976**, *17*, 345.

[15] L. Wild, T. R. Ryle, D. C. Knobeloch, I. R. Peat, *J. Polym. Sci. Pol. Phys.* **1982**, *20*, 441.

[16] L. Wild, *Adv. Polym. Sci.* **1991**, *98*, 1.

[17] L. Wild, C. Blatz, *New Adv. Polyolefins*, Plenum Press, New York, **1993**.

[18] E. Cossoul, L. Baverel, E. Martigny, T. Macko, C. Boisson, O. Boyron, *Macromol. Symp.* **2013**, *330*, 42.

[19] T. Macko, H. Pasch, *Macromolecules* **2009**, *42*, 6063.

[20] B. Monrabal, J. Blanco, J. Nieto, J. B. P. Soares, *J. Polym. Sci. Pol. Chem.* **1999**, *37*, 89.

[21] J. B. P. Soares, S. Anantawaraskul, *J. Polym. Sci. Pol. Phys.* **2005**, *43*, 1557.

[22] T. Macko, R. Bruell, Y. Zhu, Y. Wang, *J. Sep. Sci.* **2010**, *33*, 3446.

[23] B. Monrabal, L. Romero, *Macromol. Chem. Phys.* **2014**, *215*, 1818.

[24] R. Cong, W. de Groot, A. Parrott, W. Yau, L. Hazlitt, R. Brown, M. Miller, Z. Zhou, *Macromolecules (Washington, DC, U. S.)* **2011**, *44*, 3062.

[25] B. Monrabal, *Adv. Polym. Sci.* **2013**, *257*, 203.

[26] R. Chitta, T. Macko, R. Bruell, C. Boisson, E. Cossoul, O. Boyron, *Macromol. Chem. Phys.* **2015**, *216*, 721.

[27] F. Brunel, O. Boyron, A. Clement, C. Boisson, *Macromol. Chem. Phys.* **2019**, *220*, 1800496.

[28] E. Roumeli, A. Markoulis, T. Kyratsi, D. Bikiaris, K. Chrissafis, *Polym. Degrad. Stabil.* **2014**, *100*, 42.

[29] T. Usami, Y. Gotoh, S. Takayama, H. Ohtani, S. Tsuge, *Macromolecules* **1987**, *20*, 1557.

[30] S. Duc, N. Lopez, *Polymer* **1999**, *40*, 6723.

[31] O. Boyron, T. Marre, A. Delauzun, R. Cozic, C. Boisson, *Macromol. Chem. Phys. 2019*, 1900162.

[32] J. L. Koenig, M. K. Antoon, *Appl. Opt.* **1978**, *17*, 1374.

[33] C. Baker, P. David, W. F. Maddams, *Makromol. Chem.* **1979**, *180*, 975.

[34] J. B. Huang, J. W. Hong, M. W. Urban, *Polymer* **1992**, *33*, 5173.

[35] F. M. Mirabella, *Appl. Spectrosc. Rev.* **1985**, *21*, 45.

[36] K. Sahre, U. Schulze, K.-J. Eichhorn, B. Voit, *Macromol. Chem. Phys.* **2007**, *208*, 1265.

[37] A. Cherfi, G. Févotte, *Macromol. Chem. Phys.* **2002**, *203*, 1188.

[38] M. P. B. Van Uum, H. Lammers, J. P. De Kleijn, *Macromol. Chem. Phys.* **1995**, *196*, 2023.

[39] L. M. Santos, M. J. Amaral, C. Dariva, E. Franceschi, A. F. Santos, O. Boyron, T. F. L. McKenna, *Macromol. React. Eng.* **2017**, *11*, 1700007.

[40] E. Caro, E. Comas, *Talanta* **2017**, *163*, 48.

[41] M. A. McRae, W. F. Maddams, *Makromol. Chem.* **1976**, *177*, 449.

[42] K. Sano, M. Shimoyama, M. Ohgane, H. Higashiyama, M. Watari, M. Tomo, T. Ninomiya, Y. Ozaki, *Appl. Spectrosc.* **1999**, 53, 551.

[43] M. Shimoyama, T. Ninomiya, K. Sano, Y. Ozaki, H. Higashiyama, M. Watari, and M. Tomo, J. Near Infrared Spectrosc. 1**998**, 6, 317.

[44] R. W. Gerlach, B. R. Kowalski, H. O. A. Wold, *Anal. Chim. Acta* **1979**, *112*, 417.

[45] P. Bastien, V. E. Vinzi, M. Tenenhaus, *Comput. Stat. Data Anal.* **2005**, *48*, 17.

[46] B. S. Dayal, J. F. MacGregor, *J. Chemometr.* **1997**, *11*, 73.

[47] F. Lindgren, P. Geladi, S. Wold, *J. Chemometr.* **1993**, *7*, 45.

[48] S. Rännar, F. Lindgren, P. Geladi, S. Wold, *J. Chemometr.* **1994**, *8*, 111.

[49] O. Boyron, B. Macqueron, M. Taam, J. Thuilliez, C. Boisson, *Macromol. Chem. Phys.* **2018**, *219*, 1700609.

[50] W. Kaminsky, *Macromolecules* **2012**, *45*, 3289.

[51] W. Kaminsky, A. Funck, H. Hähnsen, *Dalton Trans.* **2009**, 41, 8803.

[52] H. Sinn, W. Kaminsky, H.-J. Vollmer, R. Woldt, *Angew. Chem. Int. Ed.* **1980**, *19*, 390.

[53] F. Prades, J.-P. Broyer, I. Belaid, O. Boyron, O. Miserque, R. Spitz, C. Boisson, *Acs Catalysis* **2013**, *3*, 2288.

[54] J. C. Randall, J. *Macromol. Sci. Polymer Rev* **1989**, *29*, 201.

[55] N. Inwong, S. Anantawaraskul, J. B. P. Soares, A. Z. Al- Khazaal, *Macromol. Symp.* **2015**, *356*, 54.

[56] B. Monrabal, N. Mayo, R. Cong, *Macromol. Symp.* **2012**, *312*, 115.

[57] A. Z. Al-Khazaal, J. B. P. Soares, *Macromol. Chem. Phys.* **2014**, *215*, 465.

[58] A. Alghyamah, J. B. P. Soares, *Ind. Eng. Chem. Res.* **2014**, *53*, 9228.

[59] F. M. Rugg, J. J. Smith, L. H. Wartman, *J. Polym. Sci.* **1953**, *11*, 1.

[60] A. H. Willbourn, *J. Polym. Sci.* **1959**, *34*, 569.

[61] S. Krimm, C. Y. Liang, G. B. B. M. Sutherland, *J. Chem. Phys.* **1956**, *25*, 549.

[62] K. Rossmann, *J. Chem. Phys.* **1955**, *23*, 1355.

[63] M. Mizushima, T. Kawamura, K. Takahashi, K.-h. Nitta, *Polym. J.* **2011**, *44*, 162.

[64] S. Watanabe, J. Dybal, K. Tashiro, Y. Ozaki, *Polymer* **2006**, *47*, 2010.

[65] A. Höskuldsson, *J. Chemometr.* **1988**, *2*, 211.

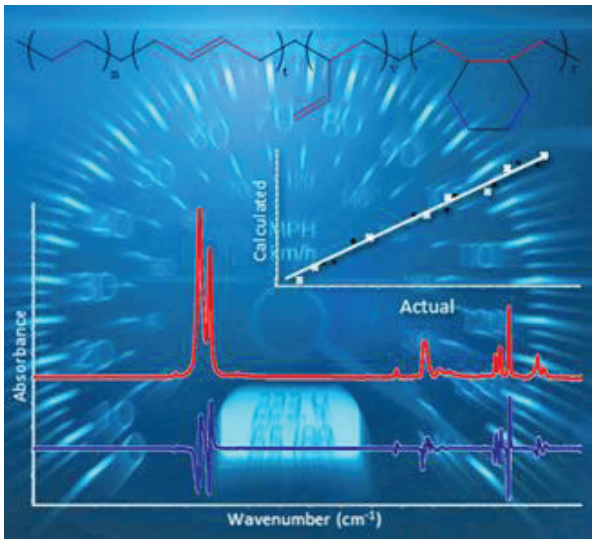
[66] J. Luo, K. Ying, J. Bai, *Signal Process.* **2005**, *85*, 1429.

[67] A. Savitzky, M. J. E. Golay, *Anal. Chem.* **1964**, *36*, 1627.

[68] P. A. Gorry, *Anal. Chem.* **1990**, *62*, 570.

4.2 RAPID DETERMINATION OF THE CHEMICAL COMPOSITION OF ETHYLENE-BUTADIENE COPOLYMERS USING FTIR SPECTROSCOPY AND CHEMOMETRICS

FTIR method coupled with chemometrics elaborated with our LLDPE models has shown that it was particularly fast and efficient to determine the chemical composition of unknown samples. We have taken advantage of the method developed for LLDPEs with simple structures to transfer it to ethylene-butadiene copolymers which present particularly complex microstructures.



Infrared spectroscopy by attenuated total reflection (ATR-FTIR), combined with partial least square (PLS) method provides a fast characterization of ethylene-butadiene copolymers intricate composition. The PLS regression method is constructed to quantify ethylene, 1,2-butadiene (vinyl), trans-1,4-butadiene and 1,2-cyclohexane units in the copolymer. These rings are formed by intramolecular cyclisation during polymerization. The performance of PLS models is evaluated by comparing the result obtained by ^{13}C NMR and the model for three unknown samples. It is shown that the proposed method allows to accurately estimate the chemical composition of ethylene-butadiene copolymers in a much shorter time than NMR.

4.2.1 INTRODUCTION

Neodymium metallocenes are unique catalysts for the copolymerization of ethylene with butadiene. A new class of elastomers was obtained using metallocene complexes of supported *ansa*-bis(fluorenyl) neodymium complexes in combination with MgR_2.[1,2] These elastomers, obtained with readily available monomers (ethylene and butadiene) display an intricate and original microstructure. The butadiene insertion leads to unsaturated moieties consisting of unsaturated groups: internal trans double bonds and

vinyl branches. In addition, this insertion leads to the formation of 1,2-cyclohexane rings. These rings are formed by a mechanism of intramolecular cyclisation involving vinyl units.[1,2] Properties of the ethylene-butadiene copolymers are directly linked to their composition and consequently it is highly relevant to fully characterize their chemical composition. The characterization of these polymers was performed by ^{1}H and ^{13}C NMR analyses.[3,4] NMR investigations permitted an accurate determination of the chemical composition of these copolymers. However, these analyses are reliable and accurate but are time consuming due to the sample preparation, the time required to record the spectrum and process the data. In many instances, for example in the case of high throughput experiments, it is desirable to determine the polymer composition in a shorter time.

Infrared spectroscopy is a consistent and an essential analytical method for exploring polymer composition.[5-9] More specifically, Fourier transform infrared spectroscopy in attenuated total reflection mode (ATR-FTIR)[10-12] might be advantageous for measuring the chemical composition of ethylene-butadiene copolymers as this technique requests straightforward sample preparation. Because structural changes in aliphatic ethylene-butadiene copolymers, cause low modifications in FTIR spectra, the use of chemometrics techniques are required to highlight differences in the polymer spectra. Partial least-squares (PLS) regression is a popular algorithm and generally used to improve the resolution of signals that can be superimposed in complex materials.[13-17] In particular, MIR spectroscopy combined with PLS methods is used to develop quantitative determination of copolymer composition.[18,19]

A combination of ATR-FTIR spectroscopy and chemometric tools was developed in the present article to quantify the chemical composition of ethylene-butadiene copolymers. The FTIR was calibrated by using NMR as a direct technique for measuring copolymer composition.

4.2.2 EXPERIMENTAL SECTION

4.2.2.1 Materials

Three neodymium metallocene complexes were selected: $[Me_2(C_{13}H_8)_2Nd(BH_4)_2Li(THF)]_2$ (**1**), $[Me_2Si(C_5H_4)(C_{13}H_8)Nd(BH_4)_2][Li(THF)]$ (**2**) and $[Me_2Si(C_5Me_4)(C_{13}H_8)Nd(BH_4)]$ (**3**). The preparation of complexes **1** and **2** was reported previously.[1,2,20,21] Complex **3** was obtained as a green powder by reaction of $Me_2Si(C_{13}H_8)(C_5Me_4)Li_2Et_2O$[22] with $Nd(BH_4)_3(THF)_3$ in tetrahydrofuran (THF).

4.2.2.2 Polymerization procedure

Polymerizations were performed in toluene using precatalysts **1, 2** and **3** in association with n-butyl-n-octyl-magnesium (BOMAG). In a typical procedure, a catalyst solution was prepared by successive addition of n-butyl-n-octyl-magnesium and of one precatalyst in toluene. The catalyst solution was stirred during 10 minutes and then introduced in a reactor. The polymerization was started by addition of the mixture of monomers at the desired temperature. At the end of polymerization, the reaction was quenched with methanol. The reaction medium was then poured in a solution of methanol containing 2,2'-Methylenebis(6-tert-butyl-4-methylphenol) (0.5 wt%). The polymer was filtered off, washed with methanol and dried under vacuum

4.2.2.3 Analytical techniques

Depending on the solubility of polymers, molar masses were measured with ambient size exclusion chromatography (SEC) in tetrahydrofuran (THF) or with high temperature size exclusion chromatography (HT-SEC) in 1,2,4-trichlorobenzene (TCB).

Size exclusion chromatography in THF

SEC measurements were performed with a Viscotek TDAmax system from Malvern Instruments that consists of a sample delivery module (GPCmax) and a tetra detector array, including light scattering, a four-capillary differential viscometer, a differential refractive index detector (RI), and a diode array UV detector. THF was used as the mobile phase at a flow rate of 1 mL min^{-1}. All polymers were injected at a concentration of 3 mg mL^{-1} after filtration through a 0.45 µm pore-size membrane. The separation was carried out on a guard column and three columns (SDVB, 5 µm, 300 × 7.5 mm I.D.) from Polymer Standard Service. Columns and detectors were maintained at 40 °C. The OmniSEC 5.02 software was used for data acquisition and data processing. A conventional calibration constructed with narrow polystyrene (Polymer Standards Service, Mainz, Germany) was used to calculate average molar masses.

High temperature size exclusion chromatography

HT-SEC analyses were performed using a Viscotek system, from Malvern Instruments, equipped with a combination of three columns (Polefin 300 mm x 8 mm I.D. porosity of 1 000 Å, 100 000 Å and 1 000 000 Å) from Polymer Standards Service. Samples were dissolved in 1,2,4-TCB with a concentration of 5 mg mL^{-1} by heating the mixture for 1 h at 150°C. 200 µL of sample solutions were injected and eluted in 1,2,4-TCB

using a flow rate of 1 mL min^{-1} at 150 °C. 2,6-di-tert-butyl-4-methylphenol (BHT) was added to the eluent (200 mg L^{-1}) in order to stabilize the polymer against oxidative degradation. Online detection was performed with a differential refractive index detector. A conventional calibration curve, obtained with polystyrene standards (Polymer Standards Service, Mainz, Germany) in the range of 500 to $4.2x10^6$ g mol^{-1}, was used to calculate the molar mass distribution of the samples. Data were acquired and processed with the OmniSEC 5.02 software.

Nuclear magnetic resonance spectroscopy

The chemical composition of ethylene-butadiene copolymers was determined by NMR using a Bruker 400 Avance III spectrometer operating at 400 MHz for ^1H and 100.6 MHz for ^{13}C. ^1H spectra were obtained with a 5 mm BBFO+ probe at 363 K and the ^{13}C spectra were obtained with a 10 mm PA-SEX probe at 363 K. A 3:1 volume mixture of tetrachloroethylene and benzene-d6 was used as solvent. Chemical shifts were measured in ppm using benzene (at 7.15 ppm) as reference for ^1H NMR and polyethylene chains (30.00 ppm) for ^{13}C NMR the resonance.

Fourier transform infrared spectroscopy

Infrared spectra were recorded using a Nicolet iS50 FTIR spectrometer from Thermo Fisher Scientific. The spectrometer is equipped with a diamond crystal ATR accessory and a deuterated triglycine sulfate (DTGS) detector and KBr optics. Before each measurement, the diamond crystal was carefully cleaned with ethanol and dry in ambient air. A small amount of sample in powder state was pressed directly on the diamond crystal with a constant pressure of 27 kg. Background and sample were acquired using 32 scans at a spectral resolution of 4 cm^{-1} from 4 000 to 400 cm^{-1}. At least every 60 minutes a new background spectrum was acquired. Spectral data were obtained with OMNIC Software from Thermo Fisher Scientific.

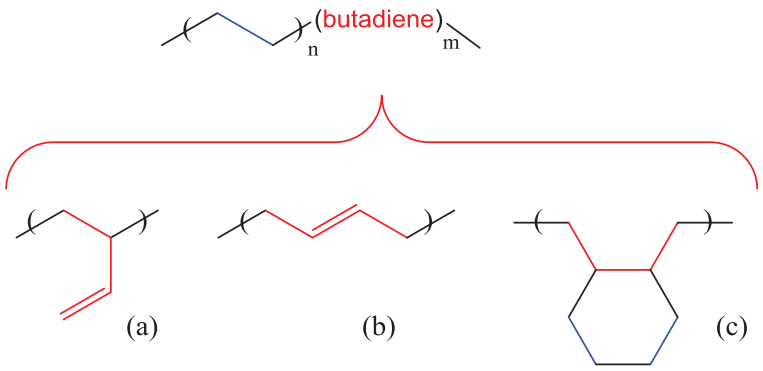
Chemometric analysis of the copolymer spectra was achieved using a partial least squares (PLS) method with *TQ Analyst software* from *Thermo Fisher Scientific*.

4.2.3 RESULTS AND DISCUSSION

4.2.3.1 Chemical composition of ethylene-butadiene copolymers

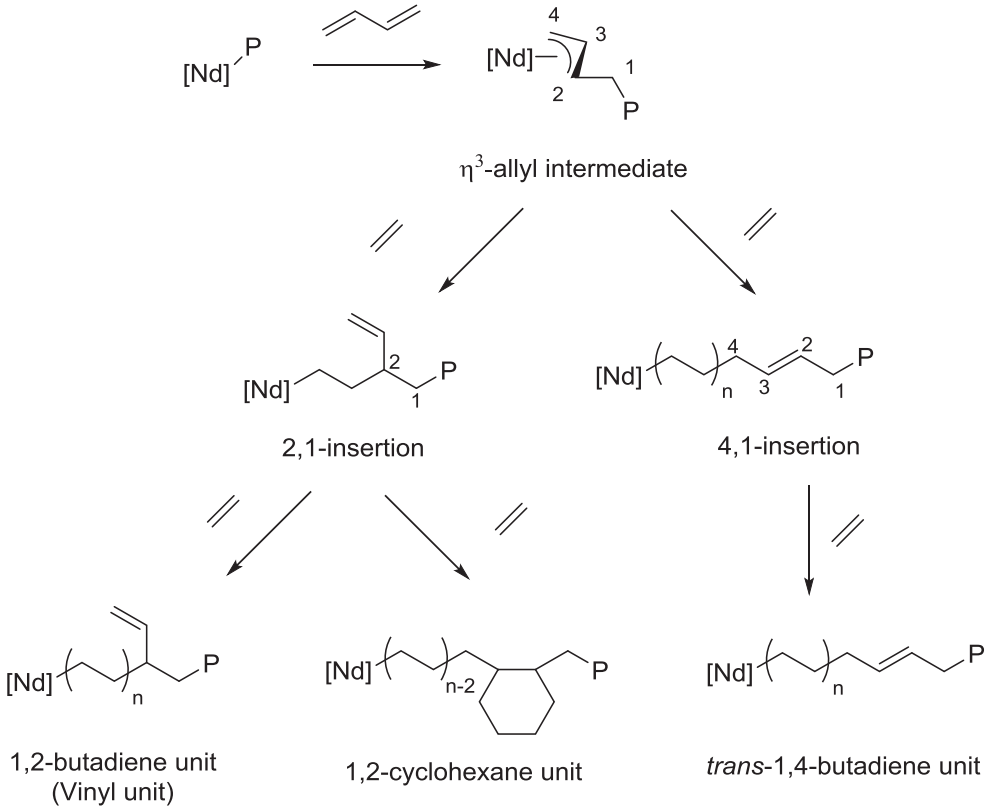
The present work was developed to determine the chemical composition of intricate ethylene-butadiene copolymers in a straightforward way. The copolymerization of ethylene with butadiene using neodymium

metallocene catalysts provides polymers with various chemical structures involving butadiene units: *trans*-1,4, vinyl and 1,2-cyclohexane (Scheme 4-2).



Scheme 4-2: Chemical composition of ethylene-butadiene copolymers vinyl (a), trans-1,4 (b) and 1,2-cyclohexane (c) units

The modification of the ligand around the metal center alters the regioselectivity of butadiene insertion. As shown in Scheme 4-3, insertion of butadiene leads to an allyl intermediate.



Scheme 4-3: Various units obtained after butadiene insertion for ethylene-butadiene copolymers.

Insertion of ethylene in the central carbon corresponds to a 2,1-butadiene insertion providing a vinyl unit and possibly the formation of a cyclohexane moiety via a subsequent intramolecular cyclisation involving two ethylene units.[1, 2, 23, 24] Insertion of ethylene on the terminal carbon corresponds to a 4,1-butadiene insertion providing exclusively trans-1,4-butadiene units. The regioselectivity of butadiene insertion (2,1 vs 4,1) is obtained considering the ratio between vinyl and cyclohexane units versus trans-1,4 units. This ratio follows the order of complex 1 > 2 > 3. Since there is competition between chain growth and cyclisation after the formation of a vinyl branch, the ratio between cyclohexane and vinyl units can be changed varying the monomer concentration. The lower the monomer concentration, the higher the number of cyclohexane units.

Taking advantage of the impact of the catalyst structure and of the polymerization conditions on the chemical structure of ethylene-butadiene copolymers a vast range of copolymers was prepared by changing these reaction parameters. Results reported in Table 4-7 show the impact of the catalyst properties and polymerization conditions on the chemical composition of copolymers.

Table 4-7: Chemical composition of ethylene-butadiene copolymers obtained by the combination of complex 1, 2 or 3 and BOMAG.

Complex	Sample	$\bar{M}_n$ (Đ)[a]	Ethylene[b]	*Trans*-1,4[b]	Vinyl[b]	1,2-cyclohexane[b]	Usage[c]
		[kg mol^{-1}]	*[mol%]*	*[mol%]*	*[mol%]*	*[mol%]*	
1	1	21.4 (3.9)	72.7	7.6	11.4	8.3	C
	2	31.3 (2.0)	80.7	4.9	5.3	9.1	C
	3	13.6 (1.5)	79.3	4.2	8.6	7.8	V
	4	14.0 (1.4)	79.8	3.8	9.1	7.4	V
	5	24.8 (2.3)	73.0	7.3	11.3	8.3	C
	6	25.8 (2.2)	73.5	6.9	11.2	8.4	C
	7	29.2 (1.6)	72.9	7.1	11.9	8.2	C
	8	31.3 (1.6)	73.5	6.7	11.6	8.2	V
	9	32.5 (2.0)	80.8	4.9	5.2	9.1	V
	10	45.7 (1.5)	80.3	4.6	6.7	8.4	C
	11	40.3 (1.4)	80.8	4.4	6.4	8.3	C
	12	9.2 (1.9)	82.1	3.1	11.5	3.3	C
	13	-	86.0	2.5	10.0	1.5	V
	14	18.5 (1.9)	76.2	4.1	18.0	1.7	C
	15	-	91.9	1.5	6.0	0.6	C
	16	-	83.2	2.7	12.4	1.7	C
	17	-	92.9	1.3	5.0	0.8	V
	18	13.2 (1.3)	93.6	1.6	1.1	3.7	C
	19	23.3 (1.6)	94.5	1.1	1.1	3.3	C
	20	44.7 (1.9)	95.6	0.8	0.7	2.9	C
2	21	16.0 (1.9)	60.5	38.2	1.1	0.2	V
	22	14.6 (1.9)	64.3	34.5	1.0	0.2	C
	23	9.4 (2.7)	73.2	25.9	0.7	0.2	C
	24	13.3 (2.1)	72.4	26.7	0.7	0.2	V
	25	13.2 (2.0)	71.7	27.3	0.8	0.2	C
3	26	47.7 (2.0)	61.5	25.1	11.3	2.1	C
	27	53.4 (2.0)	65	22.9	9.8	2.3	V
	28	59.5 (1.7)	63.8	24.1	9.7	2.4	C
	29	40.5 (2.2)	68.5	20.9	8.4	2.2	V
	30	79.3 (1.9)	61.9	24.9	11.2	2.1	C

[a] Number average molar mass and dispersity obtained with ambient SEC and HT-SEC, [b] determined with 1H NMR and 13C NMR, [c] C: calibration standards used to create the model V: validation standards used to calculate the performance index.

4.2.3.2 Interpretation of NMR spectra

The precise determination and quantification of the chemical composition of ethylene-butadiene copolymers by ^{1}H NMR and ^{13}C NMR analyses have been reported.[4] For NMR analyses, samples must be dissolved in aggressive solvent and more than 4 hours of acquisition are necessary in order to obtain good resolution. Figure 4-10 shows the high field resonance region of ^{13}C NMR spectra for three polymers synthetized with metallocene catalysts **1-3**. Although well documented,[4,25,26] the assignment of the chemical shifts and the determination of the chemical composition are tedious. This figure highlights the complex chemical structure of ethylene-butadiene copolymers.

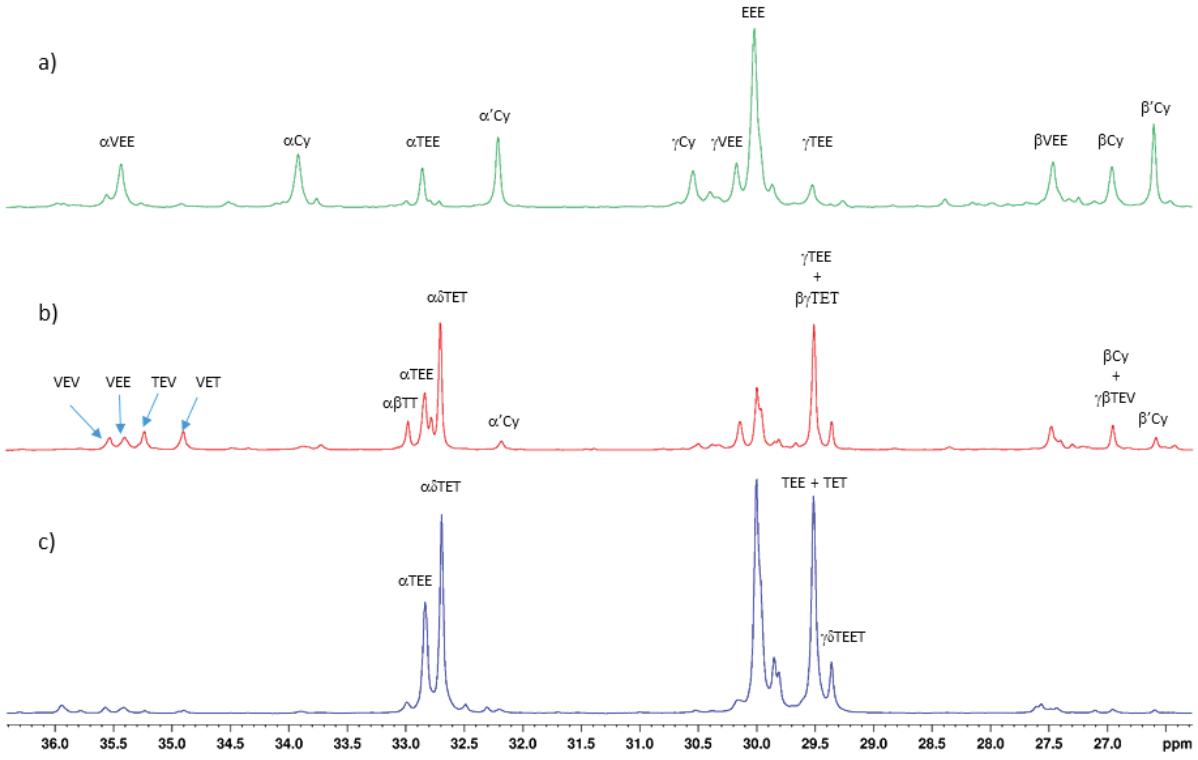


Figure 4-10: High field resonance region of 13C NMR spectra (TCE/C6D6, 363 K) of copolymers synthetized using the 3 different complexes selected for this study (V = vinyl unit; Cy = 1,2-cyclohexane unit; T = trans-1,4 unit). Sample 3 complex 1 a), sample 26 complex 3 b), sample 25 complex 2 c).

NMR analyses are reliable since the molar masses (M_n) of all polymers are high enough to neglect any inaccuracy due to the signals of chain-ends.

Molar masses of samples were determined by SEC (Table 4-7).

4.2.3.3 Interpretation of IR spectra

Copolymer samples were analysed with ATR-FTIR spectroscopy. Figure 4-11 shows the comparison of FTIR spectra of a homopolyethylene and three copolymers synthesized using catalysts based on complexes **1**-**3**.

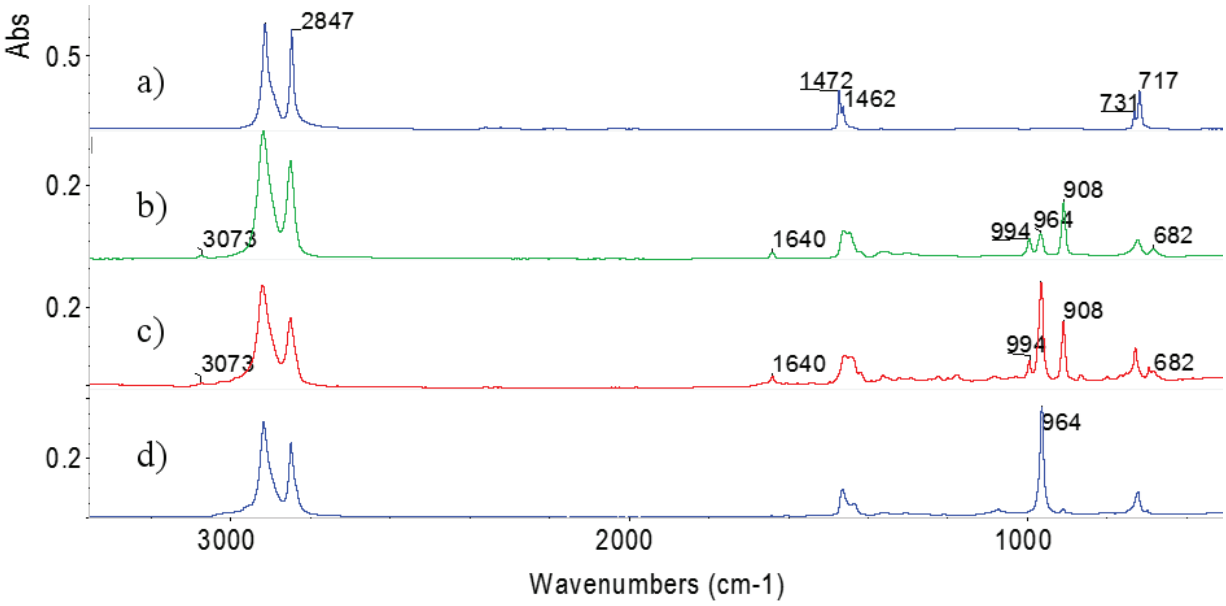


Figure 4-11: MIR spectra of a polyethylene a) and of copolymers synthetized using the 3 different complexes. Sample 3 complex 1 b), sample 26 complex 3 c), sample 25 complex 2 d).

Polyethylene shows a relatively simple infrared spectrum (Figure 4-11a). The splitting of bands (717-731 cm^{-1} and 1462-1472 cm^{-1}) is due to interactions between chains in the crystalline phase.[27, 28]

The absorption bands corresponding to vinyl units and *trans*-1,4-butadiene units are well known in the literature.[29-34] They were assigned to the corresponding vibrational mode of each type of monomer unit in the ethylene-butadiene copolymers (Table 4-8). To determine the quantity of vinyl units and *trans*-1,4-butadiene units in polybutadiene, an infrared band specific to each unit has been identified by Morero et al [35]. Those specific bands are known as 908 cm^{-1} for vinyl units and 964 cm^{-1} for *trans*-1,4-butadiene units. *trans*-1,4-butadiene units which possesses a zero dipole moment do not show stretching of the double bond at 1640 cm^{-1}. This band is only assigned to vinyl units.

The IR spectra of cyclohexane include a strong band at 2914 cm^{-1} of stretching absorption and a band at 1472 cm^{-1} of bending and scissoring absorption. These bands, corresponding to the cyclohexane unit

absorption, are difficult to identify because they overlap to that of other units present in the polymer backbone.

Due to the complexity of assigning a peak to cyclohexane units, chemometric analysis was developed and validated in this study.

Table 4-8: Major bands in MIR spectra of polyethylene and ethylene-butadiene copolymers

Spectrum	Wavenumber *[cm^{-1}]*	Assignment	Comments
PE	2914	νCH_2	Asymmetric and symmetric stretching of CH2
	2847	νCH_2	Intense and sharp
	1472	δCH_2	Bending of CH2, intense, doublet due to
	1462	δCH_2	crystallinity
	730	ρCH_2	Rocking of CH2, medium, doublet due to
	718	ρCH_2	crystallinity
Copolymer	3073	$\nu=CH_2$	Weak, sharp (vinyl unit)
	1640	νC=C	Medium sharp (vinyl unit)
	994	ωCH	Weak (vinyl unit)
	964	ωCH	Intense (*trans*-1,4 double bond)
	908	ωCH_2	Intense (vinyl unit)
	682	ωCH	Intense (vinyl unit)

ν =stretching, δ = bending, ρ =rocking, ω =wagging

4.2.3.4 Chemometric study

Calibration set

In order to determine composition of an unknown ethylene-butadiene copolymer, a calibration was created with our fully characterized samples described above. The wide range of composition of available ethylene-butadiene copolymers is particularly interesting for this purpose (Table 4-9).

Table 4-9: Composition range of ethylene-butadiene copolymers used in the model

Unit	**Range** ***[mol%]***
Ethylene	60.5 - 95.6
trans-1,4-butadiene	0.8 - 38.2
Vinyl	0.7 - 18
1,2-Cyclohexane	0.2 - 9.1

The idea is to determine with an ATR-FTIR analysis the composition of an unknown copolymer: ethylene content and the percentage of *trans*-1,4-butadiene units, vinyl units and cyclohexane units respectively. A partial least squares regression (PLS) model[36-39] was used with the four components and their relative compositions. The PLS calibration model was developed and popularized in analytical science by Wold in the 1960's[40-42] and was extensively used in chemistry by Martens,[37] Naes,[37,43,44] and Höskuldsson.[45]

Many ways for optimizing the calibration curve of the chemometric method were considered (Table 4-10).

Performance index

The effect of the choice of spectral range, the format of the data or the smoothing method (Norris or Savitzky-Golay smoothing[46-48]) were studied. This smoothing is frequently used as a pre-treatment that can eliminate noises such as baseline-drift. The performance index (PI) was chosen to measure the accuracy of the method. This number indicates the adequacy between the calculated polymer compositions and NMR measurements for the four units. The higher the performance index (range 0-100), the better the agreement between calculated values and NMR data. This allowed us to determine whether the changes made to optimize the method improved its performance.

Table 4-10: Performance index (PI) for different tests

Method	**Spectral range [cm^{-1}]**	**Data format**	**Smoothing**	**PI[a]**
1	400-4000	No derivative	No	94.0
2	400-4000	First derivative	No	95.9
3	600-1800 and 2600-3200	First derivative	No	96.1
4	600-1800 and 2600-3200	First derivative	Norris	97.0

5	600-1800 and 2600-3200	First derivative	SG[b]	96.9
6	600-1800 and 2600-3200	Second derivative	Norris	96.2

[a]Performance index, [b]Savitzky-Golay smoothing (data point was set at 7 and polynomial order was set at 3)

The following procedure was chosen. Only the spectral ranges containing structural information were selected and the part contributing to the noise was removed. In this study the spectral ranges from 600 to 1800 cm^{-1} and from 2600 to 3200 cm^{-1} were both selected. The first derivate of the IR signal was chosen in order to reduce the baseline offset and the instrumental drift. In the derivation process, noise can increase which requires a smoothing. Norris derivative filter were used for smoothing the signal and to reduce the impacts of varying baseline, variable path lengths, and high stray lights due to scatter effects. In the Norris smoothing, the segment length and the gap between segments were both set at 5.

Prediction performance

Two parameters [49] were used as indicators of the validity of the proposed model:

- *RMSEC*: root mean square error of calibration - the value corresponds to the error calculated using the calibration standards. RMSEC is expressed in mol% (Equation 4-3).

$$RMSEC = \sqrt{\sum_{i=1}^{N}(\hat{y}_i - y_i)^2 / (N - A - 1)} \qquad (4\text{-}3)$$

- *RMSEP*: root mean square error of prediction – Some of our samples are used as internal standards for validation of the method (Table 4-7). This value is a measure of the average uncertainty that can be expected when predicting new samples. RMSEP is expressed in mol% (Equation 4-4).

$$\boldsymbol{RMSEP} = \sqrt{\sum_{i=1}^{N_p}(\hat{\boldsymbol{y}}_i - \boldsymbol{y}_i)^2 / (\boldsymbol{N_p})} \qquad (4\text{-}4)$$

N = number of samples; N_p = number of samples in prediction set; $\hat{y}_i$ = model predicted value for sample *i*; *A* = number of PLS factors in model; r^2: the correlation coefficient provides the same information for these methods as it does for simple Beer's law.

In order to validate the model, RMSEC and RMSEP values have to be low and similar and r^2 close to one.

Number of factors in PLS regression

Figure 4-12 illustrates the change in autopredictive error for different numbers of PLS factors.

Root mean squared error of cross-validation (RMSEC) were plotted as a function of the number of PLS factor used in the calibration models. As the number of PLS factors is increased, the prediction error reduces. When the curve reaches its minimum, this value corresponds to the optimum number of PLS factors. Including more PLS factors, the model will fit the calibration set better but can lead to an 'over-fitting'[50] of the model and to a poorer prediction for unknown sample.

From Figure 4-12, it is possible to determine that 3 parameters could be suitable for the quantification of ethylene, *trans*-1,4-butadiene and vinyl units and 6 factors are adequate for cyclohexane units.

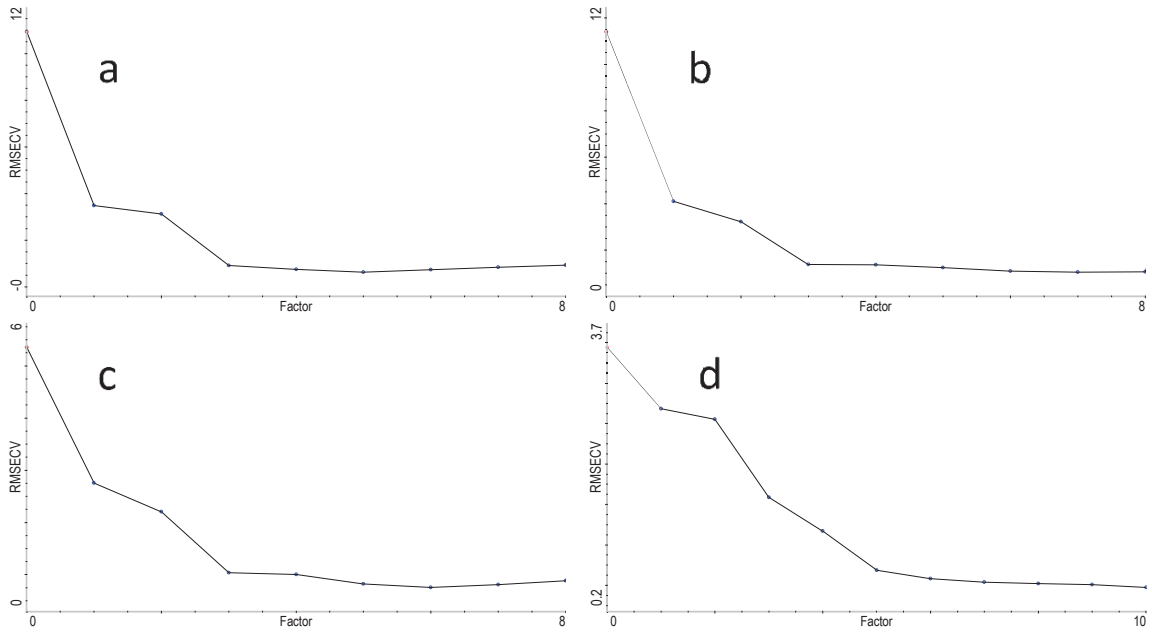


Figure 4-12: Evolution of RMSEC in function of the number of PLS factor used for ethylene (a), trans-1,4-butadiene (b), vinyl (c) and cyclohexane (d) units.

Calibration and validation

With all those optimised parameters the model was created using 20 calibration samples and 10 validation samples (Table 4-7). Figure 4-13 shows the calibration curve for the quantification of each units in the copolymers.

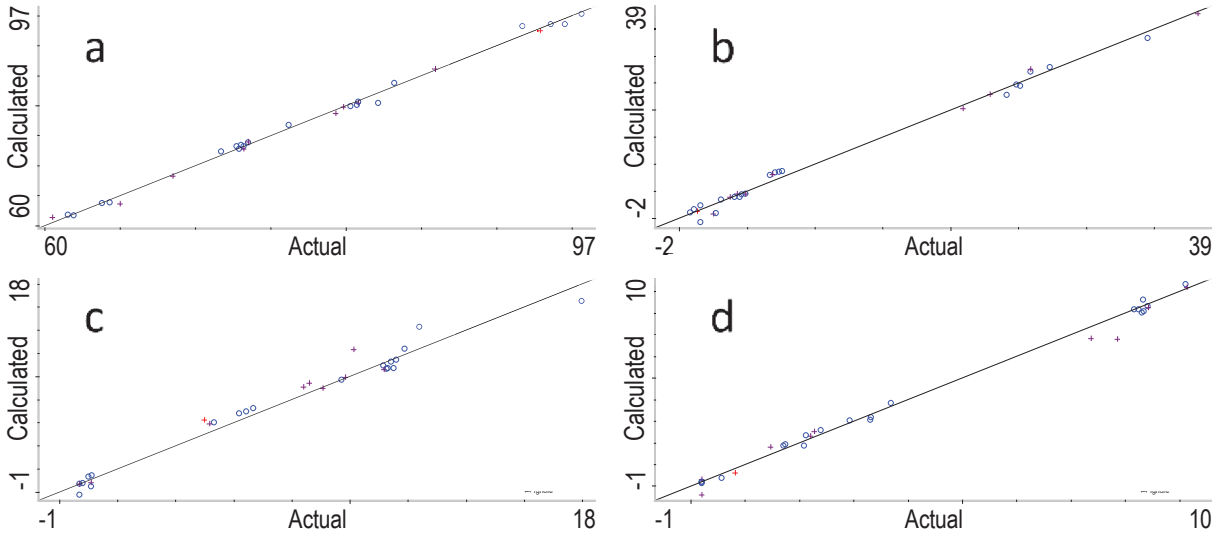


Figure 4-13: Correlation diagrams between the IR predicted values and the reference values for ethylene (a), trans-1,4 (b), vinyl (c) and 1,2-cyclohexane (d) units obtained by NMR. o stands for calibration points, + stands for validation points. The axes units are expressed in mol%.

For each parameter, a high value was obtained for the correlation coefficient; except for 1,2-cyclohexane, RMSEP/RMSEC ratio is close to 1. For 1,2-cyclohexane units number of factor is higher than that obtained for other units. Finally, it appears that the method is reliable for the determination of the content of ethylene in copolymers and for the measure of trans-1,4 and vinyl units. The prediction of 1,2-cyclohexane units seems to be the weakness of this method but considering the accuracy of all other parameters we can also evaluate efficiently cyclohexane units by difference.

Table 4-11: Calibration and validation parameters of PLS models for each paramters

	Ethylene	***trans*-1,4**	**Vinyl**	**1,2-cyclohexane**
RMSEC	0.64	1.04	0.74	0.18
r^2	0.998	0.995	0.990	0.999
RMSEP	0.61	0.89	0.92	0.45
r^2	0.998	0.998	0.980	0.993
Number of factors	3	3	3	6

Repeatability of the model

To verify repeatability of the method, an unknown ethylene-butadiene copolymer was measured 10 times with the same operator. Afterwards the PLS model was applied on all FTIR spectra to quantify each unit.

Table 4-12: Calibration and validation parameters of PLS models for each units.

Test	**1**	**2**	**3**	**4**	**5**	**6**	**7**	**8**	**9**	**10**	**Average**	**σ**
Ethylene *[mol%]*	75.6	78.6	78.2	77.3	77.4	76.9	77.8	74.8	78.9	76.9	77.2	1.3
Trans-1,4 *[mol%]*	8.6	6.3	6.1	6.7	6.6	8.2	6.4	8.2	6.0	7.0	7.0	1.0
Vinyl *[mol%]*	10.7	9.1	9.3	9.9	9.9	10.5	8.7	10.5	9.0	10.1	9.8	0.7
Cyclohex *[mol%]*	5.5	6.8	6.2	6.0	6.0	5.7	6.8	5.9	6.9	6.1	6.2	0.5

A good repeatability for all parameters was observed based on the data reported in Table 4-12. Since low sigma values were calculated, we can conclude that the proposed model is precise.

Validation of the model

With all those observations it seems that the method for the quantification of an unknown copolymer is feasible. In order to validate the model in real conditions, three new ethylene-butadiene copolymers were synthesized and analysed with both NMR and the proposed FTIR models. The results are given in Table 4-13. The predicted values obtained by FTIR are quite close to NMR results, which shows that the PLS model can be applied as a routine analysis. Considering this result, we can also conclude that the proposed model is precise and also accurate.

Table 4-13: Comparison of NMR and IR data of three unknown ethylene-butadiene copolymers for the validation of the chemometric method.

Sample	**A**		**B**		**C**	
	NMR	**IR**	**NMR**	**IR**	**NMR**	**IR**
Ethylene [mol%]	77.9	79.3	81.9	82.2	79.0	78.1
Trans-1,4 [mol%]	4.0	3.7	3.3	2.5	3.9	3.9
Vinyl [mol%]	8.3	9.0	12.7	12.5	15.3	14.5
Cyclohexane [mol%]	10.7	8.1	2.1	2.0	1.8	2.3

4.2.4 CONCLUSION

In this study an ATR-FTIR method combined with PLS modeling was developed for the simultaneous determination of 4 units in ethylene-butadiene copolymers. A series of 30 original copolymers with a wide variety of chemical composition was synthetized, characterized by NMR and then analysed by ATR-FTIR. The obtained infrared spectra were exploited using chemometric tools. A PLS model was then performed using the correlation between the chemical structure of ethylene-butadiene copolymers determined by NMR and FTIR spectra. The PLS method was revealed to be rapid, highly efficient and low-cost for determining the composition of ethylene-butadiene copolymers even if characteristic vibrations of the 1,2-cyclohexane groups were indistinguishable in FTIR spectrum. The proposed methodology provides also the great advantage of non-destructive measurement. The method is highly satisfactory based on its good repeatability and precise results. This study shows that chemometric analysis of ATR-FTIR spectrum is an easy and a valuable tool to understand the chemical composition of copolymers and can be extended to other kind of intricate polymers. The developed models can now be use for routine analysis of unknown samples with satisfactory results.

REFERENCES - CHAPTER 4.2

[1] J. Thuilliez, L. Ricard, F. Nief, F. Boisson, C. Boisson, *Macromolecules* **2009**, *42*, 3774.

[2] V. Monteil, R. Spitz, F. Barbotin, C. Boisson, *Macromol. Chem. Phys.* **2004**, *205*, 737.

[3] M. I. Lobach, I. A. Poletayeva, A. S. Khatchaturov, N. N. Druz, V. A. Kormer, *Polymer* **1977**, *18*, 1196.

[4] M. F. Llauro, C. Monnet, F. Barbotin, V. Monteil, R. Spitz, C. Boisson, *Macromolecules* **2001**, *34*, 6304.

[5] J. L. Koenig, M. K. Antoon, *Appl. Opt.* **1978**, *17*, 1374.

[6] L. M. Santos, M. J. Amaral, C. Dariva, E. Franceschi, A. F. Santos, O. Boyron, T. F. L. McKenna, *Macromol. React. Eng.* **2017**, *11*, n/a.

[7] A. Cherfi, G. Févotte, *Macromol. Chem. Phys.* **2002**, *203*, 1188.

[8] M. P. B. Van Uum, H. Lammers, J. P. De Kleijn, *Macromol. Chem. Phys.* **1995**, *196*, 2023.

[9] C. Baker, P. David, W. F. Maddams, *Makromol. Chem.* **1979**, *180*, 975.

[10] J. B. Huang, J. W. Hong, M. W. Urban, *Polymer* **1992**, *33*, 5173.

[11] F. M. Mirabella, *Appl. Spectrosc. Rev.* **1985**, *21*, 45.

[12] K. Sahre, U. Schulze, K.-J. Eichhorn, B. Voit, *Macromol. Chem. Phys.* **2007**, *208*, 1265.

[13] P. Geladi, B. R. Kowalski, *Anal. Chim. Acta* **1986**, *185*, 1.

[14] A. Borin, R. J. Poppi, *Vib. Spectrosc.* **2005**, *37*, 27.

[15] A. L. H. Muller, E. M. M. Flores, E. I. Muller, F. E. B. Silva, M. F. Ferrao, *J. Braz. Chem. Soc.* **2011**, *22*, 1903.

[16] P. Bastien, V. E. Vinzi, M. Tenenhaus, *Comput. Stat. Data Anal.* **2005**, *48*, 17.

[17] H. J. Luinge, J. H. van der Maas, T. Visser, *Chemom. Intell. Lab. Syst.* **1995**, *28*, 129.

[18] E. Marengo, V. Longo, E. Robotti, M. Bobba, F. Gosetti, O. Zerbinati, S. D. Martino, *J. Appl. Polym. Sci.* **2008**, *109*, 3975.

[19] J. Guilment, L. Bokobza, *Vib. Spectrosc.* **2001**, *26*, 133.

[20] F. Barbotin, V. Monteil, M.-F. Llauro, C. Boisson, R. Spitz, *Macromolecules* **2000**, *33*, 8521.

[21] J. Thuilliez, R. Spitz, C. Boisson, *Macromol. Chem. Phys.* **2006**, *207*, 1727.

[22] M. H. Lee, J.-W. Hwang, Y. Kim, J. Kim, Y. Han, Y. Do, *Organometallics* **1999**, *18*, 5124.

[23] H. Nsiri, I. Belaid, P. Larini, J. Thuilliez, C. Boisson, L. Perrin, *ACS Catal.* **2016**, *6*, 1028.

[24] WO2004035639A1 (2004), Societe De Technologie Michelin, Fr.; Michelin Recherche Et Technique S.A.; Atofina Research . invs.: V. Monteil, R. Spitz, C. Boisson;

[25] M. Bruzzone, A. Carbonaro, C. Corno, *Makromol. Chem.* **1978**, *179*, 2173.

[26] A. S. Rodrigues, E. Kirillov, B. Vuillemin, A. Razavi, J. F. Carpentier, *Polymer* **2008**, *49*, 2039.

[27] S. Krimm, C. Y. Liang, G. B. B. M. Sutherland, *J. Chem. Phys.* **1956**, *25*, 549.

[28] H. Hagemann, R. G. Snyder, A. J. Peacock, L. Mandelkern, *Macromolecules* **1989**, *22*, 3600.

[29] P. G. Wang, A. E. Woodward, *Makromol. Chem.* **1989**, *190*, 875.

[30] F. Severini, R. Gallo, S. Ipsale, N. Del Fanti, *Polym. Degrad. Stab.* **1986**, *14*, 341.

[31] J. M. Chalmers, "Infrared Spectroscopy in Analysis of Polymers and Rubbers", in *Encyclopedia of Analytical Chemistry*, John Wiley & Sons, Ltd, 2006.

[32] D. F. N.A., B. Kathryn, B. Michael, I. Federico, W. Jerry, "IR Spectroscopy of Polymers", Thermo Electron Corporation edition, Thermo Electron Corporation, 2007.

[33] V. Arjunan, S. Subramanian, S. Mohan, *Spectrochim. Acta, Part A* **2001**, *57*, 2547.

[34] D. Chen, H. Shao, W. Yao, B. Huang, *Int. J. Polym. Sci.* **2013**, 937284.

[35] D. Morero, A. Santambrogio, L. Porri, F. Ciampelli, *Chem. Ind.* **1959**, *41*, 758.

[36] M. J. Adams, "*Chemometrics in Analytical Spectroscopy, 2nd Edition*", Royal Society of Chemistry, 2004, p. 223 pp.

[37] H. Martens, T. Naes, *NATO ASI Ser., Ser. C* **1984**, *138*, 147.

[38] S. D. Brown, *Appl. Spectrosc.* **1995**, *49*, 14A.

[39] l. E. Frank, J. H. Friedman, *Technometrics* **1993**, *35*, 109.

[40] R. W. Gerlach, B. R. Kowalski, H. O. A. Wold, *Anal. Chim. Acta* **1979**, *112*, 417.

[41] H. Wold, "11 - Path Models with Latent Variables: The NIPALS Approach*", in *Quantitative Sociology*, Academic Press, 1975, p. 307.

[42] H. O. A. Wold, "*Nonlinear Estimation by Iterative Least Square Procedures*", 1968.

[43] T. Næs, "*A user-friendly guide to multivariate calibration and classification*", NIR Publications, Chichester, UK, 2004, p. viii.

[44] H. Martens, T. Næs, "*Multivariate calibration*", Wiley, Chichester England ; New York, 1989, p. xvii.

[45] A. Höskuldsson, *J. Chemom.* **1988**, *2*, 211.

[46] S. R. Delwiche, J. B. Reeves Iii, *Appl. Spectrosc.* **2010**, *64*, 73.

[47] P. A. Gorry, *Anal. Chem.* **1990**, *62*, 570.

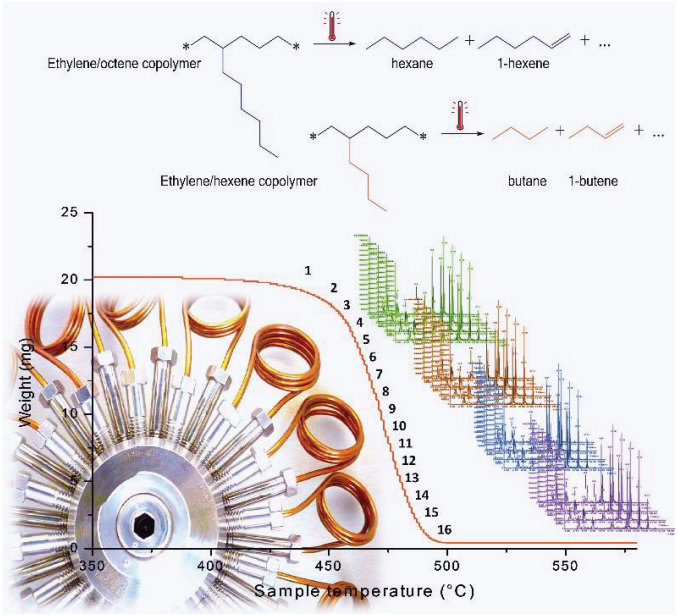
[48] A. Savitzky, M. J. E. Golay, *Anal. Chem.* **1964**, *36*, 1627.

[49] C. O. Chan, C. C. Chu, D. K. W. Mok, F. T. Chau, *Anal. Chim. Acta* **2007**, *592*, 121.

[50] W. Li, H. Qu, *J. Pharm. Biomed. Anal.* **2010**, *52*, 425.

4.3 AN ADVANCED TECHNIQUE FOR LINEAR LOW-DENSITY POLYETHYLENE COMPOSITION DETERMINATION: TGA–IST16–GC–MS COUPLING

An innovative technique TGA-IST16-GC-MS, thermogravimetric analysis combined with gas chromatography and mass spectrometry, was used to characterize LLDPE. We have used our well-defined copolymer models to validate this original method. The IST16 interface collects the gases produced during the degradation of the copolymer before GC-MS analysis. A specific signature of the comonomer present in LLDPE is identified and can be used for quantitative analysis of comonomer content.



An innovative method based on thermogravimetric analysis combined with gas chromatography and mass spectrometry, TGA–IST16–GC–MS, was developed for measuring the comonomer type and the comonomer content in a series of linear low-density polyethylene (LLDPE). LLDPE such as copolymers of ethylene and octene or ethylene and hexene were synthetized using the Et(Ind)2ZrCl2 / MAO zirconium-metallocene catalyst. Their characterization with TGA-IST16-GC-MS system were compared to the one of polyethylene prepared under similar conditions and used as reference. TGA-IST16-GC-MS allowed discriminating the comonomer type (hexene or octene) and content.

Combining the versatility of thermal analysis and the accuracy and sensitivity of mass spectrometry, this original method proved to be very useful for routine characterization of LLDPE. It has the advantage of being quicker and more easily performed that traditional means of obtaining copolymer compositions such as nuclear magnetic resonance (NMR), or through separation techniques such as TREF.

4.3.1 INTRODUCTION

Polyethylenes (PEs), which include low-density polyethylene (LDPE), linear low-density polyethylene (LLDPE) and high-density polyethylene (HDPE), constitute the most common industrial class of synthetic polymers with an annual global production of approximately 100 million tons[1, 2]. LLDPE is produced by copolymerization of ethylene with an α-olefin which introduces short-chain branching (SCB) and thereby decreases the crystallinity of final polymer[3]. The most commonly used α-olefins for this purpose are 1-butene, 1-hexene and 1-octene[4, 5] which allow fine tuning of the crystallinity and thereby the properties of resulting polyolefin. The suitability for different applications can be achieved just by variation of the comonomer content. Therefore, it is of high interest to measure the amount of comonomer units (or SCB) incorporated into the PE chains.

Various analytical methods have been employed to determine the nature and degree of SCB. Spectroscopic methods like carbon-13 nuclear magnetic resonance ^{13}C-NMR[6-8] and infrared (IR) [9-12] have been widely developed to measure SCB. More recently liquid chromatography based on crystallisation and thermal fractionation has been developed by Wild, Monrabal, Soares, Cong and Macko through temperature rising elution fractionation (TREF)[13-15], crystallization analysis fractionation (CRYSTAF)[13, 15-18] and interactive liquid chromatography[19-23]. Thermal analysis with pyrolysis–GC[24-26] has been also employed to measure branching in PE.

This work proposes a new method based on thermogravimetric analysis (TGA). TGA is generally associated to mass spectrometry (MS) [27] and IR spectroscopy [28, 29] in order to identify the gaseous compounds emitted during thermal decomposition. However, for polymer with complex microstructures like LLDPE, IR and direct MS cannot unambiguously determine the nature of most components of gas mixtures. In these cases, coupling TGA with GC–MS offers promising advantages. The emitted compounds are first separated by GC, then identified and quantified by MS.

In this paper, an innovative coupling technic is introduced, which significantly increases the number of data points collected. It combines TGA, GC-MS and an innovative gas-storage interface (IST16) with a 16-loop fractions collector inserted between the TGA and the GC [30]. The analytical tool is called hereafter TGA-IST16-GC-MS and provides an efficient way to take advantage of the MS technique.

Copolymers containing various proportions of 1-hexene and 1-octene were prepared using the zirconium catalyst *rac*-Et(Ind)$_2$ZrCl$_2$ activated with methylaluminoxane (MAO) [31-33]. The average composition of the

copolymers obtained was then elucidated using TREF, ^{1}H and ^{13}C-NMR spectroscopy. Subsequently, the copolymers were further investigated by TGA–IST16–GC–MS.

4.3.2 EXPERIMENTAL PART

4.3.2.1 Method of polymerization

Experiments were performed in a dry-argon atmosphere, using Schlenk techniques. Metallocene complex *rac*-Et(Ind)$_2$ZrCl$_2$ and methylaluminoxane (MAO, 10 wt% in toluene) were purchased directly from Sigma-Aldrich. The comonomer, 1-hexene and 1-octene, were distilled over CaH_2. Toluene and *n*-heptane were dried over 3 Å molecular sieves. Polymerizations were performed in a 500 mL glass reactor equipped with a blade stirrer and an external water jacket for temperature control as described in a previously article[34]. Polymerization was stopped by adding methanol and the mixture obtained was poured into methanol. The precipitated polymer was collected by filtration, washed with methanol, and dried under vacuum.

4.3.2.2 Characterization

High temperature size exclusion chromatography (HT-SEC)

HT-SEC analyses were performed using a Viscotek system, from Malvern Instruments SA, equipped with three columns (PLgel Olexis from Agilent Technologies, 300 mm × 7.5 mm, 13µm). 200 µL of a sample solution with a concentration of 5 mg mL^{-1} were injected and eluted in 1,2,4-trichlorobenzene at a flow rate of 1 mL min^{-1} at 150 °C. The mobile phase was stabilized with 2,6-di(tert-butyl)-4-methylphenol (200 mg L^{-1}) to avoid polymer degradation. Online detection was performed with a differential refractive-index detector and a dual light-scattering detector (LALS and RALS) for absolute molar mass determination. OmniSEC software version 5.2 was used for data acquisition and calculation.

NMR spectroscopy

The comonomer contents were determined by NMR spectroscopy using a Bruker Avance III 400 spectrometer operating at 400 MHz for ^{1}H-NMR and at 100.6 MHz for ^{13}C-NMR spectroscopy. ^{1}H-NMR and ^{13}C-NMR spectra were obtained at 90 °C with a 5 mm QNP probe and a 10 mm PA-SEX probe respectively. A 3:1 mixture of 1,2,4-trichlorobenzene and toluene-d_8 was used as the solvent. Chemical shifts were measured in ppm using the toluene signal (CHD_2 at 2.185 ppm) for ^{1}H-NMR spectroscopy and the polyethylene backbone signal (at 30.06 ppm) for ^{13}C-NMR spectroscopy.

^{1}H-NMR analyses were preferentially used to determine the α-olefin content in copolymers. The spectrum is composed of two main peaks: the signals of the CH_2 and CH protons of the polyethylene chain at 1.3 ppm and the signal of the methyl side groups at 0.9 ppm. Since high molar mass copolymers were synthetized, the methyl chain ends were neglected.

However, at low comonomer contents (< 1 mol%, samples 2 and 5), the resolution obtained in the ^{1}H-NMR spectra was too low and the methyl chain could not be neglected. In these cases, the ^{13}C-NMR spectra were used for the determination of the α-olefin content as described in a previous article. [34]

Temperature rising elution fractionation (TREF)

TREF measurements were performed to measure the chemical composition distribution (CCD) of sample. They were carried out using a CRYSTAF-TREF 300 model manufactured by Polymer Char S.A. The fractionation in TREF is based on the progressive deposition of polymer with decreasing crystallinity on an inert glass beads support inside the column (from Polymer Char S.A. 150 mm × 9 mm). The polymer is thus segregated in layers with different chemical structures. Experimentally, 80 mg of sample were dissolved in 20 mL of 1,2,4-trichlorobenzene stabilized with 2,6-di(tert-butyl)-4-methylphenol at 150 °C. 0.5 mL of the sample solution was loaded into the column. The temperature was slowly decreased to 35 °C at a rate of 0.5 °C min^{-1} to allow the polymer to crystallize. A reverse cycle was performed to quantify these fractions by rinsing solvent through the column while gradually increasing the temperature at 1 °C min^{-1}. Eluted fractions corresponding to increasing crystallinity and decreasing comonomer content were thus obtained. The concentration of the polymer solution was monitored with an IR detector measuring the total CH absorption in the range from 2700 to 3000 cm^{-1}.

4.3.2.3 TGA–IST16–GC–MS experiments

The on-line combination of GC–MS with TGA was applied to characterize gases released during the thermal degradation of the LLDPE samples.

Thermogravimetric analysis (TGA)

TGA was performed with a Mettler Toledo TGA/DSC 1, equipped with a DSC heat flow element for simultaneous detection of enthalpy variations. The temperature sensor of the equipment was calibrated using indium and zinc standards. All samples were accurately weighed (20 mg) into 150 µL aluminum oxide

crucibles. The samples were heated from 40 °C to 600 °C at 10 °C min^{-1} in dry nitrogen atmosphere at a flow rate of 30 mL min^{-1}.

Storage interface (IST16)

The composition of the gas mixture emitted during TGA experiment varies too quickly for a direct analysis by GC–MS instrument. These gases released during thermal decomposition were first collected in the IST16 device. A preheated transfer line between the TGA and IST16 storage device allowed the gases to enter one of the sixteen storage loops. These gases were stored until completion of the TGA run (Figure 4-14a). Afterwards, facilitated by the second transfer line connecting the IST16 with the GC, each fraction collected were injected into the chromatographic column for separation (Figure 4-14b). Sixteen detailed gas chromatograms were acquired, and emitted compounds can be identified. All loops, valves and inert flow paths were installed in an isothermal oven and maintained at 250 °C. The temperature of both transfer lines was set at 250 °C. For all samples, the decomposition events took place between 400 °C and 540 °C. The storage temperatures were therefore chosen accordingly, as listed in Table 4-14.

Table 4-14. Corresponding storage temperatures and loop numbers.

TGA: *T* in °C	–	400	420	430	440	450	460	470	480	490	500	510	520	530	540	–
IST16 loop [a)]	1	2	3	4	5	6	7	8	9	10	11	12	13	14	15	16

The listed temperatures are the upper limits of the ranges.

[a)] Loops 1 and 16 are used for blank samples before and after sample decomposition. No decomposition products were collected in these storage loops.

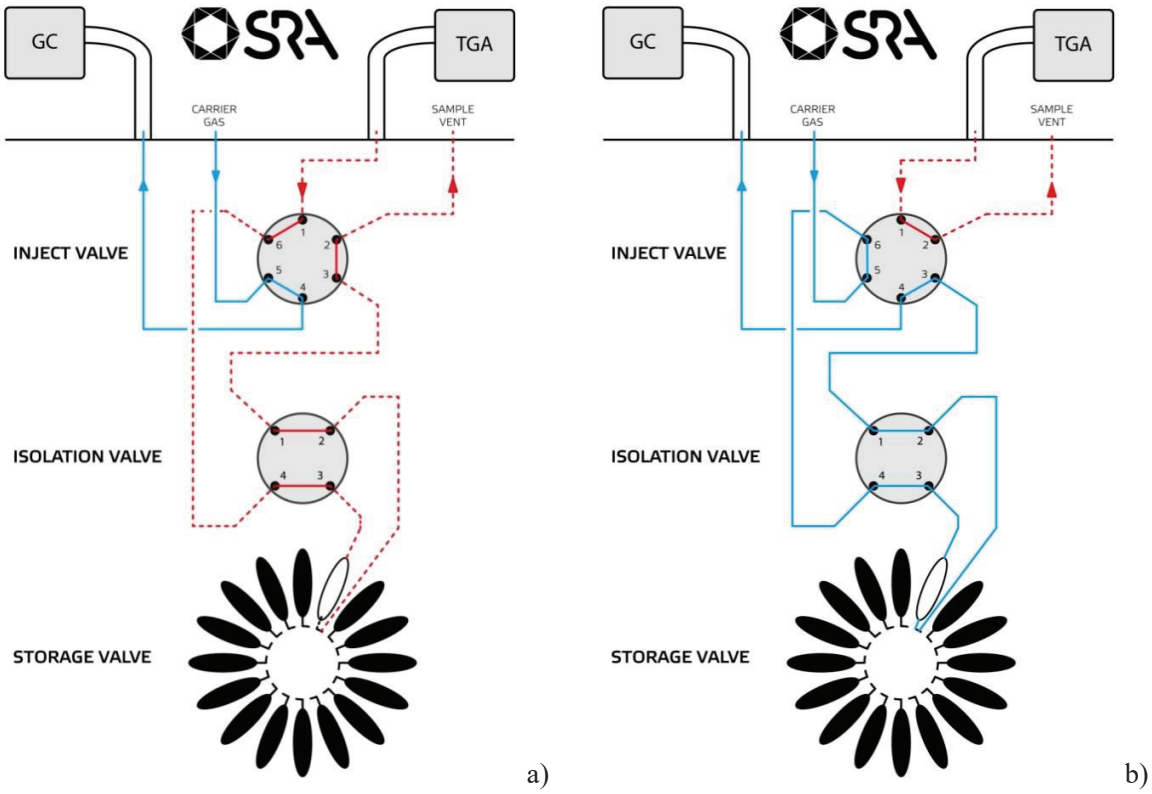


Figure 4-14: IST16 in storage mode a) and in injection mode b).

Gas chromatography–mass spectrometry (GC–MS)

A 7890B GC instrument, equipped with a capillary column and a 5977C mass selective detector from Agilent Technologies were used.

Helium was selected as the GC carrier gas. The flow rate through the chromatographic column was set at 1 mL min^{-1} with a split ratio of 4:1. The column temperature was held initially at 40 °C for 10 minutes, increased up to 300 °C at 10 °C min^{-1} and held at 300 °C for 24 minutes. The injector temperature was set to 280 °C.

The mass spectrometer was operated in the conventional electron ionization mode at an electron multiplier voltage gain of 1 V/V, with a mass scan range from 5 to 500 amu at a scan rate of 5.6 sec^{-1}. The National Institute of Standards and Technology spectra library was used to identify the compounds.

4.3.3 RESULTS AND DISCUSSION

Copolymers of ethylene with 1-hexene or 1-octene (Table 4-15) were prepared using the zirconium-metallocene catalyst $Et(Ind)_2ZrCl_2$ / MAO. A homopolymer (HDPE - sample 1) was also synthesized and used as a reference. The comonomer distribution of the synthesized samples was measured by TREF and the comonomer content was determined by NMR spectroscopy. All samples were subsequently investigated by TGA–IST16–GC–MS coupling.

4.3.3.1 Polymer characterization

The molar masses and the dispersity of polymers were determined by HT-SEC (Table 4-15). The copolymers exhibited a unimodal molar mass distribution. The TREF peak temperature of the samples gradually decreases as the comonomer content decreases, as observed in the previous works.[34, 35] Due to the high comonomer content in samples 7 and 8, the resulting copolymers are soluble at ambient temperature, and no peak was observed in TREF experiments.

TREF profiles in Figure 4-15 show that the signals collected are rather narrow and confirm that all copolymers are homogeneous in composition as expected with a metallocene catalyst. Because of their uniform comonomer distribution the copolymers are further employed below as models for TGA-IST16-GC-MS measurements.

Table 4-15: Characterizations for the ethylene–α olefin copolymers.

Sample	α-olefin	$\bar{M}_n$ ($Đ$)[a)]	α-olefin content[b)]	T_e[c)]
		Kg mol^{-1}	mol%	°C
1	–	60.2 (2.9)	0	101.8
2	Octene	41.0 (2.6)	0.6	96.2
3	Octene	32.4 (1.8)	1.7	89.5
4	Octene	32.2 (1.8)	5.6	66.4
5	Hexene	24.4 (3.4)	0.5	97.7
6	Hexene	29.5 (1.8)	5.1	68.1
7	Hexene	26.4 (2.3)	13.6	*
8	Hexene	26.4 (2.3)	20.7	*

[a)] Determined by HT-SEC with light scattering detector. $Đ$ = dispersity. [b)] Determined by ^{1}H- or ^{13}C-NMR spectroscopy. [c)] Elution temperature determined by TREF, * no peak observed in TREF experiment.

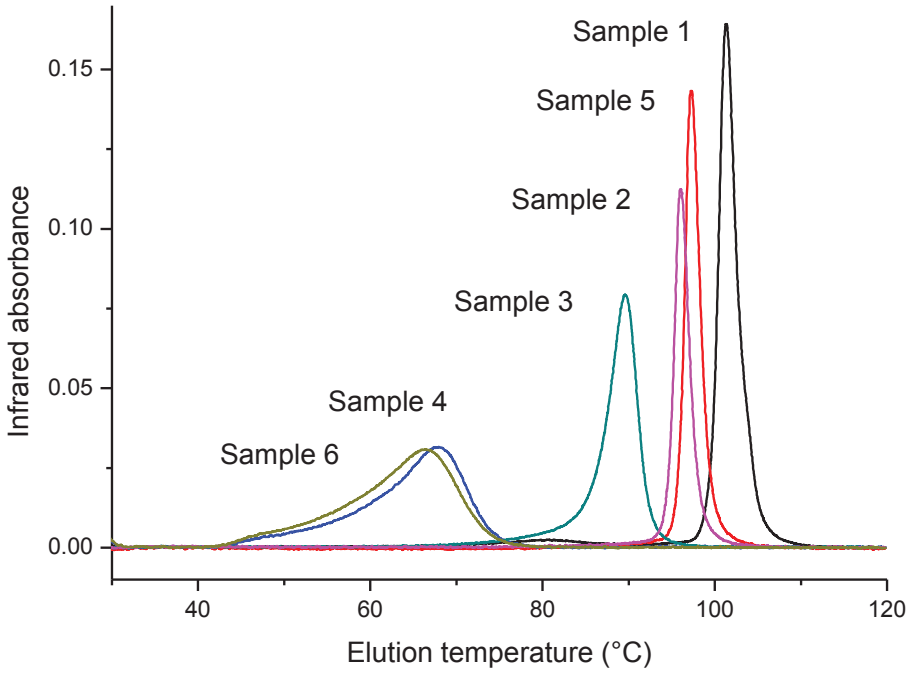


Figure 4-15: TREF profile of poly(ethylene-co-octene) (samples 2-4) and poly(ethylene-co-hexene) (samples 5-8) copolymer with a crystallization rate of 0.5 °C min^{-1}

4.3.3.2 Thermal decomposition of the HDPE

The comonomer-free sample (sample 1), used as a reference, was analyzed first with the TGA-IST16-GC-MS setup. The TGA curve in Figure 4-17 shows that the thermal decomposition occurs in a temperature range between 430 °C and 500 °C. Only one step of mass loss is observed in the thermogram of Figure 4-17.

The mass spectrum of Figure 4-16 shows that HDPE typically cleaved in a specific manner and its thermal decomposition produced three types of aliphatic hydrocarbons: α, ω-diene, α-alkene, and *n*-alkane. Alkanes and alkenes were the main emitted products. The major compounds observed during the degradation contained 9 and 10 carbons.

The mechanism of thermal decomposition has been postulated in previous studies. [36-39] according to the authors, the thermal decomposition of PE is a radical chain reaction. It can be separated into 3 steps, comparable to the polymerization of vinyl compounds, with an initiation step, a depropagation step and a termination step.

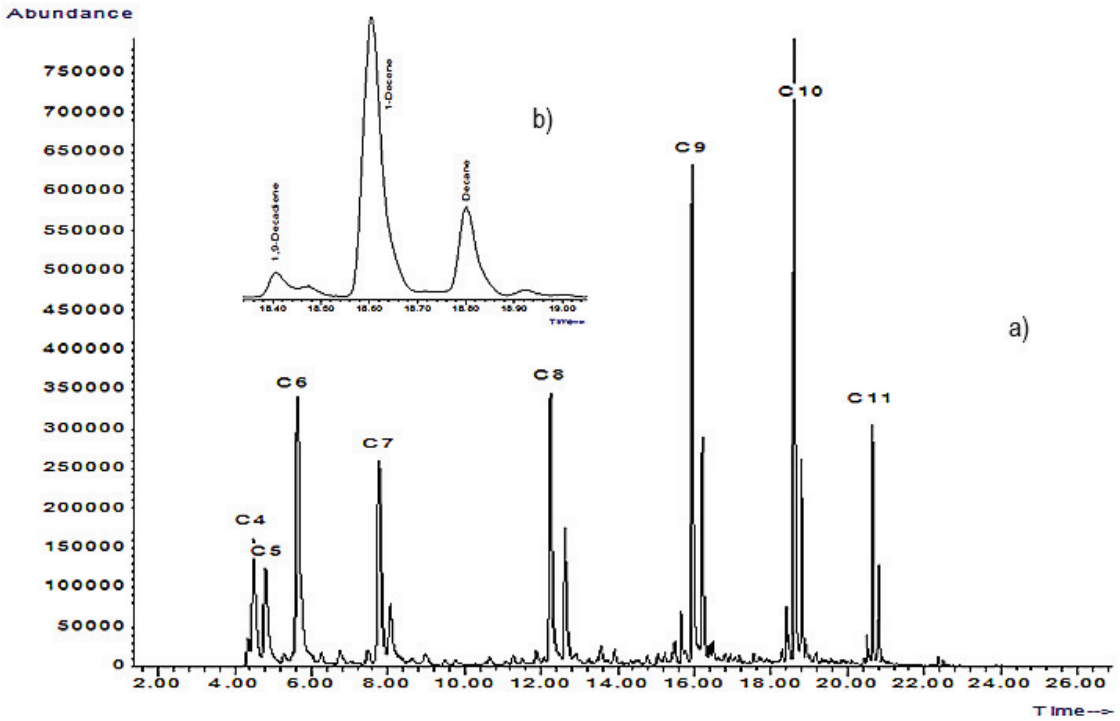
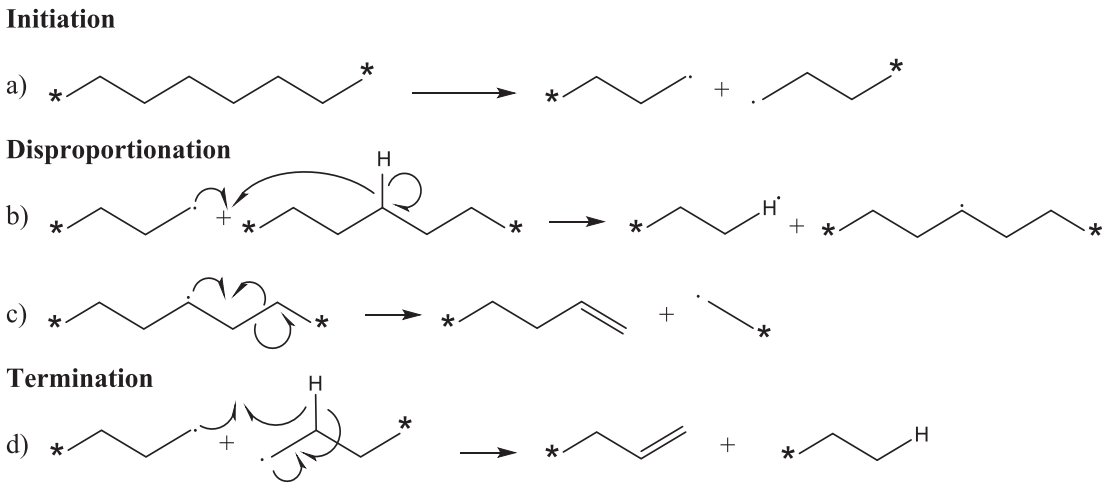


Figure 4-16: Mass spectrum (Total Ion Current) resulting from the thermal degradation of a HDPE polymer (sample 1). Each triplet consists of α, ω-diene, α-alkene and n-alkane at each carbon number. a) total spectrum b) zoom on C_{10}.



Scheme 4-4: HDPE decomposition into alkane and alkene a) thermal cleavage of HDPE into two radicals, b) intermolecular hydrogen transfer leading to an alkane fragment, c) β-scission of the radicals into α-alkene fragments d) radical disproportionation, in which 2 radicals form an alkane and an alkene fragment.

The decomposition starts with a thermal homolytic chain scission at random locations in the chain backbone and leads to two radicals (Scheme 4-4a). Once radicals are made, the polymers go through a depropagation step with a hydrogen transfer reaction, which leads to the creation of an *n*-alkane fragment and a new radical (Scheme 4-4b). Radicals can decompose by β-scission into α-alkene fragments (Scheme 4-4c). Finally, two radicals can react by coupling and disproportionation and lead to alkane and alkene fragments (Scheme 4-4d).

This mechanism explains well the formation of n-alkane and α-alkene fragments that we observed during the thermal decomposition of sample 1.

Figure 4-17 shows the amount of different main alkenes and alkanes observed corresponding to different temperatures during TGA experiment. Each substance was identified by MS and its amount was calculated from the peak intensity in the gas chromatogram (Figure 4-16).

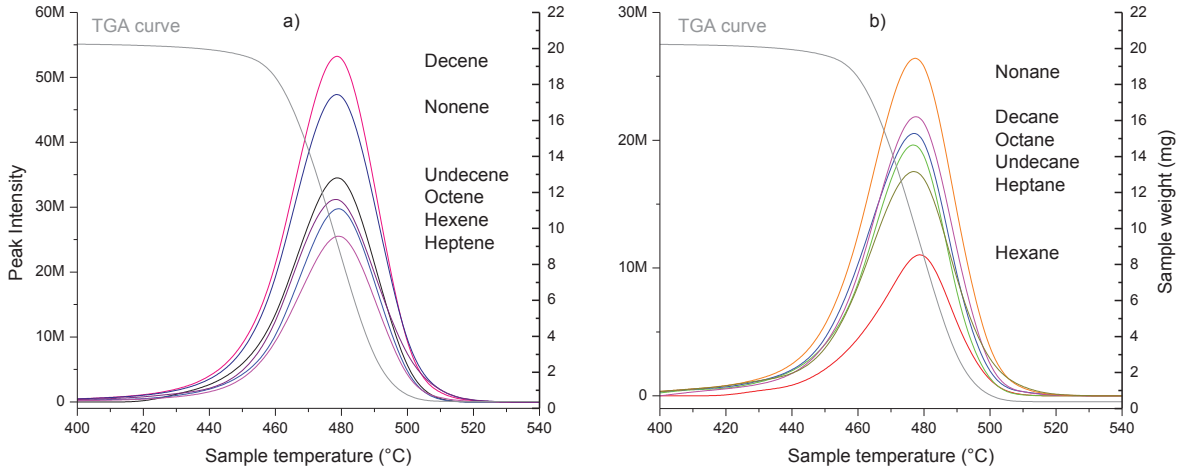


Figure 4-17: Emission profiles of a) alkenes and b) alkanes compounds from TGA analysis of sample 1 (HDPE). The left ordinate axis corresponds to the peak intensities in the gas chromatograms for each alkane and alkene component. The right ordinate axis refers to the TGA curve.

Minor amounts of cyclic compounds were also detected; in decreasing order, we found cyclopropane, cyclopentene, toluene, benzene, cyclohexene, cyclohexane and cyclopentane.

For this work, we will focus on the major alkane and alkene degradation products from C4 to C11. Table 4-16 shows the retention time of the mean peaks observed in the mass spectrum and the name of the corresponding fragments.

Table 4-16: Alkenes and alkanes compounds and corresponding retention time.

Compound	1-Butene / butane	1-Pentene/pentane	1-Hexene	Hexane	1-Heptene	Heptane	1-Octene	Octane	1-Nonene	Nonane	1-Decene	Decane	1-Undecene	Undecane
RT (min)	4.6	5.1	5.8	5.9	8.0	8.3	12.6	12.9	16.2	16.5	18.6	18.8	20.6	20.8

4.3.3.3 Thermal decomposition of ethylene-octene copolymer

Degradation profiles were obtained for the ethylene-octene copolymers (samples 2, 3 and 4) under conditions similar to those used for the reference sample.

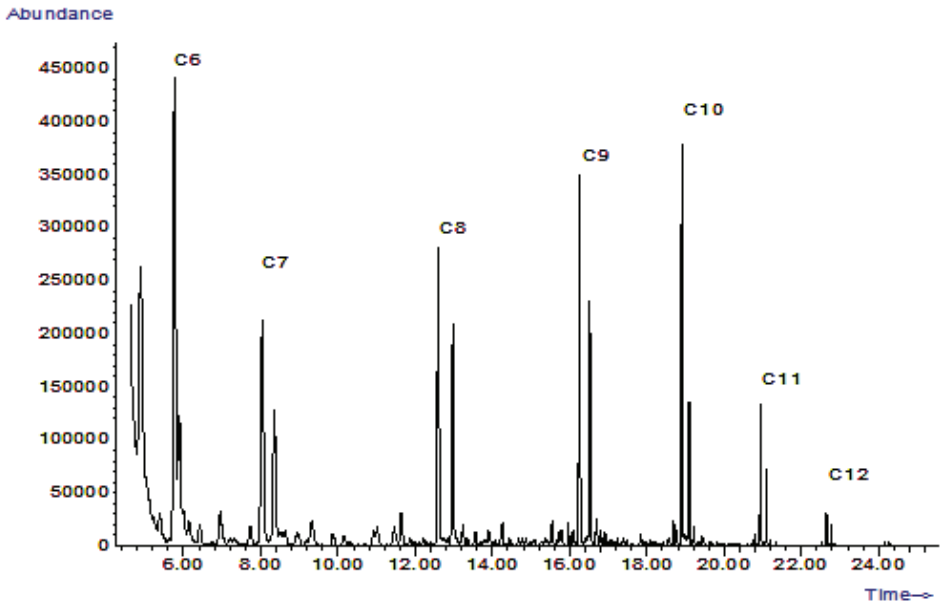
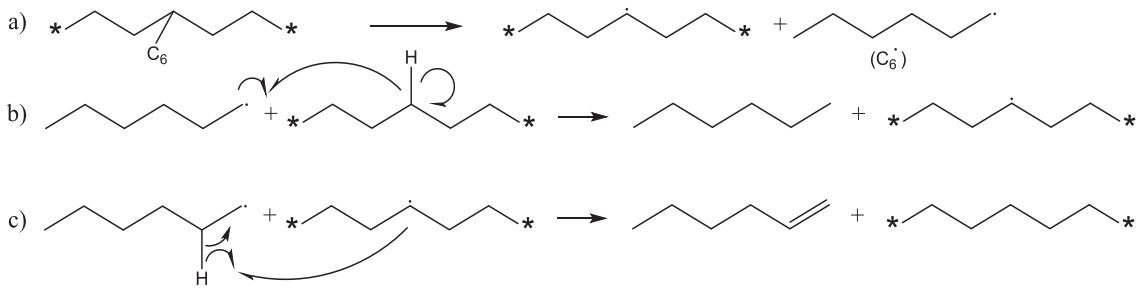


Figure 4-18: GC/MS result (extracted ion m/z = 41) for ethylene-octene copolymer, sample 3.

Similar to sample 1, the same distribution of three compounds (α, ω-diene, α-alkene, and *n*-alkane) were observed in Figure 4-18. In regard to LLDPE, new specific fragments predominate compared to the HDPE reference.



Scheme 4-5: Formation of hexane and hexene fragments for an ethylene-octene copolymer a) α scissions on a tertiary carbon atom, b) intermolecular hydrogen transfer leading to a hexane fragment, c) radical disproportionation, in which 2 radicals form an alkane and an hexene fragments.

The polymer chain breaks preferentially at the branches. This outcome relies on the branched structure of copolymers [40-42]. Ethylene-octene copolymers display hexyl branches (C_6). As a result of the scission of these branches, the C_6 fragments increased significantly in the mass spectra. According to the mechanism proposed in Scheme 4-5, these fragments result from the α scissions on a tertiary carbon atom.

Figure 4-19 clearly showed that C_6 compound (hexane and 1-hexene cumulated amounts), compared to other fragments, increase significantly as the octene content increases in the copolymer. We therefore considered that the C_6 compounds are the main signature of ethylene-octene copolymers.

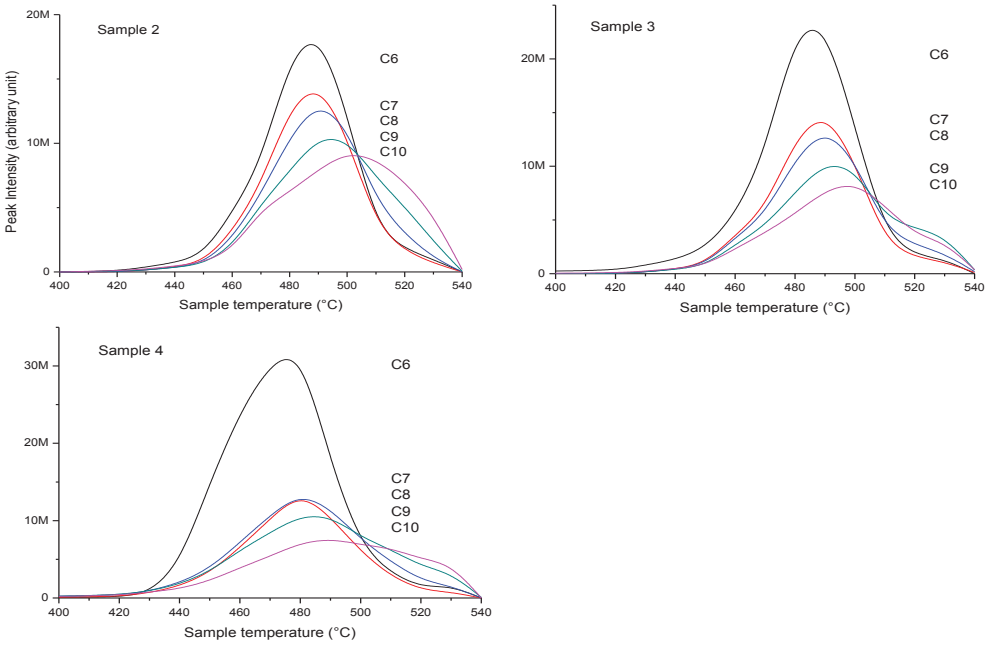


Figure 4-19: Emission profiles from the TGA analysis of ethylene-octene copolymers (sample 2, 3 and 4). The ordinate axis corresponds to the peak's intensities in the gas chromatograms for each component, alkane and alkene fragments were cumulated (C_6 = hexane and hexene fragments cumulated).

4.3.3.4 Thermal decomposition of ethylene-hexene copolymers

If C_6 fragments characterize ethylene-octene copolymers degradation, it would be expected that ethylene-hexene copolymers degradation would yield mainly to C_4 fragments. When analyzing ethylene-hexene copolymers (samples 5 to 8), a larger amount of C_4 compounds was identified in mass spectra as observed in Figure 4-20.

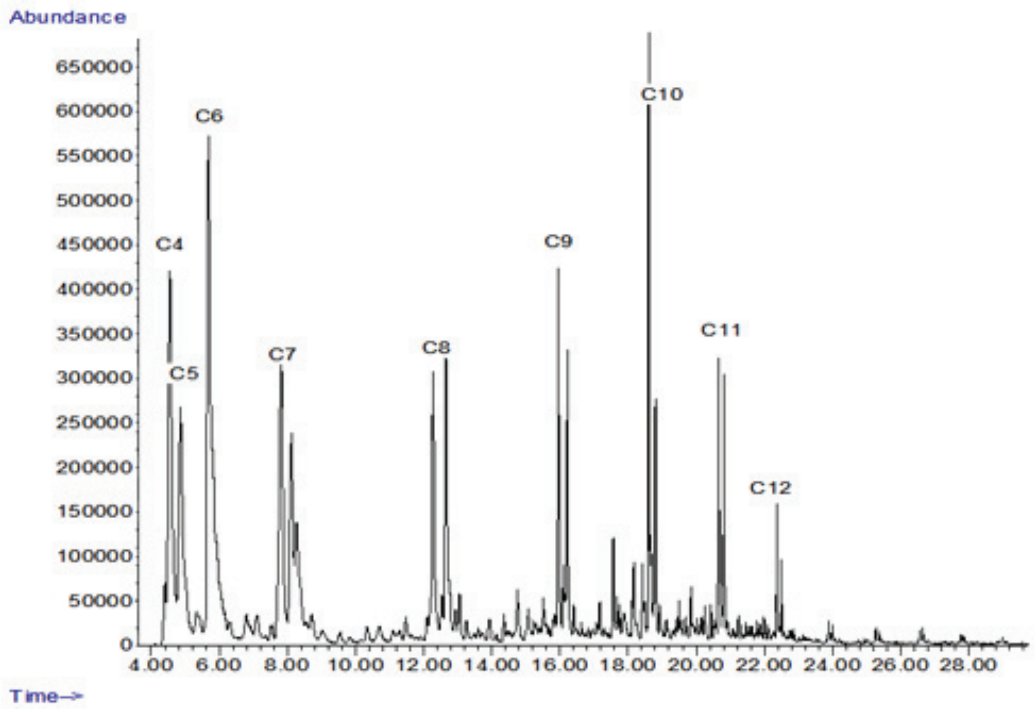


Figure 4-20: GC–MS result (extracted ion m/z = 41 or total ion current) for an ethylene-hexene copolymers, sample 8.

Indeed, the thermal decomposition of ethylene-hexene copolymers leads to more butane and 1-butene signals in the corresponding spectra and C_4 content increases significantly as the hexene content increases in the copolymer. This C_4 fragments were the result of α-scissions on the butyl branch and were obtained in a similar way as C_6 fragments previously proposed for ethylene-octene copolymers.

The scission mechanism proposed by Haney [36] supports the results observed with a main formation of C_4 compounds for ethylene-hexene copolymers and C_6 compounds for ethylene-octene copolymers.

Based on the strong correlation between the degradation products measured by TGA-IST16-GC-MS and the type of comonomer inserted into LLDPE, this method can provide very valuable information on the nature of branching. The sensitivity of this method is obviously high as low amount of comonomer, down to 0.5 mol% could be detected. Based on these results, our TGA-IST16-GC-MS system was calibrated and use in the following to efficiently quantify the amount of comonomer for unknown samples.

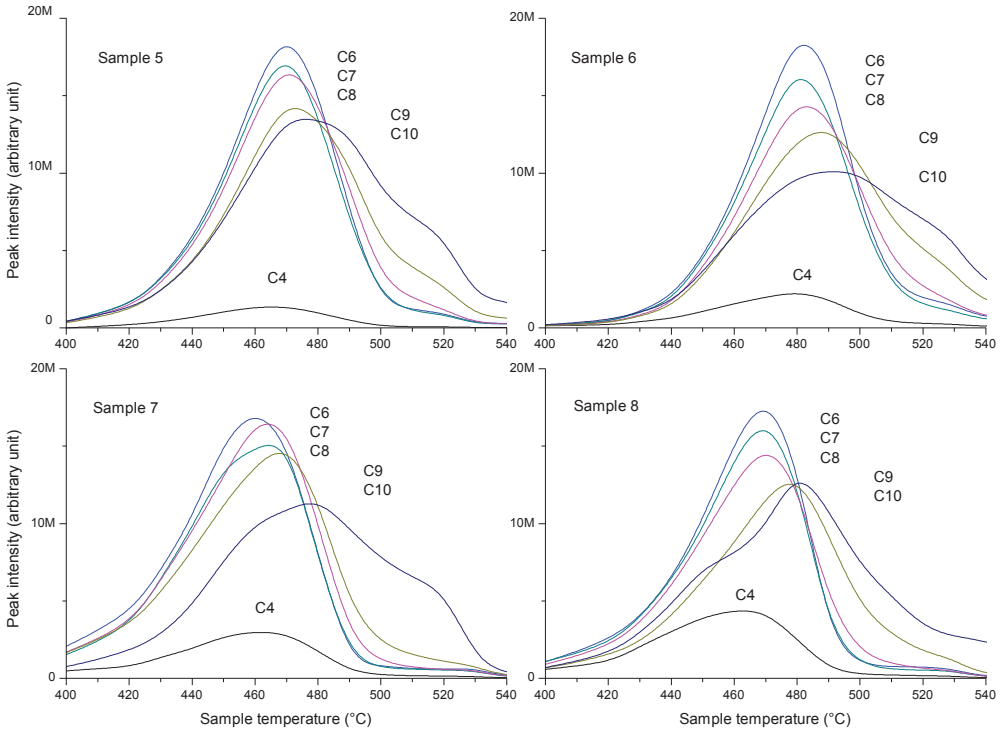


Figure 4-21: Emission profiles from the TGA analysis of ethylene-hexene copolymers (sample 5-8). The ordinate axis corresponds to the peak's intensities in the gas chromatograms for each component.

4.3.3.5 Quantitative calibration

Since 1-hexene and hexane could be separated in the mass spectrum of ethylene-octene copolymer, two separate calibrations were performed, one from the hexane fragments and the other from 1-hexene fragments.

Many parameters can affect the polymer degradation including the mass of samples, the contamination and the cleanliness of the system particularly of the transfer line. Thus, in order to normalize the peak intensities of hexane and 1-hexene, we used the peak of decane and 1-decene as internal standards, respectively. This assumes that decane and 1-decene were produced by the polymer backbone degradation independently of the comonomer content. Then, the area ratios obtained were plotted as a

function of the comonomer content previously determined by NMR (Table 4-15) to construct the calibration curves.

For ethylene-octene copolymers (samples 2-4), two curves were created. In Figure 4-22a, the curve based on alkane detection displays $\sum_{420°C}^{540°C} \frac{\text{area of hexane peak}}{\text{area of decane peak}}$ and the curve based on alkene detection displays $\sum_{420°C}^{540°C} \frac{\text{area of hexene peak}}{\text{area of decene peak}}$ versus the mole fraction of octene inserted in the copolymer and measured by NMR. Sample 1 was used as a reference and provided the background signal value of hexane and 1-hexene fragments for an unbranched polymer.

For ethylene–hexene copolymers (samples 5-8), only one curve was created because the butane and the 1-butene fragments were not resolved by GC-MS. The curve in Figure 4-22b shows $\sum_{420°C}^{540°C} \frac{\text{area of C4 peak}}{\text{area of C10 peak}}$ versus the mole fraction of hexene inserted in the copolymer and measured by NMR. Sample 1, which had no branching, was again used as a reference.

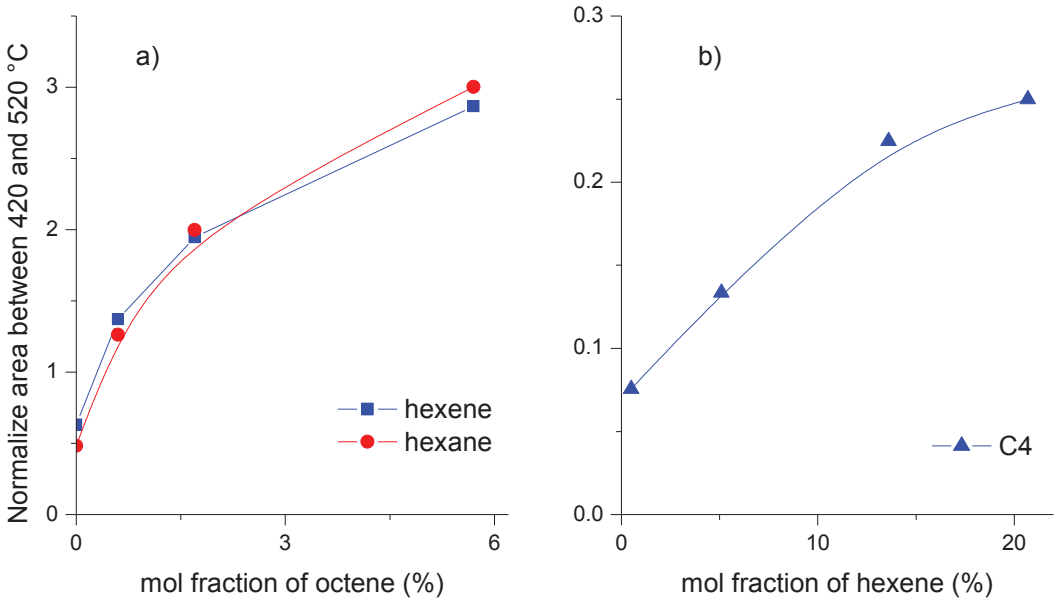


Figure 4-22: Calibration curve for a) ethylene-octene copolymers obtained with samples 2 to 4 b) ethylene-hexene copolymers obtained with samples 5 to 8. Hexene and hexane fragments measured during the degradation of ethylene-octene copolymers between 420°C and 540°C. C_4 fragments measured during degradation of ethylene-hexene copolymer between 420°C and 540°C.

The calibration curves show, that for low amounts of octene or hexene comonomers, the method is very

sensitive because the slope of the curve is very high. This slope decreases and apparently ends up reaching a plateau beyond 20 mol% of hexene.

4.3.4 CONCLUSIONS

The present paper describes a novel approach based on thermal degradation for the assessment of nature and degree of SCB in LLDPE samples. This method was applied for two classes of prepared homemade LLDPE. Ethylene-hexene and ethylene-octene copolymers were synthesized with a metallocene complex catalyst and characterized by HT-SEC and TREF to assess their homogeneity. SCB or comonomer content were measured by NMR. The TGA–IST16–GC–MS coupling system, working on an inert atmosphere, was used to provide further details on LLDPE composition. Its main advantage is that various LLDPE decomposition products can be identified and quantified despite the very complex decomposition mechanism. As previously described, alkane, alkene and diene fragments were observed from LLDPE degradation. In addition, we also observed aromatic compounds like benzene, toluene and cyclopentene.

This novel approach allows determining the nature and total content of SCB in copolymers. We demonstrated that during the degradation of LLDPE, a major detection of C_4 fragments or C_6 fragments was respectively signature of ethylene-hexene or ethylene-octene copolymers. With the help of a calibration created during this work, comonomer content could be determined. This method appears as a good substitute to NMR analysis that requires toxic solvent and long dissolution times.

The recycling process of plastic waste is of increasing economic and ecological importance. It is an objective that the recycling industry is trying to achieve. In order to identify different LLDPE to be recycled, the proposed approach can be effectively applied in a recycling process after specific separation step (flotation, magnetic, eddy currents…). LLDPE prepared by metallocene catalysis are of course simple samples with low chemical composition distribution and low molar mass dispersity. They have served as effective models for developing and validating the method. The study could be now generalized to more complex polyolefin like LLDPE resulting from heterogeneous catalysis or mixtures of different type of LLDPE as we can find during recycling process.

REFERENCES - CHAPTER 4.3

[1] W. D. Sauter, M. Taoufik, C. Boisson, *Polymers* **2017**, *9,185*.

[2] T. J. Hutley, M. Ouederni, *Polyolefin Compounds and Materials: Fundamentals and Industrial Applications*, M. Al-Ali AlMa'adeed and I. Krupa, Eds., Springer International Publishing, Cham, **2016**.

[3] M. M. Stalzer, M. Delferro, T. J. Marks, *Catal. Lett.* **2015**, *145*, 3.

[4] R. Mulhaupt, *Macromol. Chem. Phys.* **2003**, *204*, 289.

[5] M. P. McDaniel, *Adv. Catal.* **2010**, *53*, 123.

[6] J. C. Randall, *J. Polym. Sci. B* **1973**, *11*, 275.

[7] D. E. Dorman, E. P. Otocka, F. A. Bovey, *Macromolecules* **1972**, *5*, 574.

[8] W. Liu, P. L. Rinaldi, L. H. McIntosh, R. P. Quirk, *Macromolecules* **2001**, *34*, 4757.

[9] A. H. Willbourn, *J. Polym. Sci.* **1959**, *34*, 569.

[10] J. P. Blitz, D. C. McFaddin, *J. Appl. Polym. Sci.* **1994**, *51*, 13.

[11] E. Caro, E. Comas, *Talanta* **2017**, *163*, 48.

[12] A. Prasad, *Polym. Eng. Sci.* **1998**, *38*, 1716.

[13] L. Wild, C. Blatz, *New Adv. Polyolefins, New York* **1993**, 147.

[14] L. Wild, *Trends in Polymer Science* **1993**, *1*, 50.

[15] L. Wild, *Adv. Polym. Sci.* **1991**, *98*, 1.

[16] L. Wild, T. R. Ryle, D. C. Knobeloch, I. R. Peat, *J. Polym. Sci. B* **1982**, *20*, 441.

[17] B. Monrabal, J. Blanco, J. Nieto, J. B. P. Soares, *J. Polym. Sci. A* **1999**, *37*, 89.

[18] J. B. P. Soares, S. Anantawaraskul, *J. Polym. Sci. B* **2005**, *43*, 1557.

[19] T. Macko, R. Bruell, Y. Zhu, Y. Wang, *J. Sep. Sci.* **2010**, *33*, 3446.

[20] B. Monrabal, L. Romero, *Macromol. Chem. Phys.* **2014**, *215*, 1818.

[21] R. Cong, W. de Groot, A. Parrott, W. Yau, L. Hazlitt, R. Brown, M. Miller, Z. Zhou, *Macromolecules* **2011**, *44*, 3062.

[22] B. Monrabal, *Adv. Polym. Sci.* **2013**, *257*, 203.

[23] R. Chitta, T. Macko, R. Bruell, C. Boisson, E. Cossoul, O. Boyron, *Macromol. Chem. Phys.* **2015**, *216*, 721.

[24] E. Roumeli, A. Markoulis, T. Kyratsi, D. Bikiaris, K. Chrissafis, *Polym. Degrad. Stab.* **2014**, *100*, 42.

[25] S. Duc, N. Lopez, *Polymer* **1999**, *40*, 6723.

[26] T. Usami, Y. Gotoh, S. Takayama, H. Ohtani, S. Tsuge, *Macromolecules* **1987**, *20*, 1557.

[27] M. Statheropoulos, S. Kyriakou, A. Pappa, *Thermochim. Acta* **1999**, *329*, 83.

[28] S. Materazzi, R. Curini, *Appl. Spectrosc. Rev.* **2001**, *36*, 1.

[29] C. Larabi, W. a. Maksoud, K. C. Szeto, O. Boyron, A. Roubaud, P. Castelli, C. C. Santini, J. J. Walter, *J. Anal. Appl. Pyrolysis* **2013**, *100*, 81.

[30] J.-M. Letoffe, R. Chiriac, C. Sigala, J. Carre, *Spectra Anal.* **2004**, *33*, 37.

[31] W. Kaminsky, R. Steiger, *Polyhedron* **1988**, *7*, 2375.

[32] W. Kaminsky, A. Laban, *Appl. Catal., A* **2001**, *222*, 47.

[33] V. F. Tisse, C. Boisson, T. F. L. McKenna, *Macromol. Chem. Phys.* **2014**, *215*, 1358.

[34] E. Cossoul, L. Baverel, E. Martigny, T. Macko, C. Boisson, O. Boyron, *Macromol. Symp.* **2013**, *330*, 42.

[35] B. Monrabal, *Encyclopedia of Analytical Chemistry*, R. A. Meyers, Ed., John Wiley & Sons Ltd., **2000**.

[36] M. A. Haney, D. W. Johnston, B. H. Clampitt, *Macromolecules* **1983**, *16*, 1775.

[37] Y. Sugimura, S. Tsuge, *Macromolecules* **1979**, *12*, 512.

[38] R. Simha, L. A. Wall, P. J. Blatz, *J. Polym. Sci.* **1950**, *5*, 615.

[39] L. A. Wall, S. Straus, *J. Polym. Sci.* **1960**, *44*, 313.

[40] U. Hujuri, A. K. Ghoshal, S. Gumma, *Waste Manag.* **2010**, *30*, 814.

[41] H. Bockhorn, A. Hornung, U. Hornung, D. Schawaller, *J. Anal. Appl. Pyrolysis* **1999**, *48*, 93.

[42] T. Shin, O. Hajime, *Applied Pyrolysis Handbook*, CRC Press, **2006**.

FULL PAPER

Macromolecular Chemistry and Physics
www.mcp-journal.de

Chemical Composition of Hexene-Based Linear Low-Density Polyethylene by Infrared Spectroscopy and Chemometrics

Olivier Boyron, Manel Taam, and Christophe Boisson*

Mid and near infrared (MIR and NIR) spectroscopy associated with the partial least squares (PLS) method makes it possible to rapidly characterize the composition of linear low-density polyethylene (LLDPE) in a large range of 1-hexene content from 0 to 21 mol%. LLDPEs are produced using zirconocene catalysts activated with methylaluminoxane. PLS regression methods for MIR and NIR are constructed from this series of LLDPEs to quantify the 1-hexene content in unknown copolymers. In this case, the PLS regression method aims to correlate the 1-hexene content in the copolymers with their IR spectra. Multivariate calibration models are constructed by the PLS algorithm on pretreated data of MIR and NIR analyses. They are tested and validated by comparing results obtained by nuclear magnetic resonance and the PLS analyses for four unknown ethylene-1-hexene copolymers.

1. Introduction

With an annual global production of approximately 100 million tons, polyethylenes (PEs) are the main commercial polymeric materials.[1,2] They are typically classified into three main families such as high-density polyethylene (HDPE; 0.940 to 0.970 g cm^{-3}), low-density polyethylene (LDPE; 0.910 to 0.940 g cm^{-3}), and linear low-density polyethylene (LLDPE; 0.916 to 0.940 g cm^{-3}). HDPE has no or only a small amount of branching, LDPE contains a combination of long (>C_6) and short chain branching (SCB), while the branching in LLDPE is predominantly from short chain branching. This last one is synthetized by copolymerization of ethylene and an α-olefin which allows the insertion of a short-chain branching into the main chain and thus impacts the crystallinity of the material.[3] The frequently used α-olefins are 1-butene, 1-hexene, and 1-octene.[1,4] The crystallinity and then the physical properties of LLDPE can be adjusted using different content of comonomer.[5,6] Consequently, it is highly relevant to quantify the amount of comonomer units incorporated into LLDPE during the polymerization process.

Various analytical techniques have been developed to quantify the short chain branching content. It has been widely investigated using spectroscopy like Fourier transform infrared (FTIR)[7–10] and proton and carbon nuclear magnetic resonance (H-NMR and ^{13}C-NMR).[11–14] Liquid chromatography based on crystallibility of polyolefins has been established by Wild, Monrabal, Soares, and Pasch through temperature rising elution fractionation (TREF)[15–19] and crystallization analysis fractionation (CRYSTAF).[20,21] However, these techniques cannot be used for the separation of amorphous fractions of the polymers. The combination of high-temperature liquid chromatography with a Hypercarb column operating with a temperature gradient[22–27] was introduced by Cong and Macko and allows the analysis of amorphous polymers. These high-temperature fractionation techniques were able to determine the chemical composition distribution (CCD) of LLDPE. In addition, thermal analysis coupled with mass spectrometry[28–31] has been employed to measure the branching type and the content of α-olefins in LLDPE.

However, these approaches are time consuming due to the sample preparation (dissolution at high temperature with toxic solvent) for most techniques and the time required to record and process the data. In many instances, for example, in the case of high throughput experiments or during recycling process, it is desirable to determine the polymer composition in a shorter time.

Infrared spectroscopy is a consistent and an essential analytical method for exploring polymer composition.[32,33] More specifically, FTIR spectroscopy in attenuated total reflection mode (ATR-FTIR)[34–36] and near infrared (NIR)[37–39] equipped with an integrating sphere might be advantageous for measuring the chemical composition of LLDPE, as inexpensive sample preparation is sufficient for theses technique. While many previous studies[9,40,41] are based on absorbance attributable to branch type, there are few publications on quantitative studies.[7,42,43] In the work of Blitz and McFaddin,[7] FTIR calibration for different branch type (methyl, ethyl, butyl, hexyl) in LLDPE based on absorption of only one wavelength was reported. Sano et al. and Shimoyama et al. described methods to predict density in

O. Boyron, M. Taam, Dr. C. Boisson
Université de Lyon, Université Lyon 1
CPE Lyon
CNRS UMR 5265
Laboratoire de Chimie Catalyse Polymères et Procédés (C2P2)
Equipe LCPP, Batiment 308F, 43 Bd du 11 Novembre 1918, F-69616
Villeurbanne, France
E-mail: olivier.boyron@univ-lyon1.fr

The ORCID identification number(s) for the author(s) of this article can be found under https://doi-org.docelec.univ-lyon1.fr/10.1002/macp.201900376.

DOI: 10.1002/macp.201900376

© 2019 WILEY-VCH Verlag GmbH & Co. KGaA, Weinheim

FULL PAPER

Chemometrics

Macromolecular Chemistry and Physics
www.mcp-journal.de

Rapid Determination of the Chemical Composition of Ethylene/Butadiene Copolymers Using FTIR Spectroscopy and Chemometrics

Olivier Boyron, Benoît Macqueron, Manel Taam, Julien Thuilliez, and Christophe Boisson*

Fourier transform infrared spectroscopy by attenuated total reflection (ATR-FTIR), combined with the partial least square (PLS) method provides a fast characterization of ethylene/butadiene copolymers' intricate composition. The PLS regression method is constructed to quantify ethylene, 1,2-butadiene (vinyl), *trans*-1,4-butadiene, and 1,2-cyclohexane units in the copolymer. These rings are formed by intramolecular cyclization during polymerization. The performance of PLS models is evaluated by comparing the result obtained by ^{13}C NMR and the model for three unknown samples. It is shown that the proposed method allows to accurately estimate the chemical composition of ethylene/butadiene copolymers in a much shorter time than NMR.

1. Introduction

Neodymium metallocenes are unique catalysts for the copolymerization of ethylene with butadiene. A new class of elastomers was obtained using metallocene complexes of supported by *ansa*-bis(fluorenyl) neodymium complexes in combination with MgR_2.[1,2] These elastomers obtained with readily available monomers (ethylene and butadiene) display an intricate and original microstructure. The butadiene insertion leads to unsaturated moieties consisting of unsaturated groups: internal *trans* double bonds and vinyl branches. In addition, this insertion leads to the formation of 1,2-cyclohexane rings. These rings are formed by a mechanism of intramolecular cyclisation involving vinyl units.[1,2] Properties of the ethylene/butadiene copolymers are directly linked to their composition and consequently it is highly relevant to fully characterize their chemical composition. The characterization of these polymers was performed by ^{1}H and ^{13}C NMR analyses.[3,4] NMR investigations permitted an accurate determination of the chemical composition of these copolymers. However, these analyses are reliable and accurate but are time consuming due to the sample preparation, the time required to record the spectrum and process the data. In many instances, for example in the case of high throughput experiments, it is desirable to determine the polymer composition in a shorter time.

Infrared spectroscopy is a consistent and an essential analytical method for exploring polymer composition.[5–9] More specifically, Fourier transform infrared spectroscopy in attenuated total reflection mode (ATR-FTIR)[10–12] might be advantageous for measuring the chemical composition of ethylene/butadiene copolymers as this technique requests straightforward sample preparation. Because structural changes in aliphatic ethylene/butadiene copolymers, cause low modifications in FTIR spectra, the use of chemometrics techniques are required to highlight differences in the polymer spectra. Partial least-squares (PLS) regression is a popular algorithm and generally used to improve the resolution of signals that can be superimposed in complex materials.[13–17] In particular, MIR spectroscopy combined with PLS methods is used to develop quantitative determination of copolymer composition.[18,19]

A combination of ATR-FTIR spectroscopy and chemometric tools was developed in the present article to quantify the chemical composition of ethylene/butadiene copolymers. The FTIR was calibrated by using NMR as a direct technique for measuring copolymer composition.

O. Boyron, Dr. B. Macqueron, M. Taam, Dr. C. Boisson
Université de Lyon
Univ. Lyon 1
CPE Lyon
CNRS UMR 5265
Laboratoire de Chimie Catalyse Polymères et Procédés (C2P2)
Equipe LCPP
Bat 308F, 43 Bd du 11 Novembre 1918, F-69616 Villeurbanne, France
E-mail: olivier.boyron@univ-lyon1.fr
Dr. B. Macqueron, Dr. J. Thuilliez
MFP Michelin
23 Place des Carmes Dechaux 63040, Clermont-Ferrand, France
The ORCID identification number(s) for the author(s) of this article can be found under https://doi-org.docelec.univ-lyon1.fr/10.1002/macp.201700609.

DOI: 10.1002/macp.201700609

2. Experimental Section

2.1. Materials

Three neodymium metallocene complexes were selected: $[Me_2(C_{13}H_8)_2Nd(BH_4)_2Li(THF)]_2$ (**1**), $[Me_2Si(C_5H_4)(C_{13}H_8)Nd(BH_4)_2][Li(THF)]$ (**2**), and $[Me_2Si(C_5Me_4)(C_{13}H_8)Nd(BH_4)]$ (**3**). The preparation of complexes **1** and **2** was reported previously.[1,2,20,21] Complex **3** was obtained as a green powder by reaction of $Me_2Si(C_{13}H_8)(C_5Me_4)Li_2Et_2O$[22] with $Nd(BH_4)_3(THF)_3$ in tetrahydrofuran (THF).

© 2018 WILEY-VCH Verlag GmbH & Co. KGaA, Weinheim

FULL PAPER

Polyolefin Characterization

Macromolecular Chemistry and Physics
www.mcp-journal.de

An Advanced Technique for Linear Low-Density Polyethylene Composition Determination: TGA–IST16–GC–MS Coupling

Olivier Boyron, Tiffany Marre, Alain Delauzun, Ronan Cozic, and Christophe Boisson*

An innovative method based on thermogravimetric analysis combined with gas chromatography and mass spectrometry, TGA–IST16–GC–MS, is developed for measuring the comonomer type and the comonomer content in a series of linear low-density polyethylenes (LLDPE). LLDPE such as copolymers of ethylene and octene or ethylene and hexene are synthetized using the $Et(Ind)_2ZrCl_2$ zirconium-metallocene catalyst. Their characterization with TGA-IST16-GC-MS system is compared to one of the polyethylenes prepared under similar conditions and used as reference. TGA-IST16-GC-MS allows discriminating the comonomer type (hexene or octene) and content. Combining the versatility of thermal analysis and the accuracy and sensitivity of mass spectrometry, this original method proves to be very useful for routine characterization of LLDPE. It has the advantage of being quicker and more easily performed that traditional means of obtaining copolymer compositions such as nuclear magnetic resonance, or through separation techniques such as temperature rising elution fractionation (TREF).

1. Introduction

Polyethylenes (PEs), which include low-density polyethylene (LDPE), linear low-density polyethylene (LLDPE), and high-density polyethylene (HDPE), constitute the most common industrial class of synthetic polymers with an annual global production of approximately 100 million tons.[1,2] LLDPE is produced by copolymerization of ethylene with an α-olefin which introduces short-chain branching (SCB) and thereby decreases the crystallinity of final polymer.[3] The most commonly used α-olefins for this purpose are 1-butene, 1-hexene, and 1-octene[4,5] which allow fine tuning of the crystallinity and thereby the properties of resulting polyolefin. The suitability for different applications can be achieved just by variation of the comonomer content. Therefore, it is of high interest to measure the amount of comonomer units (or SCB) incorporated into the PE chains.

Various analytical methods have been employed to determine the nature and degree of SCB. Spectroscopic methods like carbon-13 nuclear magnetic resonance ^{13}C-NMR[6–8] and infrared (IR)[9–12] have been widely developed to measure SCB. More recently liquid chromatography based on crystallization and thermal fractionation has been developed by Wild, Monrabal, Soares, Cong, and Macko through temperature rising elution fractionation (TREF),[13–15] crystallization analysis fractionation (CRYSTAF)[13,15–18] and interactive liquid chromatography.[19–23] Thermal analysis with pyrolysis–GC[24–26] has been also employed to measure branching in PE.

This work proposes a new method based on thermogravimetric analysis (TGA). TGA is generally associated to mass spectrometry (MS)[27] and IR spectroscopy[28,29] in order to identify the gaseous compounds emitted during thermal decomposition. However, for polymer with complex microstructures like LLDPE, IR and direct MS cannot unambiguously determine the nature of most components of gas mixtures. In these cases, coupling TGA with GC–MS offers promising advantages. The emitted compounds are first separated by GC, then identified and quantified by MS.

In this paper, an innovative coupling technic is introduced, which significantly increases the number of data points collected. It combines TGA, GC-MS, and an innovative gas-storage interface (IST16) with a 16-loop fractions collector inserted between the TGA and the GC.[30] The analytical tool is called hereafter TGA-IST16-GC-MS and provides an efficient way to take advantage of the MS technique.

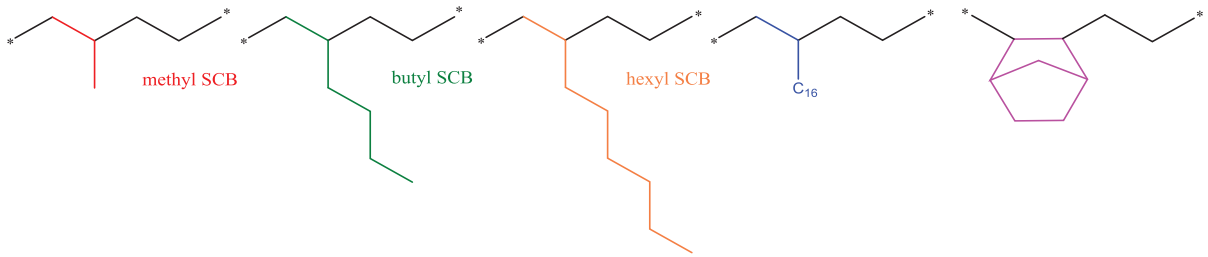
Copolymers containing various proportions of 1-hexene and 1-octene were prepared using the zirconium catalyst *rac*-$Et(Ind)_2ZrCl_2$ activated with methylaluminoxane (MAO).[31–33] The average composition of the copolymers obtained was then elucidated using TREF, ^{1}H, and ^{13}C-NMR spectroscopy. Subsequently, the copolymers were further investigated by TGA–IST16–GC–MS.

O. Boyron, Dr. C. Boisson
Université de Lyon
Univ. Lyon 1, CPE Lyon, CNRS UMR 5265
Laboratoire de Chimie Catalyse Polymères et Procédés (C2P2), Equipe CPP, Bat 308F
43 Bd du 11 Novembre 1918 69616, Villeurbanne, France
E-mail: olivier.boyron@univ-lyon1.fr
T. Marre, A. Delauzun, Dr. R. Cozic
SRA Instruments
210 rue des Sources 69280, Marcy l'Etoile, France
The ORCID identification number(s) for the author(s) of this article can be found under https://doi-org.docelec.univ-lyon1.fr/10.1002/macp.201900162.

DOI: 10.1002/macp.201900162

 © 2019 WILEY-VCH Verlag GmbH & Co. KGaA, Weinheim

GENERAL CONCLUSION



Thanks to the development in polymerization chemistry based on the design of single-site catalysts, and advances in polymer engineering with the use of cascade reactor systems, the properties and performances of polyolefins can be tuned and optimized for specific applications. The chains structures of tailor-made polyolefin have become even more complex. These remarkable advances present great challenges for characterization. Indeed, the measurement of average chemical content by NMR and density by melt flow index is not enough to predict the polymer properties. We should access to complete molar mass distribution (MWD) and chemical composition distribution (CCD) of polyolefins.

To achieve these objectives, original tools, invented by talented researchers such as Monrabal, Soares, Cong, Pasch, Brull and Macko, have been commercialized. This PhD work focuses on the implementation and development of methods based on thermal fractionation techniques that allow access to CCD in LLDPE.

All these fractionation techniques are based on the separation of polymer chains by crystallization or by interaction on a column. These techniques are relative techniques, which must be calibrated by correlating the crystallization or elution temperature with the comonomer content in order to obtain quantitative information.

To achieve these objectives, several sets of ethylene/α-olefin copolymers synthesized with metallocene catalysts under controlled conditions were prepared and used as standard. Eighty-eight LLDPE samples were synthesized and characterized by NMR to measure the levels of inserted comonomer. As the type of comonomer has an impact on separation, several samples with different types of comonomers (propene, hexene, octene, norbornene, octadecene) and different levels of comonomers (up to 20%) were used to calibrate the fractionation technique, each leading to an equation appropriate for the different types of LLDPE. These calibration curves are brought together for the first time in a single work. They have been and will be used to access the chemical composition distribution (CCD) of polyethylenes (HDPE and LLDPE) with heterogeneous composition as shown in Figure 1.

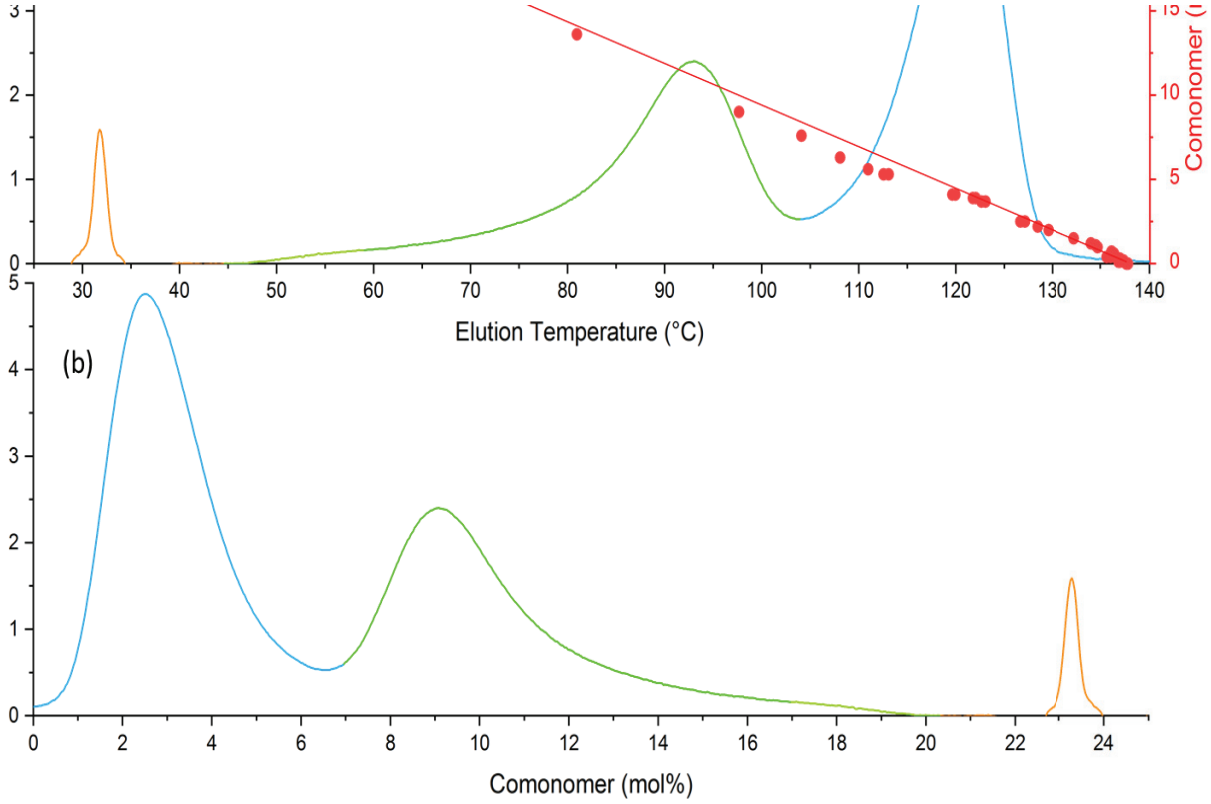


Figure C1: Chromatogram acquired by TGIC for a heterogeneous sample (a) and chemical composition distribution curve obtained from the calibration (b). Calibration for ethylene/hexene copolymers.

Parallel to this calibration work, investigations have shown certain characteristics specific to each technique.

1- The effect of molar mass on separation was studied. As reported by several researchers, a low molar mass has an impact on the elution time, but we also observed that a very high molar mass (higher than 10^6 g mol^{-1}) also has an impact on the elution time. The specific organization of crystallites in the case of high molar masses shifts the elution temperatures upwards, especially for CEF.

2 - The TGIC profiles of the LLDPE models have been compared to that of CEF profiles. The TGIC chromatograms were broader than the CEF profiles, indicating a poorer resolution mainly for low comonomer contents. Conversely, TGICs offer a wider analytical range.

3- The CCD analysis range derived from SGIC was broader than those obtained with CRYSTAF. The physical principles underlying the two methods are different: CRYSTAF is based on crystallization and SGIC on polymer adsorption-desorption. Consequently, SGIC is applicable to the whole composition range of LLDPE

(from 0 to 100% of comonomer), whereas crystallization-based techniques are limited to semi-crystalline components.

4- A new thermodynamic framework to understand the fractionation mechanism in TGIC was proposed. Using simulation methods, we have discussed the enthalpic and entropic interactions between LLDPE chains and the graphene column. The adsorption energy of various samples of LLDPE on graphene at different temperatures was calculated, showing that the steric hindrance of the comonomer (or SCB) reduces the number of contacts between the polymer chain and graphene and thus the enthalpy of adsorption. When the density of the comonomer is low, the measured adsorption energy remains negative (favorable for adsorption) above the elution temperature of the polymer. However, for this polymer, an increase in persistence length is observed during adsorption. The increase in persistence length would decrease the conformational entropy of the polymer and thus counteract the favorable adsorption energy. This entropic contribution could explain the narrowing of the peak observed experimentally for a low density of comonomers, at a high elution temperature. This model accurately reproduced the elution temperatures measured experimentally by the TGIC.

We have shown that fractionation techniques are unique ways to access distribution in chemical composition. However, these separation techniques are considered as a demanding task due to the requirement of toxic solvents and high temperature for sample dissolution. In this context, care must be taken to ensure that the polymer is properly dissolved and to avoid any degradation. This delicate preparation requires long analysis times. It was of real interest for research and analysis laboratories to develop in parallel faster and simpler techniques to access the chemical composition.

The LLDPE models, which are well defined and well characterized, have thus been used for the development of alternative methods for measuring chemical composition. Spectrometry techniques, widely used by research laboratories, have been considered as alternative tools. We are particularly interested in FTIR and in the coupling of thermal analysis to mass spectrometry.

FTIR has been used for many years for polyolefin characterization. The development of chemometrics (mathematical and statistical tools to obtain information from a large amount of data) allows a new approach in the exploitation of the obtained spectra. Chemometrics makes it possible to obtain information on polymers by observing all the significant wavelengths of the information sought. We have shown that it can be efficiently applied both in the mid-infrared and near-infrared on LLDPE but also on other types of copolymers such as ethylene/butadiene which have complex microstructures. Our model

polymers have been used to build chemometric methods, applied to IR spectra, for the prediction of comonomer content in unknown samples. As they are fast, simple and without sample preparation, these chemometric methods have shown their great potential to characterize polymers.

Lastly, the coupling of thermo-gravimetric analysis (TGA) with mass spectrometry has revealed its full potential for understanding the structure of LLDPE. The coupling allowed, by thermal degradation, to obtain significant fragments of the analyzed LLDPE which are then identified by mass spectrometry. This method allows the identification of the type of α-olefins used during the synthesis.

This thesis work shows on the one hand the unique contribution of thermal fractionation techniques to access the CCD and on the other hand the power of spectrometry to quickly obtain the average chemical composition of olefin copolymers.

All these methods developed allow us to better identify the structure of the polyolefins synthesized in our laboratory, to better understand the chemical mechanisms that take place during the different stages of polymerization, and to efficiently enhance the polymerization processes. These tools will benefit the current and future research topics of the laboratory, the research work of my fellow researchers and my industrial partners who wish to better understand the materials they have produced and used.

Beyond the synthesis of our LLDPE models, the main contributions of this thesis in the field of polyolefin characterization are summarized below and in Figure C2:

- ^{1}H NMR and ^{13}C NMR methods were described to measure the comonomer content.
- High temperature was implemented:
    - for the molar masses' determination
    - for long chain branching measurement
    - for short chain branching measurement
- Method to measure comonomer content by DSC through melting and crystallization temperature and melting and crystallization enthalpy were constructed.
- We have calibrated different thermal fractionation techniques.
    - based on crystallization (CRYSTAF, TREF, CEF)

- based on interactions (TGIC, SGIC)

A complete table of calibration curve for all fractionation techniques and for a wide range of LLDPE (propylene, hexene, octene, octadecene, norbonene) is now available.

Finally, our well-defined LLDPE models were also used to develop original spectrometric methods.

- The combination of FTIR and chemometrics has proven to be a rapid method for measuring the comonomer content in polyolefins.
- The coupling of TGA and mass spectrometry has proven to be a valuable tool to access the type of comonomer.

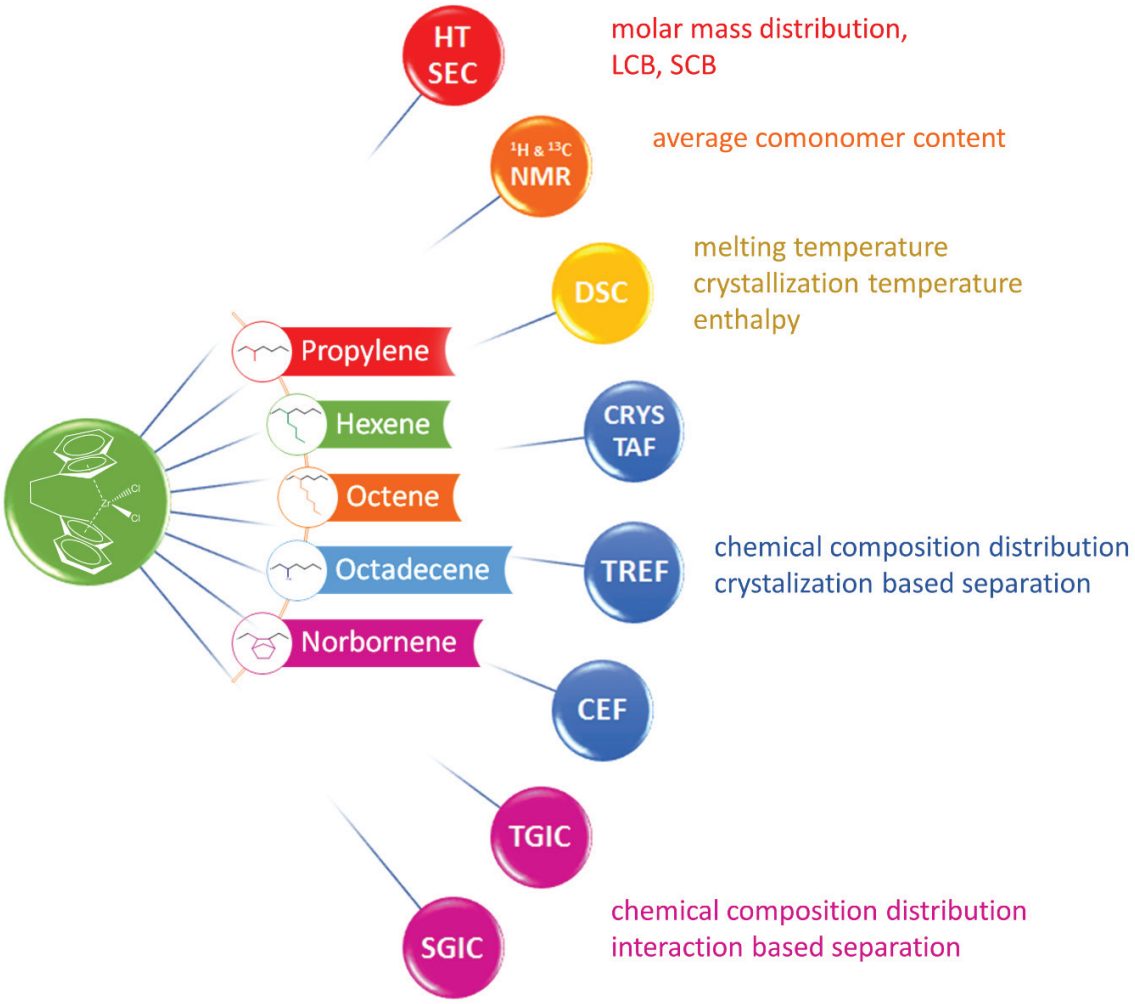


Figure C2: Overview of the thesis work carried out from the synthesis of different types of ethylene/α-olefin copolymers with a metallocene catalyst to the calibration of thermal fractionation techniques.

This work has opened up new routes for analysis of polyolefins.

Other copolymers are currently being studied by thermal fractionation techniques:

- Ethylene/vinyl acetate copolymers

Ethylene/vinyl acetate (EVA) copolymers are important commercial polymer materials. Their properties can be adjusted according to the vinyl acetate content, so it is necessary to precisely quantify the comonomer content. Different methods can be used to analyze the average chemical composition of EVAs such as NMR, TGA and FTIR. In future work, a new method will be developed to measure by thermal fractionation the chemical composition and especially its distribution. TGIC appears to be appropriate for separating EVA copolymers according to their composition.

- Ethylene/butadiene copolymers

Ethylene/butadiene copolymers are elastomers obtained from simple monomers but have a complex and original structure. Indeed, the insertion of butadiene leads to unsaturated fragments (internal trans double bonds and vinyl branches) as well as 1,2-cyclohexyl rings. The properties of these elastomers are directly related to their composition and it is therefore important to fully characterize their chemical composition. The ability of these fragments to interact with the TGIC column has not yet been demonstrated.

The ability to use other analytical techniques to measure the comonomer content in LLDPE is being explored using our LLDPE models:

- Rheology

Rheology is generally used to obtain information about LCB on polyolefins but few publications describe the effect of SCB on rheological behavior. Our LLDPE models will be measured by rheology to assess the impact of short chain branching. This work will provide calibration curves for rheology and show that it is possible to predict the co-monomer content in LLDPE using rheological measurements. The first measurements of the branch contents predicted from the zero shear viscosity analysis of the samples are in good agreement with those evaluated by NMR.

- Raman spectroscopy

Raman spectroscopy is a powerful technique for qualitative and quantitative analysis, it is non-destructive and can be integrated into industrial applications. It offers several advantages over other conventional spectroscopic techniques, for instance Raman spectra have intense and well resolved spectral peaks.

These peaks often correspond to fundamental transitions and thus provide direct and easy-to-interpret chemical information. Our LLDPE models will be analyzed by Raman spectroscopy in order to construct a new PLS model for the prediction of comonomer content in unknown samples. The use of statistics and chemometrics is also essential to the success of this project.

Applications

- Industrial applications

The methods developed in this work have been used regularly for industrial partners to better understand the materials they use or synthesize. The comonomer content for LLDPE as well as the PE or PP content in the case of a mixture are recurrently measured by thermal fractionation techniques and through the calibrations set up. For example, the methods have been applied as part of analytical services for various industrial companies to characterize polyolefin cosmetic bottles, electrical cable jacketing, and food and medical packaging.

- Plastic in ocean

Working in the polymer field is very fascinating and I really believe in the benefits of plastics for our future society. I also believe that we have not been able to manage our waste, especially plastics, and that it is now high time to change our behavior. Therefore, it is quite natural that I am also involved in the issue of plastics pollution in the oceans.

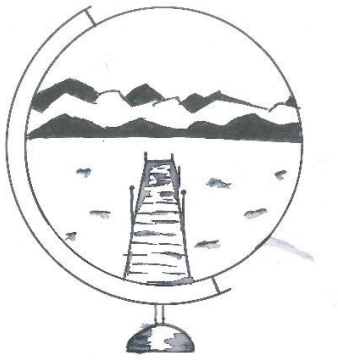
The characterization of plastic marine debris is necessary to better understand their fate in the environment and their interaction with organisms. These marine debris are mainly composed of polyolefins. In this field, I am working on the characterization of plastic debris collected in the subtropical gyre of the north Atlantic during the “Expedition 7th Continent” maritime campaign.[1-3] These thesis works will most likely find new and concrete applications to face these societal challenges.

REFERENCES

[1] A. ter Halle, L. Ladirat, M. Martignac, A. F. Mingotaud, O. Boyron, E. Perez, *Environ. Pollut. (Oxford, U. K.)* **2017**, *227*, 167.

[2] C. J. Garvey, M. Impéror-Clerc, S. Rouzière, G. Gouadec, O. Boyron, L. Rowenczyk, A. F. Mingotaud, A. ter Halle, *Environmental Science & Technology* **2020**, *54*, 11173.

[3] L. Rowenczyk, A. Dazzi, A. Deniset-Besseau, V. Beltran, D. Goudounèche, P. Wong-Wah-Chung, O. Boyron, M. George, P. Fabre, C. Roux, A. F. Mingotaud, A. T. Halle, *Environ Sci Technol* **2020**, *54*, 4102.



APPENDIX - LIST OF LLDPE MODELS

Sample	α-olefin		T_m	ΔH_f	T_c	ΔH_c	X	$\bar{M}_n$	$\bar{M}_w$	Đ	Log[η]
		mol%	°C	J g^{-1}	°C	J g^{-1}	%	Kg mol^{-1}	Kg mol^{-1}		dL g^{-1}
ECP1	propylene	9.1	92.3	76.2	71.1	70.4	26.0	29.5	50.1	1.7	
ECP2	propylene	4.2	115.0	135.4	98.6	89.0	46.2	33.0	59.4	1.8	
ECP3	propylene	2.3	121.9	173.0			59.0	33.1	62.9	1.9	
ECP4	propylene	5.0	109.0	138.0	93.0	73.8	47.1	26.2	53.0	2.0	
ECP5	propylene	2.7	119.8	143.6			49.0	31.3	73.3	2.3	
ECP6	propylene	3.7	113.0	153.5	103.3	149.8	52.4	33.8	76.0	2.2	
ECP7	propylene	6.4	101.5	111.3			38.0	26.7	48.2	1.8	
ECP8	propylene	6.2	108.1	125.1	93.6	121.7	42.7	41.7	88.4	2.1	
ECP9	propylene	9.9	90.8	75.1	70.1	69.5	25.0	27.7	49.1	1.8	
EC01	hexene	0.0	138.0	170.2	113.4	168.5	59.5	60.2	172.9	2.9	1.06
EC02	hexene	0.0	138.2	179.2	114.5	191.0	62.7	51.1	164.8	3.2	1.59
EC04	hexene	2.2	114.6	138.6	100.4		47.0	39.8	69.0	1.7	0.93
EC05	hexene	0.0	138.3	165.1	115.2	167.3	57.7	49.8	167.4	3.4	1.60
EC06	hexene	2.0	115.1	125.8	101.4	124.2	44.0	35.7	65.2	1.8	0.97
EC07	hexene	3.7	106.3	114.3			39.0	33.4	60.2	1.8	0.99
EC08	hexene	1.1	120.3	154.2	107.8	110.7	53.9	40.4	104.4	2.6	1.10
EC09	hexene	0.0	138.4	177.1	111.8	175.6	61.9	43.7	130.9	3.0	1.49
EC10	hexene	0.0	136.7	179.9	112.9	181.3	62.9	58.9	168.2	2.9	1.16
EC11	hexene	0.0	136.7	194.8	116.5		66.0	51.3	161.2	3.1	1.88
EC12	hexene	2.5	113.3	131.7	97.1		45.0	39.7	76.1	1.9	1.00
EC13	hexene	6.3	91.0	71.4	72.1	72.8	25.0	36.9	65.3	1.8	0.91
EC14	hexene	2.2	113.3	118.3	98.9	118.8	41.4	40.2	79.0	2.0	1.02
EC15	hexene	5.3	99.4	67.3	77.5	74.8	23.5	41.4	74.3	1.8	0.86
EC17	hexene	5.8	93.2	83.6			48.0	45.2	105.8	2.3	0.72
EC18	hexene	0.4	129.9	180.1	110.8	179.3	63.0	20.5	45.3	2.2	1.18
EC19	hexene	5.1	99.4	94.4			32.0	20.7	44.3	2.1	0.98
EC20	hexene	2.2	114.0	119.9	99.3	119.3	41.9	28.0	61.2	2.2	0.82
EC22	hexene	9.0	76.9	67.1	58.5	80.6	23.5	59.9	243.8	4.1	1.06
EC23	hexene	0.4	133.8	119.1	119.8	119.1	41.7	40.7	154.0	3.8	1.36
ECBu1	hexene	1.2	120.3	149.3	104.5	148.3	52.2	55.6	171.9	3.1	2.21
ECBu2	hexene	1.5	118.6	100.8	105.6	98.6	35.2	52.1	188.4	3.1	2.05
ECBu3	hexene	0.0	136.1	181.5			62.0	74.2	203.3	2.7	2.03
ECBu4	hexene	0.5	121.2	171.5	111.3	168.3	60.0	24.4	84.1	3.4	1.47
ECBu5	hexene	0.2	131.2	177.2	115.3	175.7	62.0	48.7	147.1	3.0	2.12
ECBu7	hexene	2.0	114.2	105.7	102.0	106.7	37.0	34.6	80.9	2.3	1.46
ECHS1	hexene	2.5	112.4	110.4	96.5	108.6	38.6	40.4	88.2	2.2	1.43
ECHS2	hexene	3.6	105.1	90.9	88.5	92.5	31.8	40.4	86.4	2.1	1.46
ECHS3	hexene	1.6	123.4	128.0	109.6	125.1	44.7	53.9	142.0	2.6	1.68
ECHS4	hexene	7.6	85.6	56.0	65.8	64.4	19.6	39.7	83.7	2.1	1.31
ECHS5	hexene	5.6	97.3	56.7	78.6	64.7	19.8	45.9	93.7	2.0	1.21

ECHS6	hexene	13.6	55.1	43.2	39.8	52.6	15.1	55.6	113.1	2.0	0.78
ECHS7	hexene	20.7	21.0	7.9	3.1	11.5	2.8	26.4	60.7	2.3	
IB04-1	hexene	0.7	129.7	135.6	107.3	133.3	47.4	36.5	113.5	3.1	
IB06-2	hexene	0.2	132.5	157.4	115.0	155.4	55.0	49.3	143.2	2.9	
IB09-1	hexene	0.03	138.1	178.4	112.5	176.8	62.4	40.3	122.6	3.0	
IB10	hexene	0.1	136.6	155.4	111.4	156.8	54.3	49.0	158.0	3.2	1.1
IB11-1	hexene	0.6	130.6	165.1	110.7	166.1	57.7	34.3	103.5	3.0	
IB22	hexene	1.5	123.7	135.5	109.3	135.2	47.4				
IB23	hexene	2.2	119.4	129.4	100.1	131.2	45.2				
IB23-15mn	hexene	2.2	122.0	108.4	99.0	106.5	37.9				
IB23-5mn	hexene	1.5	124.6	120.2	109.5	115.9	42.0				
IB26	hexene	1.1	120.6	124.8	104.7	124.9	43.6				
IB27	hexene	1.0	118.4	112.2	104.8	110.4	39.2				
IB29	hexene	3.9	113.0	92.5	91.3	100.2	32.4				
IB29-1	hexene	4.1	106.7	87.0	89.1	88.9	30.4				
IB29-10	hexene	2.3	115.3	108.9	97.0	114.1	38.1				
IB30	hexene	1.0	123.9	126.5	110.7	119.6	44.2				
IB31	hexene	2.3	118.9	116.9	105.5	114.1	40.9				
IB32	hexene	0.7	128.5	144.6	110.2	140.3	50.5				
IB34	hexene	3.7	108.6	97.9	92.9	97.9	34.2				
EC µ1	octene	3.4	108.1	112.9			38.5	32.1	57.9	1.8	0.80
EC µ2	octene	4.6	98.5	69.0	86.1		23.6	31.1	102.6	3.3	0.57
EC µ3	octene	1.7	116.6	124.8	102.4	125.8	43.6	32.4	58.3	1.8	0.97
EC µ4	octene	0.6	126.6	157.7	109.9	154.5	55.1	41.0	106.6	2.6	1.18
EC µ6	octene	5.6	97.9	86.6			29.6	32.2	58.0	1.8	0.74
EC µ7	octene	0.4	130.8	167.1	110.9	168.2	58.4	48.4	116.2	2.4	0.84
EC µ8	octene	12.5	55.0	40.1	38.8	50.1	15.0	38.2	75.2	1.9	
BPC1801	octadecene	1.7	116.5	111.3	103.2	79.5	38.0	35.8	93.1	2.6	0.74
BPC1802	octadecene	0.7	126.0	137.7	109.5	46.1	47.0	26.0	65.1	2.5	0.50
BPC1803	octadecene	1.5	118.1	108.4	114.9	115.2	37.0	40.9	99.2	2.4	0.91
BPC1804	octadecene	2.1	114.0	67.4	100.2	62.7	23.0	38.8	73.7	1.9	0.79
BPC1805	octadecene	6.9			98.8	40.9		113.5	203.2	1.8	0.35
BPC1806	octadecene	2.7	110.0	90.8	82.8	39.4	31.0	26.1	60.0	2.3	0.61
BPC1807	octadecene	4.1	92.0	44.0	102.6	63.7	15.0	74.9	165.5	2.2	0.70
BPC1808	octadecene	3.3	96.4	46.9	99.9	59.9	16.0	43.2	82.1	1.9	1.02
BPC1809	octadecene	2.9	106.0	61.5			21.0	25.6	59.0	2.3	0.65
BPNOR01	norbornene		133.6	4.7	119.5	4.8	1.7				
BPNOR02	norbornene	1.0	134.4	2.8	118.9	2.0	1.0	120.9	278.3	2.3	1.03
BPNOR03	norbornene	3.8	103.9	79.4	87.0	81.0	27.8	40.2	102.7	2.6	1.22
BPNOR04	norbornene	3.2	105.5	85.7	93.2	88.1	29.9	46.7	102.6	2.2	1.03
BPNOR05	norbornene		104.6	51.4	93.3	50.9	18.0				
BPNOR06	norbornene	4.0	101.8	69.5	84.6	69.3	24.3	43.9	96.9	2.2	1.06
BPNOR07	norbornene	2.4	128.9	93.9	104.7	93.6	32.8	55.5	138.7	2.5	1.08
BPNOR08	norbornene	4.7						49.9	126.4	2.5	1.08

BPNOR09	norbornene	2.5	122.6	116.9	105.8	116.2	40.9	55.1	141.1	2.6	1.06
BPNOR10	norbornene	1.9	111.1	102.9	100.8	105.0	36.0	59.2	117.2	2.0	1.06
BPNOR11	norbornene	6.7	76.8	39.1	65.9	39.3	13.7	77.4	148.1	1.9	0.92
BPNOR12	norbornene	1.0	121.8	129.9	107.8	129.5	45.4	51.5	118.1	2.3	0.00